BIOGEOCHEMICAL NITROGEN TRANSFORMATIONS UNDER CONTRASTING MIXING REGIMES IN TWO COASTAL WATER COLUMNS

by

Sebastian Haas

Submitted in partial fulfilment of the requirements
for the degree of Doctor of Philosophy

at

Dalhousie University
Halifax, Nova Scotia
October 2020

Dedication

Für meine Familie und Freunde in der allzu fernen Heimat

TABLE OF CONTENTS

LIST OF TABLES

LIST OF FIGURES

ABSTRACT

The biogeochemical cycling of nitrogen (N) in coastal water columns is of high importance due to anthropogenic N input and its role in fueling primary production and eutrophication. Using highly resolved field observations of a wide variety of environmental parameters, this thesis explores how microbiological, geochemical and physical variables control N cycling in two contrasting coastal water columns. In Chapter 2, metagenomes and the 16S rRNA phylogenetic marker gene were used in conjunction with geochemical measurements to characterize the microbial community and its functional capacities along an oxic-suboxic-sulfidic-ferruginous-methanogenic gradient in permanently stratified Powell Lake, British Columbia. This revealed potential micro-aerobic nitrifiers, facultative anaerobic potential in the widespread freshwater lineage acI (*Actinobacteria*) and evolutionarily divergent microbial lineages in the bottom water containing ancient seawater. Chapters 3 and 4 focus on the Bedford Basin (BB), Nova Scotia, a seasonally stratified coastal basin. In the dark BB bottom water (60 meters), accumulated ammonium (~20 μmol kg^{-1}) is oxidized to nitrate during stratified periods. Chapter 3 describes results from four years (2014–2017) of weekly time series measurements in BB bottom water of geochemical concentrations as well as functional and phylogenetic marker genes. Analyses in conjunction with a biogeochemical model suggested strong physical mixing in some years caused dilution of nitrifier biomass, which led to nitrification delay and temporary nitrite accumulation by delaying the regrowth of ammonia oxidizer and nitrite oxidizer populations. In Chapter 4, the N isotopic signatures ($\delta^{15}N$) of particulate N, ammonium, nitrite and nitrate associated with these nitrification patterns were analyzed, using two distinct "natural experiments": in 2014, ammonia oxidation was performed almost entirely by archaea and nitrite did not accumulate beyond 0.5 μmol kg^{-1}. In 2017, bacterial ammonia oxidation played a role in nitrite accumulation to about 8 μmol kg^{-1}. N isotope fractionation patterns were analyzed with the support of a numerical model and high-confidence, *in situ* isotopic enrichment factors ($^{15}\varepsilon$) were determined. Overall, this work identified key controls on the aquatic N cycle, its interaction with other biogeochemical cycles, microbial communities and climate, as well as controls on N isotope distributions in the context of different stratification regimes.

LIST OF ABBREVIATIONS AND SYMBOLS USED

α = Isotopic fractionation factor (generic)

$^{15}\alpha$ = Nitrogen ($^{14}N/^{15}N$) isotopic fractionation factor

δ = Isotope signature (generic)

δ_P = Isotope signature of the reaction product (generic)

δ_S = Isotope signature of the reaction substrate (generic)

$\delta^{15}N$ = Nitrogen isotope signature

ε = Isotopic enrichment factor (generic)

$^{15}\varepsilon$ = Nitrogen ($^{14}N/^{15}N$) isotopic enrichment factor

ANOSIM = Analysis of Similarities

AO = Ammonia Oxidation

AOA = Ammonia Oxidizing Archaea

AOB = Ammonia Oxidizing Bacteria

AOO = Ammonia Oxidizing Organism

ASV = Amplicon Sequence Variant

ASW = Ancient Seawater (environmentally relevant zone in Powell Lake)

BB = Bedford Basin

BNF = Biological Nitrogen Fixation

C = Carbon

C_{org} = Organic carbon

Chl = Chlorophyll

CTD = Conductivity-Temperature-Depth sensor

DIN = Dissolved Inorganic Nitrogen

DNA = Desoxyribo-Nucleic Acid

DNRA = Dissimilatory Nitrate Reduction to Ammonium

DOC = Dissolved Organic Carbon

f = fraction of unreacted substrate

Fe = Iron

KEGG = Kyoto Encyclopedia of Genes and Genomes

K_M = half saturation constants (Michaelis Menten)

KO = KEGG Orthologues

mOMZ = marine Oxygen Minimum Zone

MAG = Metagenome Assembled Genome

Mn = Manganese

N = Nitrogen

nanoSIMS = nano scale secondary ion mass spectrometry

N^2 = Buoyancy Frequency

NCBI = National Center for Biotechnology Information

nifH = Nitrogenase gene

NMDS = Non-Parametric Multidimensional Scaling

NO = Nitrite Oxidation

NOB = Nitrite Oxidizing Bacteria

N_{org} = Organic Nitrogen

nxr = Nitrite oxidoreductase gene

OTU = Operational Taxonomic Unit

P = Phosphorus

POC = Particulate Organic Carbon

PON = Particulate Organic Nitrogen

PNM = Primary Nitrite Maximum

qPCR = Quantitative Polymerase Chain Reaction

rRNA = Ribosomal ribonucleic acid

S = Sulfur

SD = Standard Deviation

SIMPER = Similarities Percentage Breakdown

ssu = small sub-unit

SW = Surface Water

V_{max} = Maximum reaction velocity

VSMOW = Vienna Standard Mean Ocean Water

ACKNOWLEDGEMENTS

First and foremost, I would like to thank my advisor Doug Wallace for supporting my research intellectually and financially, for his remarkable gift of always remaining positive, and for letting me follow my own research interests to an unusual degree even into areas beyond his scientific comfort zone.

Furthermore, I would like to thank my immensely supportive and knowledgeable advisory committee: Rich Pawlowicz, Carly Buchwald, Julie LaRoche, Chris Algar and Markus Kienast. I was truly lucky to be advised by a committee with such a high amount of expertise.

My doctoral stipend was funded by the Killam Foundation, the Nova Scotia Graduate Scholarship initiative, CERC.OCEAN as well as by the Dalhousie President's Award.

Without the support of the technical staff, I could not have produced the large amounts of data that form the basis of this work. Claire Normandeau, Liz Kerrigan and Anna Haverstock provided invaluable expert support in analyzing samples and were always available for discussions on method improvements and troubleshooting. Perhaps just as important, it was always a pleasure chatting with them, no matter how annoying the methodological problem at hand. Anna Haverstock along with many others, including Shona MacDonald, Jessie Jawanda, Chris Payne and Larysa Pakhomova, carried out or supported me in taking the innumerable water samples from Bedford Basin and Powell Lake used for this thesis. Dariia Atamanchuk and the CERC.OCEAN engineers have ensured the success of sensor deployments and resulting data analysis. Furthermore, I am grateful to the Bedford Institute of Oceanography for starting and sustaining the Bedford Basin time series and allowing us to use their infrastructure for sampling.

All past and present members of the CERC.OCEAN group have helped me to one or another degree over the years, but Jackie Hurst and Sarah Al-Shaghay deserve special mention for helping out with the uncountable little organizational or administrative problems that arose over the years as well as major logistical issues. I am also grateful to Tim Kalvelage for starting the Bedford Basin nitrogen biogeochemical project and for doing the initial work of establishing sampling and analysis protocols that were invaluable

to me at the start. Finally, while offices got shuffled around over the years, Qiang Shi was my office mate during most of the time and always fun chatting with, even though we have yet to find a connection between the nitrogen and iodine cycles.

Beyond the CERC.OCEAN group, I thank Julie LaRoche and her lab group, particularly Dhwani Desai, Brent Robicheau and Jennifer Tolman, for fruitful collaboration and for providing expertise in the field of molecular ecology, enabling the interdisciplinary research I was envisioning for my work. I am very grateful also to Chris Algar and Subhadeep Rakshit for introducing me to the world of biogeochemical modeling and providing invaluable expertise in this area.

I would like to thank the Dalhousie Oceanography department and particularly the graduate student society DOSA for creating a welcoming and active community that immediately made me feel at home after my arrival. Many new-found friends made the time in Halifax worthwhile and provided the psychological (and sometimes scientific) support no PhD student can succeed without, and among them I would like to emphasize Lorenza Raimondi and Francesco Usai, Ricardo Arruda, Colin Hughes, Helen Packer and Fabian Fürle as well as Nadine Lehmann.

Last but not least, there was an older friend who was there from the start and without whom I could not have arrived at this point: Thank you, Tatjana, for your endless love and support!

CHAPTER 1

INTRODUCTION

1.1. The Aquatic Nitrogen Cycle and its Importance

Nitrogen (N) is a limiting nutrient for primary production by photosynthetic organisms in many aquatic environments (Canfield 1983; Falkowski 1997; Howarth and Marino 2006; Xu et al. 2010). This is despite the high atmospheric abundance of N_2, as the chemically inert N_2-molecule can only be used by specialized N_2-fixing microorganisms. All other organisms rely on "fixed nitrogen", which includes diverse organic forms of N and the dissolved inorganic nitrogen (DIN) species ammonium (NH_4^+), nitrite (NO_2^-) and nitrate (NO_3^-). The sum of the mostly biotic processes producing, transforming and removing fixed N in its multiple different chemical forms constitute the biogeochemical N cycle (Fig. 1.1).

The processes within the N cycle are highly dependent on the redox state of the environment as many are either obligately aerobic or anaerobic. Therefore, and given the delayed and slow oxygenation of the oceans during Earth's history, the anaerobic process of biological N_2 fixation (BNF) likely evolved prior to the obligately aerobic nitrification process and the obligately anaerobic, but oxidized-N dependent processes of denitrification and anammox (Falkowski 1997; Canfield et al. 2010a). During the transition period, i.e. while oceans were slowly being oxygenated after the evolution of oxygenic photosynthesis, the marine water column was likely analogous to some modern-day, permanently stratified marine basins and lakes: an oxygenated surface layer, in which nitrification could occur, overlying an anoxic bottom layer, in which downward diffusing nitrate could be reduced by denitrification and anammox (Canfield et al. 2010a; Thomazo and Papineau 2013). In the mostly well-oxygenated ocean of today, anaerobic processes are restricted to the sediments and to anoxic micro-zones within particles (Bianchi et al. 2018), anoxic coastal basins (Dalsgaard et al. 2003; Bourbonnais et al. 2013), transiently suboxic eddies (Fiedler et al. 2016) and spatially restricted, but expanding (Stramma et al. 2010; Breitburg et al.

2018) marine oxygen minimum zones (mOMZ; Lavik et al. 2009; Lam and Kuypers 2011; Kalvelage et al. 2013).

The contemporary global ocean is a net N sink, receiving more fixed N from the atmosphere and terrestrial realm than it returns, part of which is a consequence of anthropogenic activity (Gruber 2008; Fowler et al. 2013). Every year, about 40–66 Tg N are delivered to coastal ecosystems by rivers (Voss et al. 2013) and current estimates suggest that 75% of riverine DIN may reach the open ocean (Sharples et al. 2017; Jickells et al. 2017). The atmospheric deposition of reactive N from fossil fuel combustion and the widespread use of the Haber-Bosch process to fix N_2 for agricultural fertilization constitute fixed N sources that are now of similar magnitude as global BNF (Duce et al. 2008; Canfield et al. 2010a; Peñuelas et al. 2012; Fowler et al. 2013; Glibert et al. 2014; Jickells et al. 2017). This leads to increased oceanic N loads and nitrogen-to-phosphorus ratios, as well as to changes in the chemical speciation (organic vs. inorganic, reduced vs. oxidized) of fixed N (Kim et al. 2011; Peñuelas et al. 2012; Glibert et al. 2014, 2016). In coastal systems, an increased share of reduced N in fixed N has been observed with consequences for ecosystem health (Glibert et al. 2014, 2016). Similarly, fluctuations in the relative supply of organic N may disturb ecological integrity and cause harmful algal blooms (LaRoche et al. 1997). Meanwhile, in the ocean at large, a decrease in surface water nitrate concentrations is predicted as a consequence of changing stratification patterns associated with climate change (Bindoff et al. 2019).

In most present-day natural systems, DIN speciation is crucially determined by nitrification, a process at the center of the N cycle oxidizing ammonia (NH_3) via nitrite to nitrate. The ratio of ammonium to nitrate available to phytoplankton has a significant impact on phytoplankton community structure and primary productivity: high shares of ammonium in DIN have been linked to lower primary productivity and to selection for smaller algal species, which may have the potential to form harmful algal blooms (Berg et al. 2003; Yoshiyama and Sharp 2006; Domingues et al. 2011; Glibert et al. 2016). Furthermore, the production of nitrite and nitrate by nitrification is a prerequisite for fixed N removal via denitrification or anammox. Together with losses to burial and transport to other parts of the ocean (continental shelfs), denitrification constitutes a quantitatively

important removal pathway for fixed N from coastal systems (Voss et al. 2013). Local variability in the efficiency of nitrification is particularly important in the coastal ocean, where most of the sinking organic matter reaches the sediments, whereas almost all organic N sinking out of the euphotic zone in the oligotrophic open ocean is remineralized (Gruber 2008). Finally, the coastal ocean is also a major source of the greenhouse gas N_2O, which can be produced as a side product of nitrification or as an intermediary product of denitrification (Bange 2006).

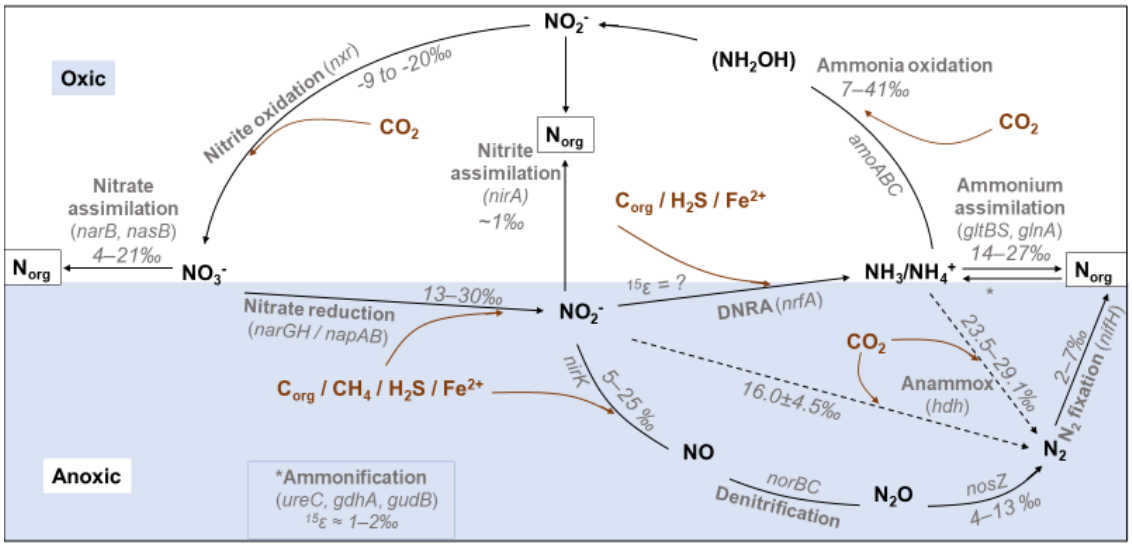

Fig. 1.1: The aquatic nitrogen cycle with functional marker genes (section 1.2) and known nitrogen isotope effects ($^{15}\varepsilon$) for each process (section 1.8) as well as potential links to the carbon, sulfur and iron cycles indicated (section 1.3).

In a changing global environment, it is especially important to understand the biogeochemical N cycle (Fig. 1.1) and how it is controlled by the interaction with other biogeochemical cycles and environmental factors, particularly the physical environment (temperature, mixing) that is subject to climate-driven changes. Moreover, detailed understanding at the intersection of geochemistry and microbiology is crucial, given that N cycle processes are mostly mediated by microbes, which use enzymes to catalyze oxidation-reduction (redox) transformations of DIN species and to convert between organic and inorganic forms of N. Well-resolved, interdisciplinary, *in situ* observations in "natural laboratories" as described in the following chapters are a key tool to gain these

insights. For example, detailed vertical profiles in stable systems close to steady state (Chapter 2) and highly resolved time series in dynamic systems (Chapters 3 and 4) are promising approaches used here to study the influence of physical factors, geochemical gradients and connected biogeochemical cycles on N cycling, with a focus on nitrification.

1.2. The N Cycle, its Microbial Players and Their Functional Marker Genes and Links to Other Elemental Cycles

To understand the N cycle and its environmental role, it is important to note that it is a complex web of processes, most of them catalyzed by microbes using organic and inorganic N compounds with different redox states for biomass growth (assimilation) or energy conservation (Fig. 1.1). BNF by taxonomically diverse bacteria or archaea (Bombar et al. 2016), collectively called diazotrophs, makes the plentiful but inert N_2 biologically available. In the ocean, BNF supported by phototrophy plays a major role, but BNF independent of light energy is increasingly recognized as quantitatively important (Bombar et al. 2016). Most known diazotrophs contain a version of the enzyme nitrogenase and the *nifH* subunit of the nitrogenase gene is typically used as a functional marker gene.

Fixed organic N can be remineralized by heterotrophic microorganisms to ammonium, in a process often called ammonification. Given the variety of organic N compounds and pathways for their remineralization, no single functional marker gene can signpost this process, but *ureC* (urease), *gdHA* and *gudB* (glutamate dehydrogenase) have been used (Lauro et al. 2011). Similarly, for ammonium assimilation no single functional marker gene can cover the incorporation of ammonium into different organic compounds, but *glnA* (glutamine synthetase) and *gltBS* (glutamate synthase) have been used (Lauro et al. 2011). Ammonium can be re-assimilated into biomass not only by phototrophs and chemolithoautotrophs but also by heterotrophs (Allen et al. 2002), thereby avoiding both the oxidative and N_2-producing portions of the N cycle.

Under oxic conditions, an alternative fate for ammonium is its oxidation via two major steps to nitrite (ammonia oxidation, AO) and further to nitrate (nitrite oxidation, NO). Typically, these two steps of nitrification are catalyzed by two taxonomically and functionally different microorganisms, ammonia oxidizing organisms (AOO) and nitrite

oxidizing bacteria (NOB). An exception to this has been found only recently, when bacteria from the genus *Nitrospira* were discovered that can conduct the entire process of oxidizing ammonium to nitrate (Daims et al. 2015; van Kessel et al. 2015). While this complete nitrification ("comammox") has mainly been found in human-made (e.g. wastewater) and some terrestrial environments (Pjevac et al. 2017; Koch et al. 2019), some environmental studies suggest that the process may be relevant also in the coastal ocean (Yu et al. 2018; Xia et al. 2018).

Nitrospira were previously known to catalyze NO, the second step of nitrification, only. Other NOB groups are the proteobacterial genera *Nitrotoga* (Alawi et al. 2007), *Nitrobacter*, *Nitrospina* and *Nitrococcus*, of which the latter two are most relevant for marine NO (Spieck and Bock 2005; Lam and Kuypers 2011). AO, the first step of nitrification, is catalyzed either by ammonia oxidizing bacteria (AOB) or -archaea (AOA). Soon after their discovery in the early 21st century, AOA were found to be the dominant ammonia oxidizing organisms (AOO) in the open ocean (Könneke et al. 2005; Wuchter et al. 2006). Known AOA are affiliated with the phylum *Thaumarchaeota* and all *Thaumarchaeota* contain the marker gene *amoA* for AO (Santoro et al. 2019), while AOB are either *Gamma-* or *Betaproteobacteria* within the orders *Nitrosococcales* and *Nitrosomonadales*, respectively.

The two main functional marker genes used in nitrification are the *amoA* subunit of the ammonia monooxygenase gene and subunits of the *nxr* gene for the nitrite oxidoreductase. Both NOB and comammox bacteria use distinct versions of *nxr* to oxidize nitrite and different versions of *amoA* are used by AOA, AOB and comammox bacteria for the first step of ammonia oxidation (Daims et al. 2015). Ammonia is first turned into hydroxylamine, an intermediate product in both bacterial and archaeal ammonia oxidation (Stein 2019). Additionally, AOB and complete nitrifiers produce nitric oxide (not shown in Fig. 1.1) as a second intermediate prior to nitrite via a hydroxylamine dehydrogenase (Caranto and Lancaster 2017). AOA may also produce NO as a side product of the final nitrite production step (Stein 2019).

Nitrification is the pre-requisite for fixed N removal via denitrification or anammox. Denitrification can be catalyzed by diverse groups of bacteria, archaea (Philippot 2002)

and even fungi (Kobayashi et al. 1996). The functional marker genes *narGH* (nitrate reductase), *nirK* (nitrite reductase), *norBC* (nitric oxide reductase) and *nosZ* (nitrous oxide reductase) are widely used as tracers for these subprocesses along the denitrification pathway (Fig. 1.1). Denitrification can be heterotrophic, using organic carbon as electron donor, or autotrophic, using reduced sulfur or iron.

Anammox, an alternative process which uses ammonium and nitrite as substrates for the removal of fixed N from aquatic environments, was also discovered relatively recently (Strous et al. 1997, 1999; Dalsgaard et al. 2003; Kuypers et al. 2003). It is an autotrophic process and organic carbon availability may therefore be an important factor in distinguishing its niche from that of heterotrophic denitrification (Algar and Vallino 2014; Hardison et al. 2015). Its marker gene hydrazine dehydrogenase (*hdh*) is a hydroxylamine oxidoreductase-like protein with high structural similarity to the hydroxylamine dehydrogenases harbored by AOB and comammox bacteria (Maalcke et al. 2016). This makes a distinction based on genetic information between AOB and anammox non-trivial and require analysis beyond the level routinely deployed for metagenomic data (Haas et al. 2019).

Dissimilatory nitrate reduction to ammonium (DNRA) is of environmental significance as it constitutes a pathway of dissimilatory N reduction that does not result in loss of fixed N. It is often associated with nitrate reduction to nitrite via the periplasmic nitrate reductase (*napAB*; Giblin et al. 2013), but the functional marker gene *nrfA* coding for the periplasmic, formate-dependent nitrite reductase that catalyzes nitrite reduction to ammonium is a more reliable identifier of genetic potential for DNRA.

Fundamental gaps in our understanding of the aquatic N cycle are still being closed. This is demonstrated by the relatively recent discoveries of the anammox (Strous et al. 1997, 1999; Dalsgaard et al. 2003; Kuypers et al. 2003) and comammox processes (Daims et al. 2015; van Kessel et al. 2015), the existence and environmental importance of archaeal ammonia oxidizers (Könneke et al. 2005; Wuchter et al. 2006), as well as the recently identified connections between denitrification and anaerobic methane oxidation (Ettwig et al. 2010; Haroon et al. 2013). Strikingly, each of these processes and associated microbes were first discovered in human-made or human-impacted environments, such as aquaria

(Könneke et al. 2005), wastewater (Strous et al. 1997, 1999), aquaculture or oil exploration pipes (Daims et al. 2015; van Kessel et al. 2015), canals or ditches (Ettwig et al. 2010), or wastewater sludge (Haroon et al. 2013). This might be explained by the typically high accessibility and economic incentive to monitor such environments, leading to a higher likelihood of chance findings that ultimately lead to discoveries.

Pure isolation of the functional microbes or their enrichment combined with microscopic imaging and/or genomic techniques was a pivotal step in the discovery process, often confirming theoretical or environmental indications for their existence (Strous et al. 1999; Könneke et al. 2005; Ettwig et al. 2010; Haroon et al. 2013; Daims et al. 2015; van Kessel et al. 2015). Subsequently, the environmental relevance was established by culture-independent methods (Dalsgaard et al. 2003; Kuypers et al. 2003; Wuchter et al. 2006; Pjevac et al. 2017). The continuing discoveries of novel processes within the N cycle is likely a consequence of its complexity, which is owed to the high number of inorganic N compounds that are stable in aqueous and solid states in the environment and that cover a wide redox range. This enables a large variety of processes that are thermodynamically feasible for energy preservation by microbes (Fig. 1.1), many of which link N compounds to other biogeochemical cycles (Lam and Kuypers 2011).

1.3. Links Between Nitrogen, Sulfur, Carbon and Metal Cycling

Given that each biotic N-biogeochemical process links the N cycle to other biogeochemical cycles via the metabolism of the catalyzing microbe, it is important to resolve these links. Each biotic process in the N cycle is linked to the carbon (C) cycle by either heterotrophy or autotrophy or potentially both (Fig. 1.1). Denitrification combined with methane or methyl compound oxidation provides additional links between the N and the C cycle (Ettwig et al. 2010; Haroon et al. 2013; Kits et al. 2015a; b; Oswald et al. 2017). Autotrophic denitrification and DNRA can be combined with sulfide or ferrous iron oxidation, thereby linking the N- to the cycles of C, sulfur (S) and iron (Fe) (Baalsrud and Baalsrud 1954; Straub et al. 1996; Jørgensen and Nelson 2004; Murphy et al. 2020). Additionally, abiotic reduction of nitrite by ferrous iron to N_2O or N_2 may be significant in iron-rich environments (Buchwald et al. 2016).

BNF can be linked to both the carbon and sulfur cycles via various processes employed by diazotrophs that include methanotrophy, methanogenesis and sulfate reduction (Bombar et al. 2016). Evidence for the occurrence of anammox (N_2 production from ammonium) with iron oxides or sulfate as electron acceptors has been found in soil and wastewater systems (Yang et al. 2012; Rikmann et al. 2012) and first indications for its occurrence were recently found also in marine sediments (Rios-Del Toro et al. 2018). Possible indications for anaerobic nitrification (NO_x^- production from ammonium) using manganese oxides (Lin and Taillefert 2014), iodate (Babbin et al. 2017) or sulfate (Rikmann et al. 2012) have not been corroborated for natural aquatic systems to date.

1.4. Nitrification at Low Oxygen Concentrations

AO and NO, the subprocesses of nitrification that constitute a focus of the following studies, are obligately aerobic processes. However, recently, they have been observed under close-to anoxic conditions (dissolved O_2 as low as <1 μM), raising questions about the lower oxygen-thresholds for these processes (Füssel et al. 2012; Buchwald et al. 2015; Bristow et al. 2016). Evidence from mOMZs suggests that the activity of specialized low-oxygen nitrite oxidizers may be limited by nitrite even under low-O_2 conditions and that higher O_2 may even partially inhibit them (Sun et al. 2017). These findings are suggestive of microaerophilic or even anaerobic nitrification. For NO, indications for activity in the absence of O_2 have been reported independently multiple times (Füssel et al. 2012; Kalvelage et al. 2013; Peng et al. 2016; Sun et al. 2017). However, these findings are inferred using natural abundance or tracer isotope techniques. Conclusions from such studies might, conceivably, be invalidated by intricate isotope effects for which evidence is only beginning to emerge and which may have the potential to explain results from these studies without invoking anaerobic nitrification (Kemeny et al. 2016; Buchwald and Wankel 2020). In Chapter 2, potential micro-aerobic nitrifiers are identified taxonomically.

The electron acceptors iodate (Babbin et al. 2017), manganese oxides (Lin and Taillefert 2014), ferric iron (Yang et al. 2012) or sulfate (Rikmann et al. 2012) are thermodynamically feasible to support the nitrification processes and some indications have been found for their environmental relevance. Evidence for ammonia oxidation to

nitrate or N_2 by sulfate reduction has been found in wastewater (Liu et al., 2008; Rikmann et al., 2012 and citations therein). Fe(III)-catalyzed oxidation of ammonium to NO_2^-/NO_3^- at neutral or high pH and to N_2 at pH<6.5 may occur in soils (Yang et al. 2012; Li et al. 2015d). Indirect evidence for Mn(IV)-catalyzed ammonia oxidation to nitrate and nitrite has been found in marine sediments (Hulth et al. 1999; Mortimer et al. 2004; Bartlett et al. 2008; Lin and Taillefert 2014).

Nitrite oxidation coupled to the dismutation of nitric oxide into O_2 and N_2 has recently been proposed to occur in mOMZs (Babbin et al. 2020). The O_2 produced during the dismutation reaction could be used to support aerobic nitrite oxidation. A similar mechanism can evidently support aerobic methane oxidation coupled to nitrite dismutation (Ettwig et al. 2010).

1.5. Kinetics of Nitrification

The kinetic properties of enzymes can be described by the maximum velocity (V_{max}) at which the process catalyzed by a given enzyme can proceed under substrate saturation, as well as the half-saturation constant (K_M), which denotes the substrate concentration at 50% V_{max} and assesses the efficiency at which the substrate can be utilized at low concentration (Menten and Michaelis 1913). In the environment, these parameters reflect evolutionary adaptations to high (high V_{max}, low K_m) or low (low V_{max}, low K_m) substrate concentrations. This can lead to niche-differentiation also in nitrifying organisms (Martens-Habbena et al. 2009) and, as shown in Chapter 3, have geochemical consequences .

Kinetic properties of nitrifying organisms suggest that they can be active at low oxygen concentrations. Lab-based studies suggest relatively high half-saturation constants for O_2 in the range of 2.6–135.3 μM for NOB, 1.3–14.9 μM for AOB and 1.2–3.9 μM for AOA (Laanbroek and Gerards 1993; Laanbroek et al. 1994; Blackburne et al. 2007; Martens-Habbena et al. 2009; Nowka et al. 2015; Ushiki et al. 2017; Qin et al. 2017). However, using data from several studies in mOMZs, Bristow et al. (2016) found apparent half-saturation constants for O_2 of 0.283±0.064 μM for AO and 0.622±0.145 μM for NO, suggesting potential for these processes at nanomolar-level oxygen concentrations. The nitrifier community in Bristow et al.'s study was likely dominated by *Thaumarchaeota* and

Nitrospina, which may explain the big difference, especially for NOB, to results from the laboratory-based studies cited above, which were conducted on *Nitrospira* and *Nitrobacter*. Bristow et al.'s study demonstrates the difficulty in distinguishing between microaerophilic and potential anaerobic nitrification, given the potential for nitrification at oxygen concentrations below the sensitivity threshold of all but the most specialized, recently developed oxygen sensors (Revsbech et al. 2011).

Differential AO and NO kinetics among nitrifying organisms can represent adaptations to different ecological niches (Blackburne et al. 2007; Martens-Habbena et al. 2009; Nowka et al. 2015). Large differences in the affinity for ammonia have been found between AOA and AOB (Martens-Habbena et al. 2009). AOA, which dominate AO in the oligotrophic open-ocean (Wuchter et al. 2006), have significantly higher affinity for ammonia ($K_m(NH_3) \approx 0.1$ μM) than AOB (2.4–8000 μM; (Suzuki et al. 1974; Ward 1987, 1990; Schramm et al. 1999; Bollmann et al. 2005; Martens-Habbena et al. 2009; Newell et al. 2013; Horak et al. 2013) which tend to be found in coastal and lacustrine environments with higher ammonium availability (Li et al. 2015b; Happel et al. 2018; Massé et al. 2019).

N-substrate affinities for NOB are in a similar range ($K_m(NO_2^-)$: 6–606 μM) as those determined for AOB, i.e. at least an order of magnitude higher than for AOA (Laanbroek and Gerards 1993; Schramm et al. 1999; Blackburne et al. 2007; Nowka et al. 2015; Ushiki et al. 2017). However, *Nitrospina*-dominated natural assemblages in an mOMZ showed much lower apparent $K_m(NO_2^-)$ for nitrite (0.254±0.161 μM), suggesting higher affinity under low nitrite concentrations (≤0.1 μM) in the ocean (Sun et al. 2017).

1.6. Nitrification in Coastal Water Columns

N cycling in coastal systems is of special significance due to their location near the land-sea interface, which makes them a direct recipient of, and filter for, anthropogenic N that is added to the ocean (Glibert et al. 2016). Excess N within coastal systems can cause ecological problems such as eutrophication and harmful algal blooms (LaRoche et al. 1997; Glibert et al. 2014, 2016; Domangue and Mortazavi 2018). As discussed above (1.1) and in Chapter 3 nitrification can play a key role in this context due to its ability to influence the crucial ammonium:nitrate ratio (Glibert et al. 2016).

As an additional challenge, global climate change and N pollution can lead to alteration of biogeochemical cycling and primary production through eutrophication and deoxygenation (Bange 2006), as well as physical changes as discussed in Chapter 3. Coastal basins and other shelf systems are also net sources of the greenhouse gas N_2O (Bange 2006). Oxygen gradients in coastal basins are of particular importance, since the availability of oxygen fundamentally influences N cycling and directly affects N_2O emissions (Punshon and Moore 2004; Bange 2006; Naqvi et al. 2010). Findings from coastal systems (Chapters 3, 4) may also help our understanding of N cycling in other globally significant marine systems, such as mOMZs and sediments.

1.6.1. Seasonal Variations and Controls of Nitrification

Seasonal maxima in nitrification have been observed frequently in coastal systems (Punshon and Moore 2004; Schweiger et al. 2007; Pitcher et al. 2011; Hollibaugh et al. 2014; Laperriere et al. 2019). They often seem to be caused by changing availability of ammonium due to mixing (Schweiger et al. 2007; Pitcher et al. 2011; Laperriere et al. 2019). In other cases, however, maximum nitrification was observed during stratified periods while low rates or nitrifier numbers were associated with mixing events (Punshon and Moore 2004; Hollibaugh et al. 2014). The latter phenomenon is explored in Chapter 3.

A frequently observed phenomenon in marine and lacustrine surface waters are near-surface wintertime blooms of nitrifying bacteria (Schweiger et al. 2007; Galand et al. 2010; Pitcher et al. 2011; Grzymski et al. 2012; Smart et al. 2015; Massé et al. 2019). In some of these cases, euphotic-zone nitrification was likely enhanced by ammonium delivery from subsurface water after stratification breaks down in early winter (Schweiger et al. 2007; Galand et al. 2010). In other cases, wintertime nitrification maxima could be facilitated by increased ammonium availability due to lower assimilative demand by phytoplankton or directly by the decreased light intensity, which allows the presumably light-sensitive nitrifiers to thrive at the surface only during this season (Smart et al. 2015).

Indications for light-inhibition of nitrification have been reported by numerous studies, but it is often difficult to distinguish between direct photoinhibition and indirect suppression of nitrification due to substrate competition from photoautotrophs (Olson

1981; Merbt et al. 2012; Hsiao et al. 2014). Also, light-intensity in mid-latitudes, where several such observations have been made (Galand et al. 2010; Pitcher et al. 2011; Massé et al. 2019), may be reduced in winter, but sunlight is still present. Moreover, there are numerous reports of euphotic zone nitrification also outside winter, proving that light-inhibition does not in principle prohibit nitrification (Wankel et al. 2007; Grundle and Juniper 2011; Stephens et al. 2019). It also seems implausible that AOA evolved high enough substrate affinity to compete with phytoplankton during spring, summer and fall, but that no AOO species additionally evolved the sunlight protection necessary to occupy this ecological niche. Instead, more direct competition may be occurring, which might include phytoplankton actively suppressing competition for ammonium from AOO, e.g. via allelopathy (Legrand et al. 2003). This still speculative idea should be tested further. Alternatively, low ammonium concentrations created by phytoplankton assimilation may simply exert a first-order limitation on nitrification rates. Low ammonium concentrations may select for "K-selected" AOO with low-K_m-low-V_{max} AO kinetics, while higher concentrations may select for AOO with the opposite kinetic properties ("r-selected"), leading to higher rates in winter. In a temperate lake in which ammonium concentrations and AO rates were highest during winter, AOA were omnipresent throughout the year while AOB were only abundant in winter (Massé et al. 2019). Based on the differential kinetics in AOA vs AOB discussed above, it is tempting to speculate that r-selected AOB caused higher rates in winter but were unable to compete with photoautotrophs for limiting ammonium during summer. At a coastal site in the Mediterranean Sea, coincident winter peaks of chlorophyll (Chl) *a* and thaumarchaeal 16S rRNA genes were reported, evidently driven by the intrusion of nutrient-rich subsurface water into the surface water (Galand et al. 2010). This suggests that substrate availability caused wintertime nitrification and that light-inhibition, at least under these circumstances, was ineffective. In summary, I argue that wintertime, near-surface nitrification maxima are more likely to be caused by increased ammonium availability due to mixing or the reduction of phytoplankton assimilation than by light-inhibition. This remains an active area of research.

1.6.2. Temporal and Spatial Nitrite Accumulations in Water Columns

Transient accumulations of nitrite have been observed in coastal waters and lakes (McCarthy et al. 1984; Gelda et al. 1999; Saccà et al. 2008; Tremblay et al. 2008; Pitcher et al. 2011; Hollibaugh et al. 2014; Heiss and Fulweiler 2016; Schaefer and Hollibaugh 2017; Laperriere et al. 2019). They are usually attributed to a decoupling of AO from NO, but it is often unclear what causes the decoupling. A wide range of factors, including high pH, high temperature, low oxygen, high organic carbon, phosphate deficiency and various chemicals including chlorate, hydroxylamine, ammonia (NH_3) and volatile fatty acids have been reported to potentially decouple nitrification (reviewed in Philips et al., 2002).

It is unclear which of these factors are most important for the transient nitrite accumulations that are often observed in coastal waters and it is possible that there is no common mechanism for the decoupling of nitrification between different systems given the differing explanations found in literature (Saccà et al. 2008; Heiss and Fulweiler 2016; Schaefer and Hollibaugh 2017). Schaefer and Hollibaugh (2017) linked high summer temperatures to rapid AOA growth, decoupling it from NOB growth. Heiss and Fulweiler (2016) also reported nitrite accumulations in an estuary during summer, with one of several predictive factors being temperature. However, there have also been several reports of nitrite accumulations in winter (Galand et al. 2010; Pitcher et al. 2011), which are likely explained by the increased and relatively sudden availability of ammonium due to resolved stratification or strong reduction of ammonium assimilation by phytoplankton, as discussed in the previous section.

A potentially unifying mechanism for many of these instances might be rapid growth and activity of AOO caused by high temperatures (Schaefer and Hollibaugh 2017) or high substrate availability (Galand et al. 2010; Pitcher et al. 2011), temporarily leading to rates of AO that exceed rates of NO while NOB adjust to the suddenly increased availability of nitrite. Chapter 3 of this thesis illustrates an example of this underlying mechanism in the special case of strong physical mixing causing eventual rapid regrowth of AOO.

These temporary nitrite accumulations in coastal water columns are distinct from the persistent primary nitrite maxima (PNM) which are located at the bottom of the euphotic

zone in the open ocean (Brandhorst 1958; Lomas and Lipschultz 2006). Two mutually non-exclusive hypotheses for PNM creation are still being debated: nitrite excretion by stressed phytoplankton (Vaccaro and Ryther 1960) as well as decoupled nitrification for which again numerous causes are plausible (Olson 1981; Lomas and Lipschultz 2006; Zakem et al. 2018).

1.7. The Influence of Physical Mixing on Biogeochemical Cycling in Water Columns

1.7.1. Biogeochemistry Under Conditions of Weak Physical Mixing

Physical mixing affects aquatic biogeochemistry, including nitrification, in many ways. When it is very low or absent, as in sediments or permanently stratified lakes (Chapter 2) or marine basins, the reduced ventilation can lead to anoxic conditions. This selects for anaerobic respiration of organic matter by use of alternative electron acceptor, which, under ideal conditions, are used in the order of their thermodynamic favourability (Froelich et al. 1979; Nealson et al. 1991; Canfield and Thamdrup 2009).

In the absence of metal or sulfur oxides, the respective steps in the electron acceptor chains would be skipped. This can lead to ferruginous (ferrous-iron rich) lake water columns where sulfate is unavailable (Crowe et al. 2014) or euxinic (sulfide-rich) water columns in which the abundance of sulfate makes sulfate reduction the dominant respiration process (Klepac-Ceraj et al. 2012; Hamilton et al. 2016). Conditions close to the theoretical scenario in which a euxinic zone underlies a ferruginous and a manganous zone can be found in many marine sediments as well as the permanently stratified Black Sea water column, for example (Froelich et al. 1979; Nealson et al. 1991; Canfield and Thamdrup 2009). Below the euxinic zone, a methanogenic zone is usually found in which CO_2, the least favorable electron acceptor is used to produce methane.

The water columns of meromictic (perennially stratified) lakes provide accessible, temporally stable model systems for in-depth studies of biogeochemical cycling along redox gradients and at interfaces. Their bottom waters present extreme endmembers on the physical mixing intensity range encountered in natural water columns.

Large differences in the chemical and physical settings of meromictic lakes cause variations between systems. The occurrence of a 'plate' of anoxygenic phototrophic bacteria is a hallmark of chemoclines that are reached by light (Schultze et al. 2017). Meromictic lake water columns often host an active methane cycle with aerobic, often gammaproteobacterial, methane oxidizers occurring in their chemoclines (Crowe et al. 2011; İnceoğlu et al. 2015a; Oswald et al. 2017). Water column-based methanogenesis has only once been measured (Iversen et al. 1987), but methanogenic archaea, specifically *Methanosarcinales* and *Methanomicrobiales*, are frequently found in meromictic lake water columns (Crowe et al. 2011; Gies et al. 2014). Generally, oxyclines of meromictic lakes provide habitat to microbial oxidizers of reductants such as ammonium, sulfide and methane from the anoxic zone.

Few studies have focused on nitrification in meromictic lakes (Joye et al. 1999; Pouliot et al. 2009), but since the relatively recent discovery of AO by marine *Thaumarchaeota*, *Thaumarchaeota* have also been found in a number of meromictic lakes (Pouliot et al. 2009; Comeau et al. 2012; Gies et al. 2014; İnceoğlu et al. 2015a; Tiodjio et al. 2015). Less is known about NOB, but sequences affiliated with *Nitrospira* have been isolated from some meromictic lakes (Gies et al. 2014; İnceoğlu et al. 2015a). Despite substantial ammonium supply to the oxygenated zone of meromictic lakes, ammonia oxidizers and the relevant marker genes are not always observed there (Lauro et al. 2011; Llorens-Marès et al. 2015). This is consequential, given the role of nitrification in providing oxidized N for N removal by denitrification or anammox. Any downward-diffusing products of nitrification can provide substrate for anaerobic nitrate reducers at the bottom of the oxycline. DNRA, anammox and denitrification have all been observed in the chemoclines of meromictic lakes and sometimes co-occur (Halm et al. 2009; Wenk et al. 2013; Michiels et al. 2017). Ferric iron enhanced nitrogen oxide reduction and sulfide-dependent lithoautotrophic denitrification were found in different meromictic lakes (Wenk et al. 2013; Michiels et al. 2017). Potential for BNF in the chemoclines and anoxic zones of meromictic lakes has also been reported based on genomic (Lauro et al. 2011; Llorens-Marès et al. 2015), isotopic (Ohkouchi et al. 2005) and experimental data (Halm et al. 2009).

Large sulfide accumulations found in many anoxic water columns depend on the activity of sulfate reducing bacteria and the presence of sulfur. Sulfur sources in meromictic lakes can be from past (e.g. Sanderson et al., 1986; Gies et al., 2014) or continuing (e.g. Andrei et al., 2015) supply of seawater or from rock deposits. Sulfide can be removed by precipitation with metals or oxidation in the chemocline (Perry and Pedersen 1993; Wenk et al. 2013). In the absence of suitable electron acceptors, disproportionation of intermediary sulfur species by heterotrophic bacteria may provide a potential source of sulfide and sulfate (Finster 2008).

1.7.2. Physical Mixing Affecting Biogeochemistry Under Oxic Conditions

Dissolved oxygen is available in most of the contemporary ocean and in most lake water, but the influence of physical mixing on biogeochemistry goes beyond its role of ventilation and the supply of oxygen. It also delivers nutrients for primary production to the euphotic zone (MacIsaac et al. 1985; Dutkiewicz et al. 2001; Johnson et al. 2010) or can mix oxygenated and ammonium-rich water masses together to favor nitrification (McCarthy et al. 1984; Schweiger et al. 2007; Galand et al. 2010). Until recently, it was generally considered that the shoaling of the mixed layer due to water column stratification initiates spring phytoplankton blooms (Sverdrup 1953). However, evidence has emerged suggesting that the initiation of phytoplankton blooms, e.g. in the North Atlantic, reflects instead the mixing-induced dilution of phytoplankton and the consequential decrease in grazer-phytoplankton encounters (Behrenfeld 2010).

Chapter 3 of this thesis presents a mechanism whereby physical dilution of nitrifier communities by mixing results in delayed and decoupled nitrification. A role for mixing in controlling the population of nitrifiers (as opposed to substrate) has only rarely been recognized previously as a potential control of nitrification rates, and thereby on biogeochemical cycling. Wollast (1978) noted dilution of nitrifying bacteria along the salinity gradient of the Scheldt Estuary and an effect of this dilution on nitrification rates, inferring that salinity-adapted nitrifiers regrew slower than freshwater-borne nitrifiers were diluted. In a very recent study, Zakem et al. (2018) inferred, primarily from modeling, that

advective transport of NOB away from their depth of optimal growth at the base of the euphotic zone may contribute to the primary nitrite maximum in the open ocean.

1.8. Nitrogen Stable Isotope Biogeochemistry

The N stable isotope composition of various N species has long been recognized as an effective tool for studying the N cycle in complex environmental systems, especially because many N-transformations are enzymatic processes involving significant isotope fractionation (Bigeleisen 1965; Delwiche and Steyn 1970; Mariotti et al. 1981; Wankel et al. 2007; Sigman et al. 2009; Santoro et al. 2011; Casciotti et al. 2013; Fuchsman et al. 2018). Kinetic isotope effects describe the preferential reaction of molecules in a chemical reaction based on the isotopic composition of its atoms. Lighter isotopes typically react faster than the heavier ones, because the higher potential energy in bonds formed by lighter isotopes (compared to heavy isotopes of a given element) causes a higher likelihood of breaking the bond by equal energy input (Fry 2006). For similar reasons, heavy isotopes concentrate on the side of an equilibrium reaction that has the stronger bonds, which forms the basis for the equilibrium isotope effect (Fry 2006).

Kinetic fractionation is characteristic of many enzymatic reactions, including microbially mediated N-transformations. The isotopic composition of a given N species can thus contain useful information about the processes responsible for producing or removing it.

Using N stable isotopes as an example, the δ-notation in units per mil (‰) is used to describe the isotopic composition of molecules in a sample in comparison to the composition in a standard or reference (Mariotti et al. 1981):

$$\delta^{15}\mathrm{N}_{\mathrm{sample}}[‰] = \frac{(15\mathrm{N}/14\mathrm{N})_{\mathrm{sample}}}{(15\mathrm{N}/14\mathrm{N})_{\mathrm{reference}}} - 1) \text{ x } 1000 \qquad 1.1$$

The N_2 of tropospheric air is commonly used as the reference for nitrogen ($\delta^{15}N$), while VSMOW (Vienna Standard Mean Ocean Water) is used for oxygen isotopes ($\delta^{18}O$).

α denotes the isotope fractionation factor and can be interpreted as a rate constant that defines by how much faster a reaction occurs for the light compared to the heavy isotope (Mariotti et al. 1981; Glibert et al. 2019):

$$^{15}\alpha = \frac{(15N/14N)_{substrate}}{(15N/14N)_{product}} \quad 1.2$$

Kinetic or equilibrium isotope effects cause α to deviate from 1. The fractionation factor can be translated into units of per mil, using the following equation that yields the isotopic enrichment factor, ε:

$$^{15}\varepsilon\ [‰] = (^{15}\alpha - 1) \times 1000 \quad 1.3$$

At steady state and if $\delta^{15}N_{substrate}$ is sufficiently small, $^{15}\varepsilon$ can be approximated as follows (Mariotti et al. 1981):

$$^{15}\varepsilon \approx \delta^{15}N_{substrate} - \delta^{15}N_{product} \quad 1.4$$

Within the N cycle, processes of nitrification, denitrification and anammox have relatively strong kinetic isotope effects (Fig. 1.1). Processes with weaker effects include ammonification ($^{15}\varepsilon$ = +1.4 to +2.3‰; Möbius, 2013) and N_2-fixation ($^{15}\varepsilon$ = 2 to +8‰; Delwiche and Steyn 1970; Macko and Fogel 1987; Zhang et al. 2014).

Isotope effects between 13 and 41‰ have been associated with bacterial and archaeal AO in laboratory studies (Delwiche and Steyn 1970; Mariotti et al. 1981; Yoshida 1988; Casciotti et al. 2003; Santoro and Casciotti 2011; Nishizawa et al. 2016). Interpretations of field measurements tend to suggest values within or slightly below this range for nitrification or ammonium utilization (Horrigan et al. 1990a; Brandes and Devol 1997; Sebilo et al. 2006; Southwell et al. 2008; Sugimoto et al. 2008, 2009), but field-based estimates usually suffer from uncertainties caused by the unconstrained influence of other processes and low measurements density. Chapter 4 provides field-based estimates of AO isotope effects that avoid these constraints and are better comparable to laboratory studies.

NO has an inverse isotopic effect ($^{15}\varepsilon$ = -9 to -21‰), i.e. its substrate becomes depleted in ^{15}N during the process. This effect, however, may only be expressed in places where nitrite accumulates, such as mOMZs or in the sub-euphotic zone oceanic primary nitrite maxima (Casciotti 2009; Casciotti et al. 2010b).

Consistent with the inverse NO isotope effect, the isotope enrichment factor of nitrite oxidation during anammox is also negative ($^{15}\varepsilon$ = -31.1 ± 3.9 ‰), while nitrite reduction

($^{15}\varepsilon$ = +16.0 ± 4.5‰) and ammonia oxidation ($^{15}\varepsilon$ = +23.5 to +29.1‰) during anammox are positive (Brunner et al. 2013). The individual steps of denitrification have similarly large N isotope effects (Fig. 1.1; Delwiche and Steyn 1970; Bryan et al. 1983; Barford et al. 1999; Ostrom et al. 2007; Granger et al. 2008). The isotope effects associated with DNRA are still unknown, representing a major knowledge gap that needs to be closed in order to improve our ability to distinguish this important process in the environment, from the fixed-N eliminating processes of NO_x^- reduction.

For assimilative processes, a wide range of N isotope enrichment factors has been reported. The available data suggest that the they can be higher for ammonium assimilation than for nitrate, and a single experiment has suggested that a very small isotope effect is associated with nitrite assimilation (Fig. 1.1; Hoch et al. 1992; Waser et al. 1998; Granger et al. 2004). However, large variations have been reported between and within microbial species for the isotope effect of nitrate assimilation (Granger et al. 2004).

Known equilibrium isotope effects in the N cycle are rare. One example is the equilibrium isotope effect between NH_3 and NH_4^+ ($^{15}\varepsilon_{NH3\leftrightarrow NH4}$ = -20 to -35‰; Bigeleisen 1949), which can affect the apparent isotope effect associated with AO (Casciotti et al. 2010a). Additionally, anammox bacteria appear to mediate an N equilibrium isotope effect between nitrite and nitrate ($^{15}\varepsilon_{NO2\leftrightarrow NO3}$ = -60.5 ± 1.0‰) during times of environmental stress, e.g. oxygen exposure (Brunner et al., 2013). This may be caused by the nitrite oxidoreductase enzyme used in anammox, nitrification and nitrate reduction. Indications for the environmental relevance of this was found in the surface Antarctic Ocean (Kemeny et al. 2016).

1.9. Biogeochemical Methods at the Intersection of Geochemistry and Environmental Microbiology

The importance of understanding geochemical distributions also on the basis of microbiological methodology has long been recognized and forms the basis of the fields of biogeochemistry and geomicrobiology. Geochemical measurements of concentrations and isotope signatures allow the quantification of processes and their effects on the environment, e.g. greenhouse gases on the climate system. Their combination with

microbiological methods can provide more profound and detailed insights, by understanding the ecological and molecular biological mechanisms underlying biotic processes.

Phylogenetic marker genes are routinely used to study microbial communities. The 18S rRNA and 16S rRNA genes are typically used to characterize the taxonomy of eukaryotic or prokaryotic microbes, respectively. Within the 16S rRNA gene, different gene regions have been used, including the V6-V8 and the V4-V5 regions. Different regions have different biases and can under- or overrepresent certain prokaryotic groups within a community (Willis et al. 2019). Despite this, 16S rRNA gene sequencing based community composition can be used for estimates of relative and absolute (after standardization to cell counts) abundance of microbial taxa (Comeau et al. 2012; Klepac-Ceraj et al. 2012; Oswald et al. 2017; Zorz et al. 2019) and is employed for these purposes in Chapters 2 and 3.

Functional marker genes provide a link between taxonomic identification of microbes and their effect on the geochemical level. They can be quantified by qPCR using primers specific to the genes of interest (as applied in Chapter 3) or their relative abundance can be estimated within metagenomes (Chapter 2), which represent approximately the entire genetic material within a given sample (Lauro et al. 2011; Llorens-Marès et al. 2015; Hamilton et al. 2016). Abundance and presence of specific functional marker genes or their transcripts can provide information on the functional potential for the respective biogeochemical process. Using phylogenetic analysis of the sequenced functional gene the function can then be linked to the underlying taxonomic group (e.g. Halm et al. 2009; Daims et al. 2015). If the functional genes are derived from metagenomes, metagenomic binning techniques can serve the same purpose and additionally provide information on the metabolic context of the marker gene and its host organism (Eren et al. 2015; Delmont et al. 2018). Near-complete metagenomic bins or metagenome-annotated genomes (MAGs) can reflect the metabolism even of uncultured microorganisms, which are otherwise difficult to describe (Kang et al. 2017; Kadnikov et al. 2019; Sun et al. 2019).

1.10. Modeling the N Cycle and Nitrification

Numerical models allow the testing of intuition, result interpretations and hypotheses that cannot be easily performed in the real world due to lack of accessibility to sampling in frequency, location or time and inability to conduct experimental manipulations or replicated experiments. Furthermore, they allow the projection of effects caused by environmental change into the future. Models of the aquatic N cycle are often integrated with models of physical circulation or have a mixing component (Fennel et al. 2011). However, this can be unnecessary in systems such as mOMZs or sediments, in which relatively low advection and steady state conditions can be assumed (Lam et al. 2011; Buchwald et al. 2018). Depending on the purpose, N cycling models can be parts of larger ecosystem models investigating higher trophic levels (Fasham et al. 1990; Yoshikawa et al. 2005; Fennel et al. 2011) or include the representation of isotope fractionation associated with N transformations (Wankel et al. 2007; Buchwald et al. 2015, 2018).

The representation of processes in published models ranges from simplistic to complex. Decisions on complexity of model design can be driven by the desired level of analysis as well as the availability of data necessary to assess model performance and adjust parameter values. Nitrification, for example, is modeled as a simple first-order function of ammonium concentration and light (inverse) by some studies (Fennel et al. 2006, 2011). Other studies distinguish the two steps of nitrification, model them dependent on functional biomass and employ complex emergent-trait approaches that select for functional groups with traits adaptive to a given situation (Bouskill et al. 2012) or parameterize AO and NO rates as functions substrate affinity among others (Zakem et al. 2018). In a similar vein, the utilization of functional genes to constrain biogeochemical dynamics in models is a promising development, linking biogeochemical modeling and molecular ecological methods, particularly metagenomics and quantitative PCRs (Reed et al. 2014). Chapter 3 provides an example of how the modeling of functional nitrifier biomass proxied by functional marker gene abundance helped to identify an important underlying biogeochemical mechanism.

The addition of stable isotope effects to biogeochemical models usually involves the modeling of a given N-containing species as a separate light-isotope and heavy-isotope

version (Buchwald et al. 2015, 2018). Such models can be parameterized with previously determined isotope fractionation factors and fit to empirical data to explain environmental distributions of concentrations and isotope signatures (Buchwald et al. 2015, 2018). They can also be used to explore possible scenarios with varying isotope fractionation factors and contributions of different processes that can explain observed environmental distributions (Wankel et al. 2007).

1.11. Objectives

The objective of this thesis was to explore the link between microbial communities, their metabolic potential and the effects these have on geochemical distributions of concentrations and stable isotope signatures in the context of different stratification regimes. Water columns of two aquatic systems with highly contrasting stratification/mixing regimes were investigated with a focus on the N cycle: The Bedford Basin (BB), Nova Scotia, Canada, is a seasonally stratified coastal ford-like basin whose water column is completely mixed at least once per year; Powell Lake, British Columbia, Canada, is a coastal lake that has been stably stratified for millennia due to its history as a former fjord that was disconnected from the ocean due to isostatic uplift associated with the end of the last glacial period. Ancient seawater from ca. 8000 years ago with heavily modified chemistry can still be detected in the bottom 50 meters as a result of the stable stratification.

Changes in microbial communities and their metabolic potential pertaining to N-, C- and S- cycles along a vertical profile through the permanently stratified water column of Powell Lake were linked to the vertical geochemical profile (Chapter 2). This enabled the analysis of metabolic and phylogenetic microbial diversity and test their alignment with the geochemical zonation along a redox gradient. In Bedford Basin, a weekly, 4-year long time series of genetic and biogeochemical parameters was constructed and analyzed in order to study the influence of environmental parameters on nitrification, its underlying microbiology (Chapter 3) and associated isotope effects (Chapter 4) *in situ*. The high (weekly) resolution of the time series allowed exceptionally detailed analysis in a “natural laboratory” under *in situ* conditions. These objectives were enabled by the large set of parallel oceanographic measurements in the framework of the Bedford Basin Time Series

as well as the natural setup of the Bedford Basin bottom water, where periods of water column stability (stratification) and pronounced nitrification are interrupted by periods of full water column mixing resetting the system akin to a natural experiment.

CHAPTER 2

GEOMICROBIOLOGY OF THE CARBON, NITROGEN AND SULFUR CYCLES IN POWELL LAKE: A PERMANENTLY STRATIFIED WATER COLUMN CONTAINING ANCIENT SEAWATER[1]

2.1. Abstract

We present the first geomicrobiological characterization of the meromictic water column of Powell Lake (British Columbia, Canada), a former fjord which has been stably stratified since the last glacial period. Its deepest layers (300-350 m) retain isolated, relict seawater from that period. Fine-scale vertical profiling of the water chemistry and microbial communities allowed subdivision of the water column into distinct geomicrobiological zones. These zones were further characterized by phylogenetic and functional marker genes from amplicon and shotgun metagenome sequencing. Binning of metagenomic reads allowed the linkage of function to specific taxonomic groups. Statistical analyses (analysis of similarities, Bray-Curtis similarity) confirmed that the microbial community structure

---

[1] Haas, Sebastian, Dhwani K. Desai, Julie LaRoche, Rich Pawlowicz, and Douglas W. R. Wallace. 2019. Geomicrobiology of the carbon, nitrogen and sulphur cycles in Powell Lake: a permanently stratified water column containing ancient seawater. Environ Microbiol **21**: 3927–3952. doi:10.1111/1462-2920.14743

Author contribution: *I planned, organized and conducted the field sampling and sensor measurements with the assistance of technicians, collaborators, administrators, etc. For laboratory work, I did DNA extractions and sulfate concentration measurements, but had help from technicians for the remaining concentration measurements. I processed and analyzed 16S and 18S rRNA amplicon sequences, and I analyzed the output from ANOSIM and SIMPER analyses as well as metagenome assembly and metagenomic binning processes, which were performed by a co-author. With advice from my co-authors, I designed the study, analyzed and interpreted the data and wrote the chapter.*

followed closely the geochemical zonation. Yet, our characterization of the genetic potential relevant to carbon, nitrogen and sulfur cycling of each zone revealed unexpected features, including potential for facultative anaerobic methylotrophy, nitrogen fixation despite high ammonium concentrations and potential micro-aerobic nitrifiers within the chemocline. At the oxic-suboxic interface, facultative anaerobic potential was found in the widespread freshwater lineage acI (*Actinobacteria*), suggesting intriguing ecophysiological similarities to the marine SAR11. Evolutionary divergent lineages among diverse phyla were identified in the ancient seawater zone and may indicate novel adaptations to this unusual environment.

2.2.Introduction

Research on the interaction between geochemistry and microbiology in redox-stratified systems is vital for our understanding of environments such as aquatic sediments, meromictic lakes and marine oxygen minimum zones (mOMZs). Studies of such systems also have implications for redox-stratified ancient oceans (Thomazo and Papineau 2013) and guide approaches to detection of life on other planets (Nealson and Berelson 2003). Perennially stratified (meromictic) lakes provide especially accessible, temporally stable model systems for the in-depth study of biogeochemical cycling along redox gradients and physico-chemical interfaces of stratified systems.

Detailed insights into the occurrence and interaction of biogeochemical processes in meromictic water columns are possible because gradients tend to be less steep than in sediments, so that redox transitions can be more readily resolved. In very stable meromictic lakes, the sustained period of separation of deeper waters from the atmosphere can lead to large accumulations of reduced compounds (Northcote and Hall 1983; Perry and Pedersen 1993; Crowe et al. 2011). In turn, long seclusion and generation of extreme chemical conditions may lead to significant divergence in the evolution of microbial species (Li et al. 2015c), so that the study of diverse environments of this type may lead to discovery of previously unexplored microbially mediated processes.

As in other stratified systems, the biogeochemistry of meromictic lakes is generally governed by the successive use of electron acceptors of decreasing thermodynamic

favourability by microbial respiration processes and abiotic reactions (Froelich et al. 1979; Nealson et al. 1991; Crowe et al. 2008b; Schultze et al. 2017). Geochemical zones can be identified based on this sequential depletion of electron acceptors along the vertical redox gradient of stratified systems (Canfield and Thamdrup 2009). Microbial community structure has long been known to vary along these geochemical gradients, reflecting their strong influence on geochemistry and, in turn, the selective pressure that geochemical distributions exert on the microbial community.

A universal microbiome for meromictic lakes likely does not exist, given the geographical, geochemical and physical diversity between different meromictic lakes, but some commonly occurring taxonomic groups can be identified. These include *Cyanobacteria*, *Alphaproteobacteria*, *Actinobacteria* and *Verrucomicrobia* (mostly in the oxic surface and oxycline), *Chlorobi*, *Beta-* and *Gammaproteobacteria* (mostly in the chemocline), *Bacteroidetes* (throughout) as well as *Deltaproteobacteria*, candidate phyla (particularly *Omnitrophica*, *Atribacteria*, *Microgenomates*) and *Chloroflexi* in the anoxic monimolimnion (Lehours et al. 2007; Lauro et al. 2011; Comeau et al. 2012; Klepac-Ceraj et al. 2012; Gies et al. 2014; İnceoğlu et al. 2015a; Llorens-Marès et al. 2015; Baatar et al. 2016). Anoxygenic photoautotrophy by green (*Chlorobi*) or purple (*Chromatiales*) sulfur bacteria and also chemolithoautotrophy are typical processes in meromictic water columns (Cloern et al. 1983; Overmann and Tilzer 1989; Overmann et al. 1992; Casamayor et al. 2012; Zadereev et al. 2017). *Thaumarchaeota* and *Betaproteobacteria* (ammonium oxidation), *Nitrospirae* (nitrite oxidation), *Gammaproteobacteria* (methanotrophy), *Betaproteobacteria*, *Chromatiales* and *Chlorobi* (sulfide oxidation) have been linked to the processes that oxidize the inorganic reductants that diffuse upwards into the chemoclines and oxyclines of meromictic lakes (Pouliot et al. 2009; Crowe et al. 2011; İnceoğlu et al. 2015a; Llorens-Marès et al. 2015; Baatar et al. 2016; Oswald et al. 2017).

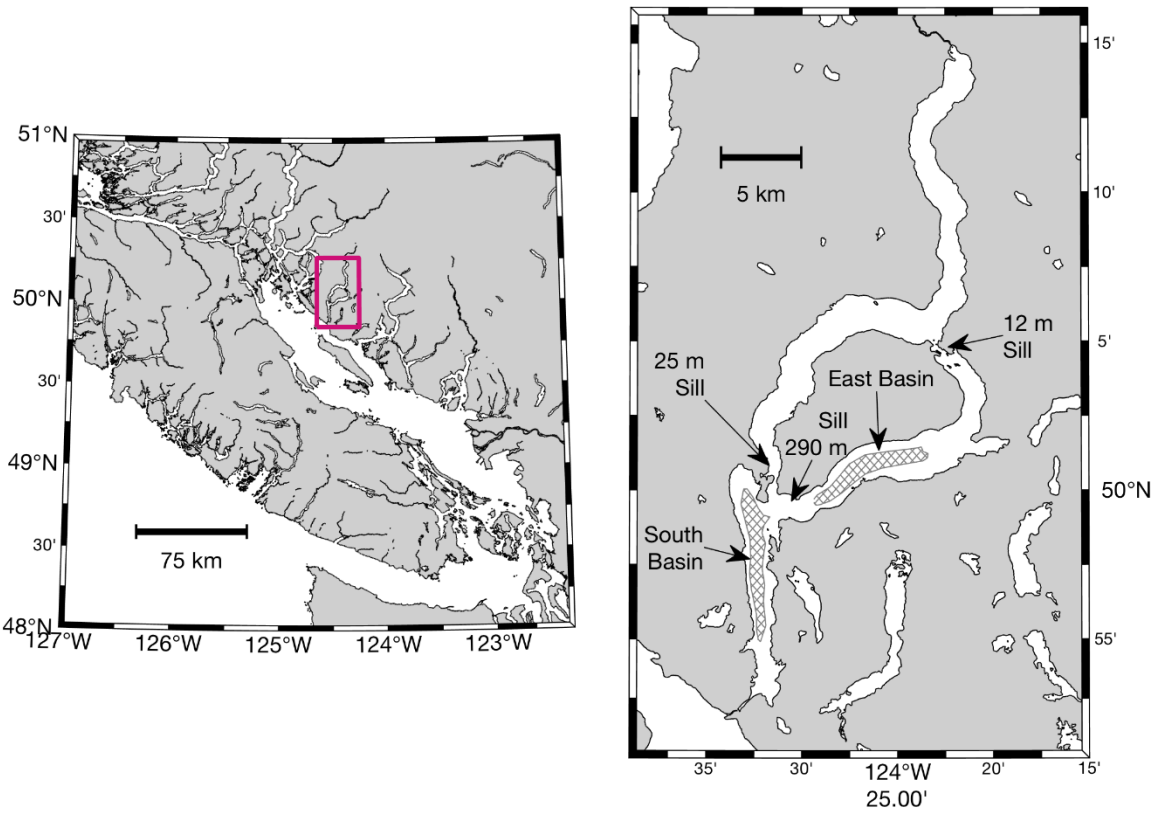

Figure 2.1. Maps of Powell Lake. Location of the South and East basins as well as depths of surrounding sills are indicated. Grey checked areas highlight flat basin bottoms containing ancient seawater and the red cross indicates sampling location.

This study describes the microbial community and geomicrobiology of meromictic Powell Lake in British Columbia, Canada (Figure 2.1). The lake contains an 'ectogenic' meromictic water column (Hutchinson 1957) with permanent stratification caused by freshwater overlaying saltwater. The former fjord was disconnected from the Pacific Ocean by isostatic uplift after the last glacial period. Altered seawater from this period remains trapped at the bottom of its southern basin and has been separated from the atmosphere for about 11,000 years (Williams et al. 1961; Sanderson et al. 1986). Given that the oceanic conveyor belt circulation overturns the deep waters of the world ocean on time scales <2000 years (Gebbie and Huybers 2012; Khatiwala et al. 2012), Powell Lake's deepest layers may contain some of the "oldest" seawater on the planet (in the sense of contact with atmosphere or ventilation). Although other lakes, such as Lake Matano and Fayetteville Green Lake, are known to have had a stable stratification for similar or even longer times

(Torgersen et al. 1981; Katsev et al. 2010), these other lakes experience continuous deep water renewal by groundwater inflow, substantially shortening their deep water residence time despite the stable stratification. The Black Sea, which is the Earth's largest contemporary meromictic water column, may be most similar to Powell Lake with respect to long-term stratification. It was established as a marine basin by connection to the Mediterranean Sea at approximately the same time as Powell Lake was disconnected from the ocean (Yanko-Hombach et al. 2014), but the "age" of Black Sea deep waters is estimated to be <1000 years (Fontugne et al. 2009; Soulet et al. 2019).

Eddy diffusivity in Powell Lake's water column decays rapidly with depth (Sanderson et al. 1986), so that molecular diffusion and double-diffusion govern vertical transfer below 320 meters (Scheifele et al. 2014), resulting in long-term meromixis (Sanderson et al. 1986). The long isolation time and the role of molecular diffusion has led to major geochemical changes to the original seawater (Sanderson et al. 1986). Documentation of the contemporary geochemical regime is mostly restricted to metal-sulfur cycling, including the formation of iron sulfides in the anoxic zone (particularly 250-280 m) and the accumulation of dissolved sulfide in the ancient seawater (Perry and Pedersen 1993). The sulfate once contained in the original seawater has been transformed and/or removed so that presently sulfate is found only in small amounts in the oxic zone and around the chemocline (Perry and Pedersen 1993). Because it contains deep water that has remained anoxic and unrenewed by advective mixing events or groundwater inflows for several millennia (Sanderson et al. 1986), Powell Lake's deeper water column is likely to have attained a geochemical steady state, making it an important model system for studying the interaction of geochemistry and microbiology (i.e. geomicrobiology) without the need to consider the possible influence of sporadic advective processes such as dense intrusions of oxygenated water. Despite this unusual potential, there have been no prior geomicrobiological studies of Powell Lake.

Here, we expand the scope of previous studies of Powell Lake's physics and geochemistry (Sanderson et al. 1986; Perry and Pedersen 1993). We define geomicrobiological zones based on the classical sequence of electron acceptors with decreasing thermodynamic favourability (Froelich et al. 1979; Canfield and Thamdrup

2009) and characterize the microbial community structure and functional genetic potential within each of these zones. This study of Powell Lake's meromictic basin presents detailed vertical profiles of geochemical parameters and microbial community composition based on amplicon sequencing of the V4-V5 variable region of the 16S rRNA gene. The metabolic potential of the microbial communities in each geomicrobiological zone is assessed from the distribution of functional gene markers in the processed reads of ten metagenomes from selected depths. Metagenomic bins derived from the co-assembly of these metagenomes from selected depths along a vertical profile were used to link the functional marker genes to taxonomic groups. We focused on the carbon, nitrogen and sulfur cycles and identified unexpected geomicrobiological features, including nitrogen fixation under ammonium excess, potential micro-aerobic nitrifiers and genetic potential for deep anoxygenic photosynthesis.

2.3.Results

2.3.1. Physical Setting and Geochemical Zonation in Powell Lake's South Basin

At the time of sampling, a shallow, warm summer epilimnion (~10 m) was separated from a cold hypolimnion (25-130 m) by a thermocline (Table 2.1). Below the hypolimnion, a 20-meter thick layer with both O_2 and H_2S below detection limit, and which was hence either suboxic (no O_2, no H_2S) or micro-oxic (small, undetectable amounts of O_2), extended to 150 meters, where dissolved hydrogen sulfide was first detected (Figure 2.2B). These depths are consistent with previous measurements, including measurements taken during different seasons (Perry, 1990; Perry and Pedersen, 1993; Scheifele et al., 2014), suggesting that the positions of these interfaces are stable over time. Below the suboxic-sulfidic interface, concentrations of dissolved iron (reflecting Fe^{2+}) and manganese (Mn^{2+}+MnS_2+$MnCO_3$+MnCl; Perry, 1990; Davison, 1993; Perry and Pedersen, 1993; Albrechtsen and Christensen, 1994) showed maxima at 200 and 230 meters, respectively. Salinities in the oxic part of the water column did not exceed 0.1 g kg^{-1} but increased quasi-exponentially below. The halocline (290-310 m) separated an upper, comparatively low-

salinity (0.2-6.4 g kg^{-1}) sulfidic layer from the relict seawater of the deepest waters, which had distinctly higher salinity (15.0-16.7 g kg^{-1}), sulfide and nutrient concentrations compared to the overlying water column. Phosphate was depleted in the oxic part of the water column and very low compared to ammonium below the chemocline, resulting in a very large excess of dissolved inorganic nitrogen compared to phosphate (Figure 2.2C, D).

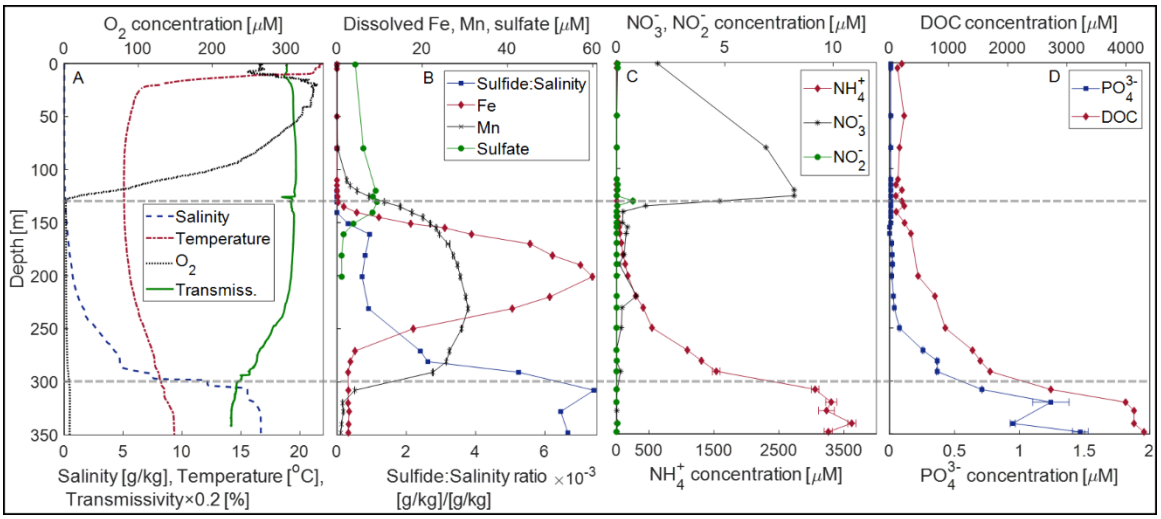

Figure 2.2. Vertical profiles of physical parameters and chemical concentrations in the center of Powell Lake's southern basin in August 2016. (A) Salinity, temperature, oxygen, transmissivity. (B) Dissolved iron (n=3), manganese (n=3) and sulfate, sulfide:salinity ratio. (C) Dissolved inorganic nitrogen: ammonium (n=2), nitrate, nitrite (n=2). (D) Phosphate (n=3), dissolved organic carbon (DOC). Error bars indicate standard deviations of technical replicates where applicable. The dashed lines indicate the depth of the oxic-suboxic interface (130 m) and the steepest part of the halocline (300 m).

Following Canfield and Thamdrup (2009), we divided Powell Lake's water column into vertical zones, using defining geochemical components (Figure 2.2) that reflect the predominant redox process in each zone (Table 2.1). The 'oxic zone' spanned the oxygenated part of the water column, but for practical purposes, we focused on the 'oxycline' portion of this zone and refer to it accordingly. The depth at which oxygen approached the detection limit coincided with the sharp nitrite peak at 130 m, which was the defining feature for the thin 'nitrogenous zone'. Below that, we defined 'manganous', 'ferruginous' and 'euxinic' zones based on the quantitatively prevailing product of the biogeochemical (biotic and abiotic) reduction processes for manganese, iron and sulfur. As an exceptional feature not found in most other stratified systems, we further defined a near-

bottom ‘ancient seawater (ASW) zone’ which was separated from the water column above by the steep halocline. Significant overlap between these zones was observed in several cases (summarized in Table 2.1), most prominently in the case of the manganous zone with dissolved manganese extending throughout the ferruginous zone to a peak in the euxinic zone. These overlaps are considered in the analysis of the distribution of taxonomic and functional markers and are further discussed below.

Although our sampling readily resolved these broad zones, the continuous transmissivity profile indicated additional, light-absorbing features near and at the bottom of the hypolimnion, which were on very small vertical scales (<5 m). While these changes were not generally resolved with water sampling at discrete depths, the two main spikes in transmissivity were represented by water samples collected from 125 and 130 m (Figure 2.2A, Table 2.1).

Table 2.1. Limnological and geomicrobiological zones in the Powell Lake water column in August 2016 with 16S rRNA sampling depths and the three indicator OTUs (rank-ordered) contributing most to the similarity of the microbial community composition between samples within a given zone (based on SIMPER analysis). For the single-sample nitrogenous zone, the three most abundant OTUs are reported instead (rank-ordered). OTUs are specified by their most detailed available taxonomic classification (with further specifications for candidate lineages) and NCBI accession number if applicable. Cases of overlapping zones are pointed out by arrows indicating whether the zone-unspecific compound intrudes from above or below.

Limnological zone	Biogeochemical zones	Overlapping zones	Physico-Chemical Characteristics	Depth range [m]	16S rRNA sampling depths [m]	Indicator OTUs
Epilimnion	Surface	-	Well-mixed, oxic	1-10	1 (duplicate)	*Chitinophagaceae* (HM129183.1) *Synechococcus* (FJ382618.1) *Roseococcus* (New.ReferenceOTU8)
Metalimnion		-	Thermocline	10-25	-	-
Hypolimnion	Oxycline	Manganous ↑	Oxic to hypoxic; Nitrate peak	25-125	80, 110, 120, 125	acI, *Actinobacteria* (FN668226.2) *Nitrospiraceae, Nitrospira* (AM167945.1) *Rhodospirillales* (GQ396920.1)
Chemocline	Nitrogenous Zone	Manganous ↑ Oxic ↓	~3.5 µM O2 (hypoxic → suboxic); Nitrite peak	130	130	acI, *Actinobacteria* (FN668226.2) *Crenothrix* (FJ502272.1) *Comamonadaceae* (GU208444.1)
Chemocline	Manganous Zone	Ferruginous ↑	Undetectable O_2 (suboxic → sulfidic); diss-Mn > diss-Fe > H_2S	135-150	135, 140, 145, 150	acI, *Actinobacteria* (FN668226.2) *Sterolibacterium* (NR_025450.1) *Bacteroidales* (AM162484.1)
Monimolimnion	Ferruginous Zone	Manganous ↓ Euxinic ↑	Sulfidic; anoxic; diss-Fe > H_2S	160-200	160, 180, 200	*Desulfobacca* (AB426203.1) *Syntrophaceae* (HQ003553.1) C20, *Chlorobi* (HM243831.1)
Monimolimnion	Euxinic Zone	Manganous ↓ Ferruginous ↓	Sulfidic, anoxic; diss-Fe < diss-Mn < H_2S	230-290	230, 250, 280, 290	SB-45, *Atribacteria* (JQ087016.1) SHA-114, AC1 (AB186797.1) *Syntrophaceae* (HQ003553.1)
Monimolimnion	Ancient Seawater Zone	Euxinic ↓	Sulfidic; anoxic; Salinity ≈ 10-16 PSU	310-350	310, 320, 330, 350	*Omnitrophica* (New.ReferenceOTU12) SB-45, *Atribacteria* (JQ087016.1) B10, *Crenarchaeota* (FN428815.1)

2.3.2. Water Column Zonation Based on Microbial Community Composition

We hypothesized that the geochemically defined zones (Table 2.1) were mirrored by specific zonation in the microbial community structure as determined by 16S rRNA gene sequencing. Based on Bray-Curtis similarity, the microbial communities in Powell Lake's water column changed markedly along the vertical profile and each of the geochemical zones contained a specific microbial community as defined by ≥60% 16S rRNA gene sequence similarity between the samples of a given zone (Figure 2.3A). A clear gradient along the vertical profile can also be observed at the phylum level (Figure 2.3B). The seven zones predicted on the basis of geochemical features were reflected by zones of microbial community dissimilarity as indicated by an analysis of similarities (ANOSIM) test applied to the operational taxonomic unit (OTU) relative abundances in groups of samples for each zone (Global R value: 0.97, significance 0.1%). In pairwise ANOSIM comparisons, zones with a sample number of $n > 2$ were significantly distinct from all other zones at the 5% significance cutoff, when ≥35 permutations were possible (Appendix A). Statistically significant differences to other zones could not be established for the surface and nitrogenous zones because of their low sample sizes ($n \leq 2$), which allowed for fewer permutations. The ferruginous and euxinic zones were also not statistically distinct from each other (significance 10%), which may be explained by the relatively small number of possible permutations in ANOSIM or may reflect the presence of dissolved sulfide as a common characteristic, leading to increased overlap of OTUs between these two zones. These analyses excluded the eukaryotic fraction of the microbial community, since a steep decrease in the number of 18S rRNA amplicon reads and simultaneous decrease in diversity (not encountered for 16S rRNA) suggested that its influence on the overall community structure was likely negligible below the nitrogenous zone (Figure A1A, B, D, E). The nitrogenous zone and the zones above it were reflected by the eukaryotic community structure (Figure A1F).

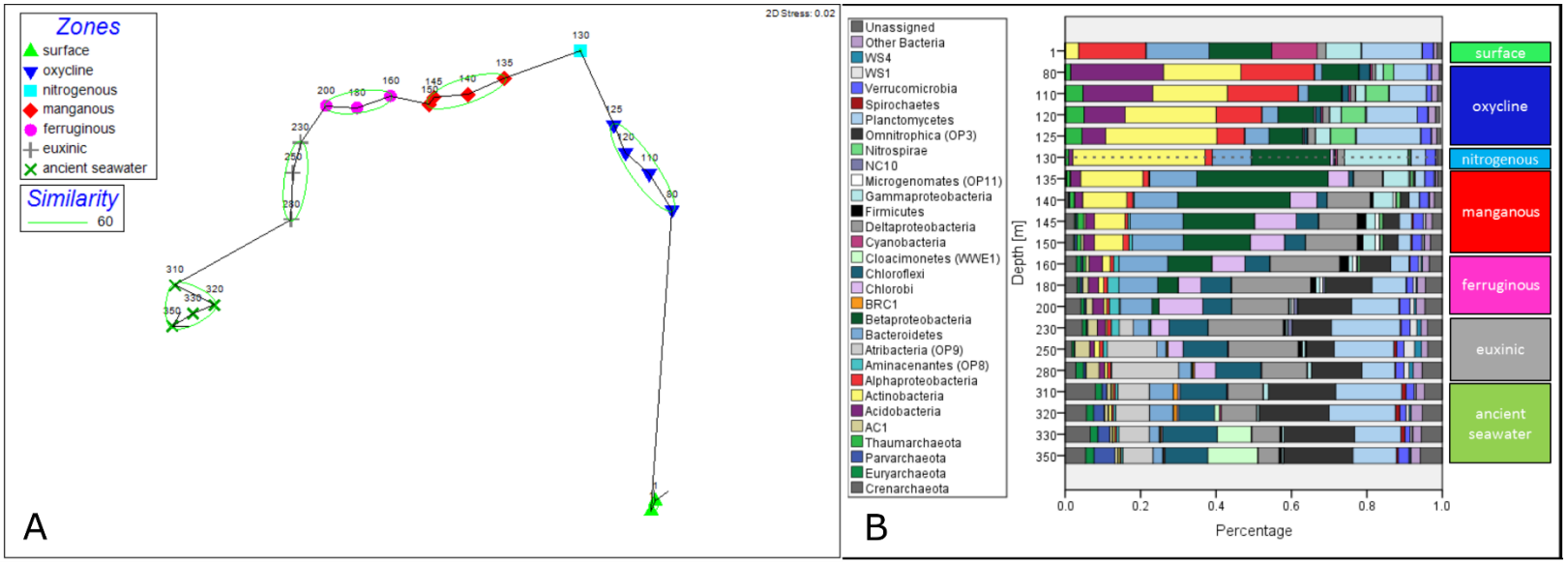

34

Figure 2.3. Microbial diversity in Powell Lake based on 16S rRNA V4-V5 amplicon sequencing. (A) Non-parametric multidimensional scaling (NMDS) plot of microbial community composition based on Bray-Curtis similarity, showing the clustering of microbial communities from different depths referenced to predicted geomicrobiological zones (Table 2.1). Geomicrobiological zones are indicated by different symbols and colors. Numbers in the plot indicate sample depths [m] and samples from neighboring depths are connected by a line. The 60%-threshold of between-sample similarity is indicated. (B) Phylogenetic composition of the bacterial and archaeal community at phylum level (including proteobacterial subphyla) by depth. The 1-meter bar represents the average of a duplicate sample. The geomicrobiological zones are indicated on the side and a dashed line indicates the oxic-suboxic interface at 130 m.

2.3.3. Description of Phylogenetic and Functional Potential Defining Geomicrobiological Zones

The following sections present detailed descriptions of the geomicrobiology of each zone. Within each zone, geochemical features (Figure 2.2) are related to abundant phyla and indicator OTUs that are based on OTU relative abundances derived from the analysis of the amplicon sequence reads of the small subunit rRNA V4-V5 variable region (Figure 2.3B, Table 2.1). Additionally, between the oxycline and the ASW zones, the genetic potential for biogeochemical processes in the carbon, nitrogen and sulfur cycles was assessed based on the relative abundances of functional marker genes in the bulk metagenomes collected at different depths (Figure 2.4). Based on their occurrence in taxonomically defined metagenomic bins (including Metagenome Annotated Genomes or MAGs), these functional marker genes were assigned to taxonomic groups (Table 2.2). Congruence between the 16S rRNA gene sequence and the metagenomic subsets of the data was suggested by high linear correlation in the vertical distribution for most microbial phyla based on 16S rRNA gene sequencing versus the vertical distribution of phyla as affiliated with metagenomic bins (Figure A2; Appendix A). In the following, OTUs strictly refer to 16S rRNA gene amplicon sequencing data, while metagenomic bins (including MAGs) describe binned shotgun sequences.

Table 2.2. Functional marker genes found in taxonomically classified metagenomic bins. Taxonomic affiliation of metagenomic bins (based on CheckM) links potential for biogeochemical processes to taxonomic groups. Reference numbers link to processes in Figure 2.5.

Biogeochemical process	Based on content of the marker genes	Taxonomic groups affiliated with biogeochemical processes	Ref.
Carbon cycle			
Aerobic respiration	*coxAC*	Bin49_*Methylophilaceae,* Bin50_*Nitrosomonadaceaa,* Bin51_MAG29_*Sediminibacterium,* Bin54_MAG7_MAG30_MAG33_*Actinobacteria,* Bin58_*Methylophilales,* Bin60_*Actinomycetales,* Bin62_*Methylotenera,* Bin66_*Verrucomicrobiales,* MAG1_*Methylococcaceae,* MAG2_*Porphyromonadaceae,* MAG3_*Verrucomicrobiaceae,* MAG4_*Opitutales,* MAG6_*Ignavibacteriales,* MAG10_*Nitrosopumilales,* MAG12_*Betaproteobacteria,* MAG14_*Bacteria,* MAG15_*Methylococcus,* MAG16_*Planctomycetaceae,* MAG18_*Deltaproteobacteria,* MAG21_MAG23_MAG34_MAG44_*Streptomycetaceae,* MAG32_*Chitinophagaceae,* MAG35_*Nitrosopumilaceae,* MAG39_*Bacteroidetes,* MAG40_*Comamonadaceae,* MAG46_*Rhodocyclaceae.*	1
High-O_2 affinity respiration	*ccoN*, *cydA*	Bin51_*Sediminibacterium,* Bin58_*Methylophilales,* Bin64_MAG32_*Chitinophagaceae,* MAG3_*Verrucomicrobiaceae,* MAG4_*Opitutales,* MAG8_MAG12_*Betaproteobacteria,* MAG13_*Bacteria,* MAG17_MAG40_*Comamonadaceae,* MAG18_*Deltaproteobacteria*, MAG22_MAG46_*Rhodocyclaceae,* MAG34_*Streptomycetaceae.*	2

Biogeochemical process	Based on content of the marker genes	Taxonomic groups affiliated with biogeochemical processes	Ref.
Calvin cycle	*prkB, rbcS*	MAG8_MAG12_*Betaproteobacteria,* MAG17_*Comamonadaceae,* MAG22_MAG46_*Rhodocyclaceae* **(*prkB+rbcS*)**. Bin50_*Nitrosomonadaceae,* Bin58_*Methylophilales* **(*prkB* only)**.	3
CO oxidation	*coxMSL*	Bin54_MAG30_MAG33_*Actinobacteria,* MAG7_*Actinomycetales,* MAG12_*Betaproteobacteria,* MAG46_*Rhodocyclaceae* **(*coxMSL*)**. MAG5_*Bacteroidetes* **(*coxMS* only)**. MAG14_*Methylococcus,* MAG17_*Comamonadaceae,* MAG31_*Deltaproteobacteria,* MAG47_*Bacteria* **(*coxS* only)**. Bin60_*Actinomycetales* **(*coxL* only)**.	4
Methane oxidation	*methane monooxygenase*	MAG1_*Methylococcaceae,* MAG19_*Nitrospiraceae.*	5
Methanol oxidation	*mxaF*	Bin49_*Methylophilaceae,* MAG1_*Methylococcaceae,* MAG14_*Methylococcus.*	6
Red. Tricarboxylic Acid Cycle	*korA, korB, frdA, aclY*	Various taxa.	7
Fermentation (lactate)	*ldh*	Bin62_*Methylotenera,* MAG3_*Verrucomicrobiaceae,* MAG15_*Planctomycetaceae.*	8
Reductive Acetyl-CoA	*acsD, acsC*	Bin65_MAG11_*Deltaproteobacteria,* MAG16_MAG47_*Bacteria* **(acs*D* only)**. MAG36_*Methanosaeta* **(acsC only)**.	9
Methanogenesis	*mcrAB*	MAG26_*Methanosarcinales* **(*mcrAB*)**. MAG36_*Methanosaeta* **(*mcrA* only)**.	10

Biogeochemical process	Based on content of the marker genes	Taxonomic groups affiliated with biogeochemical processes	Ref.
Nitrogen cycle			
Ammonification	*gudB, gdhA, ureC*	Various taxa.	11
Nitrogen assimilation	*nasB, narB, glnA, gltB, gltS*	Various taxa.	12
Ammonium oxidation	*amoABC*	MAG10_MAG28_*Nitrosopumilales,* MAG19_*Nitrospiraceae* **(*amoABC*)**. MAG35_*Nitrosopumilaceae* **(*amoBC* only)**.	13
Nitrite oxidation	*nxrAB*	MAG19_*Nitrospiraceae.*	14
Nitrate reduction	*narGH* or *napAB*	MAG1_*Methylococcaceae,* MAG3_*Verrucomicrobiaceae,* MAG17_*Comamonadaceae,* MAG21_MAG34_MAG44_*Streptomycetaceae* **(*narGH*)**. MAG8_*Betaproteobacteria*, MAG22_*Rhodocyclaceae* **(*napAB*)**.	15
Nitrite reduction (to NO)	*nirK* or *nirS*	MAG1_*Methylococccaceae,* MAG4_*Opitutales,* MAG12_*Betaproteobacteria,* MAG39_*Archaea* **(*nirK*)**. MAG8_*Betaproteobacteria, MAG17_Comamonadaceae, MAG19_Nitrospiraceae, MAG22_Rhodocyclaceae* **(*nirS*)**.	16
Denitrification	*norBC, nosZ*	Bin49_*Methylophilaceae* **(*norBC, nosZ*)**. MAG1_*Methylococcacea,* MAG8_MAG12_*Betaproteobacteria* **(*norBC* only)**. Bin65_MAG31_*Deltaproteobacteria,* MAG2_*Porphyromonadaceae,* MAG5_*Bacteroidetes* **(*norB* only)**. Bin51_*Sediminibacterium,* Bin53_*Sphingobacterales,* Bin64_*Chitinophagaceae,* MAG6_*Ignavibacteriales,* MAG15_*Planctomycetaceae,* MAG22_*Rhodocyclaceae,* MAG30_*Actinobacteria,* MAG38_*Bacteria* **(*nosZ* only)**.	17

Biogeochemical process	Based on content of the marker genes	Taxonomic groups affiliated with biogeochemical processes	Ref.
Nitrogen fixation	*nifDHK*	MAG1_*Methylococcaceae,* MAG11_*Deltaproteobacteria* **(*nifDHK*)**. MAG26_*Methanosarcinales* **(*nifH* paralog and *nifD* only)**.	18
DNRA	*nrfA*	Bin65_*Deltaproteobacteria,* MAG3_*Verrucomicrobiaceae,* MAG5_MAG39_*Bacteroidetes,* MAG8_*Betaproteobacteria.*	19
DNRA (from nitrate)	*nrfA* + *narGH* or *napAB*	MAG3_*Verrucomicrobiaceae* **(+*narGH*)**. MAG8_*Betaproteobacteria* **(+*napAB*)**.	20
Sulfur cycle			
S mineralization	*CDO1, sseA*	MAG12_*Betaproteobacteria* **(*CDO1, sseA*)**. Bin62_*Methylotenera,* MAG1_*Methylococcaceae,* MAG10_*Nitrosopumilales,* MAG15_*Planctomycetaceae,* MAG17_MAG40_*Comamonadaceae,* MAG22_MAG46_*Rhodocyclaceae,* MAG27_*Bacteria,* MAG31_*Deltaproteobacteria,* MAG35_*Nitrosopumilaceae,* MAG36_*Methanosaeta,* MAG44_*Streptomycetaceae* **(*sseA* only).**	21
S assimilation	*cysC, cysN, cysD*	Various taxa.	22
Dissimilatory sulfate reduction/ sulfide oxidation	*aprAB, dsrA*	MAG11_*Deltaproteobacteria,* MAG17_*Comamonadaceae,* MAG22_MAG46_*Rhodocyclaceae* **(*aprAB, dsrA*)**. Bin67_MAG8_MAG12_*Betaproteobacteria* **(*aprAB* only)**. Bin65_*Deltaproteobacteria,* MAG26_*Methanosarcinales,* MAG42_*Bacteria* **(*dsrA* only)**.	23

Biogeochemical process	Based on content of the marker genes	Taxonomic groups affiliated with biogeochemical processes	Ref.
Sulfide oxidation	*soxB*	Bin67_MAG12_*Betaproteobacteria,* MAG17_*Comamonadaceae,* MAG22_MAG46_*Rhodocyclaceae.*	24
FeSx formation	-	Abiotic	25
Polysulfide reduction	*phsA*	Bin65_*Deltaproteobacteria.*	26
FeSx dissolution	-	Abiotic	27
Linked and facultative processes			
Autotrophic denitrification - sulfur oxidation	[*prkB, rbcS*] + [*narGH* or *napAB* or *nirK, norBC, nosZ*] + [*aprAB, dsrA, soxB*]	MAG8_*Betaproteobacteria* **(+ [*napAB*, *norBC*, *nirK*] + *aprAB*)**. MAG12_*Betaproteobacteria* **(+ [*norBC, nirK*] + [*aprAB*, *soxB*)**. MAG17_*Comamonadaceae* **(+ [*narGH, nirK*] + [*aprAB, dsrA, soxB*)**. MAG22_*Rhodocyclaceae* **(+ [*napAB, nirK, nosZ*] + [*aprAB, dsrA, soxB*])**.	28
Autotrophic DNRA - S oxidation	[*prkB, rbcS*] + *nrfA* + [*dsrA, aprAB*]	MAG8_*Betaproteobacteria* **(+ *aprAB*)**.	29
(Facultative) anaerobic methylotrophy	*coxAC* + [*pMMO* or *mxaF*] + [*narGH, nirK, norBC, nosZ*]	Bin49_*Methylophilaceae* **(*mxaF* + [*norBC, nosZ*])**. MAG1_*Methylococcaceae* **(*coxAC* + *pMMO* + [*narGH, nirK, norBC*])**. MAG14_*Methylococcus* **(*coxAC* + *mxaF* + *nosZ*)**.	30
Facultative anaerobes	[*coxAC* or *ccoN*] + [*narGH* or *napAB*]	MAG1_*Methylococcaceae*, MAG21_*Streptomycetaceae*, MAG44_*Streptomycetaceae* **(*coxAC* + *narGH*)**. MAG3_*Verrucomicrobiaceae*, MAG17_*Comamonadaceae* **(*ccoN* + *narGH*)**. MAG8_*Betaproteobacteria*, MAG22_*Rhodocyclaceae* **(*ccoN* + *napAB*)**. MAG34_*Streptomycetaceae* **([*ccoN, coxAC] narGH*)**.	

Our analyses of the vertical distributions of functional and phylogenetic marker genes focuses on changes in relative abundance of marker genes in different metagenomes. Sequencing depths between the ten metagenomes varied and was lowest for the 310 m sample (Table A2). The shallow sequencing depth may have led to over-representation of genes from the most abundant fraction of the microbiome in a given metagenome, and genes from rare taxa may remain undetected. Particularly the metagenomic bins and MAGs tend to represent the dominant fraction of the microbiome. Oversight of rare genes or taxa, however, would not considerably bias the analysis of relative distribution of the dominant marker genes throughout the water column.

2.3.3.1. Epilimnion: Primary Producers and Degraders

The epilimnion contained dissolved inorganic nitrogen (ammonium and nitrate), but very little phosphate (Figure 2.2C, D). The top indicator OTUs were affiliated with *Chitinophagaceae*, likely representing heterotrophic degraders, the aerobic photochemotrophic genus *Roseococcus* (Yurkov and Beatty, 1998) and the photoautotrophic genus *Synechococcus* (Table 2.1, Table A3). Dinophytes, potential photoautotrophic primary producers, dominated the eukaryotic microbial fraction (Figure A1C).

2.3.3.2. Oxycline: Dominated by Potential Organic Matter Degraders and Nitrifiers

Actinobacteria dominated at the phylum level (Figure 2.3B) and indicator OTUs for the microbial community of the oxycline zone were affiliated with groups known as potential nitrifiers (*Nitrospirae*) and aerobic organic matter degraders (*Actinobacteria*, *Planctomycetes;* Table 2.1). The location of the sulfate maximum in the lower oxycline and chemocline may be explained by overrepresentation of marker genes for sulfur mineralization in the corresponding metagenomes (Figure 2.2B, Figure 2.4C).

The nitrate maximum (120-125 m) within the lower oxycline zone indicated aerobic nitrification of ammonium diffusing upwards from the monimolimnion (Figure 2.2C). The genetic potential for nitrification was found in metagenomic bins affiliated with

Nitrospiraceae and *Nitrosopumilales* (Table 2.2). The highest relative abundance of 16S rRNA gene sequences affiliated with these and other potentially nitrifying groups was found in the oxycline zone, coinciding with the nitrate peak (Figure A3A). All *Thaumarchaeota*-affiliated OTUs showed similar distributions with a maximum in the oxycline and a secondary peak in the manganous zone (Figure A3A). Ammonium oxidizing bacteria (AOBs; *Nitrosomonadaceae*) were consistently less abundant than ammonium oxidizing archaea (AOAs; *Thaumarchaeota*). However, a group of *Betaproteobacteria*-affiliated OTUs that were relatively abundant in the manganous zone (up to 5.8%) may represent additional AOBs. While poorly classified by the Greengenes database, they were affiliated with the ammonium-oxidizing group *Nitrosomonadaceae* (*Betaproteobacteriales*, *Gammaproteobacteria*) based on SILVA classification (Figure A4).

2.3.3.3. Nitrogenous Zone: Co-dominated by *Crenothrix* and acI-*Actinobacteria*

In the narrow (<10 m around 130 m) nitrogenous zone, oxygen (3.5 μM) dropped to levels close to the empirically determined detection limit, nitrate decreased rapidly, and there was a sharp nitrite peak (Figure 2.2C). The nitrite peak could be produced by incomplete denitrification (NO_3^- to NO_2^-) or ammonium oxidation decoupled from nitrite oxidation (Bristow et al. 2015) and, indeed, a contribution from ammonium oxidation was suggested by the percentage of the marker gene for ammonium oxidation being similar to that found at the nitrate maximum in the oxycline (Figure 2.4B). Consistent with the rapid nitrate decrease, the highest relative abundance of marker genes for denitrification was observed in the metagenome from the nitrogenous zone. Several marker genes for anoxygenic photosynthesis were found, at low abundance, in the nitrogenous zone (Table A4).

A sharp minimum of alpha-diversity confined to the nitrogenous zone (Figure A1A; Appendix A) was caused by the very high relative abundance of two OTUs that together made up 41.8% of 16S rRNA gene sequences at 130 m: one was affiliated with acI (*Actinobacteria*) and another, which was almost exclusively found at this depth, was affiliated with the gammaproteobacterial genus *Crenothrix* (*Methylococcales*; Table 2.1).

Crenothrix sp. are known methanotrophs and the genetic potential for methane oxidation was highest in the nitrogenous zone (Figure 2.4A). The marker gene for methane oxidation was found exclusively in a bin affiliated with *Methylococcaceae* (MAG1; Table 2.2), but since MAG1 did not contain a 16S rRNA gene, it could not definitively be linked to the *Crenothrix*-affiliated OTU. MAG1 as well as other metagenomic bins affiliated with beta- and gammaproteobacterial methylotrophs and methanotrophs also contained the genetic potential for denitrification (Table 2.2).

2.3.3.4. Manganous Zone: Dominated by Denitrifying and Methylotrophic *Betaproteobacteria*

In the center of the manganous zone (135-150 m), nitrate fell below the detection limit (Figure 2.2). Sulfide was first detectable at the bottom of this zone, but in the rest of the manganous zone as well as the nitrogenous zone, micro-oxic conditions cannot be excluded, given the µM-level accuracy range of the utilized oxygen sensor and the occurrence of high oxygen-affinity terminal electron acceptor genes (Figure 2.4A). The highly abundant acI OTU was the prime indicator OTU also in the manganous zone (Table 2.1). At the phylum level, however, *Betaproteobacteria* dominated the manganous zone (Figure 2.3B), and an additional indicator OTU was affiliated with the potential denitrifier *Sterolibacterium* (*Rhodocyclaceae;* 99% Blast ID with *S. denitrificans*; Table 2.1). Several *Betaproteobacteria*-affiliated bins (including *Rhodocyclaceae*) contained marker genes for denitrification, sulfide oxidation (*SOX*, *dsrA*, *aprAB*) and the Calvin cycle, suggesting potential for autotrophic denitrification by sulfur oxidation (Table 2.2). *Betaproteobacteria* from the order *Methylophilales* were also associated with potential methylotrophy in the manganous zone (Table 2.2, Figure A3B).

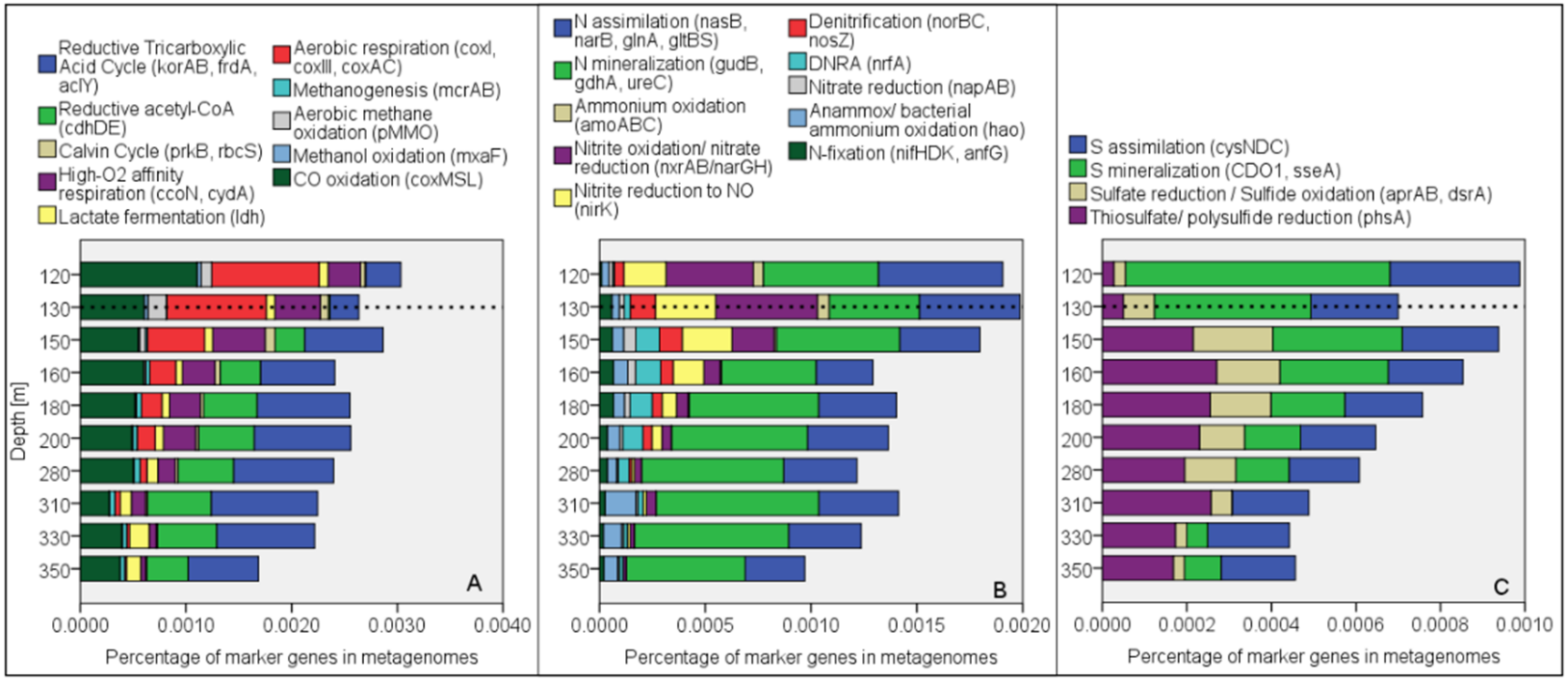

Figure 2.4. Genetic potential for biogeochemical processes in the (A) nitrogen, (B) sulfur and (C) carbon cycles, based on the relative abundance of functional marker genes in each bulk metagenome, sorted by depth. Note that the shallowest metagenome is from the oxycline zone, 120 m below the surface. The oxic-suboxic interface is indicated by dashed lines.

2.3.3.5. Ferruginous Zone: Potential for Sulfate and Nitrate Reduction

Within the ferruginous zone, dissolved manganese and iron concentrations continued to increase. Peaks of both dissolved metals around the bottom of this zone as well as sulfate decrease to levels near the detection limit indicated the co-occurrence of sulfate, manganese and iron reduction within this zone. A small sulfide/salinity maximum at 160 m further indicated that local sulfate reduction may be a source of sulfide in addition to the diffusion of sulfide from below (Figure 2.2B). The *Deltaproteobacteria*-affiliated MAG11 contained marker genes for sulfate reduction (Table 2.2) and the highest percentage of reads mapping to MAG11 was observed in the metagenome from 160 m, linking bacterial sulfate reduction to *Deltaproteobacteria* (Table A5). The prime indicator OTU was affiliated with *Desulfobacca sp.* (Table 2.1), a genus that harbors sulfate reducers (Kuever 2014) and that may also be involved in metal reduction in Powell Lake (Appendix A).

Relative abundances of *nrfA*, the marker gene for dissimilatory nitrite reduction to ammonium (DNRA) were high throughout the ferruginous zone (Figure 2.4B). Among other affiliations, it was found in two metagenomic bins affiliated with *Bacteroidetes* (Table 2.2), a phylum with high relative abundance throughout the manganous and ferruginous zones (Figure 2.3B). More specifically, MAG8, affiliated with *Betaproteobacteria*, contained marker genes for the Calvin cycle, nitrate reduction (*napAB*), denitrification, DNRA and sulfide oxidation (Table 2.2). Most reads mapping to MAG8 were found in the metagenome from the ferruginous zone (Table A5). The occurrence of MAG8 at depths where the profiles of dissolved sulfide and nitrate intersected was therefore consistent with its potential for autotrophic, sulfur-oxidizing nitrate reduction.

2.3.3.6. Euxinic and ASW Zones: Distinct Microbial Communities and Genetic Potential in the Highly Reducing, Increasingly Saline, Deep Water

The microbial communities in the two deepest zones were dominated by bacterial candidate phyla. In the euxinic zone, the candidate phyla *Atribacteria* (formerly OP9) and AC1, as well as *Syntrophaceae* (*Deltaproteobacteria*) dominated the microbial community, which was significantly different from that of the ASW zone below (Figure 2.3A, Appendix A). The greatest share of 16S rRNA gene sequences affiliated with *Archaea* (up to 13.2%), mostly *Crenarchaeota* but also *Parvarchaeota* and *Euryarchaeota*, was found in the ASW zone (Figure 2.3B; Table 2.1), as were high shares of the candidate phyla *Omnitrophica* (formerly OP3; max. 18.7%) and *Cloacimonetes* (WWE1; max. 13.2%). OTUs affiliated with these groups, including one from an unknown lineage within the *Omnitrophica*, distinguished the ASW zone from the rest of the sulfidic water column (Table A3). The differences in the microbial community structure between the two deepest zones also suggested the presence of two distinct syntrophic communities (Appendix A). A phylogenetic tree built from the OTUs that were most distinct for the ASW zone (based on SIMPER) and their nearest relatives from the SILVA database revealed OTUs branching out from phylogenetically diverse clades (Figure A5). These OTUs are detailed in *Table A6* and included a pair of novel OTUs that formed a cluster within the *Atribacteria*, novel clusters within the *Bacteroidetes*, *Deltaproteobacteria* and *Phycisphaerae*, as well as two OTUs that were unaffiliated with any known phylum. The relative abundance of taxonomically unassigned 16S rRNA gene sequences increased with depth to >5% in the ASW zone (Figure 2.3B).

Within the euxinic zone and below, the carbon and nitrogen cycles were increasingly dominated by the potential for assimilation and remineralization processes, while sulfur assimilation and thiosulfate or polysulfide reduction potential became dominant in the sulfur cycle (Figure 2.4). The share of marker genes for (potentially) anaerobic carbon fixation pathways (reductive tricarboxylic acid cycle, reductive acetyl-CoA pathway) increased with depth to a maximum around the halocline. Marker genes for methanogenesis were comparatively scarce throughout, but showed a maximum just above and below the

halocline, indicating potential for water column methanogenesis (Figure 2.4A). Consistently, the highest percentages of 16S rRNA gene sequences affiliated with *Euryarchaeota* (Figure 2.3B) were found in the same depth region and marker genes for methanogenesis were found exclusively in bins affiliated with *Euryarchaeota* (Table 2.2). The potential for CO_2 reduction via the reductive acetyl-CoA pathway in the deep water - either by acetogens or hydrogenoclastic methanogens - indicated that the full range of biogeochemically relevant electron acceptors may be operative in the water column of Powell Lake.

2.4.Discussion

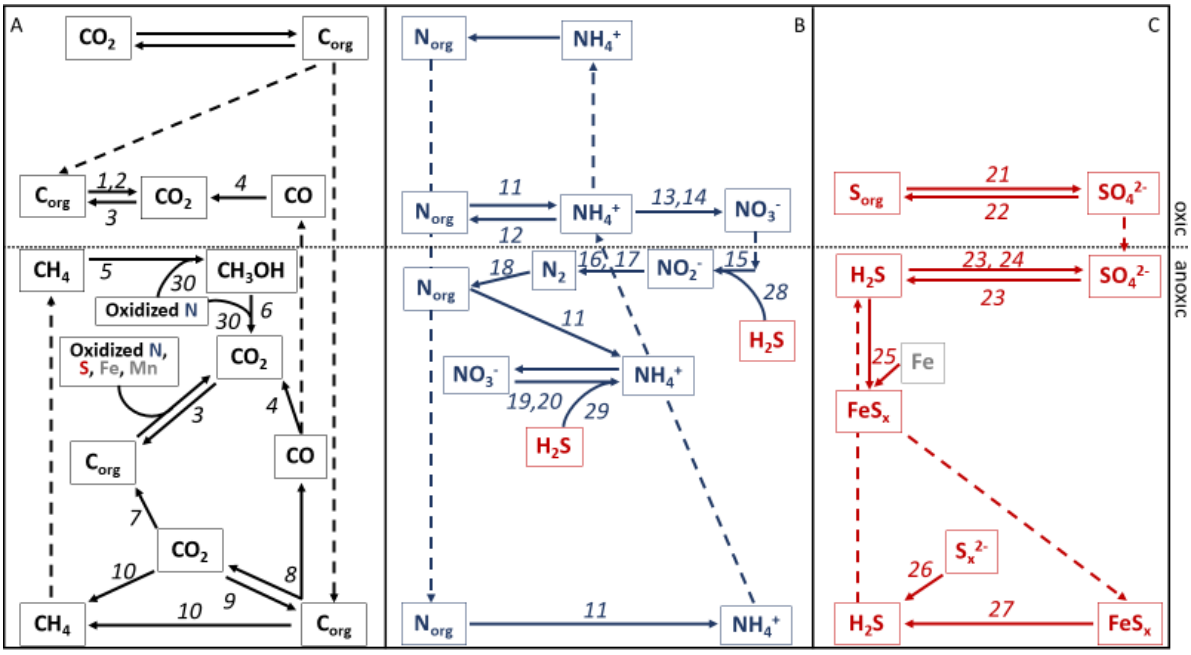

Figure 2.5. Webs of biogeochemical processes in the (A) carbon, (B) nitrogen and (C) sulfur cycles based on genetic potential found in the water column of Powell Lake. Solid arrows indicate biogeochemical processes for which genetic potential was found in the bulk metagenomes or which were inferred from geochemical profiles or dominant microbial OTUs. Dashed arrows indicate inferred physical sinking and diffusion processes. The dashed line separates processes occurring above and below the oxic-suboxic interface. Footnotes refer to Table 2.2, listing processes and the microbial taxa to which they were assigned via marker genes found in metagenomic bins. C_{org} = organic carbon.

Our results laid out the functional genetic potential for biogeochemical cycling in Powell Lake's water column (Figure 2.5) and linked it taxonomically to the microbial community

(Table 2.2). Functional potential and dominant microbial groups found in a given geomicrobiological zone were generally consistent with its geochemical characteristics. However, several inconsistencies and anomalies relative to expectations and differences based on prior studies were also evident and will be discussed following a comparison of Powell Lake's geomicrobiological characteristics to those of other stratified water columns.

2.4.1. Comparison with Other Redox-Stratified Systems

Chemocline-based anoxygenic phototrophic plates are hallmarks of meromictic lakes. Powell Lake's chemocline (130-150 m) is situated deeper below the water surface than that of most other meromictic lakes. In the chemoclines of the Black Sea and Lake Matano, anoxygenic phototrophic *Chlorobi* occur as deep as 80 to 160 m (Overmann *et al.*, 1992; Manske *et al.*, 2005; Marschall *et al.*, 2010) and 110 to 140 m (Crowe *et al.*, 2008; Crowe *et al.*, 2014), respectively. In Powell Lake, almost all 16S rRNA gene sequences were affiliated either with the non-phototrophic *Ignavibacteria* (Iino et al. 2010) or with the uncultivated lineages BSV26 or SJA-28. Yet, many marker genes central to anoxygenic photosynthesis in *Chlorobi* were found in our metagenomes, albeit at low relative abundance (Table A4; compare to relative abundances of marker genes in Figure 2.4). The detected marker genes included *pufML* (photosynthetic reaction center subunits), *pscC*, encoding a component of the photosynthetic reaction center that partly distinguishes phototrophic *Chlorobi* from *Ignavibacterium album* (Liu et al. 2012), as well as the gene for isorenieratene synthase, which produces a distinct marker of low-light adapted *Chlorobi* (Oren et al. 1977; Hamilton et al. 2017; Haas et al. 2018). *FmoA,* the marker gene for bacteriochlorophyll *a*, could not be detected, but the presence of this central pigment may be suggested by detection of *bchF*, encoding an enzyme central to bacteriochlorophyll *a* synthesis (Bryant et al. 2012). These marker genes were found most consistently at 120 m and 130 m (Table A4). Since hydrogen sulfide was absent there, anoxygenic phototrophs would have to rely on alternative electron donors available at these depths, which could include nitrite and ferrous iron (Figure 2.2B, C; Heising *et al.*, 1999; Griffin *et al.*, 2007). The low relative abundance of marker genes for anoxygenic photosynthesis may suggest a

parallel to the low-light adapted *Chlorobi* in the Black Sea, which have very low biomass and have only insignificant quantitative effect on biogeochemical cycling (Manske et al. 2005; Marschall et al. 2010). Since its chemocline is even deeper than that of the Black Sea, any anoxygenic phototrophy in Powell Lake is likely to have only insignificant quantitative effect on biogeochemical cycling due to low process rates. SJA-28, which is affiliated with 3.4 to 5.7% of 16S rRNA gene sequences in samples from the manganous zone, is the lineage that can be most plausibly, but tentatively, linked to anoxygenic photosynthesis, given that the distribution of other *Chlorobi*-related groups, *Ignavibacteria* and BSV26, suggests their involvement in metal reduction rather than anoxygenic photosynthesis (Appendix A). Despite the tentative metagenomic evidence for anoxygenic photosynthesis, measurements with a fluorescence sensor (data not shown) did not detect a signal suggestive of the presence of bacteriochlorophylls. Since bacteriochlorophyll *e* in the Black Sea has been detected by fluorescence sensors (Coble et al. 1991), genes related to anoxygenic phototrophs in Powell Lake may either not be expressed, expressed only seasonally, or at an even lower level than in the Black Sea as to be undetectable by the fluorescence sensor. Further investigations are warranted given that any anoxygenic phototrophs in Powell Lake would be among the deepest, and probably most low-light adapted known to date.

The dominant microbial phyla of the mixolimnion (*Alphaproteobacteria*, *Actinobacteria*), chemocline (*Actinobacteria*, *Bacteroidetes*, *Beta-* and *Gammaproteobacteria*) and monimolimnion matched the occurrence and distribution of abundant phyla in other meromictic lakes (Figure 2.3B; Lehours *et al.*, 2007; Lauro *et al.*, 2011; Comeau *et al.*, 2012; İnceoğlu, Llirós, Crowe, *et al.*, 2015; Llorens-Marès *et al.*, 2015; Baatar *et al.*, 2016). The microbial community of Powell Lake's deep monimolimnion, dominated by *Planctomycetes*, *Deltaproteobacteria*, *Atribacteria*, *Chloroflexi*, *Omnitrophica* and an increased share of *Archaea* compared to shallower depths (Figure 2.3B), resembled the microbial community of other meromictic lakes, particularly those with deep monimolimnia containing a methanogenic zone, such as Sakinaw and Kivu (Gies et al. 2014; İnceoğlu et al. 2015b). It also displayed quite striking similarities with the microbiome of deep marine, methane hydrate-bearing sediments

(Inagaki et al. 2006), suggesting functional similarity of microbial communities adapted to biogeochemically similar environments governed by fermentation and methanogenesis. Correspondingly, many of the nearest relatives of OTUs recovered from the ASW zone were isolated from deep sediments and gas hydrate environments (Figure A5). Some similarities were also observed with the microbial community of the Black Sea anoxic zone, including the presence of the anaerobic methane oxidizing lineages ANME-1 and ANME-2 (Figure A3B), methanogenic *Euryarchaeota* and putative gammaproteobacterial methanotrophs (Pimenov and Neretin 2006; Schubert et al. 2006). Recent evidence suggests that ANME-1 can be methanogens (Beulig et al. 2019), which may explain their occurrence in the ASW zone of Powell Lake (Figure A3B), where electron acceptors for methane oxidation are absent.

Despite showing similarities to the Black Sea, the microbial community of the former fjord Powell Lake is, overall, distinct from that of marine oxygen minimum zones (mOMZs). While many phyla of central significance in mOMZs, including *Proteobacteria*, *Bacteroidetes*, *Actinobacteria* and *Planctomycetes*, were also abundant in Powell Lake (Figure 2.3B), significant mOMZ groups, such as SUP05, SAR324, SAR11 and *Epsilonproteobacteria* (Wright et al., 2012), were absent. Similar niches for microbially driven, biogeochemical processes which exist in both environments were occupied by different, often distinctly terrestrial groups in Powell Lake. For example, autotrophic nitrogen oxide reduction coupled to sulfide oxidation is dominated by the gammaproteobacterial group SUP05 or *Epsilonproteobacteria* in mOMZs (Lavik et al. 2009; Walsh et al. 2009; Canfield et al. 2010b; Wright et al. 2012; Glaubitz et al. 2013), whereas in Powell Lake, this process could only be connected to *Betaproteobacteria* (Table *2.2*). And while the common mOMZ nitrite oxidizer *Nitrospina* sp. was present in the nitrogenous zone, members of the *Nitrospiraceae* were dominant among potential nitrite oxidizers in Powell Lake (Figure A3). *Methylophilales* and *Methylococcaceae*, the groups linked to methylotrophy and methanotrophy in Powell Lake (Table *2.2*), are also common in mOMZs (Wright et al. 2012; Chronopoulou et al. 2017), as well as the Black Sea (Pimenov and Neretin 2006). But at a more resolved taxonomic level, the most prevalent methanotroph-affiliated 16S rRNA gene sequence we identified was related with

Crenothrix sp., important methanotrophs in stratified lakes (Oswald et al. 2017). Similarly, *Thaumarchaeota* have been linked to ammonium oxidation both in this study and in mOMZs (Bristow et al. 2015, 2016; Ganesh et al. 2015). However, instead of the typical marine ammonium oxidizing genus *Nitrosopumilus maritimus*, the closest relatives of *Thaumarchaeota*-affiliated 16S rRNA gene sequences and MAGs were uncultured archaea from terrestrial and freshwater systems and, notably, the terrestrial AOA *Candidatus* 'Nitrosotalea devanaterra' (Figure A6; Lehtovirta-Morley et al., 2016), whose 16S rRNA gene is 98% identical to that of MAG10.

2.4.2. Facultative Anaerobic Adaptations in Widespread Actinobacterial Freshwater Lineage Suggest Ecophysiological Analogies to SAR11

The actinobacterial acI lineage is globally widespread throughout freshwater and brackish systems (Zwart et al. 2003; Lindström et al. 2005; Wu et al. 2006; Newton et al. 2007; Hugerth et al. 2015). In Powell Lake, an OTU affiliated with acI dominated the oxycline and nitrogenous zones and remained prevalent even in the manganous zone (Table 2.1). Its closest neighbor (99% sequence identity, blastN) was *Candidatus* 'Planktophila vernalis' isolate MMS-IIA-15 (NZ_CP016776.1; Neuenschwander et al. 2018). The high relative abundance of acI within and below the oxycline may be due to undocumented facultative anaerobic adaptations in Powell Lake strains (Ghylin et al. 2014). Next to marker genes for aerobic respiration, the metagenomic bins MAG7 and MAG44 contained the marker genes for CO oxidation (*coxMSL*) and nitrate respiration (*narGH*; Table *2.2*), respectively, and the closest neighbor for both bins was the acI strain SCGC AAA027-L06 (Garcia *et al.*, 2013), as affirmed by a high score by SEED (Table A5). The number of reads mapping to MAG7 and MAG44, respectively, was highest in the metagenome from the nitrogenous zone (Table A5). While small concentrations of oxygen probably prevailed in this zone, nitrate concentrations in this zone (4.8 μM) exceeded observed O_2 concentrations (3.5 μM), suggesting environmental pressure as an explanation for facultative nitrate respiration.

These facultative anaerobic adaptations in the globally widespread freshwater lineage acI, otherwise known as aerobic heterotrophs, suggest an analogy to the marine lineage

SAR11. SAR11 is highly abundant in the oxygenated surface ocean, but also in mOMZs (Wright et al. 2012; Bertagnolli and Stewart 2018). Similarities based on small genome and cell sizes between acI and SAR11 have been noted previously (Neuenschwander et al. 2018). Here we find indications that acI lineages in meromictic Powell Lake, like SAR11 lineages from mOMZs (Tsementzi et al. 2016), stand out from their strictly aerobic relatives by facultative anaerobic adaptations, notably the possession of genes for respiratory nitrate reduction. Thus, in analogy to the high abundance of SAR11 in varied marine ecosystems, versatile adaptations in some of its sub-lineages may enable acI to dominate both oxic as well as oxygen-depleted niches in freshwater systems globally.

2.4.3. Divergent Lineages Within Microbial Communities Typical of Meromictic Lakes

A high share of 16S rRNA gene sequences from the deepest zones remained unassigned (Figure 2.3B) and OTUs from the ASW zone affiliated with *Atribacteria*, *Bacteroidetes*, *Deltaproteobacteria* and *Phycisphaerae* form branches that are distinct from 16S rRNA gene sequences previously found elsewhere (Figure A5, Table A6). The long isolation time and highly reducing conditions may have led to unique evolutionary divergence that may go along with unusual functional adaptations (Li et al. 2015c). Given the metabolic potential of the ASW zone, members from these novel clades may be involved in processes that include the degradation and remineralization of organic nitrogen and carbon, possibly as syntrophic partners with other heterotrophs, acetogens or methanogens (Figure 2.4, Appendix A; Gies *et al.*, 2014). In the manganous zone, Powell Lake-specific clusters were identified among the *Betaproteobacteria* (SILVA classification: *Betaproteobacteriales*; Figure A4), a group with high relative abundance in the manganous zone and linked to a wide range of biogeochemical processes (Figure 2.3B, Table 2.2).

2.4.4. Unexpected Geomicrobiological Features in the Geochemical Profile

2.4.4.1. Deviations from the Ideal Electron Acceptor Sequence

The observed distribution of electron acceptors and donors indicative of geomicrobiological processes was very similar in Powell Lake to geochemical profiles found in other stratified systems such as the Black Sea or sediments of mixed lakes (Froelich et al. 1979; Nealson et al. 1991; MacGregor et al. 2001; Nealson and Berelson 2003; Canfield and Thamdrup 2009). In several cases, however, the zones overlapped (Table 2.1). This is not an unusual occurrence (Canfield and Thamdrup 2009) and may be a consequence of non-diffusive components of mixing that prevail above Powell Lake's ASW zone (Sanderson et al. 1986), leading to respiration of more than one type of electron acceptor within a single geomicrobiological zone. In Powell Lake, this included respiration of sulfate and manganese oxides next to iron oxides within the ferruginous zone, and the possible availability of trace levels of oxygen in addition to nitrate in the manganous zones.

A particularly notable deviation from purely thermodynamic predictions of the electron acceptor sequence and thus the zonation was the complete overlap of the ferruginous zone with part of the manganous zone, which stretched down to a deep dissolved manganese peak below the dissolved iron peak (Figure 2.2B). This may have reasons beyond vertical mixing patterns that require further investigation and may involve the occurrence of different mineral forms of manganese and iron oxides that are differentially accessible to microbes. Alternatively, the deep dissolved manganese peak may be due to horizontal input from the sides of the basin. Mn^{2+} usually does not precipitate and thus accumulates in anoxic bottom water (Calvert and Pedersen 1996), and bathymetry data suggest relatively large and relatively flat areas around 230 m at the northern and southern ends of Powell Lake's South Basin (Mathews 1962), where Mn^{2+} may accumulate above the sediment and provide a hypothetical source of reduced manganese to the center of the lake via horizontal transport. Finally, the abiotic aspects of manganese cycling in Powell Lake (saturation, possible co-precipitation) are poorly understood (Perry and Pedersen 1993), and may affect dissolved manganese distributions that are beyond the scope of this paper to resolve.

Investigations targeted at the manganese geochemistry of the lake are necessary to substantiate these speculations and explain the distribution of dissolved manganese, which may be independent of biotic processes.

While the relative locations of the dissolved manganese peak with respect to the dissolved iron peak were unusual, the initial accumulation of dissolved manganese above that of dissolved iron was consistent with the expected electron acceptor sequence observed elsewhere (Nealson *et al.*, 1991; MacGregor *et al.*, 2001; Nealson and Berelson, 2003; Canfield and Thamdrup, 2009). Above the manganous zone, the persistence of dissolved manganese far into the oxic zone is consistent with the slow kinetics of manganese oxidation (Balzer 1982). This may be exacerbated by the abiotic reduction of manganese oxides by upward-diffusing Fe^{2+} (Myers and Nealson 1988).

2.4.4.2. *Deltaproteobacteria* may be Involved in Metal-Sulfide Cycling via Polysulfide Reduction

In the euxinic zone of Powell Lake, concentrations of dissolved iron and manganese decreased due to precipitation as metal sulfides (Perry and Pedersen 1993). Below this depth, sulfide increased steeply, giving sulfide concentrations (not shown) a vertical profile similar to that of salinity. This might indicate that the ASW's sulfide pool is a relic of ancient sulfate reduction that stopped when sulfate was depleted within the trapped seawater. However, a strong increase of the sulfide:salinity ratio in the euxinic and ASW zones revealed a more complex picture, suggestive of ongoing net sulfide production in the ferruginous and ASW zones (Figure 2.2B). Sulfide produced from sulfate reduction in the ferruginous zone precipitates as metal sulfide (Perry and Pedersen 1993) and the sulfide accumulation within the ASW zone may reflect partial dissolution of sinking metal sulfide phases at depth. Intriguingly, a peak of the marker gene for polysulfide reductase coincided with the maximum of the sulfide:salinity ratio at 310 m (Figure 2.4C). This marker gene was found in only one bin, which was affiliated with *Deltaproteobacteria* (Table *2.2*). Given that polysulfide is an intermediate in metal sulfur pathways (Luther 1991), this might indicate microbial involvement in the cycling of metal sulfur compounds and possibly even in their dissolution. More research into this preliminary finding is required, as there are

potential implications ranging from processes in contemporary marine sediments, where Fe-S precipitation plays a central role in biogeochemical cycling, to paleo-oceanographic research, where pyrite is used as a proxy for anoxic conditions in ancient oceans.

2.4.4.3. Unexpected Potential for Nitrogen Fixation Despite Ammonium Excess

Marker genes for biological nitrogen fixation (BNF) were detected, predominantly in the manganous and ferruginous zones (Figure 2.4B). Genetic potential and isotopic evidence for BNF has previously been found in meromictic lakes, affiliated mostly with *Chlorobi* and sometimes *Deltaproteobacteria* (Ohkouchi et al. 2005; Halm et al. 2009; Lauro et al. 2011; Llorens-Marès et al. 2015). In Powell Lake, metagenomic bins containing marker genes for nitrogen fixation were affiliated with *Gammaproteobacteria*, *Deltaproteobacteria* and *Euryarchaeota* (Table 2.2). Active BNF in Powell Lake would not be expected, however, given that throughout the water column, dissolved inorganic nitrogen was far in excess of phosphate (Figure 2.2C,D; Perry, 1990). Total phosphorus data (measured by Inductively Coupled Plasma Optical Emission Spectrometry after acidification) from a later sampling campaign in 2018, confirmed the nitrogen excess over phosphorus (data not shown). Under these conditions, the energetically costly reaction involved in BNF is generally thought to be ecologically uncompetitive. Active BNF in the presence of high dissolved inorganic nitrogen concentrations has, however, been reported previously, but is not well understood (Großkopf and LaRoche 2012; Knapp 2012; Bombar et al. 2016). Further research is required to test whether active BNF occurs in Powell Lake and this, in turn, could lead to a better understanding of the ecological feasibility, role and geographical and environmental occurrence of BNF.

2.4.4.4. Potential for Micro-Aerobic and Anaerobic Methylotrophy and Methanotrophy

Denitrification was linked to methane and methanol oxidation in metagenomic bins affiliated with *Methylophilales* (*Betaproteobacteria*) and *Methylococcaceae* (*Gammaproteobacteria*) and occurring in the oxycline, nitrogenous and manganous zones

(Table 2.2, Table A5, Figure A3). Most notably, this included MAG1, representing a member of the *Methylococcaceae* with the potential for methane oxidation as well as both aerobic respiration and denitrification. Beyond these facultative anaerobic *Proteobacteria*, the presence of 16S rRNA gene sequences affiliated with ANME-2D (NCBI: JF304121) in Powell Lake's ferruginous zone and the candidate phylum NC10 at the depths of the dissolved metal peaks (Figure 2.3B, Figure A3B; Appendix A) may indicate obligate anaerobic methane oxidation coupled with nitrogen oxide reduction (Haroon et al. 2013; Graf et al. 2018).

The extension of beta- and gammaproteobacterial methylotrophic lineages as deep as 50 m into sulfidic waters (Figure A3B) coupled with their genetic potential for denitrification contributes additional evidence for the employment of alternative electron acceptors such as metal- or nitrogen oxides by members of these lineages (Kalyuhznaya et al. 2009; Kits et al. 2015a; b; Oswald et al. 2016, 2017). Genomic evidence for methanotrophy linked to partial denitrification by *Gammaproteobacteria*, specifically *Methylococcales*, has recently been found in laboratory cultures (Kits et al. 2015a; b), meromictic lakes (Oswald et al. 2017) and the stratified fjord Golfo Dulce (Padilla et al. 2017).

2.4.4.5. Identification of Potential Micro-Aerobic Nitrifiers Within the Manganous Zone

Several microbial taxa known as ammonium and nitrite oxidizers and with highest relative abundance around the nitrate peak (oxycline), displayed secondary maxima in relative abundance in the manganous zone (Figure A3A). Most notably, these were SAGMA-X (*Thaumarchaeota*: JN227488 and JN227488; Figure A6) and *Nitrospiraceae*. They may be represented by the taxonomically related MAG28, containing *amoABC*, and MAG19, containing *nxrAB* (Table 2.2), respectively, which also occurred in both the oxycline (120 m) and the manganous zone (150 m) metagenome (Table A5). Additionally, several OTUs among the *Betaproteobacteria*, identified as unusual sub-lineages within the ammonium oxidizing group *Nitrosomonadaceae* (Figure A4), occurred exclusively in the manganous zone. These may represent specialized nitrifiers producing nitrate and/or nitrite within this suboxic zone. Evidence from mOMZs suggests that nitrifiers inside suboxic zones can

survive on trace amounts of oxygen (Lam and Kuypers 2011; Füssel et al. 2012; Buchwald et al. 2015; Bristow et al. 2016; Babbin et al. 2017; Sun et al. 2017). Indeed, small amounts of oxygen may persist in Powell Lake's manganous zone as discussed above, and 16S rRNA gene sequences affiliated with groups of potential nitrifiers showed a secondary maximum in the manganous zone (Figure A3A).

Nitrification in the manganous zone of Powell Lake might sustain autotrophic nitrogen oxide reduction by sulfide oxidation at the suboxic-sulfidic boundary. Maxima in relative abundance of *nrfA* and *napAB* were found as deep as the upper ferruginous zone (Figure 2.4B). MAG8 (*Betaproteobacteria*) contained *nrfA* and *napAB* in combination with marker genes for sulfide oxidation and the Calvin cycle (Table 2.2). Further investigations employing detailed, highly resolved oxygen measurements in combination with rate measurements, nitrogen stable isotope analysis and/or transcriptomic approaches are necessary to confirm nitrogen oxide production within the chemocline by micro-aerobic nitrification. Here we identify the taxa described above as candidates for suboxic-zone adapted nitrifiers. Furthermore, our observations suggest that micro-aerobic nitrification may support autotrophic DNRA or denitrification by sulfide oxidation even in the presence of a broad suboxic zone that divides the oxic zone (source of nitrate from aerobic nitrification) from the sulfidic zone (source of sulfide from sulfate reduction).

2.4.5. Conclusions

Genetic potential for most of the key biogeochemical processes of the carbon, nitrogen and sulfur cycles was found in the water column of Powell Lake (Figure 2.5). These processes covered the full range of biogeochemical electron acceptors from O_2 to CO_2 and their occurrence was mostly consistent with the local geochemical conditions and composition of the microbial community. Evolutionarily divergent lineages prevalent in the ASW zone were identified within diverse phyla (*Atribacteria*, *Bacteroidetes*, *Deltaproteobacteria*, *Planctomycetes*) as well as outside known phyla, which may indicate novel adaptations to this unusual and isolated environment. Deviations from the thermodynamically predicted electron acceptor sequence, most notably the vertical inversion of the dissolved manganese and iron peaks, were observed and may point to the influence of non-diffusive mixing forces. Overall, however, the high physical stability of Powell Lake's water column allows

for repeated sampling of an invariant system, which will allow these and other unusual features of the lake to be addressed in future studies.

In this study, we resolved the change in community structure and functional genetic potential along the geochemical gradient of a meromictic water column, demonstrating close links between geochemistry and microbiology that have long been recognized (Froelich et al. 1979; Berner 1980). Yet, we also identified unexpected features, including taxa that may represent micro-aerobic nitrifiers occurring within the chemocline, the potential for facultative anaerobic methylotrophy and methanotrophy, potential for bacterial nitrogen fixation in high-ammonium, low-phosphate waters, and the presence of acI-*Actinobacteria* with facultative anaerobic adaptations. The classification scheme for stratified systems based on geochemical zonation, as suggested by Canfield and Thamdrup (2009), provided a template to identify these outlier features and relate them to findings from other stratified systems. We suggest that due to the universality of the theoretical concepts underlying this template, it should be used more systematically in similar studies to inform sampling and enable more precise interpretations and inter-comparison of microbial communities and functional potential between stratified systems.

2.5.Experimental Procedures

2.5.1. Study Site

Powell Lake's water surface is situated about 50 m above sea level on the Southwest coast of British Columbia, Canada (Figure 2.1). Sills divide the approximately 100 km long lake into six sub-basins, of which two contain relict seawater in their deepest layers (Williams et al. 1961; Sanderson et al. 1986). Samples for this study were taken from a single location in the center of the 11 km long, 2 km wide, 350 m deep southern basin (49°57' N, 124°32' W; Figure 2.1), which contains geothermally heated relict seawater with salinity of up to 16.7 g kg^{-1}. This is about half of the original salinity with the remainder having been flushed out or removed by diffusive and double-diffusive processes (Sanderson et al. 1986; Scheifele et al. 2014). In 1924, the sill that disconnects the southern basin from the ocean was enhanced by a dam, raising the water level of the lake by 10 m to its current level

(Perry and Pedersen 1993). Recorded lake water levels (since 1988) ranged within 5.4 m (σ = 1.1 m) and the water level during the time of sampling was 0.7 to 0.9 m below the 28-year average (daily data; source: dam management, Brookfield Renewable).

2.5.2. Sampling

Water from 30 depths was collected over the course of four days in August 2016, using Niskin bottles. For dissolved ion analyses (except sulfate), water was immediately filtered through 0.45 µm surfactant-free cellulose-acetate syringe filters (Nalgene, Thermo Scientific). Samples for nutrients (ammonium, nitrate, nitrite, phosphate) and DOC were collected in acid-washed containers and subsequently frozen until analysis. For dissolved iron and manganese samples (50 mL), the pH was adjusted to <4 by addition of 20 µL concentrated HCl upon sampling. Samples for dissolved sulfate and sulfide were fixed with 5% zinc acetate (1 mL per 10 mL and 4 mL sample, respectively).

Water samples (approximately 1-4 L per sample) for nucleic acids extraction were pre-filtered through a 160 µm nylon mesh (NITEX, Dynamic Aqua-supply Ltd., Canada), and microbial cells subsequently concentrated on sterile 0.2 µm, 47 mm polycarbonate filters using a peristaltic pump. Between samples, the entire filtration system was sequentially flushed with several centiliters of 10% HCl, MilliQ water and the new sample water. Filters were immediately frozen on liquid N_2 for transport to the lab, where they were stored frozen until extraction.

2.5.3. Physico-chemical Measurements

2.5.3.1.Sensor Measurements

A conductivity-temperature-depth sensor (CTD, SBE19+, Sea-Bird Scientific) equipped with a dissolved oxygen optode (4330, Aanderaa Data Instruments AS, Norway) was deployed in parallel to water sampling to record continuous vertical profiles of salinity, temperature, pressure and dissolved oxygen. To avoid bias in oxygen concentrations resulting from slow sensor response time, the package was stopped for several minutes at

depths of interest. Dissolved oxygen data were post-corrected for salinity, temperature, depth (according to standard protocol from the manufacturer) and sensor drift (Miloshevich et al. 2004). Despite these corrections, measured oxygen concentration values did not go below 2.6 to 3.0 µM even in sulfidic waters (presumed to be anoxic). This relatively small offset from zero was within the accuracy range declared by the manufacturer (<8 µM) and we interpret the ~3 µM measured at the top of the sulfidic zone as an empirically determined zero-value for the sensor. Additionally, an unknown effect (the optodes used are not sensitive to H_2S; manufacturer information) caused the sensor to show an apparent oxygen increase in the deepest water, which again is presumed to be anoxic. Water clarity was measured by a transmissometer (C-star, Sea-Bird Scientific) with 25 cm path length using 650 nm light. Salinity measured from conductivity is presented on the TEOS-10 Reference Composition Salinity Scale with a salinity anomaly of zero (IOC et al. 2010).

2.5.3.2.Geochemical Analyses

Dissolved phosphate (PO_4^{3-}), ammonium (NH_4^+; Kérouel and Aminot, 1997) and nitrite (NO_2^-) were measured on an auto-analyzer (San++, Skalar) according to manufacturer's instructions based on standard spectrophotometric and fluorometric methods (Kérouel and Aminot 1997; Hansen and Koroleff 1999). For ammonium analysis, deep water (≥290 m) samples had to be highly diluted (1:100) to fit the sensitivity range of the instrument, leading to large error margins that were caused by small contaminations and not fully captured by our error bars. Nitrite concentrations below 135 m were corrected for a background signal determined by running the auto-analyzer protocol but omitting addition of the coloring reagent. Dissolved nitrate (NO_3^-) concentrations were measured by chemiluminescence after nitrite removal by sulfamic acid (Granger and Sigman 2009) and reduction in a hot acidic vanadyl sulfate solution on a NO_x analyzer (Braman and Hendrix 1989). A nitrate background signal of 0.30 µM (standard deviation: 0.26 µM) was evidently introduced during sampling and caused an artifact of >0.0 µM nitrate in the monimolimnion. Total dissolved sulfide was analyzed according to Cline (1969) with a detection limit of 0.1 µM. Dissolved iron and manganese were analyzed by Atomic Absorption Spectrometry (SpectrAA Model 55B, Varian) with a detection limit of 0.18

μM. After filtration through 0.45 μm cellulose acetate filters (same as above) and subsequently through Dionex™ OnGuard™ II H Cartridges (Thermo Scientific) to remove zinc, sulfate was measured by ion-chromatography (Dionex ICS-5000, Thermo Scientific) with a background signal of ca. 0.6 μM; sulfate data from samples below 200 m are not reported, because unknown interferences caused ambiguous results. DOC was measured on a total organic carbon analyzer after acidification and purging (TOC-V, Shimadzu).

2.5.4. Nucleic Acid Extraction and Sequencing

DNA was extracted from the filters using the DNeasy Plant Mini Kit (Qiagen) with modifications to the protocol that included the application of 50 μL lysozyme (5 mg/mL) before adding lysis buffer AP1 together with 45 μL proteinase K (20 mg/mL). Successful extraction was confirmed using nucleic acid quantification by nanoDrop™ (Thermo Scientific). DNA was amplified using previously described primers targeting the V4-V5 variable region of the 16S rRNA gene of bacteria and archaea, and the V4 region of the 18S rRNA gene of Eukaryotes, respectively (Comeau et al. 2011; Walters et al. 2016; Parada et al. 2016). Tag sequencing of DNA amplicons was carried out on an Illumina MiSeq instrument using 2×300 bp paired-end v3 chemistry at the Integrated Microbiome Resource, Dalhousie University (Comeau et al. 2017). Additional sequencing of whole community metagenomes was carried out at selected depths using the Illumina Nextera XT kit as described by the manufacturer. Briefly, libraries were prepared by enzymatically shearing the samples and tagging them with adaptors, PCR-amplified while adding barcodes, and finally purified, normalized and pooled for loading onto a MiSeq (2×300 bp paired-end v3 chemistry) for deep sequencing or onto a NextSeq (2×150 bp paired-end "high-output" chemistry) for shallower sequencing depth (Table A2).

2.5.5. Processing of Nucleic Acid Reads and Bioinformatic Analyses

Three types of analyses were carried out to characterize the microbial community along the vertical geochemical gradient of Powell Lake, each with their associated benefits and limitation as described in Appendix A.

2.5.5.1. Small Subunit rRNA Gene Sequence Processing and Analysis

16S/18S rRNA gene sequences were processed using a QIIME-1 (Caporaso et al. 2010) based workflow (Langille, https://github.com/LangilleLab/microbiome_helper/wiki/; Comeau et al., 2017). This included merging of paired-end sequences using PEAR (Zhang et al. 2014a), discarding sequences <400 bp or with quality <30 over 90% of bases, as well as removing chimera by VSEARCH (Rognes et al. 2016). Using *sortmerna* (Kopylova et al. 2012) for reference picking and *sumaclust* (Mercier et al. 2013) for *de novo* picking, operational taxonomic units (OTUs; defined by 97% sequence similarity) were picked and clustered against the Greengenes (16S rRNA) and PR^2 (18S rRNA) reference databases (DeSantis et al. 2006; Guillou et al. 2013). Subsequently, low-confidence OTUs (<0.1%) were removed (Comeau et al. 2017). 16S rRNA amplicon reads were rarefied to 6614 reads, which allowed to keep all samples and did not cause perceivable differences in outcome compared to higher thresholds. 18S rRNA amplicon reads were rarefied to 1408 reads and all samples from >135 m depth fell below this threshold (Figure A1E). Phylogenetic trees of 16S rRNA gene sequences were constructed by RAxML (Stamatakis 2014) and visualized by iTOL (Letunic and Bork 2016) or using the Kimura two-parameter model (Kimura 1980) in MEGA7 (Kumar et al. 2016) after alignment with MUSCLE (Edgar 2004) or SINA (available at http://www.arb-silva.de; Pruesse *et al.*, 2012) and using reference genes from the SILVA and NCBI RefSeq databases (Pruitt et al. 2007; Yilmaz et al. 2014). Diversity indices (Shannon-Weaver, Simpson, Richness) and curves were determined using QIIME-1 scripts. Rank-dominance plots for the 16S and 18S rRNA gene sequences were generated in PRIMER v6 (Clarke 1993, 2006). As applied by Desai *et al.* (2012), Bray-Curtis similarity analysis, ANOSIM and SIMPER routines from the PRIMER v6 program were used to analyze the microbial community structure in different samples and zones predicted by the geochemical profile. Bray-Curtis similarities in community structure at the OTU level, between each pair of samples were ordinated and visualized on an NMDS plot. The relevance of the geochemical zonation was tested for statistical significance in the microbial community structure by ANOSIM. Additionally, SIMPER was used to determine indicator OTUs, which were i) OTUs that contribute most to

similarity within a zone (Table 2.1), as well as ii) OTUs that contribute most to dissimilarity between two zones (Table A3).

2.5.5.2. Metagenomic Annotation, Assembly and Binning

Bulk metagenomic reads were annotated using the pipeline described at https://github.com/LangilleLab/microbiome_helper/wiki/Metagenomic-standard-operating-procedure based on the Microbiome Helper toolkit (Comeau et al. 2017). Reads were trimmed and filtered using Trimmomatic (Bolger et al. 2014), which filtered out 11.2-17.7% of reads in the NextSeq metagenomes and 0.6% of reads in the MiSeq metagenomes. The resulting read number was similar between most metagenomes with lower numbers in the metagenomes from 280 m and 310 m (Table A2). The program Nonpareil (Rodriguez-R and Konstantinidis 2014) was used to estimate the coverage and sequencing depth for each metagenome (Table A2).

For functional analysis of the bulk metagenomes, KEGG (Kyoto Encyclopedia of Genes and Genomes) orthologs (KOs) were assigned to metagenomic reads (e-value threshold: <0.001) using HUMAnN (Abubucker et al., 2012). HUMAnN quantified the relative abundance of each KO based on total reads within a given bulk metagenome, whereby the number and length of reads mapping to a given KO were normalized to gene length. KOs affiliated with functional marker genes for biogeochemically relevant processes with a focus on the carbon, nitrogen and sulfur cycles were extracted from these metagenome datasets using the method developed by Lauro et al. (2011) and enhanced by Llorens-Marès et al. (2015). Beyond the selection by Llorens-Marès et al. (2015), we added further marker genes from the KEGG database to cover additional processes as well as to improve the representation of existing processes (Table A7). Specifically, potential for the processes of methanol oxidation (*mxaF*; Lau *et al.*, 2013), as well as respiration using high-O_2 affinity terminal electron acceptors (*ccoN* and *cydA*; Morris and Schmidt, 2013) was covered additionally by adding the respective marker genes. The marker gene *ureC* was added to more accurately represent potential for the N remineralization process and *nirK* was used as an additional functional marker gene in the nitrogen cycle as a marker for NO-forming nitrite reduction used in anammox, denitrification and bacterial ammonium oxidation.

Additionally, we investigated the vertical distribution of several functional marker genes not included in the KEGG database (Table A4). For this, we used prodigal (Hyatt et al. 2010) to call genes from the metagenomes and subsequently scanned Hidden Markov Models (HMMs), which were either retrieved from the FunGene repository (Fish et al. 2013) or custom-made based on Uniprot entries, using HMMer (Eddy 2011). We further note that the marker gene *hao* (hydroxylamine oxidoreductase; Table A7) is not process-specific based on KEGG orthology (K10535), because the gene for hydroxylamine oxidoreductase used by AOBs (Kozlowski et al. 2016) and the hydrazine dehydrogenase gene (*hdh*) found in anammox bacteria are both paralogs of octaheme hydroxylamine oxidoreductase (Maalcke et al. 2016). *Hao* was thus interpreted to represents the sum of aerobic and anaerobic bacterial ammonium oxidation.

Metagenomic reads from bulk metagenomes were co-assembled and binned following the workflow published online (Delmont http://merenlab.org/data/ 2017_Delmont_et_al_HBDs) which is described in (Delmont et al. 2018), based on the Anvi'o platform (Eren et al. 2015), using previously published applications (Delcher et al. 2002; Hyatt et al. 2010; Eddy 2011; Langmead and Salzberg 2012; Alneberg et al. 2014; Li et al. 2015a; Parks et al. 2015; Kim et al. 2016). Briefly, the paired-end reads were filtered for quality using the parameters described in Minoche *et al.* (2011) and implemented in the package Illumina utils (Eren et al. 2013). On average, around 92% of the reads per sample passed the quality filtering step. The filtered reads were then co-assembled using Megahit (Li et al. 2015a) and contigs ≥5000 bases in length were binned using Concoct (Alneberg et al. 2014). The bins with ≥50% completion and ≤20% redundancy, in terms of presence of a set of 139 bacterial single copy marker genes (Campbell et al. 2013), were labelled as Metagenome Assembled Genomes (MAGs). From the 72 bins obtained by this protocol, 47 were defined as MAGs. Relative to HUMAnN output, between 5 and 69% of reads from the different metagenomes were mapped to bins (Table A2). The program CheckM (Parks et al. 2015) was used to associate taxonomic affiliation to the bins and SEED was used to identify their closest neighbor (Overbeek et al. 2014). Protein coding genes identified in the contigs in each bin by using the program Prodigal (Hyatt et al. 2010) were functionally annotated using the RAST server (Aziz et al.

2008). As summarized in Table 2.2, functional marker genes of interest (Table A7) identified in different metagenomic bins were linked to taxonomic groups, using the taxonomic affiliation of the bins. In some cases, the annotation of selected functional marker genes found in the bins was refined using PSI-Blast, specifically to detect subunits of the ammonium monooxygenase gene (*amoABC*) as well as to distinguish different types of nitrate reductases (*napAB*, *nrfA*, *narB*, *narGH*, *nxrAB*) and nitrite reductases (*nirBD*, *NIT-6*), respectively, which were not detected or sufficiently resolved by RAST. In the same way, it was tested whether genes annotated as 'hydroxylamine reductase' were genes that have a function in the anammox process.

2.5.5.3. Sequence Deposition

Nucleotide sequence data have been deposited into NCBI databases under the Bioproject PRJNA489439. Raw sequences from small subunit rRNA genes as well as raw bulk metagenome sequences were submitted to the Short Read Archive (SRA) under accession number SRP159945 (individual accession numbers: SRR7798723-43 (16S rRNA), SRR7798745-65 (18S rRNA), SRR7801934-41 (metagenomes)). Assembled and rarefied 16S rRNA gene sequences have been deposited at DDBJ/EMBL/GenBank under the accession KCEW00000000. Metagenomic bin sequences can be accessed via the Genome database under accession numbers QYOT00000000-QYRM00000000.

CHAPTER 3

PHYSICAL MIXING CONTROLS AND DECOUPLES NITRIFICATION VIA BIOMASS DILUTION[2]

3.1. Abstract

Our study demonstrates that dilution of nitrifying microorganisms by physical mixing can delay and decouple nitrification in subsurface waters of a seasonally stratified, eutrophic coastal basin. The findings are based on analysis and biogeochemical modeling of four years of weekly oceanographic time-series measurements in Bedford Basin, Nova Scotia, Canada, that included measurements of functional (*amoA*) and phylogenetic (16S rRNA) marker genes for nitrifiers.

In years with colder winters, more intense winter mixing resulted in strong dilution of the resident nitrifier population causing delays in nitrification, lasting weeks to months despite the presence of sufficient oxygen and ammonium substrate. Delayed regrowth of nitrifiers following dilution led to transient accumulations of nitrite (3–8 μmol kg_{sw}^{-1}) by decoupling the two steps of nitrification, ammonia- and nitrite oxidation. Nitrite accumulation was enhanced by fast ammonia oxidation kinetics of ammonia-oxidizing bacteria (*Nitrosomonadaceae*), which transiently outcompeted *Nitrosopumilus*-like ammonia-oxidizing archaea that dominated under more stable conditions. We propose a mechanism whereby intensity of mixing controls nitrifier biomass and community

---

[2] Haas, Sebastian, Brent M. Robicheau, Subhadeep Rakshit, Jennifer Tolman, Christopher K. Algar, J. LaRoche, and Douglas W. R. Wallace. Physical mixing controls and decouples nitrification via biomass dilution. Under Review, PNAS.

Author contribution: *I conceived of the study and wrote the chapter with contributions from co-authors, notably 2 other doctoral students who brought in knowledge from their specializations, marine microbiology and numerical modeling. Supported by co-authors, I interpreted the data and reached the main conclusions. I helped further develop the model, which was initially developed of by co-authors, and I processed and analyzed the 16S rRNA amplicon sequencing data. DNA extraction, nutrient and qPCR analyses, as well as most field sampling was performed by technicians or co-authors.*

composition, leading to variable delays in their regrowth and variability in nitrification rates. Such mixing-induced, transient effects on biomass and diversity of microbial communities with biogeochemical implications are likely to be relevant in other intermittently stratified water columns. The mechanism links climate-sensitive and variable physical mixing with microbially-driven nitrification and the speciation of nitrogen supply to marine phytoplankton. This study emphasizes the value of high-frequency, multi-parameter time series for identifying and modeling controls of complex microbial and biogeochemical processes in dynamic aquatic systems.

3.2. Introduction

Coastal waters worldwide are subject to inputs of anthropogenic nitrogen (N) which impact primary production and marine ecosystems through alteration of both the quantity and speciation (oxidized/reduced, inorganic/organic) of N (Peñuelas et al. 2013; Glibert et al. 2016). These are key controls on phytoplankton growth and community composition, altering patterns and magnitude of primary production, causing eutrophication and harmful algae blooms and impacting carbon flux (Yoshiyama and Sharp 2006; Domingues et al. 2011; Glibert et al. 2016). For example, relative increase in ammonium over nitrate supply can shift phytoplankton community compositions toward smaller species with the potential to cause harmful algal blooms and reduced productivity (Glibert et al. 2016). The speciation of N also exerts control on key microbial N-cycling pathways, including the fixed-N removal processes anammox and denitrification. These pathways depend on the availability of oxidized forms of N that can be converted to N_2 and thereby removed from the pool of readily bioavailable N within ocean waters.

It is therefore essential to understand the processes and environmental factors that control the speciation of dissolved inorganic nitrogen (DIN= $NO_3^- + NO_2^- + NH_3/NH_4^+$) between oxidized (nitrate and nitrite) and reduced (ammonium/ammonia) forms, as well as between organic and inorganic forms (LaRoche et al. 1997; Glibert et al. 2016). A key-process controlling DIN-speciation is nitrification, the two-step oxidation of ammonia (NH_3) to nitrate (NO_3^-) via nitrite (NO_2^-). Ammonia-oxidizing organisms (AOO), either archaea

(AOA) from the phylum *Thaumarchaeota* or bacteria (AOB), catalyze the oxidation of ammonia to nitrite:

Ammonia oxidation (AO): $2NH_3 + 3O_2 \rightarrow 2NO_2^- + 2H^+ + 2H_2O$ 3.1

AO kinetics differ between the two AOO groups, with higher maximum reaction velocities (V_{max}) and ammonium half-saturation constants (K_m) in AOB (Suzuki et al. 1974; Ward 1987; Bollmann et al. 2005) compared to AOA (Martens-Habbena et al. 2009; Horak et al. 2013; Peng et al. 2016). Nitrite-oxidizing bacteria (NOB) are responsible for the second step from nitrite to nitrate:

Nitrite oxidation (NO): $2NO_2^- + O_2 \rightarrow 2NO_3^-$ 3.2

Recently, an exception to the two-organism nitrification paradigm (Daims et al. 2015; van Kessel et al. 2015) has been recognized through the discovery of complete ammonia oxidation to nitrate ("comammox") by individual *Nitrospirae* bacteria (Daims et al. 2015; van Kessel et al. 2015). This could play a role in coastal marine waters under some conditions (Xia et al. 2018).

In the ocean, nitrification maxima typically occur at or below the base of the euphotic zone, spatially separated from photosynthetic primary production (Horak et al. 2013; Santoro et al. 2013; Peng et al. 2016). However, vertical transport can supply products of nitrification to the euphotic zone (Yool et al. 2007; Johnson et al. 2010). Incomplete nitrification may therefore affect phototrophic communities, since the speciation of externally-supplied N (e.g. ammonium vs. nitrate) can significantly impact both the structure and productivity of phytoplankton (Glibert et al. 2016).

Accumulation of the intermediate product of nitrification, nitrite, has been documented in a wide range of marine systems, including at the base of the oceanic euphotic zone (Lomas and Lipschultz 2006), in oxygen deficient zones (Buchwald et al. 2015; Bristow et al. 2015), and transiently in coastal bays and estuaries (Horrigan et al. 1990b; Heiss and Fulweiler 2016; Schaefer and Hollibaugh 2017; Laperriere et al. 2019). In many cases, the presence of nitrite can be attributed to decoupling of AO and NO, which are usually tightly coupled despite ecophysiological differences between AOA and NOB (Kitzinger et al.

2020). A large variety of environmental factors have been associated with the decoupling of nitrification in marine systems (Philips et al. 2002; Bristow et al. 2015; Heiss and Fulweiler 2016; Schaefer and Hollibaugh 2017). Here we describe nitrite accumulation arising from nitrifier regrowth following physical dilution, which might point to a general mechanism for decoupling nitrification in seasonally stratified water columns.

Physical transport is widely recognized to control phytoplankton growth in aquatic systems, for example through supply of nutrients to the euphotic zone from below (Dutkiewicz et al. 2001; Johnson et al. 2010). Mixing also plays a role in the initiation of spring blooms according to the "dilution-recoupling" hypothesis (Behrenfeld 2010), according to which dilution of both phytoplankton and grazer biomass leads to fewer grazer-phytoplankton encounters. It has been shown that nitrification can be enhanced by the mixing of ammonium-rich waters into well-oxygenated waters (McCarthy et al. 1984; Laperriere et al. 2019), whereas the mixing-induced transport of NOB biomass away from the depth of optimal growth at the base of the euphotic zone has recently been implicated as a factor explaining local nitrite accumulation (Zakem et al. 2018). Here, we describe a different negative control of mixing on nitrification, whereby seasonal and inter-annual variations in mixing lead to temporally variable rates of nitrification as a consequence of nitrifier biomass dilution.

High-frequency, long-term measurements of the physical and chemical environment along with the associated microorganisms have been shown to be a valuable tool set for determining environmental controls on microbial processes (Punshon and Moore 2004; Li and Harrison 2008; Johnson et al. 2010; Robidart et al. 2012; El-Swais et al. 2015; Ma et al. 2019). However, such time series are rare because of the sustained, multi-disciplinary effort and teamwork they require.

Here, we present results of such a time-series based study of nitrification within the bottom water (60 m) of Bedford Basin (BB), a eutrophic, anthropogenically impacted, fjord-like embayment located within the Halifax Regional Municipality on the Atlantic coast of Nova Scotia, Canada (see *SI Materials and Methods* sections for more details). Restricted water exchange with the open ocean and annual cycles of stratification and winter mixing make BB a useful natural laboratory to study the relationship between

microbial growth phases, geochemistry and physical processes. Based on four years of weekly observations of ammonia monooxygenase subunit A (*amoA*) gene copy numbers (via quantitative PCR; qPCR), microbial community composition (16S rRNA gene amplicon sequencing), nutrient concentrations, and a biogeochemical model enhanced by functional gene modeling, we observed variable dilution of the nitrifier population following winter mixing events. We propose that intense winter mixing during cold winters flushes the resident nitrifier population from the basin bottom waters, resulting in delay in nitrification and decoupling of AO and NO until the nitrifier community can reestablish. During warmer winters, when mixing is less intense, growth can keep pace with mixing and effectively prevent dilution.

3.3. Study Settings and Time Series Context

The 4-year time series of molecular and chemical data from BB bottom water presented here (*SI Materials and Methods*) was collected between January 2014 and December 2017, at the center of the basin (44°41'37"N, 63°38'25"W). Our study was conducted in the context of a longer, weekly oceanographic time series established in 1992 (Li and Harrison 2008; Li 2014). BB (70 m maximum depth) experiences annual cycles of turbulent winter mixing and seasonal stratification. Water above the sill depth (20 m) is subject to circulation and tidal exchange with the Atlantic Ocean (Scotian Shelf) throughout the year (Petrie and Yeats 1990; Fader and Miller 2008; Shan et al. 2011), while the bottom water is effectively disconnected from this circulation during stratified periods. Stratification is established in spring (~April) and persists into winter (November–February), when it breaks down due to intense cooling (Shan et al. 2011; Li 2014). In some years, the stratified period is interrupted by the intrusion of relatively warm and saline water from the Scotian Shelf into the bottom water of the basin (Platt et al. 1972; Punshon and Moore 2004; Burt et al. 2013). Unlike the more extended periods of convective mixing during winter, these intrusions are short-lived and do not break down the vertical stratification, but they do ventilate the bottom water and modify its biogeochemistry (Punshon and Moore 2004; Burt et al. 2013). The fate of "older" bottom water that is displaced following an intrusion is not

well-characterized but presumably involves upwelling and mixing into near-surface layers followed by exchange with continental shelf-water.

AOA peptides and the presence of *Nitrospina*-type NOB have previously been detected in BB bottom water (Georges et al. 2014), which is dark (Taguchi and Platt 1977) and has a microbial community that is distinct from than in the near-surface waters (El-Swais et al. 2015). Despite continuous availability of ammonium (mostly >1 μmol kg_{sw}^{-1}), AO rates are highly variable (Punshon and Moore 2004).

3.4. Results

3.4.1. Physical Mixing and Nutrient Cycling in Bedford Basin, 2014–2017

The mixing regime within BB between 2014 and 2017 displayed a sequence of full water column winter/spring mixing followed by stratification throughout summer and fall (Figure 3.1) that was consistent with longer-term observations (Figure B1). During stratified periods the bottom water was relatively isolated from surface water as indicated by consistently cold temperatures (~1–4°C) despite strong near-surface temperature variability (1–18°C). Dissolved oxygen was an especially clear indicator of active mixing due to its non-conservative nature and near-surface source: periods of stratification were marked by a steady oxygen decrease in bottom waters and were clearly distinguishable from periods of mixing when oxygen was delivered to the bottom water (Figure 3.2A).

The event markers M14, PM15, M16 and M17 in Figure 3.2A show the end of winter mixing and onset of stratification each year around April as indicated by the beginning of steady oxygen decrease. The stratified periods were interrupted by occasional shelf-water intrusions into the bottom water (Events I14, I16a, I16b and I17: Figure 3.1, Figure 3.2A). In July 2017, there was an intrusion of shelf water to mid-depth layers (~30 m) of BB (Shi and Wallace 2018). Some of this intruding water also got entrained into the bottom layers during the subsequent weeks, as indicated by nitrate decrease and a delayed oxygen decrease at 60 m (Event MDI17: Figure 3.2A,B).

The intrusions generally delivered warmer (0.5–2.3°C temperature increase) and saltier (0.2–0.6 PSU salinity increase) offshore water to the bottom of BB, whereas winter mixing decreased both the temperature and salinity of the bottom water (Figure 3.1A,B). The cooling and freshening effect of winter mixing and the contrasting effect of intrusions on BB bottom water are reflected in the "spiciness" of the water, where spiciness is a derived parameter that is proportional to both temperature and salinity and can be used to distinguish water types that share the same density (Flament 2002). Sudden increases in spiciness occurred with each intrusion event (Events I14, I16a, I16b, I17).

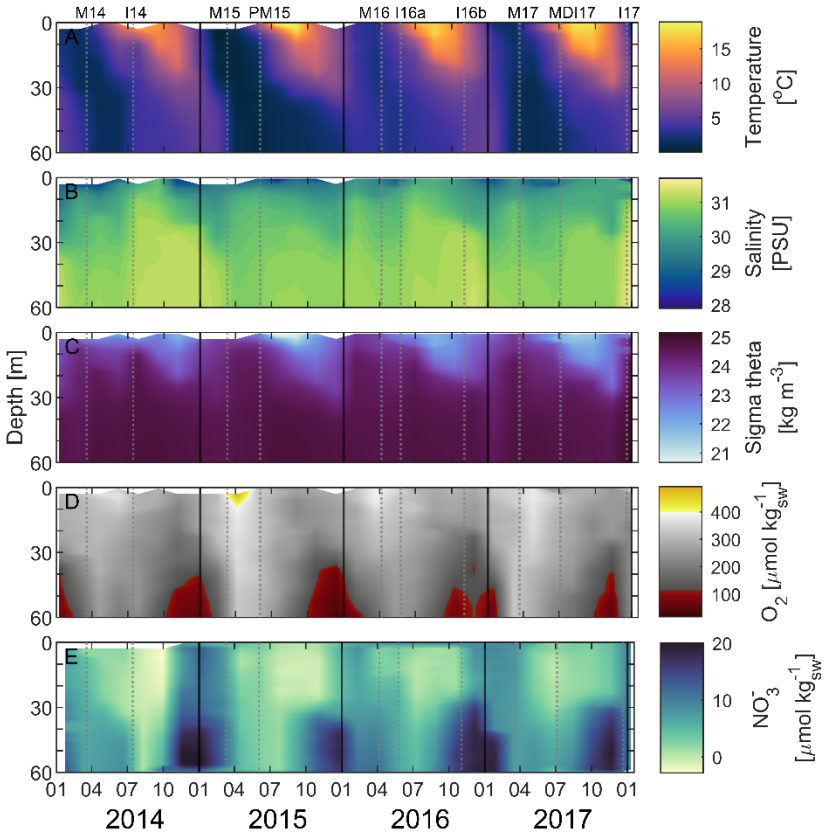

Figure 3.1. Time series of weekly vertical profiles of temperature (A), salinity (B), sigma theta (potential density) (C), dissolved oxygen (D), nitrate (E) in Bedford Basin between January 2014 and December 2017. Event numbers indicate winter mixing ("M") or intrusion events ("I"). "MDI17" is an intrusion to mid-depth waters of BB. PM15 indicates the prolonged phase of winter mixing in 2015.

In contrast, rapid decreases in spiciness associated with winter mixing adding relatively cold and fresh water to the bottom layer occurred in early 2014, 2015 and 2017 (Events

M14, M15, M17; Figure 3.2A). They co-occurred with rapid increases in oxygen concentration indicating intense winter mixing (Figure 3.2A). The spiciness decrease in winter 2016 was much less pronounced (M16), whereas lowest spiciness was observed in late April 2015 (Figure 3.2A), suggesting more intense winter mixing in 2015 compared to other years, especially 2016.

This is consistent with lower air temperatures during winter 2015 compared to winter 2016. Low temperatures drive winter mixing in BB through cooling of surface water (Li and Harrison 2008; Shan et al. 2011), and average January–March atmospheric temperatures recorded at Environment and Climate Change Canada's Bedford Basin station were lowest in 2015 (-4.4°C) and highest in 2016 (-0.5°C), with intermediate values observed in 2014 (-2.7°C) and 2017 (-1.6°C). The average January–March temperatures since 2008, when data became available at this station, have been -1.5°C (standard deviation: 1.3°C) and the winter temperatures in 2015 were the coldest on record at this station.

Additionally, higher buoyancy frequency (N^2) in winter 2016 indicated stronger stratification than in other years (Figure 3.2A). Taken together, these observations indicate that winter mixing was particularly weak in 2016 and particularly intense in 2015, whereas 2014 and 2017 represented intermediate cases.

Both winter mixing and intrusions led to increased dissolved oxygen and decreased DIN concentrations in the bottom water (Figure 3.2A,B). In all four years, ammonium concentrations increased with the onset of stratification (~April) due to remineralization of organic nitrogen, reaching maximum concentrations of 13–18 μmol kg_{sw}^{-1} during the stratified period (Figure 3.2B). The proportion of nitrate in DIN increased in late summer, indicating that nitrification exceeded the rate of N remineralization. Continuous water column profiles measured by a nitrate sensor (*SI Materials and Methods*) showed that the nitrate maximum in each year was located close to our standard sampling depth of 60 m (Figure 3.1E). At the end of the stratified periods, ammonium typically decreased to relatively low concentrations ≤2.0 μmol kg_{sw}^{-1}. However, in 2015, ammonium remained above ~6 μmol kg_{sw}^{-1} (Figure 3.2B).

Despite these repeating patterns of physical mixing and ammonium accumulation, the timing of nitrate accumulation differed between years. The derivative of nitrate with respect to time (Figure 3.3D) indicates that in 2016, nitrate began to increase immediately after the onset of stratification, whereas a delay in accumulation was observed following winter mixing in 2014 and 2015 (Figure 3.2B).

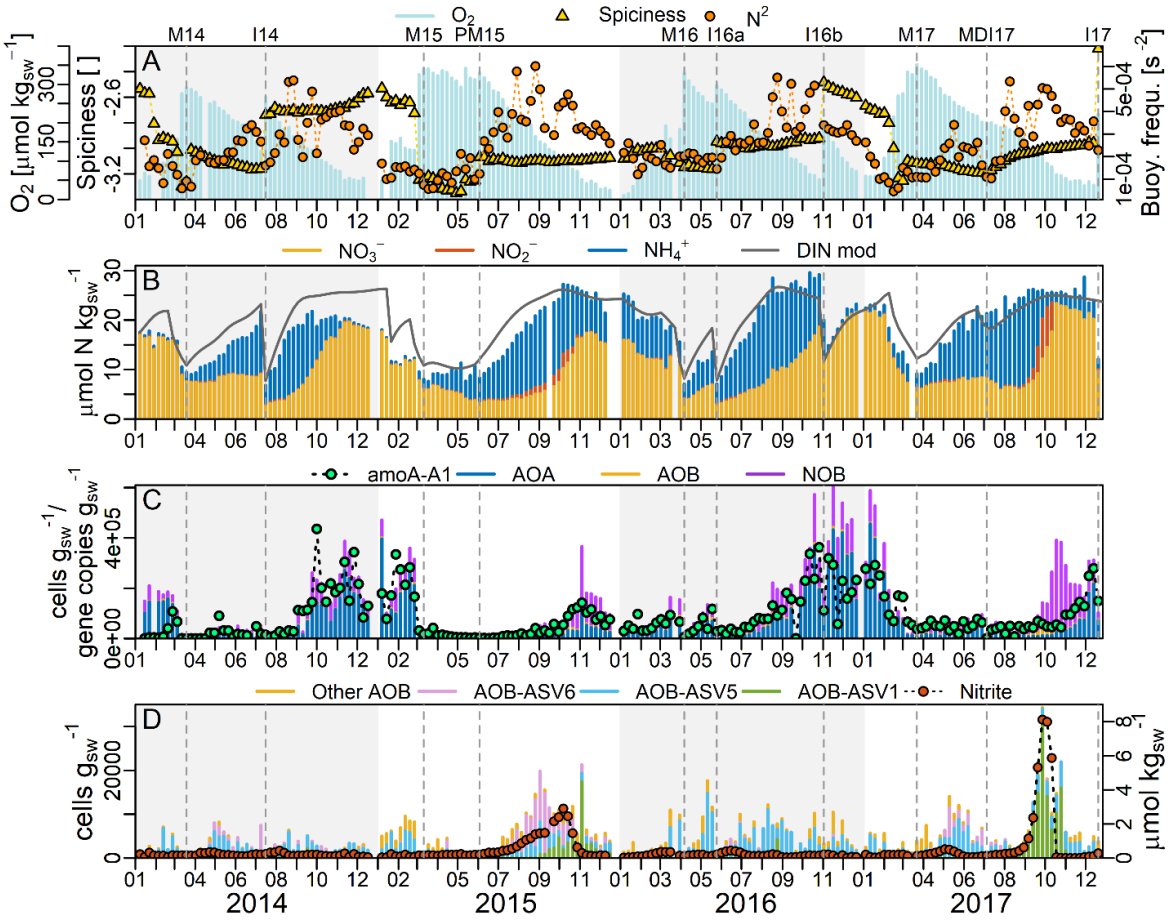

Figure 3.2. Time series of biogeochemical parameters observed at 60 m in Bedford Basin, 2014–2017. A) Buoyancy frequency (N^2), spiciness and oxygen concentration. B) Ammonium, nitrite and nitrate concentration along with modeled DIN concentrations. C) Abundance of *Thaumarchaeota* (AOA), *Nitrospinaceae* (NOB) and *Nitrosomonadaceae* (AOB) affiliated ASVs, as well as amoA-A1. D) Nitrite concentration and the abundance (based on % total 16S rRNA amplicon sequences scaled to total cell counts) of ASVs affiliated with *Nitrosomonadaceae* (NOB). Event numbers ("M", "I", "PM", "MDI") as in Figure 3.1.

3.4.2. Diversity of 16S rRNA Genes Affiliated with Nitrifiers

To examine the diversity of nitrifiers during the time series period, we analyzed the abundance of amplicon sequence variants (ASV) affiliated with the known nitrifiers *Thaumarchaeota* (AOA), *Nitrosomonadaceae* (AOB) and *Nitrospinaceae* (NOB). Relative abundances of nitrifier-affiliated ASVs were scaled to total microbial cell counts (Figure 3.2C,D; *SI Materials and Methods*). The relative abundance of ASVs affiliated with nitrifiers (sum of *Thaumarchaeota*, *Nitrosomonadaceae*, *Nitrospinaceae*) in the microbial community ranged from <0.1% to 38%, which corresponded to 2.1×10^2 – 6.1×10^5 cells g_{sw}^{-1} after scaling to microbial cell counts (Figure 3.2C). AOA abundance (max. 4.5×10^5 cells g_{sw}^{-1}) was similar to other coastal systems (Pitcher et al. 2011; Robidart et al. 2012).

Overall, the AOA ASVs were the dominant ammonia oxidizers in BB. The two most abundant *Thaumarchaeota*-affiliated ASVs, AOA-BB-ASV2 and AOA-BB-ASV3, were closely related with each other and formed a distinct clade within the genus *Nitrosopumilus* (Figure B2B). AOA-BB-ASV3 was most abundant in 2015, while AOA-BB-ASV2 dominated in the remaining years.

AOB were affiliated with the betaproteobacterial family *Nitrosomonadaceae* (beta-AOB; Figure B2A). The relative abundance of beta-AOB was low compared to AOA (Figure 3.2C), but the larger cell sizes of AOB compared to AOA may entail higher biogeochemical impact per cell (Martens-Habbena et al. 2009). Beta-AOB-BB-ASV6, which formed a clade independent of the *Nitrosomonas* and *Nitrosospira* clades (bootstrap support >80%), showed a distinct maximum in fall 2015 (Figure 3.2D; Figure B2A). Beta-AOB-BB-ASV1, which fell into a cluster of *Nitrosomonas*-like BB sequences, had a maximum in fall 2017 and a smaller amplitude maximum in late fall 2015.

NOB were affiliated with the genus *Nitrospina* (Figure B2A). The three most abundant *Nitrospina*-affiliated ASVs showed minima in summer and maxima in fall/winter. *Nitrospirae*-affiliated 16S rRNA genes were present in only a few samples at very small percentage (<0.1%) and did not fall within the genus *Nitrospira* (Figure B2A), suggesting no role for comammox in BB bottom water during the study period (Xia et al. 2018).

3.4.3. Controls on the Temporal Distribution of *amoA* and Nitrifier-Affiliated 16S rRNA ASVs

To investigate how the timing of nitrification may be controlled by variations in nitrifier biomass and diversity, we further characterized the AOA by quantifying six marine phylotypes of the functional gene for ammonia oxidation, *amoA*. The most abundant archaeal phylotype was amoA-A1 (up to 4.4×10^5 *amoA* copies g_{sw}^{-1}), which has been found primarily in ocean surface waters (Sintes et al. 2016). Strong correlation between *Thaumarchaeota*-affiliated ASV and amoA-A1 abundance (Spearman's rho: $R^2 = 0.66$, $p<1\times10^{-47}$; Figure 3.2C) suggested that amoA-A1 variations tracked AOA abundance. The much lower abundance of the other phylotypes ($\leq1.1\times10^4$ copies g_{sw}^{-1}) and their association with mixing events rather than nitrate concentration (Figure B3; Table B1), suggest that these rarer phylotypes were transient populations, which were transported from surface or shelf waters but were unable to establish themselves in the bottom water of BB (*Supplementary Discussion B1*).

Only phylotype amoA-A1 correlated with nitrate (Spearman's rho: $R^2 = 0.42$; $p<1\times10^{-24}$) and its abundance decreased during both winter mixing and intrusion events (Figure 3.2C), which explains its inverse correlation with oxygen (Table 3.1; Table B1; Figure B4). This suggests that amoA-A1 was active and the dominant phylotype. However, in 2017, amoA-A1 abundance did not increase until after the period of rapid nitrite and nitrate increase (September/October; Figure 3.2B,C). A peak in the abundance of *Nitrosomonadaceae*-affiliated ASVs coinciding with this period of steep nitrite and nitrate increase in 2017, suggests a significant role for beta-AOB (Figure 3.2B,C,D).

Table 3.1. Results from Spearman's Rho correlation tests between oxygen concentration, spiciness, nitrifier abundances and their time derivatives (dx/dt) using 2014–2017 BB bottom water data.

Parameter pair		n	r	p
O_2	amoA-A1	196	-0.59	3.90E-20
	AOA	197	-0.6	6.20E-21
	NOB	197	-0.76	6.20E-39
$d(O_2)/dt$	d(amoA-A1)/dt	188	-0.19	0.0105
	d(AOA)/dt	190	-0.28	0.0001
	d(NOB)/dt	190	-0.27	0.0002
d(spiciness)/dt	d(amoA-A1)/dt	193	-0.18	0.0106
	d(AOA)/dt	195	-0.27	0.0001
	d(NOB)/dt	195	-0.14	0.046

A statistically significant correlation was identified between oxygen increase and decreases in the nitrifier proxies amoA-A1 as well as in the AOA and NOB cell densities (Table 3.1). This suggests mixing-associated decreases that can be explained by dilution with BB near-surface water, which was depleted in AOA and NOB (Figure B5) and flushed by the near-surface estuarine circulation and tidal exchange (Petrie and Yeats 1990; Fader and Miller 2008; Shan et al. 2011). Thus, physical mixing with the surface water can act as a net sink for nitrifier biomass, diluting it within the bottom water. Winter mixing coincided with more pronounced nitrifier decreases than the intrusion events of 2014 and 2016 (I14, I16a, I16b; Figure 3.2C). The degree of amoA-A1 dilution by winter mixing varied between years, with more dilution in 2014 (minimum: 11 copies g_{sw}^{-1}, dilution factor $\approx 10^3$) and 2015 (min: 1.0×10^3 copies g_{sw}^{-1}, dilution factor $\approx 10^2$) compared to 2016 (5.6×10^3 copies g_{sw}^{-1}, dilution factor ≈ 10) and 2017 (4.1×10^4 copies g_{sw}^{-1}, dilution factor ≈ 10).

After the strong dilution following winter mixing in 2014 and 2015 (Events M14, M15: Figure 3.2C), delayed regrowth of the nitrifier population was observed, which coincided with delayed nitrate accumulation during the same periods. Conversely, nitrate increased immediately following cessation of winter mixing in 2016 and 2017 (Events M16, M17: Figure 3.2C), when amoA-A1 wintertime minima were less pronounced. The increase in

nitrate and amoA-A1 at the beginning of the 2017 stratified period was interrupted by the mid-depth intrusion of July 2017 (Event MDI17: Figure 3.2C).

3.4.4. A Biogeochemical Model of Nitrogen Cycling in BB Bottom Water

To gain mechanistic insight into the influence winter mixing may have on nitrifier growth dynamics and nitrification rates, a simple N-cycling box model was constructed for the BB bottom water (Figure B6; Table B2, Table B3, Table B4). Conceptually this model is analogous to a bioreactor, where a resident population of nitrifiers actively grows below the pycnocline but can be diluted through time-varying exchange with BB near-surface water (by winter mixing) or Scotian Shelf water (by intrusions; Figure B6). During the stratified period, the nitrifiers remain relatively isolated from the surface water and dilution is negligible. During winter mixing or intrusion events, the population is subjected to dilution as the exchange term increases. If the dilution rate is much faster than the growth rate, then washout of the "bioreactor" can occur. At the low dilution rate applied during stratified periods, net population growth can occur.

Use of a single set of rate constants for N remineralization, AO and NO (Table B4) was sufficient to reproduce the overall seasonal trends in DIN and *amoA* copies observed at 60 m from 2014–2017 (Figure 3.3). Much of the observed inter- and intra-annual variability was resolved by this simple model, including the delayed nitrate production in 2014 (pre-intrusion) and 2015, as well as the immediate nitrate increases following 2015/16 winter mixing and the intrusion events in 2014 and 2016 (Figure 3.3). A Q_{10}-type temperature dependence for the rate constants of AO, NO and N remineralization was required to represent the increased ammonium and nitrate production rates following the intrusion events, which delivered warmer water (Figure 3.1B; Table B4; *Supplementary Discussion B2*).

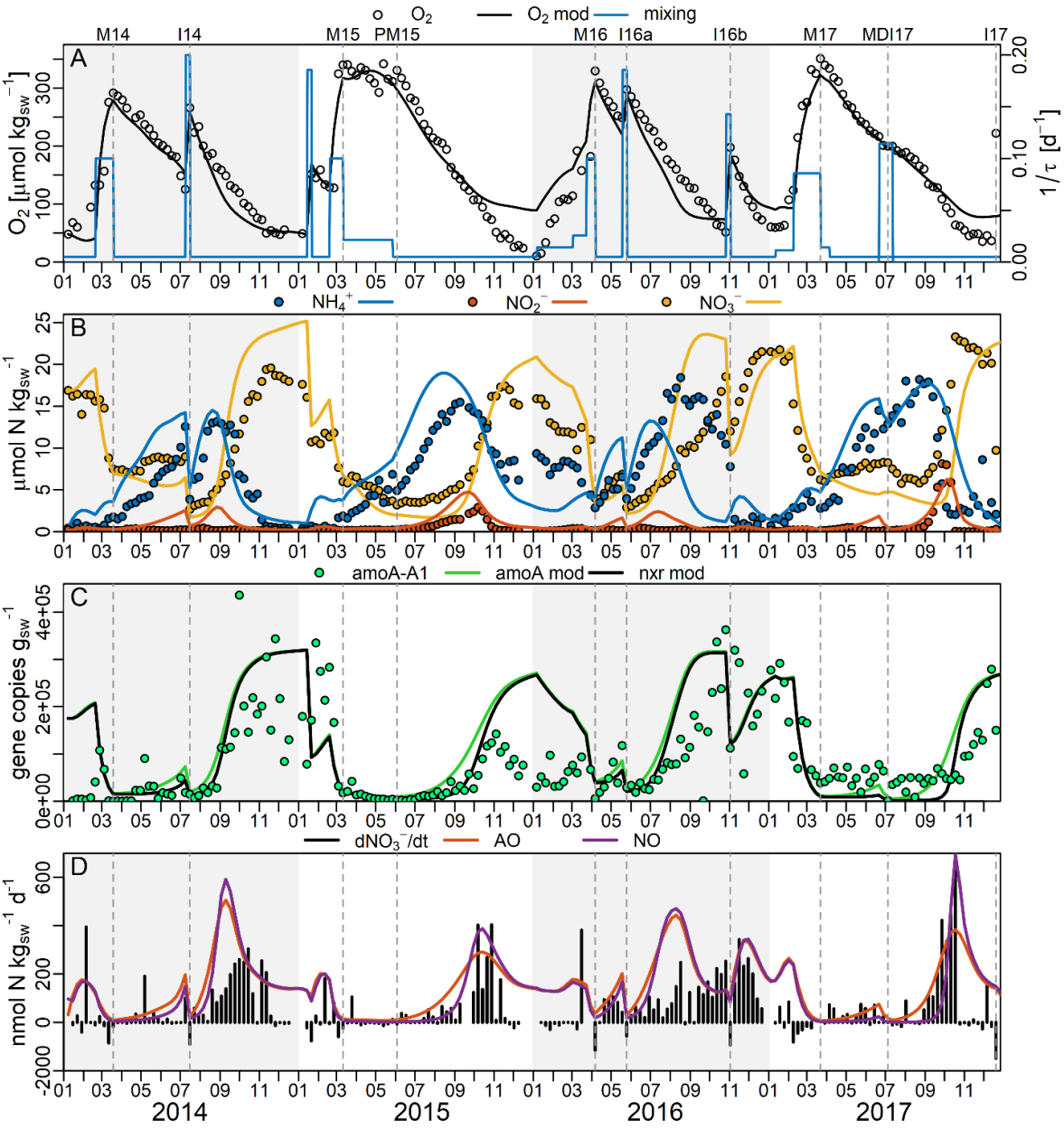

Figure 3.3. Time series of observed (scatter or bar) and modeled (lines: "mod") biogeochemical parameters at 60 m in Bedford Basin, 2014–2017. A) Oxygen concentrations (modeled and observed) and the inverse of residence time τ, describing the timescale of exchange of Bedford Basin bottom water with water from the basin surface or the shelf. B) Observed and modeled ammonium, nitrite and nitrate concentrations. C) AmoA-A1 (modeled and observed) and *nxr* (modeled) gene abundance. D) Modeled rates of ammonia oxidation and nitrite oxidation as well as time derivative of observed nitrate concentration, dNO_3^-/dt (note the less detailed scale for negative values). Event numbers ("M", "I", "PM", "MDI") as in Figure 3.1.

3.4.5. Variability in Modeled Nitrification Rates was Caused Mainly by the Dilution of Nitrifier Biomass by Physical Mixing

The modeled representation of AOO population density, which was parameterized as a function of growth by AO as well as dilution by mixing (Table B2), approximated the observed time series of amoA-A1 abundance (Figure 3.3). After the long and intense winter mixing period of 2015 (Events M15, PM15: Figure 3.3A), which reduced the nitrifier population to very low levels (Figure 3.2C), the modeled AO rate took several months to increase substantially (Figure 3.3D) despite the presence of >5 μmol kg_{sw}^{-1} ammonium during this period of delayed nitrification. In 2016, when shorter and less intense winter mixing resulted in less dilution of the nitrifier population, nitrification rates increased immediately after mixing ceased.

Experiments with the model supported the interpretation that dilution of the AOO population during winter delayed nitrification: manipulation of the diluting effect of 2015 winter mixing on *amoA* gene copy numbers, while holding its effect on all other parameters constant, resulted in extended (increased influence of mixing on nitrifiers) or shortened (decreased influence) delay in both nitrifier growth and nitrate production (Figure 3.4).

Further empirical support for the role of winter mixing in delaying nitrification came from a statistical evaluation of physical and geochemical parameters from the full-length BB time series (>10 years; Appendix B; Table B1, Table B5). Spiciness during the years 2014–2017 was lowest in March of 2015 (Event M15: Figure 3.2A). Using data from the full-length time series, we observed that the magnitude of the annual spiciness minimum during winter (January–April) as well as the annual average oxygen concentration correlated with both the annual average nitrate concentration and the annual average value of the nitrate/ammonium ratio (Table B5). The minimum spiciness and annual average oxygen concentration parameters may represent empirical indices of winter mixing intensity (minimum spiciness) and mixing intensity in general (average oxygen) so that these correlations are consistent with an overall negative effect of mixing on nitrification in BB.

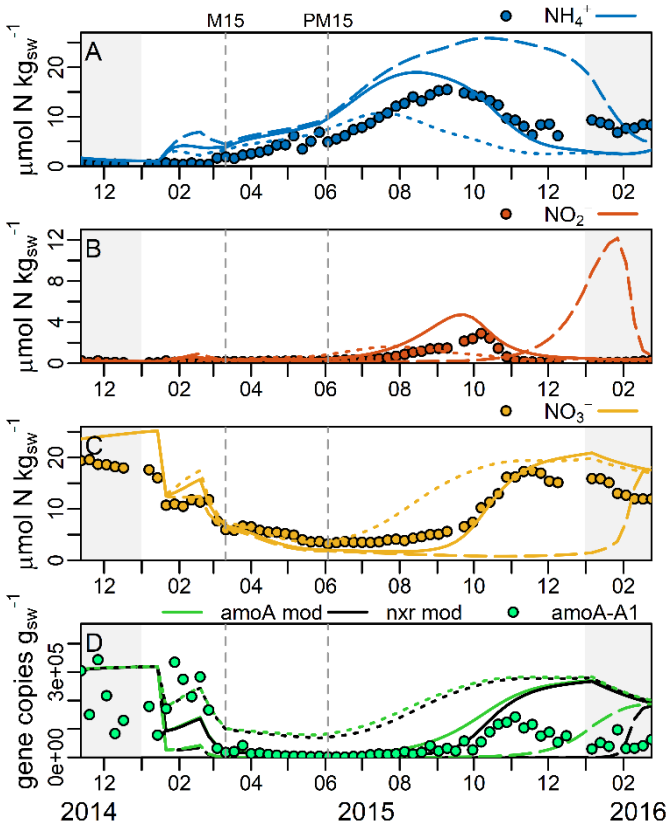

Figure 3.4 Observations and model output as in Figure 3.3, but focused on the year 2015 and showing the output from experimental model runs for which the effect of winter mixing on *amoA* and *nxr* was manipulated during winter mixing of 2015 (January 14th – May 27th). For this manipulation, the diluting effect of mixing on the nitrifier marker gene populations was multiplied by 2 (dashed lines) or divided by 2 (dotted lines) compared to the standard model (solid lines). A) Ammonium concentrations; B) nitrite concentrations; C) nitrate concentrations; D) *nxr* (modeled only) and *amoA* concentrations. Event numbers ("M", "I", "PM", "MDI") as in Figure 3.1.

3.4.6. Nitrite Accumulation as Another Consequence of Nitrifier Biomass Dilution

The model was able to represent the nitrite peaks observed in September/October 2015 and 2017 (Figure 3.3B). They appeared when modeled *amoA* exceeded *nxr* (the modeled functional gene for NO) during periods of regrowth following dilution of these populations (Figure 3.3B,C). This implies that nitrite accumulated due to decoupled regrowth of the two nitrifier populations after their dilution. Experiments with the model additionally

demonstrated that increased dilution of nitrifier populations by mixing could have increased (and delayed) the accumulation of nitrite (Figure 3.4).

Hence, despite the model's use of a much higher rate constant for NO compared to AO (Table B4), AOO growth temporarily outpaced NOB growth following strong dilution. This was partly because ammonium had accumulated during the nitrification delay, whereas the production of nitrite (by AO) was slow. When the populations are strongly diluted by mixing (as in 2015), substantial NOB regrowth can only begin following production of nitrite by AOO: this causes temporary decoupling of AO from NO. With weaker mixing, sufficient AOO and NOB are retained in the bottom water from the previous year so that AO and NO remain closely coupled, precluding accumulation of nitrite (as in 2016). Although not represented in the model, decoupling may be enhanced by the activity of beta-AOB, which showed maxima coinciding with both the 2015 and 2017 nitrite maxima (Figure 3.2D).

3.5. Discussion

The discussion starts with an examination of the role of beta-AOB in enhancing nitrite accumulation and factors that influence their growth. It is argued that physical mixing not only dilutes nitrifier biomass but can also cause transient shifts in community composition which have biogeochemical consequences. Lastly, the broader relevance, implications as well as unknowns related to the mixing-induced, transient changes in nitrifier biomass and diversity observed in the Bedford Basin time-series are discussed.

3.5.1. Transient Beta-AOB Growth Associated with Nitrite Accumulation Suggests Mixing-induced Shifts in the Dominant Ammonia Oxidizer

Nitrosopumilus-like *Thaumarchaeota* (AOA) of the amoA-A1 phylotype were consistently present in BB bottom water and were the overall dominant ammonia oxidizers during the 4-year period. However, short-lived peaks in beta-AOB-affiliated ASVs were also observed, which coincided with the largest observed nitrite accumulations and were followed by steep nitrate increases (Figure 3.2B,D). These AOB peaks appeared when high

ammonium concentration coincided with strong dilution of the nitrifier community in 2015 and after the mid-depth intrusion of July 2017, which suggests that opportunistic, fast-growing AOB may have temporarily outcompeted slower-growing AOA and were involved in creating the relatively large (>1 μmol kg_{sw}^{-1}) nitrite accumulations.

We suggest that mixing may have created temporary niches for the beta-AOB. AOB have higher V_{max} (~300 μM N h^{-1}) and K_m (2–10,000 μmol L^{-1}; Suzuki et al. 1974; Ward 1987; Bollmann et al. 2005) compared to AOA (K_m: ≤0.1 μmol L^{-1}, V_{max}: 0.9 μM N h^{-1}; Martens-Habbena et al. 2009; Horak et al. 2013; Peng et al. 2016). Generally, organisms adapted to lower nutrient concentrations ("K-selected") have lower growth efficiency and are favored in stable environments (Pianka 1970; Vallino 2011; Dutkiewicz et al. 2013). Hence, faster-growing, "r-selected" AOB may have temporarily outcompeted "K-selected" AOA in 2015 and 2017 following strong dilution of the nitrifier community. The high ammonium concentrations would then additionally favor faster-growing beta-AOB. As these AOB eventually became substrate-limited by depleting the ammonium below their K_m, the AOA population re-established its dominance (Figure 3.2C,D). In 2016, relatively weak mixing during the prior winter allowed a resident AOA population to persist so that it was ready to utilize ammonium as it became available following the onset of stratification (Figure 3.2A,B,C). Even when ammonium accumulated to high concentrations later that year, AOA were established in a stable environment, which allowed them to outcompete AOB.

The relatively steady nitrate increase and negligible nitrite accumulation observed in 2016 may reflect the lower V_{max} of the AOA that were dominant in that year. The steeper nitrate increases following the nitrite accumulations of 2015 and 2017 likely reflect the higher V_{max} of beta-AOB (Suzuki et al. 1974; Bollmann et al. 2005; Martens-Habbena et al. 2009), whose appearance coincided with both nitrite maxima (Figure 3.2D). Hence, fast enzyme kinetics of beta-AOB likely enhanced nitrite accumulation by promoting the decoupling from NOB growth and further translated into steep nitrate increases once the NOB population was large enough to decrease the initially accumulated nitrite.

We note that the slow and steady nitrate increase of the 2016 stratified period, when AOB played a negligible role, was overestimated by the model, whereas the steep nitrate

increase in September/October 2017, which was associated with the highest abundance of AOB-affiliated ASVs (Figure 3.2C,D), was more closely reproduced (Figure 3.3C). This suggests that the fixed set of rate constants employed in the model are more representative of faster "AOB-type" nitrate production (2015, 2017) than slower "AOA-type" nitrate production (2014, 2016). This may also explain the "false" nitrite peaks generated by the model during the AOA-dominated years 2014 and 2016 (Figure 3.3B). Indeed, use of a different AO parameterization in an otherwise identical model was able to better represent the absence of strong nitrite accumulation and the steady nitrate increase observed in 2016, but strongly overestimated the delay in nitrate accumulation in 2015 and 2017 (Figure B7). It appears that a more complex model with at least two kinetically distinct AOO populations would be required to explore the competition based on kinetic differences suggested by these observations. The observations demonstrate how mixing can affect not only the biomass of nitrifiers but also their community composition with consequences for the transformation of nitrogen species. This, in turn, suggest that explicit modeling of nitrifier biomass and its diversity may be important for understanding nitrogen cycling in dynamic coastal systems and projecting its response to variable climate forcing.

3.5.2. Model-Observation Mismatches

Mismatches between model and observations can point to unknown influencing factors or levels of complexity not captured by the model. As described in the previous sections, some of the smaller mismatches of the model with nitrate concentration data shown in Figure 3.3B were likely a result of attempting to model the entire four-year period using a fixed AO rate constant, despite known kinetic differences between AOB and AOA. The largest model-data mismatch occurred in November 2015, when nitrate accumulation stopped and amoA-A1 abundance started to decrease, despite ~6 μmol kg_{sw}^{-1} ammonium still being present (Figure 3.3B,C). This observation was not captured by the model and may have been due to a combination of grazing (which is not represented in the model) and low prevailing oxygen concentrations (~50 μmol kg_{sw}^{-1}, decreasing further to the 4-year minimum of 11 μmol kg_{sw}^{-1}). Oxygen concentrations were overestimated by the model during this period, which may also be a consequence of stronger stratification in 2015

compared to other years. We hypothesize that low oxygen concentrations may have limited AO and caused AOO growth rates to fall below the level of grazing rates (Verhagen and Laanbroek 1992; Anderson et al. 2012; Qin et al. 2017). Once this threshold was crossed and oxygen concentration continued to decrease (as observed; Figure 3.2A), AOO growth could not exceed losses to grazing, leading to continued decrease until the system was reset by mixing. Identification and quantification of grazers as well as a more complex model that includes grazing would be required to explore this hypothesis further.

3.5.3. Broader Relevance of the Model-Derived Ammonia Oxidation Rates and Underlying Microbiology

Similar ranges and variability in AO rates to those described here were observed in BB bottom water by Punshon and Moore (2004), who measured AO rates using isotopic labelling experiments throughout 2002, but did not have supporting data describing the nitrifier community. Notably, they found low rates associated with mixing: in two successive weeks at the end of the 2002 winter mixing period, rates were undetectable in the presence of ammonium concentrations >1 μmol kg_{sw}^{-1}. Overall, they found no correlation of their AO rates with either temperature or ammonium concentration, which led them to speculate about an influence of variable nitrifier biomass on AO rates.

Here we show that this lack of correlation as well as variable AO rates can indeed be understood from the effect of variable nitrifier biomass, which masks the effect of ammonium and temperature on AO rates. Our model, which parameterizes the influence of nitrifier biomass, temperature and ammonium concentration on AO rates (Table B3), was able to reproduce the trends observed in BB bottom water during 2002 following adjustment of the mixing and surface boundary conditions to reflect the conditions of that year (Figure B8). That is, using model parameterizations that had been tuned to represent the 2014–2017 time series (Figure 3.3), it was possible to reproduce the independently collected nitrate and ammonium concentration data and AO rates measured in 2002 (Figure B8). This suggests that dilution of ammonia oxidizer biomass by winter mixing was the reason for the low rates of AO measured in March 2002 (Punshon and Moore 2004).

In order to compare nitrification rates and the underlying nitrifier community observed in BB with other regions of the ocean, we estimated single-cell AO rates from the annual maximum modeled volumetric rates and the annual maximum observed *amoA* copies g_{SW}^{-1}. Given that *Nitrosopumilus* contain only one *amoA* copy per genome (Walker et al. 2010), we assumed that *amoA*-based rates equal rates per AOA cell. The estimated rates in the AOA-dominated years 2014 and 2016 then were 1.5 and 1.3 fmol NH_3 $cell^{-1}$ d^{-1}, respectively. These values are within the range of cell-specific AO rates for AOA (1–8 fmol NH_3 $cell^{-1}$ d^{-1}) measured in the Gulf of Mexico (Kitzinger et al. 2019, 2020). Further, the most abundant NOB ASVs found in BB (NOB-BB-ASVs 3–5) were phylogenetically related to NOB from the Gulf of Mexico based on their 16S rRNA gene sequences (Figure B9). Although the most abundant AOA ASVs found in the BB (AOA-BB-ASVs 2&3) formed a separate clade from Gulf-of-Mexico ASVs, they were still closely related (98–99% similarity) to those and other environmentally relevant *Nitrosopumilus* species (Figure B10). This suggests that microbial diversity and AO kinetics underlying the time series observations in BB are representative of nitrifiers in other parts of the ocean.

3.5.4. The Cause of Nitrite Accumulations and Nitrification Delay in BB Bottom Water

Our analyses of the time series reveal a negative control by winter mixing on nitrate production via its effect on nitrifier biomass and diversity (Figure 3.2, Table 3.1). During winter, surface water cooling drives convective mixing, which dilutes the bottom waters with nitrifier-depleted surface water (Figure B5). The estuarine circulation and tidal exchange in the surface layers can then remove the nitrifiers from the basin (Petrie and Yeats 1990; Fader and Miller 2008; Shan et al. 2011). Colder winters with stronger mixing were associated with stronger nitrifier biomass dilution and subsequent nitrification delay, nitrite accumulation and beta-AOB growth (Figure 3.2). The importance of mixing is corroborated by statistical analyses of the long-term time series which shows negative correlation between mixing proxies and the annual average nitrate concentration (Table B5; Table B6; Appendix B). Additionally, a simple model with uniform rate constants was

able to reproduce observed inter-annual differences in nitrifier regrowth and the timing of nitrate accumulation based on variations in mixing intensity (Fig. 3, Figure 3.4).

On this basis, we propose a mechanism by which mixing dilutes nitrifier biomass, leading to both delay and decoupling of nitrification due to delays in nitrifier regrowth. As observed, ammonium that accumulated during periods of AO delay can eventually fuel fast AOO growth. Temporarily, this can outpace regrowth of the NOB, which require time to adjust their population size once increased amounts of nitrite become available. The resulting high AO rates temporarily exceed NO rates, which drives nitrite accumulation. An additional effect of mixing on nitrifier community composition favored beta-AOB in their competition with AOA, which enhanced the nitrite accumulation.

The transient response of the nitrifier community has some analogy with the well-known effect observed in laboratory incubations, in which a substrate for nitrification, either ammonium or organic matter, is added to a batch of seawater depleted in nitrifiers. Sequential accumulation of ammonium and nitrite is typically observed in such experiments prior to nitrate accumulation and is generally attributed to delayed, transient growth of AOO and NOB responding to availability of their respective substrates (von Brand et al. 1937; Buchwald et al. 2012). For example in the classical experiment of von Brand et al. (1937), a dark incubation of filtered, low-DIN seawater with added particulate organic matter resulted in the sequential accumulation of ammonium and nitrite prior to eventual accumulation of nitrate after a ~1-month delay.

Our results demonstrate that sufficiently strong physical mixing is a natural mechanism that can "reset" nitrifier biomass to low levels and initiate sequential accumulation of ammonium, nitrite and nitrate. This mechanism adds to a variety of environmental factors including light, copper and temperature, which are known to potentially inhibit, limit or decouple nitrification (Groeneweg et al. 1994; Joye and Hollibaugh 1995; Philips et al. 2002; Merbt et al. 2012; Amin et al. 2013; Schaefer and Hollibaugh 2017). Mixing has previously been shown to impact nitrification by bringing ammonium-rich waters in contact with oxygenated water (McCarthy et al. 1984; Laperriere et al. 2019). Recently, a modeling study suggested that steady-state accumulation of nitrite as a function of depth

in the water column of the oligotrophic ocean may be controlled, in part, by the mixing of NOB biomass away from their optimal depth (Zakem et al. 2018).

Our study provides detailed observations coupled with a mechanistic representation showing how mixing can control the temporal dynamics of nitrifier populations and nitrification in an intermittently stratified system. This implies that there are levers with which variable climate and weather conditions can impact the timing of nitrification and thereby the composition of DIN produced (ammonium:nitrite:nitrate ratio). It is therefore worthwhile considering whether this mechanism is relevant elsewhere or even globally.

3.5.5. Broader Significance of Mixing-Induced Dilution and Shifting of Nitrifier Communities

Any water column subject to intermittent, sufficiently strong physical mixing disrupting less turbulent periods may, in principle, be susceptible to the identified mechanism. If water brought in by mixing or advection is relatively poor in viable nitrifier biomass but contains ammonium or organic N, ammonium and nitrite may consequently accumulate due to delayed nitrification and associated temporal decoupling of nitrification. This may apply to subsurface waters of seasonally mixed lakes where climatic variations can affect the extent of spring mixing (Salmaso 2005), fjord-like basins and estuaries similar to BB with stratification-mixing cycles and/or irregular intrusion events (Horrigan et al. 1990b; Ma et al. 2019; Kelly et al. 2020), and even shelf systems subject to seasonal blooms and sinking of organic matter, periodic upwelling or seasonal changes in shelf-slope exchange (Mordy et al. 2010; Santoro et al. 2013).

Hence, the identified mechanism may be widespread, but high-frequency time series of long duration that include microbiological markers to trace biomass variations may be required to recognize and elucidate its global distribution. The sparsity of such time series datasets, especially those with high temporal resolution, might explain why this mechanism has not been described previously.

There are, however, some indications in the literature for its occurrence. For example, higher *Thaumarchaeota* numbers were observed in near-surface waters of Monterey Bay during stratification in fall compared to relatively unstratified waters in spring (Robidart et

al. 2012). Hollibaugh et al. (Hollibaugh et al. 2014) made similar observations in coastal surface waters off Georgia (USA), using seasonal sampling: the highest copy numbers of thaumarchaeal *amoA* and 16S rRNA genes were found at the end of the stratified period, while much lower numbers were found earlier in the stratified period and prior to the onset of stratification. A follow-up study on the same system suggested that accelerated growth of AOA under high summer temperatures might have been responsible for decoupling of nitrification and nitrite accumulation (Schaefer and Hollibaugh 2017). However, the observed increase of AOA during the stratified period may also be consistent with the mechanism presented here, whereby physical mixing dilutes the nitrifier community, causing nitrite peaks upon AOA regrowth.

Seasonal variations in nitrification and nitrifier biomass as well as transient nitrite accumulation have been observed in many other marine coastal and shelf systems and the causal mechanisms are often poorly understood (Horrigan and Springer 1990; Mordy et al. 2010; Robidart et al. 2012; Hollibaugh et al. 2014; Schaefer and Hollibaugh 2017; Laperriere et al. 2019). Schaefer and Hollibaugh (Schaefer and Hollibaugh 2017) suggested that high temperature may decouple nitrification by promoting rapid AOO growth. Decoupling by rapid AOO growth may also underly observations of nitrification decoupling associated with sudden availability of ammonium (Pitcher et al. 2011; Ma et al. 2019). The mechanism involving physical dilution described here relies on a similar principle to decouple nitrification by eventual fast AOO growth (following delayed AOO regrowth), leading to AO>NO and nitrite accumulation (Figure 3.4B,D). This suggests that, rather than NOB inhibition or limitation, AOO growth variations that cannot be immediately matched by NOB growth may be a common driver of transient nitrite accumulation in many aquatic systems.

3.5.6. Physical Nitrifier Biomass Dilution as a Link Between Climate, Nitrification and Phytoplankton Ecology

Our analysis of the BB time series demonstrates a link between weather- and climate variability and sub-euphotic zone nitrification with potential implications for phytoplankton ecology. Atmospheric forcing plays an important role in stratification-

mixing patterns of ocean waters (Capotondi et al. 2012). For example, infrequent deep water renewal events in a coastal basin have been linked to freshwater run-off and other atmospherically controlled variables (Kelly et al. 2020). In BB, winter mixing is largely driven by heat loss to the atmosphere (Li and Harrison 2008; Shan et al. 2011). Particularly in 2014 and 2015, large spikes in spiciness and oxygen occurred from one week to the next (Events M14, M15: Figure 3.2) and suggested that winter mixing occurs episodically on weekly or sub-weekly timescales, possibly driven by individual storms or cold-weather periods. Since sufficiently strong winter mixing can delay nitrification, winter temperatures and possibly individual storm- or cold-weather events could strongly influence the timing and extent of nitrification for the remainder of the year.

Further, the DIN from below or near the base of the euphotic zone, where most nitrification takes place in BB and elsewhere in the ocean (Horak et al. 2013; Santoro et al. 2013; Peng et al. 2016), can be delivered to the euphotic zone upon destratification or by other upward transport mechanisms (Johnson et al. 2010), including, for example, the intrusions in BB. Within the euphotic zone, variations in DIN supply can impact phytoplankton ecology and the health of aquatic ecosystems. For example, a high share of ammonium in DIN supply has been linked to lower primary productivity and selection against diatoms and towards smaller algal species with higher potential to form harmful algae blooms (Yoshiyama and Sharp 2006; Domingues et al. 2011; Glibert et al. 2016). Hence, the identified link between physical mixing and nitrification may have important impacts on seawater chemistry linked to phytoplankton-driven primary productivity in coastal systems.

For Atlantic Canada, as for many other temperate regions, the increase in winter temperatures and changes in storm patterns observed over the past decades are projected to continue in the future as a result of climate change (Greenan et al. 2019; Zhang et al. 2019). This may alter the frequency of winters with weak mixing facilitating rapid nitrification in BB, thus constituting an effect of climate change on DIN composition and, by extension, phytoplankton ecology (Glibert et al. 2016). Future research on mixing-induced shifts in nitrifier diversity and biomass in other coastal systems is necessary to

elucidate the quantitative importance of this mechanism and its climate sensitivity on local and global scales.

3.5.7. Concluding Remarks

The time series and modeling study presented here demonstrates a biogeochemically relevant impact of climate-sensitive physical processes on both nitrifier community composition and biomass. Model-observation mismatches (Figure 3.3) suggest an influence of additional factors that were not parameterized in the model, including the explicit representations of AOA and AOB functional types as well as biomass loss terms, such as grazing. Similarly detailed time series of functional microbial biomass and diversity may be required to investigate the distribution, and therefore global significance, of such mixing-induced, dynamic effects on nitrification. Such data is also needed to tune or test biogeochemical models. This study emphasizes the importance of multi-parameter, high-frequency oceanographic time series and of biogeochemical models that explicitly parameterize kinetically distinct nitrifier community members.

3.6.Materials and Methods

3.6.1. Bedford Basin Study Site, Sampling and Time Series Context

Descriptions of the study site, the long-term time series context, sampling procedures and the source of atmospheric data are detailed in *SI Materials and Methods*.

3.6.2. Analysis of Bulk Nutrient, Particulate and Chlorophyll *a* Concentrations

Nutrients, particulates and chlorophyll *a* were analyzed by standard methodology, as detailed in *SI Materials and Methods*.

3.6.3. Numerical Modeling

A box model was used to simulate annual N cycling in the bottom water of BB and investigate possible mechanisms for temporal decoupling of N remineralization, AO and

NO (Figure B6). The use of a box model was motivated by a lack of spatial resolution in our data set, and the philosophy of not making the model more complicated than the resolution of the data we are seeking to understand. The model equations (Table B2) compute the change in state variable concentration *(dC/dt)* with time. These include chemical concentrations (O_2, NH_3/NH_4^+, NO_2^-, NO_3^-), and two microbial populations, represented by the marker genes for ammonia (*amoA*) and nitrite oxidation (*nxr*). A complete list of differential equations, reactions and rate parameters are presented in Table B2, Table B3 and Table B4. The initial remineralization reaction was forced by weekly particulate organic carbon (POC) data from 60 m and accounted for seasonal variability in remineralization (e.g. the spring bloom), which was not explicitly represented in the model. Remineralization consumes POC and O_2, producing NH_3/NH_4^+ according to the Redfield ratio (Table B3). Nitrification was modelled as a two-step process: AO ($NH_3/NH_4^+ \rightarrow NO_2^-$) facilitated by ammonia oxidizers (*amoA*) and NO ($NO_2^- \rightarrow NO_3^-$) facilitated by nitrite oxidizers (*nxr*), both also consuming O_2. A Q_{10} formulation was used to represent the influence of temperature on the rate constants for remineralization and nitrification (Table B3). A loss term for NO_3^- was included, representing the loss of NO_3^- to N assimilation by chemoautotrophs as well as denitrification, both in the sediment and potentially the anoxic micro-zones associated with particles (Bianchi et al. 2018). Empirically, it accounts for the fact that remineralization with Redfield stoichiometry over-predicts DIN concentrations in the latter half of each year when DIN:P ratios decline at 60 m in BB (Figure B11). An additional loss term for O_2 represents sediment uptake and respiration by higher organisms in the water column that produce organic N instead of ammonium and therefore are not covered by the remineralization term (*R.remin*).

The model assumes that the bottom water of BB is one stable box that only marginally interacts with the surface water (5 m) during the stratified period which prevails for most of the year. During mixing periods (winter/spring), the water column overturns, mixing the bottom water with surface water. Additionally, short-lived, randomly timed intrusions introduce shelf-water into the bottom water. Mixing was implemented with the following mathematical relationship:

$$\left.\frac{\partial C_i}{\partial t}\right|_{mix} = \frac{1}{\tau} \cdot \left(C_i^{5m} - C_i\right) \quad 3.3$$

Where C_i is the concentration at 60 m of the state variable in question, C_i^{5m} is its concentration in the surface water (5 m) and τ is the exchange timescale of bottom water with surface water from within the basin or the Scotian Shelf. For the stratified period, this timescale was chosen based on the eddy diffusivity values from Bedford Basin determined by Burt et al. (2013) and a length scale from the depth of the sill to the bottom of basin (~50 m) according to the relation h^2/K_z. During the intrusion events, τ was decreased to a small value to recreate the sudden step-like O_2 concentration changes observed in our weekly timeseries. During winter, when convective cooling and storms homogenize the basin water, τ was decreased to reproduce the specifically observed increase in bottom water O_2 during this time. O_2 was used as tracer of mixing, because its non-conservative nature makes it a particularly sensitive tracer of active mixing. Since the surface was the only source of O_2 to the bottom water, active mixing at a rate exceeding oxygen consumption was needed to increase or maintain oxygen concentrations. Conservative tracers, on the other hand only provide evidence of past mixing. It is assumed that the timeseries of weekly measurements at 5 m depth for O_2, NO_3^-, NO_2^-, NH_3/NH_4^+, are representative of the surface water that is exchanged with the basin bottom water and are used as the top boundary condition. The concentrations of *amoA* and *nxr* were taken to be 0 in the surface water (Figure B5). Unlike the remaining intrusion and winter mixing events, the 2017 mid-depth intrusion was modeled as an exchange of 60-meter water with a water mass representing BB mid-depth water (200 µmol O_2 kg_{sw}^{-1}, 12 µmol NH_4^+ kg_{sw}^{-1}, 5 µmol NO_3^- kg_{sw}^{-1}, 0 µmol NO_2^- kg_{sw}^{-1}, 0 gene populations).

To constrain the kinetic parameters, the O_2-half saturation constants for AO and NO were chosen from literature values (Table B4). The rate constants for remineralization (*k.remin*), AO (*k.AO*) and NO (*k.NO*) were fit to the four year times series by minimizing the cost function:

$$\sum_j \sum_i \left(\frac{y_{ij}^{mod} - y_{ij}^{obs}}{\overline{y}_i}\right)^2 \quad 3.4$$

where y_{ij}^{mod} and y_{ij}^{obs} are the modelled and observed concentrations of i (= O_2, NO_3^-, NO_2^-, NH_3/NH_4^+) at time j, and $\overline{y}_i$ is the average concentration of each in the time series. The model was coded in the programing language R, using the package 'deSolve' to solve differential equations (Soetaert et al. 2010) and the package 'FME' for least-square fitting (Soetaert and Petzoldt 2010).

3.6.4. Microbial Cell Counts

Total microbial cells <35 μm were stained with SYBR™ Green I (Invitrogen) and quantified by flow cytometry, as detailed in *SI Materials and Methods*.

3.6.5. DNA Extraction, 16S rRNA Amplicon Sequencing, Sequence Analysis and Deposition

DNA extractions of 0.2–160 μm fractionated seawater were completed as previously described (Haas et al. 2019) and amplicon sequencing of the V4-V5 variable region of the16S rRNA gene of bacteria and archaea was conducted at the Integrated Microbiome Resource, Dalhousie University (Comeau et al., 2017, and methodology therein). Illumina sequences of the 16S rRNA gene were processed using a QIIME-2 based workflow (Bolyen et al. 2019) as described in *SI Materials and Methods*. Phylogenetic trees were built as described in *SI Materials and Methods*.

3.6.6. Quantitative PCRs (qPCR)

Six oceanic archaeal phylotypes of the archaeal *amoA* gene (amoA-A1, -A2, -A3, -A4, -A5 and -A6) as defined by Sintes et al. (Sintes et al. 2016) were quantified by qPCR. Details of the assays used to quantify the different phylotypes can be found in *SI Materials and Methods* and in Table B7 and Table B8.

3.6.7. Deposition of DNA Sequences, Data and Model Code

The subset of ASV sequences used in this study (i.e. affiliated with potential nitrifiers) was deposited in GenBank under the accession numbers MT175443-MT175495. Other data as

well as model code related to this work was submitted to the Pangaea database: https://doi.pangaea.de/10.1594/PANGAEA.914705. The subset of data produced by the Bedford Institute of Oceanography can additionally be accessed under this link: http://www.bio.gc.ca/science/monitoring-monitorage/bbmp-pobb/bbmp-pobb-en.php.

CHAPTER 4

IN SITU NITROGEN ISOTOPE FRACTIONATION DURING NITRIFICATION REVEALED BY TWO YEARS OF WEEKLY TIME SERIES MEASUREMENTS IN A EUTROPHIC COASTAL BASIN[3]

4.1. Abstract

Here we analyzed nitrogen stable isotope effects associated with nitrification based on detailed *in-situ* time series measurements in a coastal basin. Measurements of $\delta^{15}N$ in multiple N species (particulate nitrogen, ammonium, nitrite, nitrate) were conducted weekly throughout two years. These year-long time series represented two contrasting natural experiments in the sub-euphotic zone, ammonium-rich bottom water (60 m) of Bedford Basin, Nova Scotia, Canada. In one year (2014) the system was dominated by archaeal ammonia oxidation and nitrite remained low (<0.5 μmol kg^{-1}), while in the other year (2017), bacterial ammonia oxidation played a role in causing transient nitrite accumulation of ~8 μmol kg^{-1}.

---

[3] Sebastian Haas, Subhadeep Rakshit, Tim Kalvelage, Carolyn Buchwald, Christopher K. Algar, Douglas W.R. Wallace: Manuscript in preparation for publication.

Author contribution: *Following up on early work by Tim Kalvelage who put in place initial protocols for N isotope analysis and analyzed samples from the first year of the time series, I performed a major part of the nitrogen isotope laboratory analyses and was responsible for optimizing the methodology and protocols within the CERC.OCEAN laboratory, but also had significant support in laboratory analysis from technicians. With inspiration and advice from my co-authors, I conceived of the study, analyzed and interpreted the data and wrote the chapter. I helped further develop the model, which was initially developed by co-authors.*

A particularly rapid $\delta^{15}N_{NH4}$ increase observed in fall 2017 was associated with high AO rates, likely driven by bacterial ammonium oxidizers. Overall, however, we found high inter-annual similarity in isotope fractionation associated with nitrification between the two years. High-confidence estimates of the isotope effect associated with ammonia oxidation ($^{15}\varepsilon_{AO}$, best estimates: 21.8 ±2.2‰ and 24.1 ±1.1‰) were derived from Rayleigh models of *in situ* data taken during periods when the bottom waters approximated a closed system. During these periods, any influence of isotope effects on these $^{15}\varepsilon_{AO}$ estimates from other processes, such as ammonium assimilation, was shown to be insignificant. Using a numerical model, we found that the best fit to the ^{15}N data required $^{15}\varepsilon_{AO}$ values (21.4‰ and 26.0‰) close to the ones determined by Rayleigh models and a $^{15}\varepsilon_{NO}$ value (-11.1‰) close to those previously reported. Furthermore, we found ^{15}N-enrichment of the particulate nitrogen pool due to the light-independent assimilation of partially nitrified ammonium. Generally, these detailed *in situ* nitrogen isotope fractionation experiments tested the validity of assumptions made for analogous *ex-situ* experiments and raised questions about the environmental relevance of the full range of $^{15}\varepsilon_{AO}$ determined by laboratory-based studies.

4.2.Introduction

Nitrification plays a central role in the nitrogen (N) cycle, oxidizing ammonia (NH_3) via nitrite (NO_2^-) to nitrate (NO_3^-), thereby determining the composition of dissolved inorganic nitrogen (DIN = ammonium/ammonia + nitrite + nitrate). This is a crucial prerequisite for the removal of bioavailable N, as oxidized DIN (nitrite or nitrate) is required for N_2 production by denitrification or anammox. DIN composition also affects phytoplankton ecology, changing primary production and shifting phytoplankton communities (Berg et al. 2003; Yoshiyama and Sharp 2006; Domingues et al. 2011; Glibert et al. 2016).

The two steps of nitrification, ammonia oxidation (AO) to nitrite and nitrite oxidation (NO) to nitrate, are typically catalyzed by two different microorganisms. In the open ocean, ammonia oxidizing archaea (AOA) from the phylum *Thaumarchaeota* are the dominant ammonia oxidizers (Francis et al. 2005; Wuchter et al. 2006). Ammonia oxidizing bacteria (AOB) from the beta- and gamma- subphyla of the *Proteobacteria* play important roles in

some other aquatic systems including some coastal systems (Li et al. 2015b; Happel et al. 2018; Massé et al. 2019) and have AO kinetics distinct from AOA determining their ecological niches (Martens-Habbena et al. 2009; Martens-Habbena and Stahl 2011).

The stable isotopic composition ($\delta^{15}N$) of DIN species has proven a useful tool for improving the understanding of N cycling, including nitrification (Casciotti 2016). Knowledge of the isotopic fractionation characteristics for key N transformations is required for the interpretation of such data.

Differences in the enzymatic AO pathways between AOB and AOA (Walker et al. 2010; Vajrala et al. 2013; Martens-Habbena et al. 2015; Kozlowski et al. 2016; Stein 2019) as well as distinct kinetic differences leading to niche separation (Martens-Habbena et al. 2009) might indicate quantitative differences in isotope fractionation. On the other hand, both AOB and AOA produce hydroxylamine as a first intermediary product from ammonia (Vajrala et al. 2013) and laboratory-based studies neither found differences in N isotope fractionation between AOA and AOB, nor a clear relationship between AO rates and $^{15}\varepsilon_{AO}$ (Casciotti et al. 2003; Santoro and Casciotti 2011; Nishizawa et al. 2016). However, these *in vitro* based findings have not been tested *in situ*.

Whereas the $\delta^{15}N$ of nitrate ($\delta^{15}N_{NO3}$), and increasingly also nitrite are used to study marine N cycling (Casciotti and McIlvin 2007; Buchwald et al. 2015; Smart et al. 2015), isotopic analyses of all three major DIN species, including ammonium (NH_4^+; dominant over NH_3 at circumneutral pH and therefore "ammonium" used here also to denote NH_3+NH_4^+ unless otherwise noted), are rare. They have been mostly limited to coastal systems (Mariotti et al. 1984; Horrigan et al. 1990a; Middelburg and Nieuwenhuize 2001; Sebilo et al. 2006; De Brabandere et al. 2007; Sugimoto et al. 2009), where higher ammonium concentrations make $\delta^{15}N_{NH4}$ measurements less challenging analytically (Zhang et al. 2007). Yet, multiple processes can affect each of the major DIN pools differently, and isotopic analysis of more than one DIN species can help to discern different consumption and production processes.

Accumulations of nitrite due to temporary decoupling of nitrification have been frequently observed in coastal systems (Chapter 3; Horrigan et al. 1990b; Soetaert et al. 2006; Pitcher et al. 2011; Heiss and Fulweiler 2016; Schaefer and Hollibaugh 2017;

Laperriere et al. 2019). However, few studies have analyzed N isotope dynamics associated with this phenomenon and a general understanding is lacking (Horrigan et al. 1990a; De Brabandere et al. 2007; Sugimoto et al. 2009). The isotopic mechanisms underlying nitrite accumulated within marine oxygen deficient zones have been investigated more thoroughly (Bourbonnais et al. 2015; Buchwald et al. 2015), but both the main production (nitrate reduction vs ammonia oxidation) and removal processes (nitrite reduction vs nitrite oxidation) of nitrite differ under anoxic conditions. A better understanding of isotope effects associated with transient nitrite accumulation under oxic conditions might help to identify the underlying causes. Since they are temporal and short-lived phenomena, detailed time series may be the optimal tools for analysis.

N isotopic fractionation ($^{15}\alpha$) or enrichment factors ($^{15}\varepsilon$) express the magnitude of the isotopic fractionation associated with a given process (Mariotti et al. 1981). For AO ($^{15}\varepsilon_{AO}$) and NO ($^{15}\varepsilon_{NO}$), as for many similar biogeochemical processes, these have been quantified under controlled laboratory settings using pure or enriched cultures in closed systems (Delwiche and Steyn 1970; Mariotti et al. 1981; Yoshida 1988; Casciotti et al. 2003, 2010a; Casciotti 2009; Santoro and Casciotti 2011; Nishizawa et al. 2016). Some other studies have been able to estimate the $^{15}\varepsilon$ for nitrification or AO on the basis of *in situ* observations via the best fit of numerical models applied to observations (Wankel et al. 2007; Buchwald et al. 2015, 2018), by fitting Rayleigh-type functions of isotope fractionation to observations (Horrigan et al. 1990a; De Brabandere et al. 2007; Sugimoto et al. 2008, 2009), or from observations made on incubated samples (Brandes and Devol 1997; Sebilo et al. 2006; Southwell et al. 2008). It is notable that the laboratory-based studies tend to report a wider range of $^{15}\varepsilon_{AO}$ in both AOB and AOA (13–42‰) compared to studies based on *in situ* observations (7–25‰). Whereas the field studies lack the control of a closed system experiment that may yield accurate analyses and results, they presumably reflect realistic environmental conditions and their microbial communities (Casciotti et al. 2010a). Detailed, long-term *in situ* time series measurements of $\delta^{15}N$ in multiple DIN species from well-constrained, temporarily stable natural systems are rare but could combine the advantages of natural complexity and absence of experimental bias provided by *in situ*

measurements on the one hand and a level of control, analytical detail and data density close to that possible in laboratory-based experiments on the other.

Here we use Bedford Basin (BB), Nova Scotia, Canada, as a natural laboratory to study nitrification and the associated stable isotope dynamics. It is an anthropogenically impacted, fjord-like coastal basin that is rich in DIN, including ammonium, which allows for analysis of $\delta^{15}N$ of all three DIN species, at most times throughout the year. Importantly, the BB experiences annual mixing-stratification cycles. During stratified periods in most years, the bottom water is disconnected from near-surface water and water outside the basin, thus creating a temporary "closed system" in which nitrification during fall can be observed approximately as in a mesocosm experiment. Mixing in winter and spring resets the bottom water by removing accumulated nitrate and nitrifier biomass (Chapter 3) and provides the conditions for another "natural experiment" during the next stratified period.

For this study we analyzed weekly $\delta^{15}N$ data of particulate organic nitrogen (PON), ammonium, nitrite and nitrate in the bottom water of BB during two years, 2014 and 2017. These years were chosen because they provide contrasting biogeochemical scenarios: in 2014, the ammonia oxidizer community was dominated by AOA and very little nitrite accumulated (<0.5 μmol kg^{-1}) during fall (Chapter 3). In contrast, nitrite accumulated to ~8 μmol kg^{-1} at the beginning of fall 2017, with AOB, occurring in succession prior to AOA, playing a crucial role for nitrification and the accumulation of nitrite (Chapter 3).

The goal of this study was to apply qualitative analysis, Rayleigh models and numerical models to the *in situ* time series of nitrogen isotopes and concentrations collected from BB, in order to improve our understanding of isotopic mechanisms underlying nitrification, including potential impacts of shifts in ammonia oxidizer community composition.

4.3.Methods

4.3.1. Bedford Basin: Study Site

The Bedford Basin is a 17 km^2 fjord-like embayment located in close proximity to an urban center, the Halifax Regional Municipality, Nova Scotia, Canada (Figure 4.1). Freshwater input (5.3 m^3 s^{-1}) is small compared to the mean tidal volume entering the basin (2.5 10^7

m^3) and the total basin volume of 5.1×10^8 m^3 (Petrie and Yeats 1990; Gregory 1993). It receives anthropogenic nutrient input from several wastewater treatment plants in the region, one of which drains directly into the BB (Kerrigan et al. 2017).

A two-layer estuarine type circulation moves relatively saline water into the basin in a deeper layer and relatively fresh water out toward the Halifax Harbour and the Scotian Shelf (Huntsman 1924; Petrie and Yeats 1990; Fader and Miller 2008; Shan et al. 2011). A shallow sill (~20 m) effectively disconnects the bottom water of the 70-m deep BB from this circulation during times of stratification.

The physical mixing regime of BB is characterized by an annual cycle of full water column mixing in winter and temperature stratification beginning in spring (~April) and lasting until December to February, when it breaks down due to strong wintertime heat loss (Li and Harrison 2008; Shan et al. 2011). Occasional shelf water intrusion events occur in many years, interrupting the isolation of the bottom water during the stratified period by introducing relatively warm, saline, nutrient-poor and oxygen-rich water from the Scotian Shelf into the bottom or mid-depths of the basin (Platt et al. 1972; Burt et al. 2013; Shi and Wallace 2018).

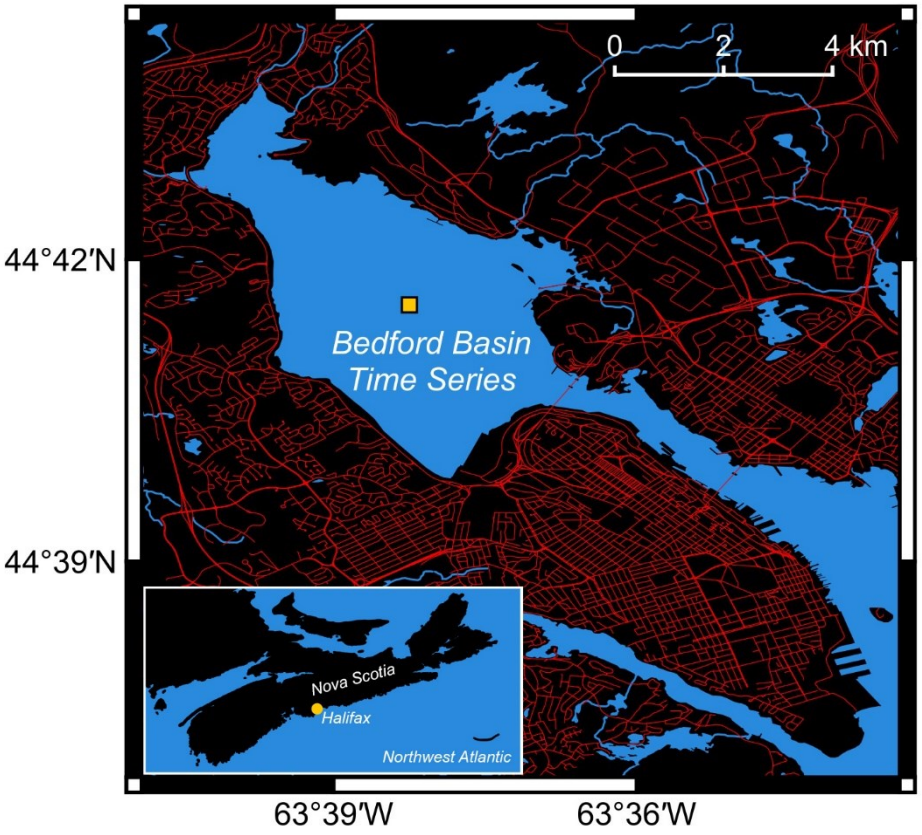

Figure 4.1: Map of Bedford Basin.

4.3.2. Sampling Program

Sampling for this study was conducted in the framework of the BB Monitoring Program led by the Bedford Institute of Oceanography (BIO), which has conducted a weekly oceanographic monitoring program (1992 to present; Li, 2014) at the Compass Buoy Station, (44°41'37"N, 63°38'25"W), situated at the central deep point of the basin (Gregory, 1993). Since 1992, continuous vertical profiles of physico-chemical parameters have been recorded weekly, using CTD (conductivity-temperature-depth), salinity, oxygen, and fluorescence probes (Li and Harrison 2008; Li 2014). Data for this study were collected with a Seabird SBE 25 instrument (including an SBE 43 oxygen sensor). Complementary, discrete samples for dissolved oxygen, chlorophyll (Chl) *a*, nutrients and other parameters were collected from Niskin bottles triggered at 1, 5, 10, and 60 m. The

2017 oxygen sensor measurements were calibrated with Winkler titrations whereas the 2014 data relied on factory calibration of the oxygen sensor.

4.3.3. Analysis of Bulk Concentrations

For Chl *a* analysis, water samples (0.5-1 L) were collected onto GF/F-filters, extracted with 90% acetone at -10°C for 24 hours and analyzed on a Turner Model 10 field fluorometer (Lorenzen 1966). Samples for dissolved inorganic nutrient (DIN) concentrations in the basin were pre-filtered (0.45 µm), stored frozen (-20°C), and measured in monthly batches on a continuous flow analyzer (AA3, Seal Analytical) at the BIO (2014 samples) or on a similar machine (San++, Skalar) in the CERC.OCEAN laboratory at Dalhousie University (2017 samples). Nitrate (NO_3^-) and nitrite (NO_2^-) were determined using standard photometric methods (Hansen and Koroleff 1999) with detection limits of 0.1 and 0.04 µmol kg^{-1} as well as precision of 0.13 and 0.01 µmol kg^{-1}, respectively. Ammonium was determined fluorometrically (Kérouel and Aminot 1997), with a detection limit of 0.1 µmol kg^{-1} and a precision of 0.11 µmol kg^{-1}. Samples for particulate organic nitrogen (PON) were collected onto combusted 25-mm glass fiber filters and stored frozen (-20°C). Upon thawing, filters were oven-dried and analysed on an elemental analyzer.

4.3.4. Nitrogen Isotopic Analyses

All glassware (combusted) and plastic items used for sampling or subsequent isotopic analyses were soaked in 10%-HCl for 24 hours and thoroughly rinsed with deionized water (DIW). Samples for determining the isotopic composition of DIN species were collected as follows: a 60-mL syringe was directly attached to the Niskin bottle via a nylon stopcock, rinsed three times with sample water, and completely filled. Using a Swin-Lok filter holder, the sample was gently forced through a pre-combusted 25-mm glass fiber filter into a 60-ml HDPE bottle (or a glass vial for $\delta^{15}N_{NH4}$ samples). About 10 mL of sample were used for rinsing and discarded before collecting the remaining volume. Samples were kept cool during transport and frozen within three hours (-20°C) until analysis.

The $\delta^{15}N$ and $\delta^{18}O$ of the various DIN species were measured following wet chemical conversion to nitrous oxide (N_2O; McIlvin and Altabet, 2005). Nitrate was first reduced to

NO_2^- with HCl-activated cadmium powder following a slightly modified version of the protocol described by Ryabenko *et al.* (2009). Briefly, a solution of 2.5 mmol L^{-1} sulfamic acid in 25% HCl was added to the samples to a final concentration of 10 µmol L^{-1} to remove any pre-existing nitrite (Granger and Sigman 2009). Then, 15 mL of sample or standard of a known isotopic composition was transferred to a 50-mL centrifuge tube. To ensure quantitative conversion of NO_3^- to NO_2^-, the salinity was increased to 5 mol L^{-1} by the addition of NaCl (combusted for 24 h at 450°C to remove any N-impurities) and the pH was buffered at about 9 by adding MgO. Approximately 0.6 g of activated cadmium was added as reducing agent. The tubes were placed on a reciprocal shaker overnight at 75 rpm. The next day, they were centrifuged and the conversion efficiency during the reduction step was checked for each sample: initial NO_3^- concentrations were compared against NO_2^- levels after cadmium reduction using the standard photometric assay after sulfanilamide and (N-(1-naphthyl)-ethylenediamine dihydrochloride) as described by Hansen and Koroleff (1999). Then a defined volume was transferred to a clean 20-mL crimp vial to achieve 15 nmol of NO_2^- and filled to 15 mL with DIW (2014 samples) or 1M NaCl (2017 samples; Appendix C). Nitrite in these samples was reduced to N_2O using a freshly prepared solution of equal volumes of 20% acetic acid and 2 mol L^{-1} sodium azide (McIlvin and Altabet 2005). Omitting the cadmium reduction step, the same procedure was applied to determine $\delta^{15}N$ of nitrite ($\delta^{15}N_{NO2}$) for 2014 samples. For 2017 $\delta^{15}N_{NO2}$ samples, method adjustments described in Appendix C were applied. The methodological modifications that allowed the additional analysis of $\delta^{18}O$ in nitrite (described in Appendix C) did not affect the $\delta^{15}N_{NO2}$ results (Figure C2).

To measure $\delta^{15}N_{NH4}$, samples were diluted to a concentration of 1.4 µmol L^{-1} with DIW and ammonium was then oxidized to NO_2^- with a basic hypobromite solution (Zhang et al. 2007). Following oxidation, sodium arsenite was added to consume excess hypobromite and the pH was neutralized using HCl. Oxidation efficiency was checked for each sample by comparing initial NH_4^+ concentrations against NO_2^- concentrations after hypobromite oxidation and was typically >90%. Nitrite was then reduced to N_2O as described above. Data from samples with hypobromite oxidation efficiency <75% were removed from analysis. This was typically the case for samples of lower concentration (<2–3 µM) that

could not be significantly diluted with DIW, which caused interferences from unknown seawater constituents. For nitrate, ammonium and partially for nitrite, sample concentration was adjusted to standard concentration. Some nitrite samples were not adjusted in this way but were instead corrected post-analysis for concentration effects using *in-house* standards run at concentration gradients with each run.

Post-analysis, $\delta^{15}N_{NH4}$ values were corrected for $\delta^{15}N_{NO2}$ measured in parallel samples. All samples were corrected for the $\delta^{15}N$ values of distilled water blanks run in parallel. *In-house* standards for each DIN species were analyzed with each batch of samples to ensure between-run precision. The average of duplicate measurements is reported, and error margins represent the empirically determined precision of each method based on long-term *in-house* standard values as standard deviation (SD; $\delta^{15}N_{NH4}$: 0.79‰, $\delta^{15}N_{NO2}$: 0.53‰, $\delta^{15}N_{NO3}$: 0.26‰). Because we determined decreasing measurement accuracy with decreasing nitrate concentration below about 5 µmol kg^{-1}, we assigned a higher margin of error around $\delta^{15}N_{NO3}$ values depending on a sample's nitrate concentration as outlined in Appendix C (Figure C1).

For isotopic analysis, the produced N_2O was quantitatively purged from the aqueous solution, cryo-focused by means of an automated trace gas pre-concentrator (PreCon, ThermoFisher Scientific) and injected into a continuous flow isotope ratio mass spectrometer (deltaV, ThermoFisher Scientific). The $\delta^{15}N$ of samples was calibrated using standards run in parallel: the international standards USGS32 ($\delta^{15}N$ = 180‰; $\delta^{18}O$ = 25.7‰), USGS34 ($\delta^{15}N$ = -1.8‰; $\delta^{18}O$ = -27.9‰), and IAEA-NO-3 ($\delta^{15}N$ = 4.7‰; $\delta^{18}O$ = 25.6‰) were used for $\delta^{15}N_{NO3}$ and USGS25 ($\delta^{15}N$ = -30.4‰), IAEA-N-1 ($\delta^{15}N$ = 0.4‰), and IAEA-N-2 ($\delta^{15}N$= 20.3‰) for $\delta^{15}N_{NH4}$. Calibrated reference material for $\delta^{15}N_{NO2}$ (2014 samples) was provided by Mark Altabet (Bourbonnais et al. 2017): MAA1 ($\delta^{15}N$ = -60.6‰), MAA2 ($\delta^{15}N$ = 3.9‰), and Zh1 ($\delta^{15}N$= -16.4‰). For 2017 samples, three new nitrite isotope standards were created as described in Appendix C: SHA1 ($\delta^{15}N$ = 17.5‰), SHA2 ($\delta^{15}N$ = 118.9‰), MAA1_NEW ($\delta^{15}N$ = -59.2‰).

The concentration and $\delta^{15}N$ ($\delta^{15}N_{PON}$) of particulate organic nitrogen were determined on an elemental analyzer coupled to an isotope ratio mass spectrometer (Isoprime 100, Elementar). $\delta^{15}N_{PON}$ was measured at a precision of 0.3‰ based on long-term variability

of *in-house* references. USGS40 ($\delta^{15}N$ = -4.5‰) and USGS41 ($\delta^{15}N$ = 47.6‰) reference materials were used to standardize $\delta^{15}N_{PON}$ values.

4.3.5. Isotope Notation and Rayleigh Model Fitting

All isotope standards mentioned previously are standardized against the nitrogen (N) stable isotope ratio of N_2 in air (^{15}N-N_2/^{14}N-N_2 = 0.0036765) and expressed in the commonly used δ notation:

$$\delta^{15}N\ [‰] = \left(\left(\frac{\left(\frac{^{15}N_{sample}}{^{14}N_{sample}} \right)}{0.0036765} \right) - 1 \right) \times 1000 \qquad 4.1$$

To determine isotopic enrichment factors, Rayleigh models were fitted following the Rayleigh closed system isotope fractionation rules outlined by Mariotti *et al.* (1981). Linear regressions were fit to the models using the Matlab (Mathworks) code "linfit" (http://memg.ocean.dal.ca/fennel/MM2009/Lab_06/linfit.m), which takes into account the y-axis error margin (SD) of each data point. 95% confidence intervals were calculated from the slope and intercept uncertainties determined by *linfit*.

If the reaction substrate's isotopic signature (δ_S) is sufficiently small, the isotopic enrichment factor (ε) can be approximated as follows (Mariotti et al. 1981):

$$\varepsilon = \frac{\delta_S - \delta_S(0)}{\ln(f)} \qquad 4.2$$

where $\delta_S(0)$ is the isotopic signature of the substrate at the beginning of the reaction and f is the fraction of unreacted substrate present at a given time point during the reaction.

4.3.6. Numerical Model of Concentrations, Isotopes and Functional Genes

We extended a model of BB bottom water N remineralization and nitrification previously described in (Chapter 3) by adding N isotope fractionation functions to the modeled ammonia oxidation (AO) and nitrite oxidation (NO) processes (Figure 4.2; Table C2; Table C3; Table C4). The model represented the state variables oxygen, ammonium, nitrite and nitrate concentration as well as the concentration of the functional marker genes for AO (*amoA* = ammonium monooxygenase) and NO (*nxr* = nitrite oxidoreductase; Table C4). These state variables changed due to the simulated processes of N remineralization, AO, NO as well as N loss (Table C3). The chain of modeled processes was initiated by forcing N remineralization with observed substrate (PON, O_2) concentrations. Each state variable was also subject to alteration as a result of mixing with the surface boundary. The surface boundary concentrations and N isotopic compositions of ammonium, nitrite and nitrate were set based on observations made in the near-surface water (5 m). Missing weekly near-surface values were interpolated. *AmoA* and *nxr* were set to zero at the surface boundary as justified by observations (Chapter 3; El-Swais et al. 2015). State variables were exchanged between the bottom water box and the surface boundary as a function of the mixing rate. The background mixing rate (= inverse of residence time; Table C4) was set to a value consistent with eddy diffusivity coefficients determined during a stratified period in BB by Burt et al. (2013). The mixing rate was increased stepwise during convective mixing and intrusion events by fitting modeled to observed oxygen concentrations as described by (Chapter 3).

For this study, we added state variables representing the concentration of the ^{15}N fraction for each DIN species (ammonium, nitrite and nitrate), while the $\delta^{15}N$ of organic matter was forced by the $\delta^{15}N_{PON}$ values measured in 2014 (also used for 2017). Each modeled process was additionally run for the ^{15}N fraction of each species and rates changing the concentration of each ^{15}N fraction were modified by multiplication with the relevant isotopic fractionation factor $^{15}\alpha$ (Table C2; Table C3; Table C4). This resulted in model output for i) [$^{15}N + {}^{14}N$], and ii) [^{15}N] for each compound which was used to compute the

respective $\delta^{15}N$. The isotopic fractionation factor (α) can be defined in terms of the isotopic enrichment factor (ε; Mariotti *et al.*, 1981):

$$\alpha = \left(\frac{\varepsilon}{1000}\right) + 1 \qquad 4.3$$

$^{15}\alpha$ was set to 1 (i.e. no fractionation) for N remineralization (Möbius 2013) and N loss, whereas for AO and NO least-square cost functions were used to determine the $^{15}\alpha$ producing the best fit of the model to the observed $\delta^{15}N$ time series.

Prior to fitting the $^{15}\alpha$ of AO and NO, we made additional changes to the model presented in (Chapter 3) to ensure optimal fit of model to the DIN concentration data. To achieve this, we forced the process rates with empirical instead of modeled O_2 concentrations to avoid inaccurate rate estimates caused by inaccurately modeled O_2 concentrations. Furthermore, different rate constants for the various processes were allowed for each of the two years in order to improve the model fit to the DIN concentration data, whereas Chapter 3 used a single set of rate constants for the entire four year time-series (2014–2017). This approach required trade-offs due to natural variability in the biology underlying rate constants between the years.

The intrusion of July 2014 and the mid-depth intrusion of July 2017 were modeled in a similar way to winter mixing, but the concentrations and $\delta^{15}N$ values of the DIN species of intruding water were not taken from the BB near-surface data. Instead, the July-2014 intrusion was assumed to bring Scotian Shelf water with negligible ammonium and nitrite concentrations (0 μmol kg^{-1}) and nitrate concentrations (2.5 μmol kg^{-1}) and $\delta^{15}N$ (4.6‰) values as observed in September 2014 in Scotian Shelf waters near Halifax (N. Lehmann, unpublished data). No such data were available as reference for the July 2017 mid-depth intrusion and so it was modeled with ammonium (13 μmol kg^{-1}; 14‰), nitrite (0.1 μmol kg^{-1} ; -16‰) and nitrate (5 μmol kg^{-1}; -1‰) concentration and isotope data that resulted in good model fit to the observations. Higher concentrations for the 2017 mid-depth intrusion are justified since it is assumed to have entrained BB mid-depth water into the bottom water.

The model was coded in the programming language R, using the packages 'FME' and 'deSolve' (Soetaert and Petzoldt 2010; Soetaert et al. 2010) for least-square fitting and for solving differential equations, respectively.

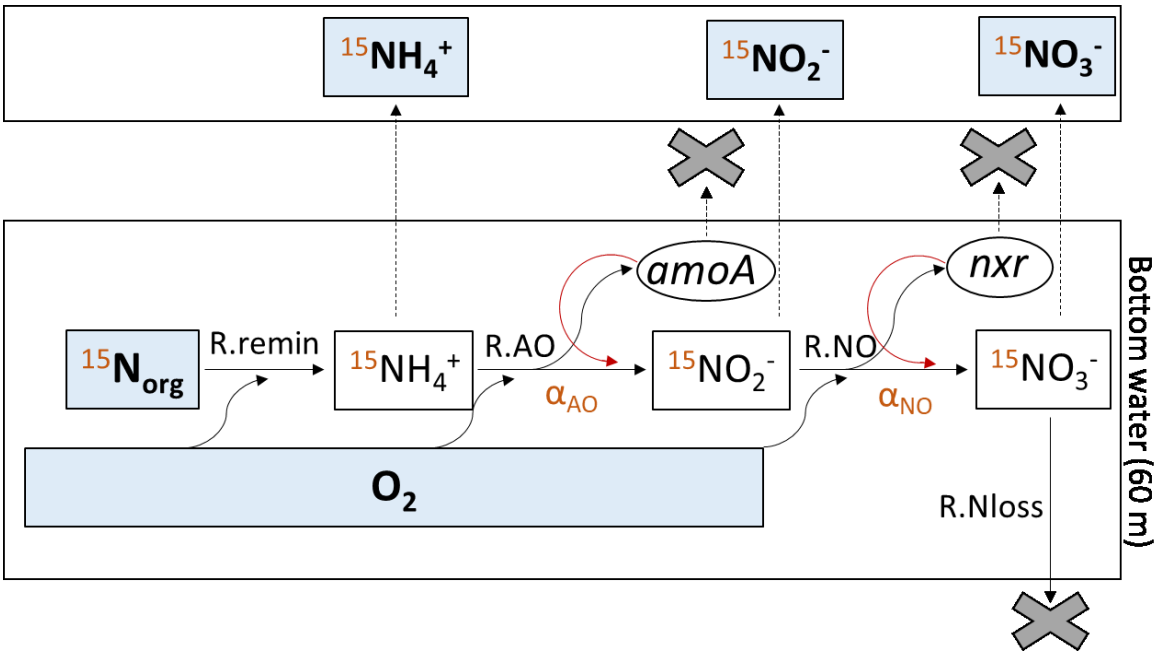

Figure 4.2: Schematic describing the numerical model including isotope fractionation. Each reaction was run i) for [^{15}N + ^{14}N], and ii) for [^{15}N], shown in orange. The [^{15}N]-only reactions were modified by an isotopic fractionation factor (α). α = 1 (no fractionation) was used for N-loss and N remineralization. Variables defined by empirical observations are highlighted in bold font within gray-shaded boxes, the remaining variables are modeled. As indicated by the red arrows, *amoA* and *nxr* growth reinforces the reactions catalyzed by them, AO and NO, respectively. Arrows toward 'X' indicate losses from the model. R.remin = remineralization rate; R.AO = ammonia oxidation rate; R.NO = nitrite oxidation rate; R.Nloss = N loss rate (= denitrification + assimilation + diffusive loss to sediment). Schematic modified from (Chapter 3).

4.4.Results

4.4.1. Physico-chemical Conditions

Increasing vertical temperature gradients (Figure 4.3A,B) and a steady oxygen decrease at 60 m (Figure 4.4A,B) indicated the beginning of seasonal stratification in March of both years (19/03/2014, 22/03/2017). The 2014 stratified period was interrupted by a shelf-water

intrusion event in mid-July, which increased temperature and salinity and caused oxygen to increase by 140 μmol kg^{-1} between two weekly measurements (Figure 4.3A, B, C; Figure 4.4A).

A comparable intrusion event indicated by a sharp oxygen increase occurred in December 2017 (Figure 4.4B). Additionally, in mid-July 2017, an intrusion to the mid-depths of the basin brought more saline water (Figure 4.3D; see also Shi and Wallace, 2018). This coincided with a slower oxygen decrease at 60 m (Figure 4.4B), indicating an influence of this mid-depth intrusion also on the bottom water chemistry.

Chl *a* maxima in the near-surface water indicated phytoplankton blooms occurred in March and April 2014 as well as in April, May and October 2017 (Figure 4.3G,H). The March 2014 and April 2017 spring blooms, but not the secondary spring blooms of each year, were followed instantly by small Chl *a* maxima in the bottom water (Figure 4.3G,H), indicating stratification was still incomplete and mixing linked the near-surface to the bottom water at least episodically. Similarly small Chl *a* maxima in June/July 2014 and July 2017 may represent phytoplankton-derived organic matter from the April 2014 and May 2017 blooms reaching the bottom water. This delay is consistent with previous estimates of particle sinking speeds (~1 m d^{-1}) in BB (Hargrave and Taguchi 1978; Petrie and Yeats 1990).

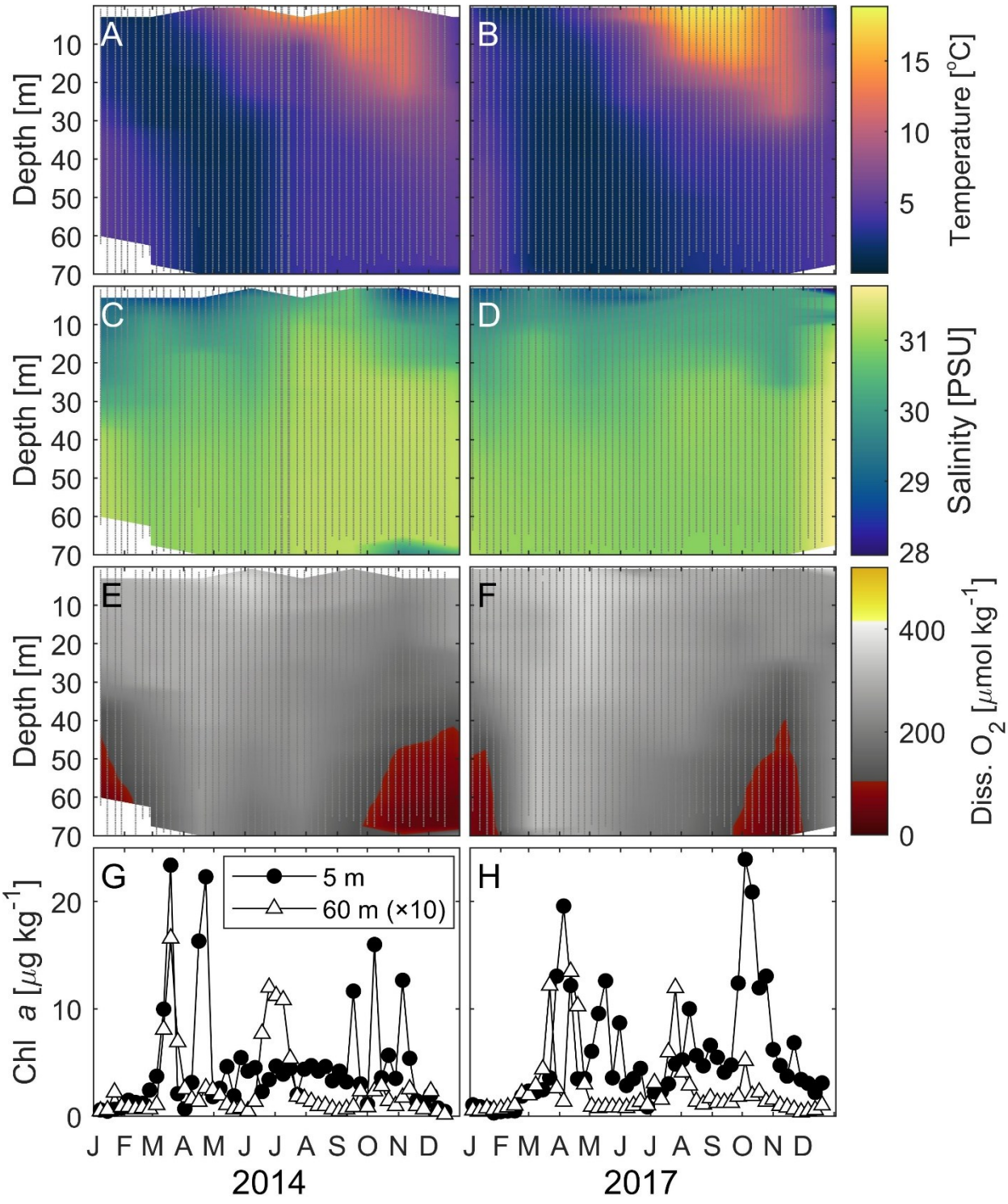

Figure 4.3: Time series of oceanographic parameters in Bedford Basin in 2014 (A, C, E, G) and 2017 (B, D, F, H): A, B) Temperature; C, D) Salinity; E, F) Dissolved oxygen; G, H) Chl *a* concentration at 5 m and 60 m.

4.4.2. Seasonal Changes in Particulate Nitrogen Concentrations and Isotopic Composition

Particulate organic nitrogen (PON) concentrations in the BB bottom water showed no clear trends and varied between ca. 1 µmol kg^{-1} and maximum values between 5 and 6 µmol kg^{-1} at various times in 2014 and 2017 (Figure 4.4C,D). In the last third of each year, PON concentrations were relatively stable between 1 and 3 µmol kg^{-1}.

$\delta^{15}N_{PON}$ showed only small variations during spring and summer 2014 with values on average 1.3‰ (SD: 1.3‰) higher than the $\delta^{15}N_{PON}$ measured near the surface (5 m) prior to September (Figure 4.4C). Starting in early September, $\delta^{15}N_{PON}$ values at 60 m increased almost steadily from 6.4‰ on September 3rd to a maximum of 13.7‰ in November, while near-surface values showed no such increase.

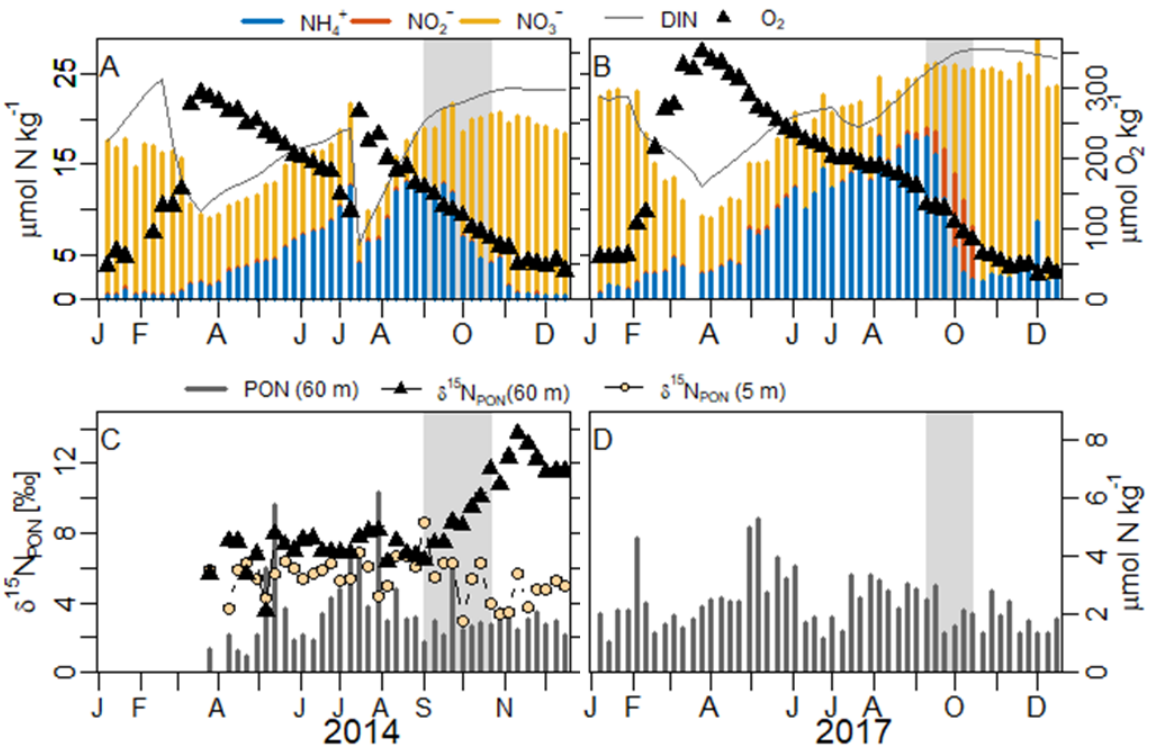

Figure 4.4: Time series of biogeochemical observations (scatter or bar plots) and model output (lines) at 60 meters depth in Bedford Basin in the years 2014 (A, C) and 2017 (B, D): A-B) Observed and modeled DIN concentrations as well as dissolved oxygen (O_2) concentrations; C-D) δ^{15}N-PON (5 m and 60 m, 2014 only) and PON concentration (60 m).

4.4.3. Dissolved Inorganic Nitrogen Speciation

DIN in bottom water ranged from 9–29 μmol kg^{-1} within the two year time frame, and each year at the onset of stratification (March/April), it began to increase due to the addition of ammonium (Figure 4.5A,B). In 2017, nitrate increased steadily by about 2 μmol kg^{-1} between the onset of stratification until July, while in 2014 there was very little change in nitrate concentration until the July intrusion event. This inter-annual difference in nitrate production has been previously explained by differences in winter mixing intensity, which dilutes the nitrifier population to different extents in different years (Chapter 3). The intrusion of July 2014 caused a sudden nitrate and ammonium decrease within one week, while the mid-depth intrusion of July 2017 coincided with smaller nitrate decrease at 60 m which extended over several weeks. In both years, nitrate increased rapidly in September and October, coinciding with a rapid ammonium decrease.

Coincident with this nitrate increase and ammonium decrease in each year, plateauing DIN concentrations (Figure 4.4A,B) suggested a strong decrease in N remineralization, which was also represented in the modeled rates (Figure 4.5A). Given stable PON concentrations around this time and increased temperatures due to the intrusion, the modeled N remineralization rates likely decreased along with the decreasing availability of O_2, as this is the only other variable which determines modeled N remineralization rates (Table C3). This suggests a switch from a period of pre-dominant N remineralization to a period of pre-dominant nitrification in early September.

During 2014, only minor nitrite accumulation was observed in late April (0.35 μmol kg^{-1}) and early August (0.44 μmol kg^{-1}; Figure 4.5E). However, in 2017, nitrite accumulated to a maximum value of 8.1 μmol kg^{-1} in late September, coinciding with the period of ammonium decrease (Figure 4.5F).

4.4.4. Nitrogen Isotope Effects Associated with Dissolved Inorganic Nitrogen Transformations

The fluctuations in concentration of the three DIN species were reflected in their isotopic compositions (Figure 4.5C–H). $\delta^{15}N_{NO3}$ in BB bottom water decreased steadily in both years starting with the beginning of the stratified period. It decreased more rapidly

following the July 2014 intrusion, leading to a minimum in September of 2014 (-5.8‰). The annual $\delta^{15}N_{NO3}$ minimum of 2017 was also reached in September (-7.4‰), following several weeks of particularly rapid decrease (Figure 4.5G–H). In both years, $\delta^{15}N_{NO3}$ started to rapidly increase following the September minima, until it levelled out in November 2014 (~19‰) and October 2017 (~23‰), respectively. Just prior to the $\delta^{15}N_{NO3}$ minima and coincident with the ammonium concentration maxima of each year, $\delta^{15}N_{NH4}$ started a rapid increase reaching annual maxima of 40.1‰ in 2014 and 78.0‰ in 2017. The sharp $\delta^{15}N_{NO3}$ increase and nitrate decrease associated with the July 2014 intrusion was consistent with an offshore source of more ^{15}N-enriched nitrate ($\delta^{15}N_{NO3}$ = 4.6‰; NO_3^- = 2.5 μmol kg^{-1}; N. Lehmann, unpublished data).

$\delta^{15}N_{NO2}$ minima in June (-20.4‰) and September 2014 (-20.3‰) as well as May 2017 (-15.2‰) corresponded with minima (0.1–0.2 μmol kg^{-1}) in nitrite concentration (Figure 4.5E,F). In contrast, the $\delta^{15}N_{NO2}$ minimum of September 2017 (-23.6‰) did not coincide with a nitrite concentration minimum but occurred near the beginning of the period during which nitrite accumulated to the two-year maximum (Figure 4.4F)

Overall, the timing and quality of the changes in $\delta^{15}N$ of the three DIN species were similar between 2014 and 2017 (Figure 4.4) despite between-year differences in nitrite accumulation, ammonia oxidizer community composition (Chapter 3) and the intensity of mid-year intrusion events. However, some parameters differed between years, including the steeper increase of $\delta^{15}N_{NH4}$ and $\delta^{15}N_{NO3}$ in fall 2017 compared to 2014.

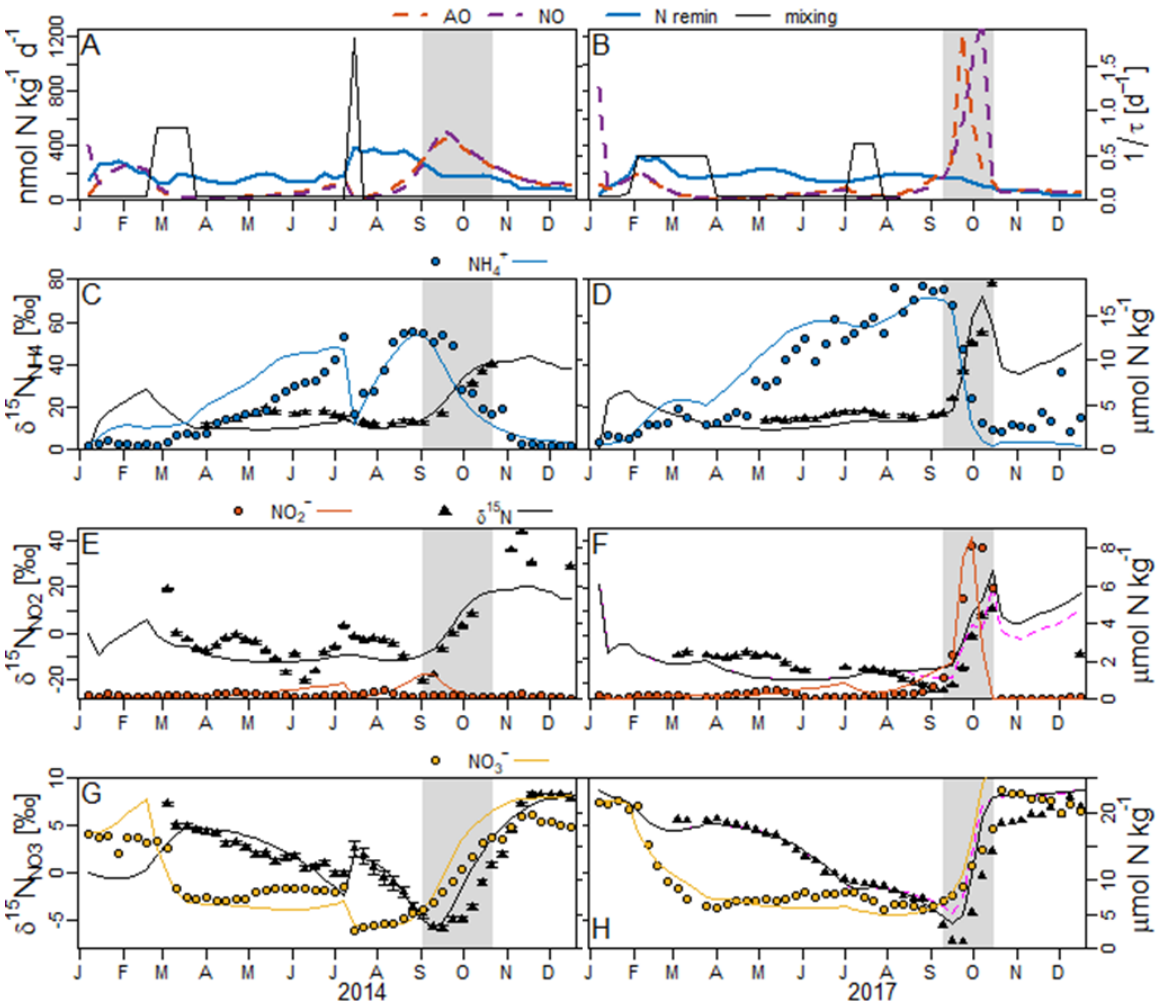

Figure 4.5: Time series of modeled rates (lines), observed (scatter) and modeled (lines) isotope signatures ($\delta^{15}N$) at 60 meters depth in Bedford Basin in the years 2014 (A, C, E, G) and 2017 (B, D, F, H). A, B) modeled rates of N remineralization, ammonia oxidation (AO) and nitrite oxidation (NO), as well as the inverse of residence time τ, describing the timescale of BB bottom water exchange with water from the basin surface or the shelf; C, D) ammonium (NH_4^+) concentration and $\delta^{15}N$; I-J) nitrite (NO_2^-) concentration and $\delta^{15}N$; E, F) nitrate (NO_3^-) concentration and $\delta^{15}N$. The gray-shaded areas indicate the closed-system nitrification period for each year. The dashed pink lines in panels F and H indicate modeled $\delta^{15}N_{NO2}$ and $\delta^{15}N_{NO3}$ after adjusting the $^{15}\varepsilon_{NO}$ value to -11.1‰ for August to December 2017. Error bars represent the empirically determined precision of each isotope analysis method (see 4.3.4), which was adjusted for concentration-dependency for $\delta^{15}N_{NO3}$ as described in Appendix C.

4.5.Discussion

4.5.1. $\delta^{15}N_{PON}$ Increase due to Dark Ammonium Assimilation

Parallel with the $\delta^{15}N_{NH4}$ increase in September and October 2014 caused by isotope fractionation during AO, we observed simultaneous increase of $\delta^{15}N_{PON}$ by ca. 7‰ (Figure 4.4C). Our method of filtering Niskin-sampled water did not distinguish between the sinking and suspended PON fractions. However, a lack of Chl *a* increase in the bottom water (Figure 4.3G) and the steady $\delta^{15}N_{PON}$ values in near-surface water throughout the year (Figure 4.4C) imply that the $\delta^{15}N_{PON}$ increase was not caused by PON sinking from surface waters, but rather by ^{15}N-enrichment of the PON suspended within the bottom-water. N remineralization has a small associated isotope enrichment effect (~2‰ ;Möbius 2013) that might explain the constant but small offset observed between near-surface and bottom water $\delta^{15}N_{PON}$ prior to September, but cannot explain the increase of almost 7‰ between September and November 2014 in bottom water only (Figure 4.4C). This increase could, however, be explained by partial transmission of the increasingly high $\delta^{15}N_{NH4}$ signal into biomass via ammonium uptake.

Elevated $\delta^{15}N_{NH4}$ may occur where nitrification of sufficiently large ammonium pools occurs along temporal (this study) or spatial (sediments, stratified water columns) gradients. At the points (in time or space) along such a gradient at which the original ammonium pool has been partially oxidized, the remaining ammonium is predicted, based on Rayleigh-type mechanisms, to become ^{15}N-enriched. Parallel ammonium assimilation could transfer this isotopic signature into the PON pool and lead to temporarily or locally elevated $\delta^{15}N_{PON}$.

Assimilation of incompletely nitrified ammonium has been recognized as a potential influence on the $\delta^{15}N_{PON}$, but so far only for phytoplankton-driven assimilation in the euphotic zone: elevated $\delta^{15}N_{PON}$ due to assimilation of incompletely nitrified ammonium by phytoplankton was observed under sea-ice in Bering Sea near-surface waters (Granger et al. 2011; Morales et al. 2014). A similar effect was inferred from an ecosystem model of the Sea of Okhotsk that required the inclusion of nitrification and ammonium assimilation

to fit observed end-of-year increases in both $\delta^{15}N_{NH4}$ and sinking $\delta^{15}N_{PON}$ (Yoshikawa et al. 2005).

Given the absence of light in BB bottom water (Taguchi and Platt 1977), we here observed an analogous situation of ^{15}N-enrichment of the biomass of heterotrophic (Middelburg and Nieuwenhuize 2000; Allen et al. 2002; Veuger et al. 2004) and/or chemolithoautotrophic microorganisms due to their assimilation of ^{15}N-enriched ammonium. This might have different implications than $\delta^{15}N_{PON}$ alteration by phytoplankton assimilation of incompletely nitrified ammonium, as it can cause $\delta^{15}N_{PON}$ increase also below the euphotic zone. The possible occurrence of a similar effect below the euphotic zone in the open ocean would be consistent with observed vertical profiles showing increasing $\delta^{15}N_{PON}$ in the suspended PON fraction with ocean depth (Altabet et al. 1991; Voss et al. 1996; Casciotti et al. 2008; Sigman et al. 2009). Within the euphotic zone, nitrification maxima are often observed seasonally in winter (Murray et al. 1998; Herfort et al. 2007; Galand et al. 2010; Pitcher et al. 2011; El-Swais et al. 2015). As previously noted by Mino et al. (2016), assimilation of partially nitrified ammonium and subsequent export of ^{15}N-enriched PON might therefore explain the winter-time maxima of $\delta^{15}N_{PON}$ that are frequently observed also below the euphotic zone (Altabet et al. 1991; Voss et al. 1996; Peña et al. 1999; Wu et al. 1999; Lourey et al. 2003; Mino et al. 2016). Studies in open ocean systems are necessary to address the question of whether the $\delta^{15}N_{PON}$ increase due to assimilation of partially nitrified ammonium found in Bedford Basin is indeed relatable to open ocean settings.

4.5.2. Evidence for Dark Ammonium Assimilation Throughout the Stratified Period

Based on coincidence of the start of $\delta^{15}N_{PON}$ and $\delta^{15}N_{NH4}$ increases in September 2014 it is tempting to speculate that nitrifiers, which are chemolithoautotrophs, were directly responsible for the ^{15}N-enrichment in the particulate matter of BB bottom water. However, the coincidence of the start of the $\delta^{15}N_{PON}$ and $\delta^{15}N_{NH4}$ increases in September 2014 does not necessarily imply that nitrifiers were directly responsible for both. As pointed out above, the increase of $\delta^{15}N_{NH4}$ due to nitrification is a necessary condition for the $\delta^{15}N_{PON}$

increase. Therefore, assimilation by non-nitrifiers occurring at a constant rate throughout the year could also explain the observed behavior of $\delta^{15}N_{PON}$.

In support of this, the data show that between April and late August 2014, $\delta^{15}N_{NH4}$ was consistently higher than $\delta^{15}N_{PON}$ by 7.9‰ (SD: 2.6‰; Figure 4.4C, Figure 4.5C). Since N remineralization would be expected to result in a $\delta^{15}N_{NH4}$ close to the $\delta^{15}N$ of substrate organic matter (Möbius 2013), this suggests the occurrence of one or more ammonium-utilizing processes with associated N isotope fractionating, such as ammonia oxidation or assimilation (Delwiche and Steyn 1970; Hoch et al. 1992). A cycle of ammonium assimilation and N remineralization, in which ammonium and PON each act as both substrate and product, should increase $\delta^{15}N_{NH4}$ and decrease $\delta^{15}N_{PON}$ in the absence of other processes, because $\varepsilon_{NH4assimilation} > \varepsilon_{N\text{-}remineralization}$ (Hoch et al. 1992; Möbius 2013). Hence, PON originating from near-surface waters should become depleted in ^{15}N after sinking into the bottom water, yet we observed consistently higher $\delta^{15}N_{PON}$ in bottom water than in surface water (Figure 4.4C). An influence of nitrification (through increasing $\delta^{15}N_{NH4}$) and a possible inter-annual memory effect of ^{15}N-enriched PON leftover in the bottom water from the previous year may act to increase $\delta^{15}N_{PON}$ in bottom water relative to that in near-surface water. This implies that ammonium assimilation may also occur prior to September 2014.

Using radioisotope labeling techniques, Taguchi and Platt (1977) demonstrated light-independent ("dark") ammonium assimilation in subsurface waters of BB at 30 m in February and, with less confidence, at 40-50 m in August. The occurrence of dark ammonium assimilation in the BB bottom water is, however, consistent with the detection of enzymes associated with ammonium assimilation in metaproteomics from BB bottom water in January 2011, when the vast majority of protein sequences, including some related to ammonium assimilation, were affiliated with ammonia oxidizing archaea (Georges et al. 2014).

Georges *et al.* (2014) found no metaproteomic evidence for nitrate assimilation in May 2010 or January 2010, despite relatively high nitrate (6.83 μmol L^{-1}) and low ammonium (0.44 μmol L^{-1}) concentrations in January (no metaproteomic data for Summer or Fall). Given this metaproteomic data, a generally observed preference for ammonium over nitrate

assimilation (Ludwig 1938; Harvey 1953; Middelburg and Nieuwenhuize 2000; Veuger et al. 2004; Glibert et al. 2016; Yan et al. 2019), as well as the agreement between Rayleigh models based on ammonium and nitrate (discussed below), we conclude that there is no evidence for significant nitrate assimilation in addition to the observed ammonium assimilation in the bottom water of BB.

4.5.3. Fitting a Closed-system Rayleigh Model to Identify the Isotopic Enrichment Factor of Ammonia Oxidation ($^{15}\varepsilon_{AO}$)

The high temporal resolution of the BB dataset allowed selection of specific time periods for which bottom water conditions were indicative of a closed system to which Rayleigh models of isotope fractionation could be applied (gray-shaded periods; Figure 4.4, Figure 4.5). Steady DIN concentrations (Figure 4.4A, B) during these periods indicated that nitrification strongly exceeded N remineralization. This was supported by modeled rates (Figure 4.5A, B). Furthermore, O_2 concentrations during these periods were too high (>85μmol kg^{-1}; Figure 4.4A, B) to allow for significant rates of denitrification or anammox in the bottom water (Jensen et al. 2008, 2009). DIN assimilation by photoautotrophs can also be excluded given that light is unavailable in BB bottom water (Taguchi and Platt 1977). The insignificance of new input or removal of DIN during these segments of the stratified period in both years justified our assumption that the BB bottom water represented a temporarily closed system for nitrification.

For both years, the "Rayleigh closed-system period" was defined to start when DIN reached a plateau and ammonium concentrations began to drop, and to end when ammonium concentration stopped decreasing. The amounts of ammonium left at the end of each year's nitrification period (2014: ~1 μmol kg^{-1}, <5% of maximum; 2017: 2 μmol kg^{-1}, 11% of maximum) were lower than in some laboratory studies of nitrification (e.g. Casciotti et al. 2003).

The isotopic enrichment factor for AO, $^{15}\varepsilon_{AO}$, can be approximated by the slope of the linear fit applied to the ammonium series on the Rayleigh model (Figure 4.6), expressed as follows (Mariotti et al. 1981):

$$\delta_S = \varepsilon \times lnf \quad 4.4$$

with δ_S denoting the $\delta^{15}N$ of the substrate and f the fraction of unreacted substrate. The slope determined for the 2014 and 2017 Rayleigh model fits in Figure 4.6A and C represented the isotopic enrichment during ammonium utilization ($^{15}\varepsilon_{AU}$). For 2014, it could be corrected for the influence of ammonium assimilation to represent the isotopic enrichment factor for AO, $^{15}\varepsilon_{AO}$, as discussed in Appendix C and shown in Figure 4.6B and Table 4.1.

Alternatively, the isotopic enrichment factor of AO can be approximated by the difference between the values of the y-intercepts of the products' (nitrate + nitrite) and substrate's (ammonium/ammonia) curves on the Rayleigh model (Mariotti et al. 1981). In the case of 2014 (Figure 4.6B), this difference (20.6 ±1.7‰) was not significantly different from the $^{15}\varepsilon_{AO}$ determined via the ammonium slope (21.8 ±2.2‰; Table 4.1). However, in 2017 (Figure 4.6C), a slightly larger, significant difference was observed between the two estimates (slope: 24.1 ±1.1‰; intercepts: 31.3 ±1.6‰). Given that an underestimation of the ammonium slope due to a small influence of ammonium assimilation, ammonification and/or the NH_4^+/NH_3 isotope effect was unlikely (Appendix C), one explanation for this discrepancy may be the possible loss of nitrification product, e.g. via denitrification, later in the Rayleigh closed-system period, which would have increased the slope of the nitrate curve and thereby decreased its intercept (Figure 4.6C).

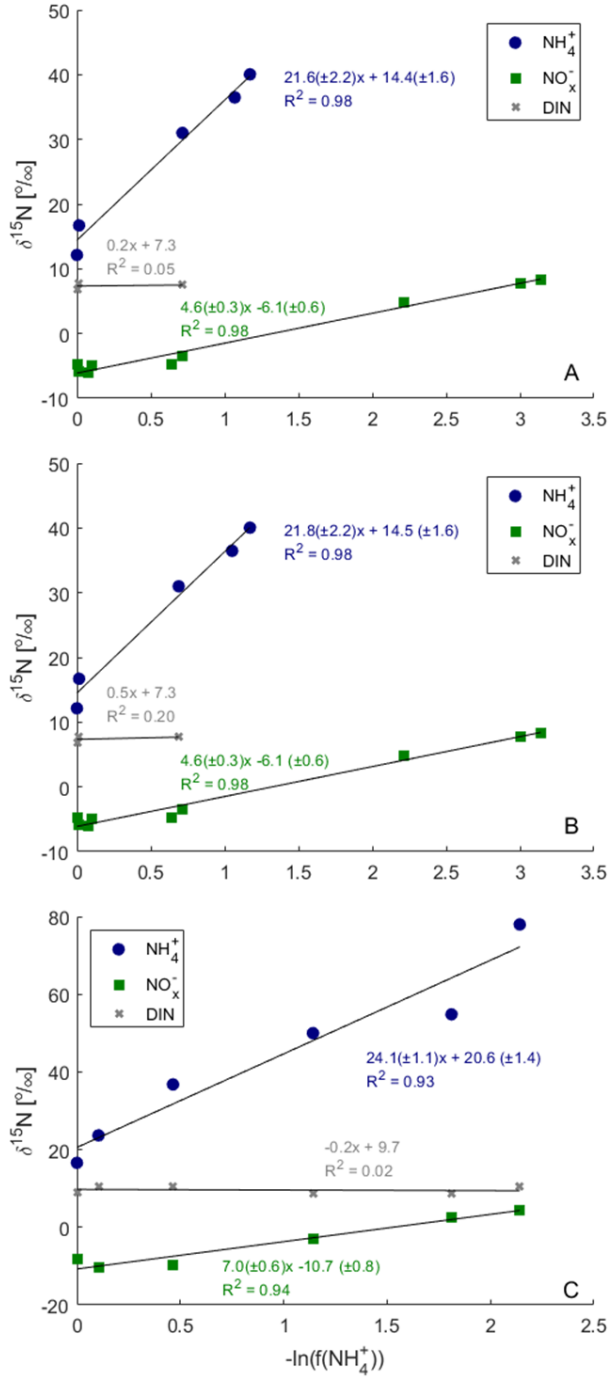

Figure 4.6: Rayleigh models for nitrification during the closed-system periods in fall 2014 and 2017. A) Rayleigh model for fall 2014 including the effects of ammonium assimilation; B) Rayleigh model for fall 2014 after correction for ammonium assimilation (see discussion); C) Rayleigh model for fall 2017 including the effects of ammonium assimilation. The uncertainties given for slope and intercept of the linear regressions represent the 95% confidence interval and take into account isotope method precision (see 4.3.4), which was adjusted for concentration-dependency for $\delta^{15}N_{NO3}$ (Appendix C).

Table 4.1: Isotopic enrichment factors determined by Rayleigh closed system models or best fit within numerical models for the years 2014 (AOA dominance, nitrite accumulation <0.5 µmol kg^{-1}) and 2017 (crucial AOB influence, nitrite accumulation of 8 µmol kg^{-1}). The uncertainties (±) represent the 95% confidence interval.

Isotopic Enrichment Factor (ε)	2014 [‰]	2017 [‰]	Estimated by
Ammonium Utilization ($^{15}\varepsilon_{AU}$)[1]	21.6 ± 2.2	24.1 ± 1.1	Rayleigh slope (NH_4^+; Figure 4.6A, C)
Ammonia Oxidation ($^{15}\varepsilon_{AO}$)	21.8 ± 2.2	-	Rayleigh slope (NH_4^+; Figure 4.6B)[2]
Ammonia Oxidation ($^{15}\varepsilon_{AO}$)	17.0 ± 1.5	24.0 ± 2.2	Rayleigh slope (NO_x^-; Figure 4.7)
Ammonia Oxidation ($^{15}\varepsilon_{AO}$)	20.6 ± 1.7	31.3 ± 1.6	Rayleigh intercept (NH_4^+-NO_x^-; Figure 4.6)
Ammonia Oxidation ($^{15}\varepsilon_{AO}$)	21.4	26.0	Best fit numerical model
Nitrite Oxidation ($^{15}\varepsilon_{NO}$)		-11.1	Best fit numerical model

[1]Likely insignificantly different from ε_{AO} also for 2017 (see 4.5.3)
[2]Based on Rayleigh model corrected for ammonium assimilation (see Appendix C)

To assess a possible influence of processes other than nitrification during the Rayleigh closed system period on nitrite or nitrate, the isotope effect associated with AO can also be assessed from the change in the $\delta^{15}N$ of the product. This can be calculated as follows (Mariotti et al. 1981):

$$\delta_P = \delta_S(0) - \varepsilon_{NH_4^+ \rightarrow NO_x^-} \times \frac{f_{NH_4^+} \times \ln\left(f_{NH_4^+}\right)}{1 - f_{NH_4^+}} \qquad 4.5$$

with δ_P denoting the $\delta^{15}N$ of the product (nitrate + nitrite = NO_x^-) and $\delta_S(0)$ the initial $\delta^{15}N$ of the substrate (ammonium). The slopes of the linear regression in Figure 4.7A and B thus approximate the $^{15}\varepsilon_{AO}$. These linear regressions were started at the datapoint representing the respective annual $\delta^{15}N_{NO3}$ minimum (Figure 4.5G, H). This was 1–2 weekly time points after the start of the Rayleigh-closed system period as defined for the Rayleigh models shown in Figure 4.6, because the subsequent increase in $\delta^{15}N_{NO3}$ could be attributed to ^{15}N-enrichment from the increasingly ^{15}N-enriched nitrification substrate (ammonium). Inclusion of the preceding $\delta^{15}N_{NO3}$ decrease (gray datapoints in Figure 4.7), which was likely a consequence of isotopic dilution of the pre-existing nitrate pool (discussed below), would have decreased the accuracy of the $^{15}\varepsilon_{AO}$ estimation.

For 2017, the $^{15}\varepsilon_{AO}$ determined in Figure 4.7B (24.0 ±2.2‰) was similar to the $^{15}\varepsilon_{AU}$ determined via the slope of the ammonium curve in the Rayleigh model shown in Figure

4.6C (see also Table 4.1). This supports the assumption that the influence of ammonium assimilation on $^{15}\varepsilon_{AU}$ was insignificant also during the 2017 Rayleigh closed system period so that it can be assumed that $^{15}\varepsilon_{AU} \approx {}^{15}\varepsilon_{AO}$. It also suggests that the observed increase in $\delta^{15}N_{NOx}$ during the Rayleigh closed-system period of 2017 was caused primarily by nitrification and that the influence of other processes (e.g. denitrification, nitrate assimilation) on the observed fractionation was negligible.

For 2014, the $^{15}\varepsilon_{AO}$ determined by the slope of the product (17.0 ±1.5‰; Figure 4.7A) was 4.7‰ smaller than the $^{15}\varepsilon_{AO}$ determined by the ammonium slope (Figure 4.6B). This might indicate an influence on $\delta^{15}N_{NOx}$ by processes other than nitrification during the Rayleigh closed-system period of 2014. However, an influence of processes such as denitrification or nitrate assimilation would cause a steeper than expected slope in Figure 4.7A, since additional nitrate consumption would lead to higher $\delta^{15}N_{NO3}$ enrichment than expected due to nitrification alone.

It remains possible that the relatively large and significant differences between the 2017 ammonium slope and ammonium-NO_x^- intercepts (Figure 4.6C) as well as the 2014 NO_x^- slope and the estimates via other approaches (Table 4.1) reflect measurement uncertainty in one of the isotope pools. Even in controlled laboratory incubation experiments, with pure AOB cultures, differences of a similar magnitude have been observed when determining the $^{15}\varepsilon_{AO}$ with these different approaches (Mariotti et al. 1981).

As established above and in Appendix C, the influence of other processes (ammonification, ammonium assimilation) on the ammonium pool was likely negligible during the relevant periods (see above and Appendix C). Since the approaches via the NO_x^- slope (Figure 4.7) and ammonium-NO_x^- intercepts require the additional assumption of the negligibility of NO_x^- utilizing processes during the Rayleigh closed system periods, the $^{15}\varepsilon_{AO}$ value determined by the ammonium slope is likely the most accurate estimate (Table 4.1). Hence, the highest (31.3 ±1.6‰) and lowest (17.0 ±1.5‰) estimates of $^{15}\varepsilon_{AO}$ may have been outliers and the most accurate estimates were likely achieved via the ammonium slope of the Rayleigh curve, 21.8 ±2.2‰ (2014) and 24.1 ±1.1‰ (2017).

Steady oxygen decrease during the Rayleigh closed system periods indicated stable stratification, but also indicated heterotrophic remineralization of organic matter, a possible

source of ammonium. Potentially, this could indicate an opening in the Rayleigh system due to N remineralization, and if N remineralization rates were balanced by denitrification rates, it could conceivably result in the observed, steady DIN concentrations. However, heterotrophic respiration can also produce nitrogenous products other than ammonium, such as urea (Bronk et al. 1998). Moreover, significant remineralization-denitrification would be expected to cause $\delta^{15}N_{DIN}$ increase due to the strong isotopic enrichment effect of denitrification (Granger et al. 2008), but steady $\delta^{15}N_{DIN}$ (Figure 4.6A,C) was observed during the Rayleigh closed system periods. This suggests a negligible role for denitrification and validates the assumption of a closed system during these periods.

Similarly, a violation of the closed-system assumption due to significant feedback on $\delta^{15}N_{NH4}$ via N remineralization of the increasingly ^{15}N-enriched PON (discussed above) is unlikely. This is because i) the $\delta^{15}N_{PON}$ increase is small compared to the $\delta^{15}N_{NH4}$ increase, and ii) the PON fraction that is being enriched in ^{15}N due to ammonium assimilation during the Rayleigh closed system period must represent an actively growing population and is therefore unlikely to simultaneously contribute significantly to the PON fraction being remineralized.

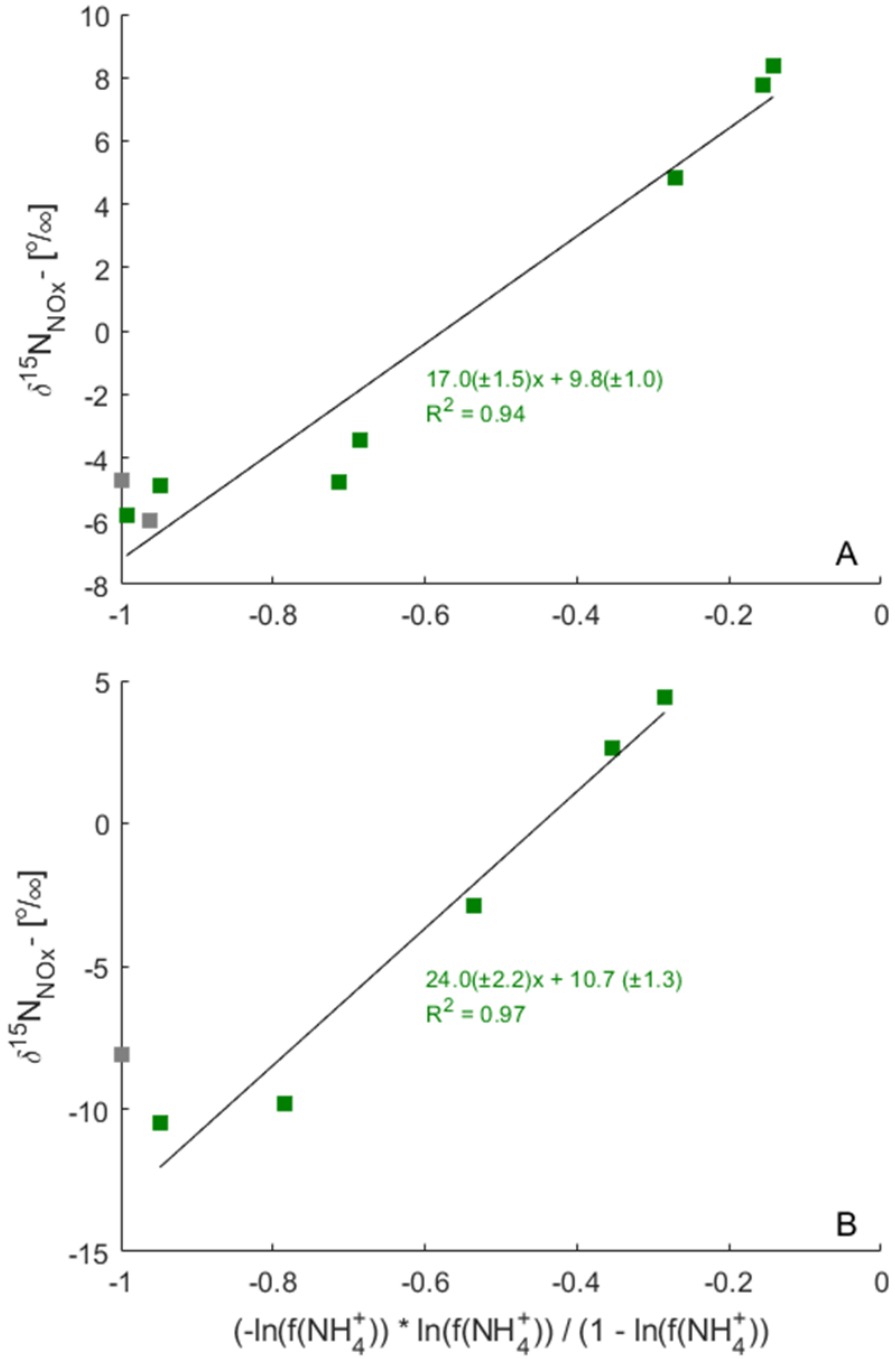

Figure 4.7: Rayleigh models based on the combined change in $\delta^{15}N$ in the nitrification products nitrate and nitrite ($\delta^{15}N_{NOx^-}$) during ammonium depletion, for the Rayleigh closed-system periods in A) 2014, and B) 2017. The gray datapoints are part of the Rayleigh closed-system period but ignored by the linear regressions, as discussed in the main text. The uncertainties given for slope and intercept of the linear regressions represent the 95% confidence interval and take into account isotope method precision (see 4.3.4), which was adjusted for concentration-dependency for $\delta^{15}N_{NO3}$ (Appendix C).

4.5.4. Interpretation of $\delta^{15}N_{NO2}$ and $\delta^{15}N_{NO3}$ Minima

In both years, periods of parallel $\delta^{15}N_{NO2}$ and $\delta^{15}N_{NO3}$ decrease ended in minima only two weeks apart (Figure 4.5E–H). Both minima were likely caused by nitrification but may have differing explanations at the level of isotope fractionation. The steady $\delta^{15}N_{NO3}$ decrease leading to the September minimum in both years can be explained by the continuous preferential transfer of ^{14}N from ammonium to the pre-existing (2.7 μmol kg^{-1}) nitrate pool (Sebilo et al. 2006). Since $\delta^{15}N_{NH4}$ was approximately constant between April and September, this led to a decrease in $\delta^{15}N_{NO3}$ (Figure 4.4G,H). This $\delta^{15}N_{NO3}$ decrease continued until its difference to $\delta^{15}N_{NH4}$ approximated the isotopic enrichment factor of nitrification.

Since the nitrite pool was always much smaller than the nitrate pool, the $\delta^{15}N_{NO2}$ minima of September 2014 and 2017 may be more readily explained as an expression of the inverse isotope effect associated with NO (Casciotti, 2009; Buchwald and Casciotti, 2010). In 2014, nitrite, which had accumulated to 0.4 μmol kg^{-1}, decreased in parallel with $\delta^{15}N_{NO2}$ until both reached their minima in early September (Figure 4.5E). In 2017, nitrite accumulation started prior to the beginning of the strong nitrification period (Figure 4.5F). Despite the opposite trend of nitrite concentrations, NO was likely active in both cases (Figure 4.5A,B) and its inverse isotope effect may have caused the observed $\delta^{15}N_{NO2}$ decrease leading to the annual minima. Subsequent to the minima, steep increases in $\delta^{15}N_{NO2}$ and $\delta^{15}N_{NO3}$ followed the rapid increase of $\delta^{15}N_{NH4}$ that was observed in September of both years and can therefore be explained by N transfer from the increasingly ^{15}N-enriched ammonium pool (Figure 4.5).

4.5.5. Best Fit of a Numerical Model Consistent with Isotopic Enrichment Factors Determined by the Rayleigh Models

To further explore these and other features of the DIN isotope time series and to compare isotopic enrichment factors between numerical models that cover the full-year time series and the Rayleigh models which are restricted to a relatively short period, we used a modified version of the numerical model for BB bottom water described in Chapter 3. The

model was optimized to fit observed trends in DIN concentrations in 2014 and 2017, and subsequently amended with isotope fractionation functions.

To model the large nitrite accumulation in September 2017, the AO rate constant was multiplied by a factor of 3.5 during the time period in which AOB growth was observed (Chapter 3). This reflects faster AO kinetics in AOB compared to AOA, which dominate AO in BB bottom water at most other times (Chapter 3; Bollmann et al. 2005; Martens-Habbena et al. 2009; Peng et al. 2016). Rate constants for N remineralization, AO and NO were adjusted for each year to fit the observed timing of ammonium decrease and nitrate increase in September (Table C4).

The model reproduced the general trends in DIN concentrations of both years (Figure 4.5C–H). Next, the $^{15}\varepsilon_{AO}$ and $^{15}\varepsilon_{NO}$ combination that produced the best fit to the time series $\delta^{15}N$ observations were chosen by a least-square fitting function from the R package FME (Soetaert and Petzoldt 2010). Using these isotope enrichment factors, the model also reproduced the overall trends observed in the N stable isotope time series (Figure 4.5C–H).

The $^{15}\varepsilon_{AO}$ values producing the best model fit to each year's observation were very similar to the $^{15}\varepsilon_{AO}$ and $^{15}\varepsilon_{AU}$ determined by Rayleigh models (Table 4.1). This was reflected by the model fit closely matching the steep $\delta^{15}N_{NH4}$ increase in the fall of each year, i.e. during the closed system periods to which the Rayleigh models were applied (Figure 4.5C,D).

The model also matched the $\delta^{15}N_{NO2}$ increase at the end of each year that was driven by the transfer of ammonium-N by AO from the increasingly ^{15}N-enriched ammonium pool (Figure 4.5E,F). However, the model did not capture the small-scale variations in nitrite concentration prior to July 2017 and throughout most of 2014, which were likely driven by small-scale variations in AO and NO. Therefore, the resulting $\delta^{15}N_{NO2}$ variations during these periods were not reflected in the model either (Figure 4.5E,F) and the $^{15}\varepsilon_{NO}$ values determined by best fit to each year's observations (-0.4 and -4.6‰ for 2014 and 2017, respectively) should not be considered meaningful. Instead, we determined a $^{15}\varepsilon_{NO}$ for the period following the July-2017 mid-depth intrusion during which modeled nitrite concentrations were close to observations (Figure 4.5F). Holding the remaining parameters of the model constant, the $^{15}\varepsilon_{NO}$ producing the best fit for the July-December 2017 period

was determined (as described above) to be -11.1‰ (Figure 4.5F). This is close to the $^{15}\varepsilon_{NO}$ ≈ -13‰ determined by laboratory experiments (Casciotti 2009).

4.5.6. Inter-Annual Similarity in $\delta^{15}N$ Patterns Despite Biogeochemical Dissimilarities

Remarkably, few significant differences were observed in the timing and quality of the overall trends in $\delta^{15}N$ of ammonium, nitrite and nitrate between the two years, despite biogeochemical differences (ammonia oxidizer type, nitrite accumulation). Even though significant nitrite accumulation only occurred in 2017, the relatively flat $\delta^{15}N_{NH4}$ that suddenly increased rapidly in September (Figure 4.5C,D), the minima of $\delta^{15}N_{NO2}$ and $\delta^{15}N_{NO3}$ at the beginning of the $\delta^{15}N_{NH4}$ increase and the eventual steep increase also of $\delta^{15}N_{NO2}$ and $\delta^{15}N_{NO3}$ (Figure 4.5E,F) were each observed in both 2014 and 2017. This suggests that there was only a minor influence of the 2017 nitrite accumulation and the dominance of either AOB or AOA on the major trends in isotope fractionation during nitrification.

Inter-annual differences in magnitude or rate of change in the $\delta^{15}N$ parameters were observed, however, and these may be associated with higher AO and NO rates in 2017 compared to 2014. This difference was probably caused by high AO rates catalyzed by the AOB that temporarily dominated AO in 2017 but not in 2014 (Chapter 3). Fast AO enabled fast NO, causing more rapid ^{15}N-enrichment of the ammonium pool in September/October 2017 than during the corresponding period in 2014. This led to higher maximum $\delta^{15}N_{NH4}$ values and steeper $\delta^{15}N_{NO2}$ and $\delta^{15}N_{NO3}$ increase in 2017 (Figure 4.5E–H).

Small inter-annual differences in $^{15}\varepsilon_{AO}$ were observed between the Rayleigh closed system periods of each year using different approaches based on Rayleigh models and the numerical model (Table 4.1). The small trend of lower $^{15}\varepsilon_{AO}$ values in 2014 compared to 2017 was significant for some of the individual approaches, but overall, the 95% confidence intervals of the upper-range $^{15}\varepsilon_{AO}$ estimates of 2014 overlapped with the lower-range estimates for 2017. Hence, these inter-annual differences in $^{15}\varepsilon_{AO}$ were statistically not significant and were also small in comparison to the large, overlapping ranges of $^{15}\varepsilon_{AO}$ reported in both AOB and AOA (Casciotti et al. 2003; Santoro and Casciotti 2011).

4.5.7. Significance of *In Situ* Isotopic Enrichment Factors for Nitrification from a Natural Experiment

Several studies have estimated isotopic enrichment factors for nitrification in aquatic water columns on the basis of *in situ* data (Horrigan et al. 1990a; Sebilo et al. 2006; De Brabandere et al. 2007; Sugimoto et al. 2008, 2009). The challenge such studies face is to discern the many processes that can influence the $\delta^{15}N$ of ammonium, nitrite and nitrate, which usually prevents a high-confidence estimation of $^{15}\varepsilon_{AO}$. The present study relies on high data density, isotopic information from PON and the three main DIN species as well as favorable environmental conditions (dark, sufficiently oxygenated) that minimize the impact of confounding processes (denitrification, N assimilation by phototrophs). This is necessary for estimates that approximate the accuracy with which these factors can be measured in laboratory-based studies and to discern any influence from processes other than nitrification.

The N isotopic enrichment factors for AO and nitrification determined here (Table 4.1) are well within the range (13–42‰) reported previously from culture-based studies (Delwiche and Steyn 1970; Mariotti et al. 1981; Yoshida 1988; Casciotti et al. 2003; Santoro and Casciotti 2011; Nishizawa et al. 2016). They are at the high end of the much smaller range (7–25‰) of $^{15}\varepsilon_{AO}$ or $^{15}\varepsilon_{AU}$ determined on the basis of *in situ* observations, environmental sample incubations or models fit to environmental observations (Horrigan et al. 1990a; Brandes and Devol 1997; Sebilo et al. 2006; De Brabandere et al. 2007; Southwell et al. 2008; Sugimoto et al. 2008, 2009; Nishizawa et al. 2013; Buchwald et al. 2018).

It remains unclear why some culture-based studies yield such high estimates of $^{15}\varepsilon_{AO}$ (Mariotti et al. 1981; Casciotti et al. 2003; Santoro and Casciotti 2011; Nishizawa et al. 2016), but it is noteworthy that field studies consistently find values ≤31‰ (this study; Horrigan et al. 1990a; Brandes and Devol 1997; Southwell et al. 2008; Sugimoto et al. 2008, 2009; Nishizawa et al. 2013). A possible explanation for any overestimation of $^{15}\varepsilon_{AO}$ in studies with laboratory cultures might be the accumulation of an AO intermediary product induced by experimental conditions such as high substrate provision (Santoro and Casciotti 2011). Evidence for nitrification intermediary products between ammonia and

nitrite now exists for both AOB and AOA (Vajrala et al. 2013; Martens-Habbena et al. 2015; Caranto and Lancaster 2017; Stein 2019). High $^{15}\varepsilon_{AO}$ determined under laboratory conditions may also be explained by the rate of AO relative to the rate of ammonium entering the cell (Casciotti et al. 2010a). Inherent in each of these explanations is the possibility that they cause an artificial bias under experimental conditions that may render the upper bounds of the $^{15}\varepsilon_{AO}$ range determined in such way inapplicable to *in situ* conditions. The high-confidence, field-based $^{15}\varepsilon_{AO}$ estimates reported here provide further indication that the environmentally relevant $^{15}\varepsilon_{AO}$ range may comprise only a smaller subset (≤31‰) of the large range determined by culture-based studies. Given that AOA dominated in 2014 whereas AOB played a dominant role in 2017 (Chapter 3), this holds true for both groups.

4.5.8. Conclusions

We analyzed two different realizations of nitrification "experiments" occurring in the closed-system natural laboratory setup provided by the bottom water of a nitrogen-rich, seasonally stratified basin. The high resolution of the available time series and the long summer-fall stratified period allowed observation and interpretation of the *in situ* isotope fraction patterns in BB bottom water that are comparable with the confidence attainable with laboratory experiments. In each of the two years, a nitrification-dominated period started in September. During these periods the BB bottom water could be viewed as a closed system in which nitrification proceeded with little interference from other N cycle processes, allowing isotopic enrichment factors for ammonia oxidation to be determined with high confidence using Rayleigh closed-system models (Table 4.1). Near the beginning of these nitrification-dominated periods, distinct $\delta^{15}N_{NO3}$ and $\delta^{15}N_{NO2}$ minima were caused by isotope fractionation during AO and inverse isotope fractionation during NO, respectively.

Isotopic enrichment factors for ammonia oxidation were determined by the best fit of a numerical model to the entire time series and found to be similar to those determined by Rayleigh models applied to a more limited time period (Table 4.1). This suggests that these factors can, in principle, be determined with reasonable accuracy by numerical models,

which are well-constrained by observations and take into account the relevant physical and biogeochemical processes. This adds confidence to the determination of isotopic enrichment factors by such well-designed numerical models, which may be more applicable than Rayleigh models in situations in which the absence of influence from other biogeochemical processes cannot be assumed.

The overall trends of N isotope signatures were similar between the two years, despite differences in nitrifier community (AOA vs AOB) and nitrite accumulation due to nitrification decoupling. Yet, the high-frequency time series allowed detection of some subtle inter-annual differences. The significant role of AOB in 2017 but not 2014 likely resulted in steeper increase of $\delta^{15}N_{NH4}$, $\delta^{15}N_{NO2}$ and $\delta^{15}N_{NO3}$ near the end of the nitrification period as a consequence of higher AO rates facilitated by the AOB. Despite decoupling of nitrification leading to nitrite accumulation in September 2017 but not in 2014, a pronounced $\delta^{15}N_{NO2}$ minimum followed by steep increase was observed during both periods, suggesting that temporary nitrification decoupling does not produce a distinct pattern in $\delta^{15}N_{NO2}$ signatures (or $\delta^{15}N$ of other DIN species).

Parallel $\delta^{15}N_{PON}$ increase to the $\delta^{15}N_{NH4}$ increase caused by nitrification in sub-euphotic zone water suggested ^{15}N-enrichment of suspended particulate organic matter via dark assimilation of partially nitrified ammonium by chemolithoautotrophs or heterotrophs. This effect should be considered when interpreting profiles or time series of $\delta^{15}N_{PON}$.

It would be worthwhile to further explore this influence of partial nitrification on $\delta^{15}N_{PON}$. Furthermore, results from this study emphasize discrepancies between laboratory- and field-based isotopic enrichment factors that should be explored further by more careful laboratory analyses and by additional detailed *in situ* time series studies in diverse environments.

5. CHAPTER 5
CONCLUSION

The findings and biogeochemical characterizations presented in Chapters 2, 3 and 4 contributed to our knowledge of biogeochemical cycling in Bedford Basin and Powell Lake. The highly resolved measurements by interdisciplinary approaches in these two natural laboratories resulted in novel insights into biogeochemical cycling of N and associated elements.

The first geomicrobiological characterization and detailed description of geochemical zones along the redox gradient of Powell Lake's water column presented in Chapter 2 established a basis for further investigation into the biogeochemistry of this unusual and extreme system. Our results confirmed, in large parts, the expected alignment between geochemical zonation and microbiological potential, but also showed interesting exceptions. For example, we identified candidate micro-aerobic nitrifiers related to the clades Sagma-X (*Thaumarchaota*) and *Nitrosomonadaceae* (*Betaproteobacteria*). Their potential production of oxidized N under micro-aerobic conditions may sustain autotrophic N reduction even in the presence of a broad suboxic zone. Moreover, we identified anaerobic adaptations in the acI lineage (*Actinobacteria*), which emphasizes their role as freshwater analogues of the ubiquitous marine SAR11 lineage. Divergent lineages from several phyla (*Atribacteria*, *Bacteroidetes*, *Deltaproteobacteria* and *Phycisphaerae*) were identified in the ancient seawater zone at the bottom of Powell Lake, which may suggest unexplored functional traits. Genetic potential for BNF provided further indications for the occurrence of this process in meromictic lakes and at high ammonium concentrations and DIN:phosphate ratios (Großkopf and LaRoche 2012; Knapp 2012; Bombar et al. 2016). Interestingly, no genetic potential for the anammox process could be identified despite the presence of ammonium and nitrite at the top of the suboxic zone. Finally, the strong observed overlap between the ferruginous and manganous zones may point to bathymetric peculiarities of Powell Lake or to poorly understood manganese biogeochemistry.

Chapter 3 identified a potentially widespread and important physical mechanism controlling nitrifier biomass, diversity and, as a consequence, product composition and rates of nitrification. Dilution of nitrifier biomass as a control on nitrification and an effect

of nitrifier diversity on nitrification product composition are poorly explored or even novel concepts. All types of nitrifiers were shown to be subject to dilution by physical mixing, which can lead to delayed nitrification following periods of strong mixing. Additionally, our results showed that the favourability of AOB over AOA in more turbulent, high-ammonium environments can lead to transient nitrite accumulation. Moreover, we identified ammonium and temperature as controls on nitrification rates in Bedford Basin. The detailed, long-term time series employing both geochemical and microbiological measurements was crucial for reaching these conclusions, because it revealed the different dynamics in nitrite, nitrate, *amoA*, AOA and AOB concentrations in different years. In conjunction with the empirical data, the numerical model simulating geochemical changes as function of physical and functional gene variations was instrumental in identifying the mechanism and making it more intuitively comprehensible. These findings are particularly relevant, because physical mixing is a climate-sensitive variable and it is conceivable that global climate change may indirectly affect nitrification below the euphotic zone in Bedford Basin and other aquatic systems via the identified mechanism.

Building on the findings and numerical model from Chapter 3, Chapter 4 explored the effect of transient AOB dominance and resulting nitrite accumulation on the isotope effects associated with nitrification, using two natural experiments provided by observations from the years 2014 and 2017. Interestingly, we found little influence of this nitrification decoupling on the isotope effect. Instead, we identified similar isotopic enrichment factors for AO and NO in both years. These isotopic enrichment factors uniquely combine the benefits of laboratory and field experiments, as they were observed under environmentally realistic *in situ* conditions while confounding processes could be controlled for effectively due to high measurement density and variety. Therefore, the reported factors will be of important use in the interpretation of N isotope effects associated with nitrification in field- and laboratory-based studies. Moreover, the analyzed time series of different N species during nitrification in Bedford Basin and the evidence for N-isotopic enrichment of PON caused by the light-independent assimilation of partially nitrified ammonium will facilitate interpretation of similar datasets even if they are of lower temporal resolution.

5.1.Potential Future Research on the Biogeochemistry of Powell Lake

The findings presented in Chapters 2–4 also suggested hypotheses and raised questions for further research and identified mechanisms with more global implications. One promising line of research emerging from the study of Powell Lake (Chapter 2) is an inquiry into any active biological nitrogen fixation and what makes it ecologically feasible in this high-ammonium, high-nitrogen-to-phosphorus environment. While phosphorus (P) rather than N limitation of primary production is the norm in lakes (Hecky et al. 1993), Powell Lake's DIN:phosphate ratio is extremely high (Guildford and Hecky 2000). Numerous meromictic lakes have a DIN:phosphate ratio exceeding the "Redfield ratio" of 16:1 despite their anoxic water column portions that allow for denitrification (Tezuka 1985; Priscu 1997; Klepac-Ceraj et al. 2012; Llorens-Marès et al. 2015). A plausible explanation for the high DIN:phosphate ratio in meromictic lakes like Powell Lake, may be the scavenging of P by the formation of minerals like vivianite observed in similar lakes (Xiong et al. 2019). However, given the genetic potential for BNF in Powell Lake, it would be worthwhile to test the hypothesis of an additional, quantitatively significant contribution of BNF to Powell Lake's high DIN:phosphate ratio in future research.

In this context, an intriguing observation not presented in this text are exceptionally high excess-N_2 concentrations in Powell Lake's anoxic zone inferred from N_2/Ar ratio measurements (Haas, Bristow, Wallace, et al.: unpublished data). Investigations into the source of this excess N_2, a potential fertilizing effect of high N_2 on BNF, as well as the cause of the high observed DIN:phosphate ratios and a possible role for BNF contributing to excess N compared to P, represent highly intriguing future lines of research. N_2/Ar and BNF rate measurements as well as a search for *nifH* gene transcripts from within the ancient seawater zone are recommended to address these questions. A wider issue such research could address by using Powell Lake as a natural mesocosm model system, is the stability of the postulated feedback loop between denitrification and BNF that is thought to stabilize the oceanic N:P ratio over geological time frames (Falkowski 1997; Tyrrell 1999; Gruber 2008; Landolfi et al. 2013).

Furthermore, due to its stability, the chemocline-region of Powell lake provides a good natural laboratory to investigate differential distribution of the N-reducing process DNRA,

denitrification and anammox along gradients of oxygen, nitrate, organic carbon and sulfide. In this context, the connection between nitrogen and methane cycling, epitomized by the well-described MAG1, deserves further investigation. The chemocline area also provides the opportunity for detailed studies of nitrification within a spatially well-defined suboxic zone on the basis of the identified potential nitrifiers occurring there. Promising methods for this research include measurement of natural abundance N and C stable isotope signatures, distributions of RNA from functional genes, detailed oxygen profiles and rate measurements. Finally, despite the tentative nature of the existing metagenomic evidence for anoxygenic photosynthesis, an investigation into the occurrence of this process in the chemocline of Powell Lake would be of significant interest given the similarity in depth and therefore light levels of the Black Sea chemocline, in which some of the most low-light adapted phototrophs on the planet have been identified (Manske et al. 2005; Marschall et al. 2010).

5.2. Potential Future Research on Nitrification in Bedford Basin and Beyond

The results from the studies on Bedford Basin (Chapters 3 and 4) should be followed up by research both inside the basin and in other aquatic systems. The global distribution of the dilution-regrowth mechanism as a control on nitrification as described in Chapter 4 should be assessed by time-series studies in other coastal, shelf and lacustrine environments, as pointed out in the discussion section of Chapter 4.

The detailed characterization of N stable isotope fractionation during nitrification in Bedford Basin described in Chapter 4 can help future studies in interpreting similar but less detailed datasets. Further attention should be paid to the unexpected finding of $\delta^{15}N_{PON}$ increase due to ^{15}N-enrichment caused by the light-independent assimilation of partially nitrified ammonium. Extension of the numerical model by the addition of an ammonium assimilation term and the addition of PON concentration and $\delta^{15}N$ as state variables is likely to be a valuable tool in exploring this effect further within Bedford Basin. A possible effect of nitrification on the $\delta^{15}N_{PON}$ of sinking organic matter should be considered and tested also in other systems, given accumulating evidence for incomplete nitrification under various conditions (Chapter 3; Yoshikawa et al. 2005; Granger et al. 2011; Morales et al. 2014). Incomplete nitrification may represent a mechanism that could explain the increase

of suspended organic N, which is typically observed below the euphotic zone (Altabet et al. 1991; Voss et al. 1996; Casciotti et al. 2008; Sigman et al. 2009). In addition to the suspended matter (Chapter 4), the pool of sinking organic N could conceivably also be affected by this: sinking chemolithoautotrophs or, in the case of euphotic-zone nitrification, phytoplankton enriched in ^{15}N due to uptake of incompletely nitrified ammonium might transport this signal to the sediments, altering the sedimentary $\delta^{15}N_{PON}$ signal. This may have implications for paleo-oceanographic studies interpreting sediment records. A recent meta-analysis suggests that the direct relationship between sedimentary $\delta^{15}N_{PON}$ and surface water $\delta^{15}N_{NO3}$ holds true on a global scale and indicates that water-column alteration does not usually affect paleo-oceanographic sedimentary $\delta^{15}N_{PON}$ analyses (Robinson et al. 2012). However, a possible influence of nitrification on $\delta^{15}N_{PON}$ increase below the euphotic zone in open ocean settings should be further investigated, since, in specific cases, it might influence even the sedimentary $\delta^{15}N$. One possible way of further investigating this effect is by use of sediment traps at the bottom of Bedford Basin or elsewhere in the ocean, where strong, (temporarily) incomplete nitrification occurs to assess the $\delta^{15}N$ of sinking PON in addition to that of suspended PON. Another approach could be the application of nanoSIMS (nano scale secondary ion mass spectrometry) technology (applied e.g. by Kitzinger et al. 2020), which could allow taxonomic identification of the microbes that take up incompletely nitrified, ^{15}N-enriched ammonium in Bedford Basin.

Together, Chapters 3 and 4 suggested that Bedford Basin could be used as a natural laboratory for a better understanding of the competition and succession between AOB and AOA and the biogeochemical consequences. It was observed that AOB outcompete AOA in times of high substrate availability and following physical disturbances, marking AOB as r-selected and AOA as K-selected. To address this question and to understand the identified effect mixing has on nitrification in Bedford Basin in more detail, the model presented and used in Chapters 3 should be further developed to allow for the competition of two or more kinetically distinct ammonia oxidizer types; one with the capability of fast, AOB-type and one with slower, AOA-type AO kinetic properties. If combined with direct AO and NO rate measurements and enrichment or culturing efforts of the dominant

nitrifiers, this would be particularly promising for further exploration of the mechanics of delayed nitrification and nitrite accumulation caused by the effect of physical mixing on nitrifier biomass and diversity. Since their discovery, AOA have taken center-stage in marine nitrification research because of their dominant role in the oligotrophic open ocean (Wuchter et al. 2006; Robidart et al. 2012; Tolar et al. 2013; Hollibaugh et al. 2014; Santoro et al. 2017). While a role for AOB in some more ammonium-rich coastal and lacustrine systems is recognized (Li et al. 2015b; Happel et al. 2018; Massé et al. 2019), the necessity of a more detailed understanding of the conditions favoring one group over another is highlighted by the biogeochemical implications of the findings presented in Chapter 3. Due to their faster kinetics, AOB likely played a crucial role in mitigating the observed nitrification delay in Bedford Basin. Had any secondary, adverse environmental conditions prohibited AOB growth in BB, nitrification would have likely been delayed even more than observed. Further elucidation of environmental factors that may affect AOB growth and their competition with AOA is therefore of high interest. Promising factors of interest include temperature, oxygen and ammonium concentration. The effect of variations in these parameters on nitrification by AOA and AOB in Bedford Bains should be tested experimentally, using Bedford Basin bottom water, ideally sampled during a stratified period before the fall nitrification peak when nitrifier populations have not yet reached their maxima. A further step could be the enrichment and cultivation of Bedford Basin nitrifiers and the use of enrichment cultures for physiological tests.

The combined impacts of climate change and anthropogenic N input on nutrient cycling in coastal systems are complex and multi-variate: climate change may affect nutrient cycling in estuaries by modifying freshwater input, stratification patterns, storm patterns and phytoplankton ecology among other factors (Statham 2012). Therefore, it is difficult to assess whether the nitrification delay mechanism described in Chapter 3 will be reinforced as a result of climate change. For example, weaker mixing due to warmer winter atmospheric temperatures could lessen the frequency and intensity of its occurrence, but stronger and more frequent storms during winter may have the opposite effect. A better understanding of the physical oceanography of Bedford Basin and how exactly it interacts with nitrifier biomass is necessary for an effective prediction of nitrification delay in this

model system. Is nitrifier biomass most effectively removed from Bedford Basin bottom water by short and intense, possibly storm-driven, events, or by longer-term atmospheric forcing better described by the average winter temperatures, or does nitrification delay as observed in 2015 require both a cold winter and late-winter storms? Similarly, the mechanism of intrusion events and susceptibility of their frequency to climate change needs to be better understood, since they represent a mechanism by which DIN of a given ammonium:nitrate ratio could be supplied to phytoplankton.

5.3. Possible Further Implications of Bedford Basin Results

While there are many differences between the ammonium-rich bottom water of the coastal Bedford Basin and the base of the euphotic zone in the oligotrophic open ocean, the dilution-regrowth mechanism might also help to understand the primary nitrite maximum consistently observed in the latter areas (Lomas and Lipschultz 2006). The seasonal movement of the base of the euphotic zone and the mixed layer due to seasonal changes in light and temperature stratification could provide the basis for continuously shifting location of maximum nitrifier biomass growth (Figure 5.1). The base of the euphotic zone may be optimal for nitrifier growth because of the lack of competition for ammonium from phytoplankton and the availability of ammonium from organic matter remineralization (Zakem et al. 2018). Bacteria and archaea cannot actively swim, hence their population maxima move to the optimal location by actively growing there via cell division. Chapter 3 shows that such growth can cause transient nitrite accumulation by temporarily decoupling AOO from NOB growth. On this basis, I speculate that fast growth of AOA at the constantly moving optimal depth for nitrification could help to explain the feature of primary nitrite maxima (Figure 5.1). This adds to existing hypotheses that postulate the excretion of nitrite by stressed phytoplankton (Vaccaro and Ryther 1960), differential light inhibition of AOO and NOB (Olson 1981), or differences in substrate affinity or yield between AOO and NOB (Zakem et al. 2018). Zakem et al. (2018) additionally propose a role for advective transport of NOB away from the site of optimal nitrification. This is different from the mixing-based model hypothesized here, which presumes that the PNM might be a temporary feature that constantly re-emerges at different depths, rather than a constant, spatially moving feature (Figure 5.1). A mechanism based on differences in AOO

and NOB biomass would be consistent with maximum AO rates and relatively high ratios of AOA vs NOB in the primary nitrite maximum off Costa Rica (Buchwald et al. 2015). However, time-series studies of nitrifier biomass as well as DIN concentrations at relevant oceanic sites are necessary to test this hypothesis. In the open ocean, this is feasible with nitrite and nitrate sensors installed on a moored profiler (Atamanchuk et al. 2020). A moored profiler may not be necessary in Bedford Basin, where weekly sampling is possible and was shown to resolve the transient nitrite accumulations well (Chapter 3). However, the addition of nitrite sensor profiles to the weekly sampling regime or water sampling with higher vertical resolution within the bottom half of the water column are necessary to understand possible vertical variations in the accumulation of nitrite over time.

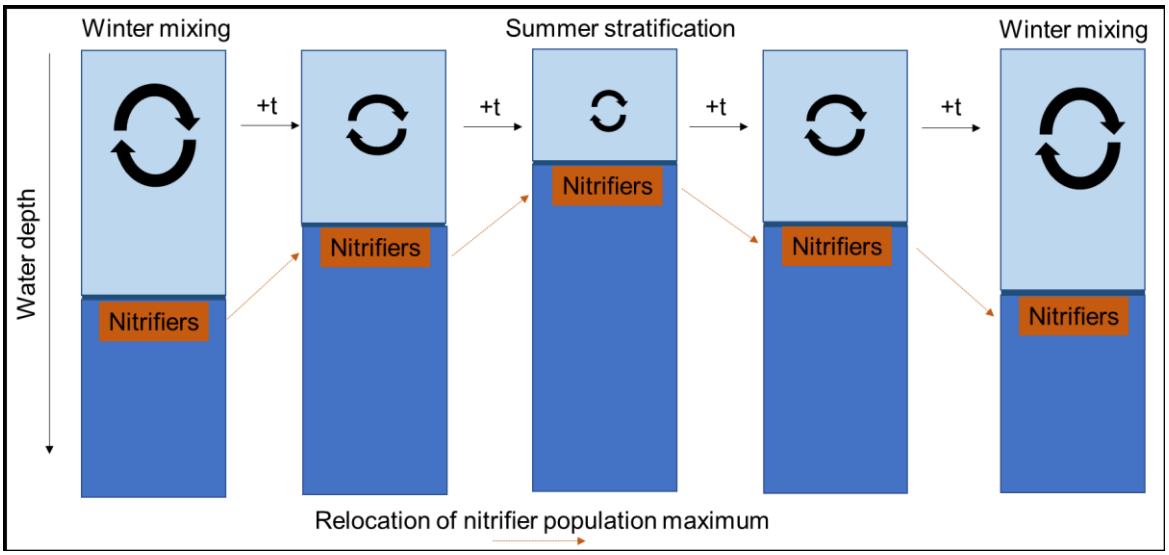

Figure 5.1: Speculative application of the nitrifier dilution-regrowth mechanism identified for Bedford Basin in Chapter 3 to the primary nitrite maximum observed at the base of the euphotic zone in the Open Ocean. Nitrifier biomass grows fastest at the ever-changing optimal location in the water column. This, as shown in Chapter 3, can cause temporary nitrite accumulation.

There may also be applied uses of the dilution-regrowth mechanism. Harmful algal blooms are known to be fueled by ammonium and there is evidence to suggest that they may be prevented or decelerated by lowering ammonium:nitrate ratios (Glibert et al. 2016). In Chapter 3 we provide evidence that in Bedford Basin, nitrifier biomass can be a limiting factor for nitrification, the key process for lowering this ratio. By extension, low nitrifier

biomass could limit nitrification in other coastal systems. Addition of viable nitrifier biomass to systems at risk for harmful algal blooms may present a preventative management tool. The viability and nitrification efficiency of the nitrifier biomass in a given environment would be a key factor for this: biological adaptations of the nitrifier biomass such as substrate affinity, low-oxygen tolerance, salinity and temperature adaptation might determine the success of such an application.

5.4. Concluding Remarks

In conclusion, this thesis highlights the importance of accessible model systems from which well-resolved, multi-disciplinary data can be extracted. Particularly, highly resolved biogeochemical time series with a strong component of functional microbial biomass are identified here as crucial tools that have the potential to link understanding in the realms of aquatic microbiology, geochemistry, physical oceanography and atmospheric forcing within dynamic systems. Notably, the technology to apply such time series also to less accessible parts of the ocean is starting to become available (Robidart et al. 2012; Atamanchuk et al. 2020).

Bedford Basin presents a typical, anthropogenically impacted coastal system, which can be assumed to be a model for contemporary systems of quantitative importance. Conversely (yet complementary), the value of much more unusual systems like Powell Lake lies in their potential analogy with Early-Earth oceans, but also in their status as conceptual end-members or extremes. Powell Lake's ancient seawater community demonstrates the microbiological and biogeochemical consequences of isolating seawater from the atmosphere for millennia. Inquiry into such systems can teach us the conditions under which paradigms about feedback and interactions between biogeochemical processes that are valid in most environments cease to hold true.

BIBLIOGRAPHY

Abubucker, S., N. Segata, J. Goll, and others. 2012. Metabolic Reconstruction for Metagenomic Data and Its Application to the Human Microbiome J.A. Eisen [ed.]. PLoS Comput Biol **8**: e1002358. doi:10.1371/journal.pcbi.1002358

Alawi, M., A. Lipski, T. Sanders, Eva-Maria-Pfeiffer, and E. Spieck. 2007. Cultivation of a novel cold-adapted nitrite oxidizing betaproteobacterium from the Siberian Arctic. ISME J **1**: 256–264. doi:10.1038/ismej.2007.34

Albrechtsen, H. J., and T. H. Christensen. 1994. Evidence for microbial iron reduction in a landfill leachate-polluted aquifer (Vejen, Denmark). Appl Environ Microbiol **60**: 3920–3925.

Algar, C., and J. Vallino. 2014. Predicting microbial nitrate reduction pathways in coastal sediments. Aquat Microb Ecol **71**: 223–238. doi:10.3354/ame01678

Allen, A. E., M. H. Howard-Jones, M. G. Booth, M. E. Frischer, P. G. Verity, D. A. Bronk, and M. P. Sanderson. 2002. Importance of heterotrophic bacterial assimilation of ammonium and nitrate in the Barents Sea during summer. J Mar Syst **38**: 93–108. doi:10.1016/S0924-7963(02)00171-9

Alneberg, J., B. S. Bjarnason, I. de Bruijn, and others. 2014. Binning metagenomic contigs by coverage and composition. Nat Methods **11**: 1144–1146. doi:10.1038/nmeth.3103

Altabet, M. A., W. G. Deuser, S. Honjo, and C. Stienen. 1991. Seasonal and depth-related changes in the source of sinking particles in the North Atlantic. Nature **354**: 136–139. doi:10.1038/354136a0

Amin, S. A., J. W. Moffett, W. Martens-Habbena, and others. 2013. Copper requirements of the ammonia-oxidizing archaeon *Nitrosopumilus maritimus* SCM1 and implications for nitrification in the marine environment. Limnol Oceanogr **58**: 2037–2045. doi:10.4319/lo.2013.58.6.2037

Amir, A., D. McDonald, J. A. Navas-Molina, and others. 2017. Deblur Rapidly Resolves Single-Nucleotide Community Sequence Patterns. mSystems **2**: e00191-16. doi:10.1128/msystems.00191-16

Anderson, R., C. Winter, and K. Jürgens. 2012. Protist grazing and viral lysis as prokaryotic mortality factors at Baltic Sea oxic−anoxic interfaces. Mar Ecol Prog Ser **467**: 1–14. doi:10.3354/meps10001

Andrei, A.-Ş., M. S. Robeson, A. Baricz, and others. 2015. Contrasting taxonomic stratification of microbial communities in two hypersaline meromictic lakes. ISME J **9**: 2642–2656. doi:10.1038/ismej.2015.60

Atamanchuk, D., J. Koelling, U. Send, and D. W. R. Wallace. 2020. Rapid transfer of oxygen to the deep ocean mediated by bubbles. Nat Geosci **13**: 232–237. doi:10.1038/s41561-020-0532-2

Aziz, R. K., D. Bartels, A. A. Best, and others. 2008. The RAST Server: Rapid Annotations using Subsystems Technology. BMC Genomics **9**: 75. doi:10.1186/1471-2164-9-75

Baalsrud, K., and K. S. Baalsrud. 1954. Studies on Thiobacillus denitrificans. Arch Mikrobiol **20**: 34–62. doi:10.1007/BF00412265

Baatar, B., P.-W. Chiang, D. Y. Rogozin, and others. 2016. Bacterial Communities of Three Saline Meromictic Lakes in Central Asia. PLoS One **11**: e0150847. doi:10.1371/journal.pone.0150847

Babbin, A. R., C. Buchwald, F. M. M. Morel, S. D. Wankel, and B. B. Ward. 2020. Nitrite oxidation exceeds reduction and fixed nitrogen loss in anoxic Pacific waters. Mar Chem **224**: 103814. doi:10.1016/j.marchem.2020.103814

Babbin, A. R., B. D. Peters, C. W. Mordy, B. Widner, K. L. Casciotti, and B. B. Ward. 2017. Multiple metabolisms constrain the anaerobic nitrite budget in the Eastern Tropical South Pacific. Global Biogeochem Cycles **31**: 258–271. doi:10.1002/2015GB005327.Received

Baer, S. E., T. L. Connelly, R. E. Sipler, P. L. Yager, and D. A. Bronk. 2014. Effect of temperature on rates of ammonium uptake and nitrification in the western coastal Arctic during winter, spring, and summer. Global Biogeochem Cycles **28**: 1455–1466. doi:10.1002/2013GB004765

Balzer, W. 1982. On the distribution of iron and manganese at the sediment/water interface: thermodynamic versus kinetic control. Geochim Cosmochim Acta **46**: 1153–1161. doi:10.1016/0016-7037(82)90001-1

Bange, H. W. 2006. Nitrous oxide and methane in European coastal waters. Estuar Coast Shelf Sci **70**: 361–374. doi:10.1016/j.ecss.2006.05.042

Barford, C. C., J. P. Montoya, M. A. Altabet, and R. Mitchell. 1999. Steady-state nitrogen isotope effects of N_2 and N_2O production in *Paracoccus denitrificans*. Appl Environ Microbiol **65**: 989–994. doi:10.1128/aem.65.3.989-994.1999

Bartlett, R., R. J. G. Mortimer, and K. Morris. 2008. Anoxic nitrification: Evidence from Humber Estuary sediments (UK). Chem Geol **250**: 29–39. doi:10.1016/j.chemgeo.2008.02.001

Behrenfeld, M. J. 2010. Abandoning Sverdrup's Critical Depth Hypothesis on phytoplankton blooms. Ecology **91**: 977–989. doi:10.1890/09-1207.1

Berg, G., M. Balode, I. Purina, S. Bekere, C. Béchemin, and S. Maestrini. 2003. Plankton community composition in relation to availability and uptake of oxidized and reduced nitrogen. Aquat Microb Ecol **30**: 263–274. doi:10.3354/ame030263

Berg, I. A., D. Kockelkorn, W. H. Ramos-Vera, R. F. Say, J. Zarzycki, M. Hügler, B. E. Alber, and G. Fuchs. 2010. Autotrophic carbon fixation in archaea. Nat Rev Microbiol **8**: 447–460. doi:10.1038/nrmicro2365

Berner, R. 1980. Early diagenesis: a theoretical approach, 1st ed. Princeton University Press.

Berounsky, V. M., and S. W. Nixon. 1990. Temperature and annual cycle of nitrification in waters of Narragansett Bay. Limnol Oceanogr **35**: 1610–1617. doi:10.4319/lo.1990.35.7.1610

Bertagnolli, A. D., and F. J. Stewart. 2018. Microbial niches in marine oxygen minimum zones. Nat Rev Microbiol **16**: 723–729. doi:10.1038/s41579-018-0087-z

Beulig, F., H. Røy, S. E. McGlynn, and B. B. Jørgensen. 2019. Cryptic CH_4 cycling in the sulfate–methane transition of marine sediments apparently mediated by ANME-1 archaea. ISME J **13**: 250–262. doi:10.1038/s41396-018-0273-z

Bianchi, D., T. S. Weber, R. Kiko, and C. Deutsch. 2018. Global niche of marine anaerobic metabolisms expanded by particle microenvironments. Nat Geosci **11**: 263–268. doi:10.1038/s41561-018-0081-0

Bigeleisen, J. 1949. The Relative Reaction Velocities of Isotopic Molecules. J Chem Phys **17**: 675–678. doi:10.1063/1.1747368

Bigeleisen, J. 1965. Chemistry of isotopes. Science **147**: 463–471. doi:10.1126/science.147.3657.463

Bindoff, N. L., W. W. L. Cheung, J. G. Kairo, and others. 2019. Changing ocean, marine ecosystems, and dependent communities, *In* H.-O. Pörtner, D.C. Roberts, V. Masson-Delmotte, et al. [eds.], IPCC special report on the ocean and cryosphere in a changing climate.

Blackburne, R., V. M. Vadivelu, Z. Yuan, and J. Keller. 2007. Kinetic characterisation of an enriched *Nitrospira* culture with comparison to *Nitrobacter*. Water Res **41**: 3033–3042. doi:10.1016/j.watres.2007.01.043

Bolger, A. M., M. Lohse, and B. Usadel. 2014. Trimmomatic: a flexible trimmer for Illumina sequence data. Bioinformatics **30**: 2114–2120. doi:10.1093/bioinformatics/btu170

Bollmann, A., I. Schmidt, A. M. Saunders, and M. H. Nicolaisen. 2005. Influence of starvation on potential ammonia-oxidizing activity and *amoA* mRNA levels of *Nitrosospira briensis*. Appl Environ Microbiol **71**: 1276–1282. doi:10.1128/AEM.71.3.1276-1282.2005

Bolyen, E., J. R. Rideout, M. R. Dillon, and others. 2019. Reproducible, interactive, scalable and extensible microbiome data science using QIIME 2. Nat Biotechnol **37**: 852–857. doi:10.1038/s41587-019-0209-9

Bombar, D., R. W. Paerl, and L. Riemann. 2016. Marine Non-Cyanobacterial Diazotrophs: Moving beyond Molecular Detection. Trends Microbiol **24**: 916–927. doi:10.1016/J.TIM.2016.07.002

Bourbonnais, A., M. A. Altabet, C. N. Charoenpong, J. Larkum, H. Hu, H. W. Bange, and L. Stramma. 2015. N-loss isotope effects in the Peru oxygen minimum zone studied using a mesoscale eddy as a natural tracer experiment. Global Biogeochem Cycles **29**: 1–19. doi:10.1002/2014GB005001.Received

Bourbonnais, A., M. F. Lehmann, R. C. Hamme, C. C. Manning, and S. K. Juniper. 2013. Nitrate elimination and regeneration as evidenced by dissolved inorganic nitrogen isotopes in Saanich Inlet, a seasonally anoxic fjord. Mar Chem **157**: 194–207. doi:10.1016/j.marchem.2013.09.006

Bourbonnais, A., R. T. Letscher, H. W. Bange, V. Échevin, J. Larkum, J. Mohn, N. Yoshida, and M. A. Altabet. 2017. N_2O production and consumption from stable isotopic and concentration data in the Peruvian coastal upwelling system. Global Biogeochem Cycles 678–698. doi:10.1002/2016GB005567

Bouskill, N. J., J. Tang, W. J. Riley, and E. L. Brodie. 2012. Trait-based representation of biological nitrification: Model development, testing, and predicted community composition. Front Microbiol **3**: 364. doi:10.3389/fmicb.2012.00364

De Brabandere, L., N. Brion, M. Elskens, W. Baeyens, and F. Dehairs. 2007. $\delta^{15}N$ dynamics of ammonium and particulate nitrogen in a temperate eutrophic estuary. Biogeochemistry **82**: 1–14. doi:10.1007/s10533-006-9047-1

Braman, R. S., and S. A. Hendrix. 1989. Nanogram Nitrite and Nitrate Determination in Environmental and Biological Materials by Vanadium(III) Reduction with Chemiluminescence Detection. Anal Chem **61**: 2715–2718.

von Brand, T., N. W. Rakestraw, and C. E. Renn. 1937. The experimental decomposition and regeneration of nitrogenous organic matter in sea water. Biol Bull **72**: 165–175.

Brandes, J. A., and A. H. Devol. 1997. Isotopic fractionation of oxygen and nitrogen in coastal marine sediments. Geochim Cosmochim Acta **61**: 1793–1801. doi:10.1016/S0016-7037(97)00041-0

Brandhorst, W. 1958. Nitrite Accumulation in the North-East Tropical Pacific. Nature **182**: 679–679. doi:10.1038/182679a0

Breitburg, D., L. A. Levin, A. Oschlies, and others. 2018. Declining oxygen in the global ocean and coastal waters. Science **359**: eaam7240. doi:10.1126/science.aam7240

Bristow, L. A., T. Dalsgaard, L. Tiano, and others. 2016. Ammonium and nitrite oxidation at nanomolar oxygen concentrations in oxygen minimum zone waters. Proc Natl Acad Sci USA **113**: 10601–10606. doi:10.1073/pnas.1600359113

Bristow, L. A., N. Sarode, J. Cartee, A. Caro-Quintero, B. Thamdrup, and F. J. Stewart. 2015. Biogeochemical and metagenomic analysis of nitrite accumulation in the Gulf of Mexico hypoxic zone. Limnol Oceanogr **60**: 1733–1750. doi:10.1002/lno.10130

Bronk, D., P. Glibert, T. Malone, S. Banahan, and E. Sahlsten. 1998. Inorganic and organic nitrogen cycling in Chesapeake Bay: autotrophic versus heterotrophic processes and relationships to carbon flux. Aquat Microb Ecol **15**: 177–189. doi:10.3354/ame015177

Brunner, B., S. Contreras, M. F. Lehmann, and others. 2013. Nitrogen isotope effects induced by anammox bacteria. Proc Natl Acad Sci USA **110**: 18994–18999. doi:10.1073/pnas.1310488110

Bryan, B., G. Shearer, J. Skeeters, and D. Kohl. 1983. Variable expression of the nitrogen isotope effect associated with denitrification of nitrite. J Biol Chem **258**: 8613–8617.

Bryant, D. A., Z. Liu, T. Li, and others. 2012. Comparative and Functional Genomics of Anoxygenic Green Bacteria from the Taxa *Chlorobi*, *Chloroflexi*, and *Acidobacteria*, p. 47–102. *In* V.W. Burnap R. [ed.], Functional Genomics and Evolution of Photosynthetic Systems. Advances in Photosynthesis and Respiration. Springer, Dordrecht.

Buchwald, C., and K. L. Casciotti. 2010. Oxygen isotopic fractionation and exchange during bacterial nitrite oxidation. Limnol Oceanogr **55**: 1064–1074. doi:10.4319/lo.2010.55.3.1064

Buchwald, C., K. Grabb, C. M. Hansel, and S. D. Wankel. 2016. Constraining the role of iron in environmental nitrogen transformations: Dual stable isotope systematics of abiotic NO_2^- reduction by Fe(II) and its production of N_2O. Geochim Cosmochim Acta **186**: 1–12. doi:10.1016/j.gca.2016.04.041

Buchwald, C., K. Homola, A. J. Spivack, E. R. Estes, R. W. Murray, and S. D. Wankel. 2018. Isotopic Constraints on Nitrogen Transformation Rates in the Deep Sedimentary Marine Biosphere. Global Biogeochem Cycles **32**: 1688–1702. doi:10.1029/2018GB005948

Buchwald, C., A. E. Santoro, S. R. HR, and K. L. Casciotti. 2015. Nitrogen cycling in the secondary nitrite maximum of the eastern tropical North Pacific off Costa Rica. Global Biogeochem Cycles **29**: 22–23. doi:10.1002/2015GB005187.Received

Buchwald, C., A. E. Santoro, M. R. McIlvin, and K. L. Casciotti. 2012. Oxygen isotopic composition of nitrate and nitrite produced by nitrifying cocultures and natural marine assemblages. Limnol Oceanogr **57**: 1361–1375. doi:10.4319/lo.2012.57.5.1361

Buchwald, C., and S. Wankel. 2020. Put it in Reverse: Isotopic Insights From a Nitrite-oxidizer Performing Nitrate Reduction. *Ocean Sciences Meeting*.

Burt, W. J., H. Thomas, K. Fennel, and E. Horne. 2013. Sediment-water column fluxes of carbon, oxygen and nutrients in Bedford Basin, Nova Scotia, inferred from ^{224}Ra measurements. Biogeosciences **10**: 53–66. doi:10.5194/bg-10-53-2013

Calvert, S. E., and T. F. Pedersen. 1996. Sedimentary geochemistry of manganese: implications for the environment of formation of manganiferous black shales. Econ Geol **91**: 36–47. doi:10.2113/gsecongeo.91.1.36

Campbell, J. H., P. O'Donoghue, A. G. Campbell, P. Schwientek, A. Sczyrba, T. Woyke, D. Söll, and M. Podar. 2013. UGA is an additional glycine codon in uncultured SR1 bacteria from the human microbiota. Proc Natl Acad Sci USA **110**: 5540–5545. doi:10.1073/pnas.1303090110

Canfield, D. E. 1983. Prediction of chlorophyll a concentrations in Florida lakes: The importance of phosphorus and nitrogen. JAWRA J Am Water Resour Assoc **19**: 255–262. doi:10.1111/j.1752-1688.1983.tb05323.x

Canfield, D. E., A. N. Glazer, and P. G. Falkowski. 2010a. The evolution and future of earth's nitrogen cycle. Science **330**: 192–196. doi:10.1126/science.1186120

Canfield, D. E., F. J. Stewart, B. Thamdrup, L. De Brabandere, T. Dalsgaard, E. F. Delong, N. P. Revsbech, and O. Ulloa. 2010b. A cryptic sulfur cycle in oxygen-minimum-zone waters off the Chilean coast. Science **330**: 1375–1378. doi:10.1126/science.1196889

Canfield, D. E., and B. Thamdrup. 2009. Towards a consistent classification scheme for geochemical environments, or, why we wish the term 'suboxic' would go away. Geobiology **7**: 385–392. doi:10.1111/j.1472-4669.2009.00214.x

Caporaso, J. G., J. Kuczynski, J. Stombaugh, and others. 2010. QIIME allows analysis of high-throughput community sequencing data. Nat Methods **7**: 335–336. doi:10.1038/nmeth.f.303

Capotondi, A., M. A. Alexander, N. A. Bond, E. N. Curchitser, and J. D. Scott. 2012. Enhanced upper ocean stratification with climate change in the CMIP3 models. J Geophys Res Ocean **117**. doi:10.1029/2011JC007409

Caranto, J. D., and K. M. Lancaster. 2017. Nitric oxide is an obligate bacterial nitrification intermediate produced by hydroxylamine oxidoreductase. Proc Natl Acad Sci USA **114**: 8217–8222. doi:10.1073/pnas.1704504114

Casamayor, E. O., M. Llirós, A. Picazo, A. Barberán, C. M. Borrego, and A. Camacho. 2012. Contribution of deep dark fixation processes to overall CO_2 incorporation and large vertical changes of microbial populations in stratified karstic lakes. Aquat Sci **74**: 61–75. doi:10.1007/s00027-011-0196-5

Casamayor, E. O., X. Triadó-Margarit, and C. Castañeda. 2013. Microbial biodiversity in saline shallow lakes of the Monegros Desert, Spain. FEMS Microbiol Ecol **85**: 503–518. doi:10.1111/1574-6941.12139

Casciotti, K. L. 2009. Inverse kinetic isotope fractionation during bacterial nitrite oxidation. Geochim Cosmochim Acta **73**: 2061–2076. doi:10.1016/j.gca.2008.12.022

Casciotti, K. L. 2016. Nitrogen and Oxygen Isotopic Studies of the Marine Nitrogen Cycle. Ann Rev Mar Sci **8**: 379–407. doi:10.1146/annurev-marine-010213-135052

Casciotti, K. L., J. K. Böhlke, M. R. McIlvin, S. J. Mroczkowski, and J. E. Hannon. 2007. Oxygen isotopes in nitrite: Analysis, calibration, and equilibration. Anal Chem **79**: 2427–2436. doi:10.1021/ac061598h

Casciotti, K. L., C. Buchwald, and M. McIlvin. 2013. Implications of nitrate and nitrite isotopic measurements for the mechanisms of nitrogen cycling in the Peru oxygen deficient zone. Deep Res Part I Oceanogr Res Pap **80**: 78–93. doi:10.1016/j.dsr.2013.05.017

Casciotti, K. L., C. Buchwald, A. E. Santoro, and C. Frame. 2010a. Assessment of nitrogen and oxygen isotopic fractionation during nitrification and its expression in the marine environment. Methods Enzymol **486**: 253–280. doi:10.1016/B978-0-12-381294-0.00011-0

Casciotti, K. L., M. McIlvin, and C. Buchwald. 2010b. Oxygen isotopic exchange and fractionation during bacterial ammonia oxidation. Limnol Oceanogr **55**: 753–762. doi:10.4319/lo.2009.55.2.0753

Casciotti, K. L., and M. R. McIlvin. 2007. Isotopic analyses of nitrate and nitrite from reference mixtures and application to Eastern Tropical North Pacific waters. Mar Chem **107**: 184–201. doi:10.1016/j.marchem.2007.06.021

Casciotti, K. L., D. M. Sigman, and B. B. Ward. 2003. Linking Diversity and Stable Isotope Fractionation in Ammonia-Oxidizing Bacteria. Geomicrobiol J **20**: 335–353. doi:10.1080/01490450303895

Casciotti, K. L., T. W. Trull, D. M. Glover, and D. Davies. 2008. Constraints on nitrogen cycling at the subtropical North Pacific Station ALOHA from isotopic measurements of nitrate and particulate nitrogen. Deep Res Part II Top Stud Oceanogr **55**: 1661–1672. doi:10.1016/j.dsr2.2008.04.017

Chronopoulou, P., F. Shelley, W. Pritchard, S. T. Maanoja, and M. Trimmer. 2017. Origin and fate of methane in the Eastern Tropical North Pacific oxygen minimum zone. ISME J **11**: 1386–1399.

Clarke, K. R. 1993. Non-parametric multivariate analyses of changes in community structure. Austral Ecol **18**: 117–143. doi:10.1111/j.1442-9993.1993.tb00438.x

Clarke, K. R. 2006. PRIMER v6: User Manual/Tutorial, R.N. Gorley [ed.]. PRIMER-E.

Cline, J. D. 1969. Spectrophotometric Determination of Hydrogen Sulfide in Natural Waters. Limnol Oceanogr **14**: 454–458. doi:10.4319/lo.1969.14.3.0454

Cloern, J. E., B. E. Cole, and R. S. Oremland. 1983. Autotrophic processes in meromictic Big Soda Lake, Nevada. Limnol Oceanogr **28**: 1049–1061. doi:10.4319/lo.1983.28.6.1049

Coble, P. G., R. B. Gagosian, L. A. Codispoti, G. E. Friederich, and J. P. Christensen. 1991. Vertical distribution of dissolved and particulate fluorescence in the Black Sea. Deep Sea Res Part A Oceanogr Res Pap **38**: S985–S1001. doi:10.1016/S0198-0149(10)80020-2

Cohen, Y. 1978. Consumption of dissolved nitrous oxide in an anoxic basin, Saanich Inlet, British Columbia. Nature **272**: 235–237.

Comeau, A. M., G. M. Douglas, and M. G. I. Langille. 2017. Microbiome Helper: a Custom and Streamlined Workflow for Microbiome Research J. Eisen [ed.]. mSystems **2**: e00127-16. doi:10.1128/mSystems.00127-16

Comeau, A. M., T. Harding, P. E. Galand, W. F. Vincent, and C. Lovejoy. 2012. Vertical distribution of microbial communities in a perennially stratified Arctic lake with saline, anoxic bottom waters. Sci Rep **2**: 1–10. doi:10.1038/srep00604

Comeau, A. M., W. K. W. Li, J.-É. Tremblay, E. C. Carmack, and C. Lovejoy. 2011. Arctic Ocean Microbial Community Structure before and after the 2007 Record Sea Ice Minimum J.A. Gilbert [ed.]. PLoS One **6**: e27492. doi:10.1371/journal.pone.0027492

Crowe, S. A., C. Jones, S. Katsev, and others. 2008a. Photoferrotrophs thrive in an Archean Ocean analogue. Proc Natl Acad Sci USA **105**: 15938–15943. doi:10.1073/PNAS.0805313105

Crowe, S. A., S. Katsev, K. Leslie, and others. 2011. The methane cycle in ferruginous Lake Matano. Geobiology **9**: 61–78. doi:10.1111/j.1472-4669.2010.00257.x

Crowe, S. A., J. A. Maresca, C. Jones, and others. 2014. Deep-water anoxygenic photosythesis in a ferruginous chemocline. Geobiology **12**: 322–339. doi:10.1111/gbi.12089

Crowe, S. A., A. H. O'Neill, S. Katsev, P. Hehanussa, G. D. Haffner, B. Sundby, A. Mucci, and D. A. Fowle. 2008b. The biogeochemistry of tropical lakes: A case study from Lake Matano, Indonesia. Limnol Oceanogr **53**: 319–331. doi:10.4319/lo.2008.53.1.0319

Daims, H., E. V Lebedeva, P. Pjevac, and others. 2015. Complete nitrification by *Nitrospira* bacteria. Nature **528**: 504–509. doi:10.1038/nature16461

Dalsgaard, T., D. E. Canfield, J. Petersen, B. Thamdrup, and J. Acuña-González. 2003. N_2 production by the anammox reaction in the anoxic water column of Golfo Dulce, Costa Rica. Nature **422**: 606–608. doi:10.1038/nature01526

Davison, W. 1993. Iron and manganese in lakes. Earth-Science Rev **34**: 119–163. doi:10.1016/0012-8252(93)90029-7

Delcher, A. L., A. Phillippy, J. Carlton, and S. L. Salzberg. 2002. Fast algorithms for large-scale genome alignment and comparison. Nucleic Acids Res **30**: 2478–2483. doi:10.1093/nar/30.11.2478

Delmont. 2017. Recovering HBDs from TARA Oceans Metagenomes – Meren Lab.

Delmont, T. O., C. Quince, A. Shaiber, and others. 2018. Nitrogen-fixing populations of Planctomycetes and Proteobacteria are abundant in surface ocean metagenomes. Nat Microbiol **3**: 804–813. doi:10.1038/s41564-018-0176-9

Delwiche, C. C., and P. L. Steyn. 1970. Nitrogen isotope fractionation in soils and microbial reactions. Environ Sci Technol **4**: 929–935. doi:10.1021/es60046a004

Desai, D. K., F. D. Desai, and J. LaRoche. 2012. Factors Influencing the Diversity of Iron Uptake Systems in Aquatic Microorganisms. Front Microbiol **3**: 362. doi:10.3389/fmicb.2012.00362

DeSantis, T. Z., P. Hugenholtz, N. Larsen, and others. 2006. Greengenes, a chimera-checked 16S rRNA gene database and workbench compatible with ARB. Appl Environ Microbiol **72**: 5069–5072. doi:10.1128/AEM.03006-05

Dimitriu, P. A., H. C. Pinkart, B. M. Peyton, and M. R. Mormile. 2008. Spatial and temporal patterns in the microbial diversity of a meromictic soda lake in Washington State. Appl Environ Microbiol **74**: 4877–4888. doi:10.1128/AEM.00455-08

Domangue, R. J., and B. Mortazavi. 2018. Nitrate reduction pathways in the presence of excess nitrogen in a shallow eutrophic estuary. Environ Pollut **238**: 599–606. doi:10.1016/J.ENVPOL.2018.03.033

Domingues, R. B., A. B. Barbosa, U. Sommer, and H. M. Galvão. 2011. Ammonium, nitrate and phytoplankton interactions in a freshwater tidal estuarine zone: potential effects of cultural eutrophication. Aquat Sci **73**: 331–343. doi:10.1007/s00027-011-0180-0

Duce, R. A., J. LaRoche, K. Altieri, and others. 2008. Impacts of atmospheric anthropogenic nitrogen on the open ocean. Science **320**: 893–897. doi:10.1126/science.1150369

Dutkiewicz, S., M. Follows, J. Marshall, and W. W. Gregg. 2001. Interannual variability of phytoplankton abundances in the North Atlantic. Deep Res Part II Top Stud Oceanogr **48**: 2323–2344. doi:10.1016/S0967-0645(00)00178-8

Dutkiewicz, S., J. R. Scott, and M. J. Follows. 2013. Winners and losers: Ecological and biogeochemical changes in a warming ocean. Global Biogeochem Cycles **27**: 463–477. doi:10.1002/gbc.20042

Eddy, S. R. 2011. Accelerated Profile HMM Searches W.R. Pearson [ed.]. PLoS Comput Biol **7**: e1002195. doi:10.1371/journal.pcbi.1002195

Edgar, R. C. 2004. MUSCLE: a multiple sequence alignment method with reduced time and space complexity. BMC Bioinformatics **5**: 113. doi:10.1186/1471-2105-5-113

El-Swais, H., K. A. Dunn, J. P. Bielawski, W. K. W. Li, and D. A. Walsh. 2015. Seasonal assemblages and short-lived blooms in coastal north-west Atlantic Ocean bacterioplankton. Environ Microbiol **17**: 3642–3661. doi:10.1111/1462-2920.12629

Eren, A. M., Ö. C. Esen, C. Quince, J. H. Vineis, H. G. Morrison, M. L. Sogin, and T. O. Delmont. 2015. Anvi'o: an advanced analysis and visualization platform for 'omics data. PeerJ **3**: e1319. doi:10.7717/peerj.1319

Eren, A. M., J. H. Vineis, H. G. Morrison, and M. L. Sogin. 2013. A Filtering Method to Generate High Quality Short Reads Using Illumina Paired-End Technology I.K. Jordan [ed.]. PLoS One **8**: e66643. doi:10.1371/journal.pone.0066643

Ettwig, K. F., M. K. Butler, D. Le Paslier, and others. 2010. Nitrite-driven anaerobic methane oxidation by oxygenic bacteria. Nature **464**: 543–548. doi:10.1038/nature08883

Fader, G., and R. Miller. 2008. Surficial geology, Halifax Harbour, Nova Scotia. Geol Surv Canada Bull **590**: 1–165.

Falkowski, P. 1997. Evolution of the nitrogen cycle and its influence on the biological sequestration of CO_2 in the ocean. Nature **387**: 272–275. doi:10.1038/387272a0

Fasham, M. J. R., H. W. Ducklow, and S. M. McKelvie. 1990. A nitrogen-based model of plankton dynamics in the oceanic mixed layer. J Mar Res **48**: 591–639. doi:10.1357/002224090784984678

Fennel, K., R. Hetland, Y. Feng, and S. DiMarco. 2011. A coupled physical-biological model of the Northern Gulf of Mexico shelf: model description, validation and analysis of phytoplankton variability. Biogeosciences **8**: 1881–1899. doi:10.5194/bg-8-1881-2011

Fennel, K., J. Wilkin, J. Levin, J. Moisan, J. O'Reilly, and D. Haidvogel. 2006. Nitrogen cycling in the Middle Atlantic Bight: Results from a three-dimensional model and implications for the North Atlantic nitrogen budget. Global Biogeochem Cycles **20**: GB3007. doi:10.1029/2005GB002456

Fiedler, B., D. S. Grundle, F. Schütte, and others. 2016. Oxygen utilization and downward carbon flux in an oxygen-depleted eddy in the eastern tropical North Atlantic. Biogeosciences **13**: 5633–5647. doi:10.5194/bg-13-5633-2016

Finster, K. 2008. Microbiological disproportionation of inorganic sulfur compounds. J Sulfur Chem **29**: 281–292. doi:10.1080/17415990802105770

Fish, J. A., B. Chai, Q. Wang, Y. Sun, C. T. Brown, J. M. Tiedje, and J. R. Cole. 2013. FunGene: the functional gene pipeline and repository. Front Microbiol **4**: 291. doi:10.3389/fmicb.2013.00291

Flament, P. 2002. A state variable for characterizing water masses and their diffusive stability: spiciness. Prog Oceanogr **54**: 493–501. doi:10.1016/S0079-6611(02)00065-4

Fontugne, M., F. Guichard, I. Bentaleb, C. Strechie, and G. Lericolais. 2009. Variations in ^{14}C Reservoir Ages of Black Sea Waters and Sedimentary Organic Carbon During Anoxic Periods: Influence of Photosynthetic Versus Chemoautotrophic Production. Radiocarbon **51**: 969–976. doi:10.1017/S0033822200034044

Fowler, D., M. Coyle, U. Skiba, and others. 2013. The global nitrogen cycle in the twenty-first century. Philos Trans R Soc B Biol Sci **368**: 20130164. doi:10.1098/rstb.2013.0164

Francis, C. A., K. J. Roberts, J. M. Beman, A. E. Santoro, and B. B. Oakley. 2005. Ubiquity and diversity of ammonia-oxidizing archaea in water columns and sediments of the ocean. Proc Natl Acad Sci USA **102**: 14683–14688. doi:10.1073/pnas.0506625102

Froelich, P. N., G. P. Klinkhammer, M. L. Bender, and others. 1979. Early oxidation of organic matter in pelagic sediments of the eastern equatorial Atlantic: suboxic diagenesis. Geochim Cosmochim Acta **43**: 1075–1090. doi:10.1016/0016-7037(79)90095-4

Frontier, S. 1985. Diversity and structure in aquatic ecosystems. Oceanogr Mar Biol **23**: 253–312.

Fry, B. 2006. Stable Isotope Ecology, Springer.

Fuchsman, C. A., A. H. Devol, K. L. Casciotti, C. Buchwald, B. X. Chang, and R. E. A. Horak. 2018. An N isotopic mass balance of the Eastern Tropical North Pacific oxygen deficient zone. Deep Sea Res Part II Top Stud Oceanogr **156**: 137–147. doi:10.1016/J.DSR2.2017.12.013

Füssel, J., P. Lam, G. Lavik, M. M. Jensen, M. Holtappels, M. Günter, and M. M. Kuypers. 2012. Nitrite oxidation in the Namibian oxygen minimum zone. ISME J **6**: 1200–1209. doi:10.1038/ismej.2011.178

Galand, P. E., C. Gutiérrez-Provecho, R. Massana, J. M. Gasol, and E. O. Casamayor. 2010. Inter-annual recurrence of archaeal assemblages in the coastal NW Mediterranean Sea (Blanes Bay Microbial Observatory). Limnol Oceanogr **55**: 2117–2125. doi:10.4319/lo.2010.55.5.2117

Ganesh, S., L. A. Bristow, M. Larsen, N. Sarode, B. Thamdrup, and F. J. Stewart. 2015. Size-fraction partitioning of community gene transcription and nitrogen metabolism in a marine oxygen minimum zone. ISME J **9**: 2682–2696. doi:10.1038/ismej.2015.44

Garcia, S. L., K. D. McMahon, M. Martinez-Garcia, and others. 2013. Metabolic potential of a single cell belonging to one of the most abundant lineages in freshwater bacterioplankton. ISME J **7**: 137–147. doi:10.1038/ismej.2012.86

Gebbie, G., and P. Huybers. 2012. The Mean Age of Ocean Waters Inferred from Radiocarbon Observations: Sensitivity to Surface Sources and Accounting for Mixing Histories. J Phys Oceanogr **42**: 291–305. doi:10.1175/JPO-D-11-043.1

Gelda, R. K., S. W. Effler, and C. M. Brooks. 1999. Nitrite and the Two Stages of Nitrification in Nitrogen Polluted Onondaga Lake, New York. J Environ Qual **28**: 1505–1517. doi:10.2134/jeq1999.00472425002800050016x

Georges, A. A., H. El-Swais, S. E. Craig, W. K. Li, and D. A. Walsh. 2014. Metaproteomic analysis of a winter to spring succession in coastal northwest Atlantic Ocean microbial plankton. ISME J **8**: 1301–1313. doi:10.1038/ismej.2013.234

Ghylin, T. W., S. L. Garcia, F. Moya, and others. 2014. Comparative single-cell genomics reveals potential ecological niches for the freshwater acI Actinobacteria lineage. ISME J **8**: 2503–2516. doi:10.1038/ismej.2014.135

Giblin, A. E., C. R. Tobias, B. Song, N. Weston, G. T. Banta, and V. H.Rivera-Monraoy. 2013. The Importance of Dissimilatory Nitrate Reduction to Ammonium (DNRA) in the Nitrogen Cycle of Coastal Ecosystems. Oceanography **26**: 124–131. doi:10.2307/24862073

Gies, E. A., K. M. Konwar, J. T. Beatty, and S. J. Hallam. 2014. Illuminating microbial dark matter in meromictic Sakinaw Lake. Appl Environ Microbiol **80**: 6807–6818. doi:10.1128/AEM.01774-14

Glaubitz, S., K. Kießlich, C. Meeske, M. Labrenz, and K. Jürgens. 2013. SUP05 dominates the Gammaproteobacterial sulfur oxidizer assemblages in pelagic redoxclines of the central Baltic and Black Seas. Appl Environ Microbiol **79**: 2767–76. doi:10.1128/AEM.03777-12

Glibert, P. M., R. Maranger, D. J. Sobota, and L. Bouwman. 2014. The Haber Bosch–harmful algal bloom (HB–HAB) link - IOPscience. Environ Res Lett **9**: 105001.

Glibert, P. M., J. J. Middelburg, J. W. McClelland, and M. J. Vander Zanden. 2019. Stable isotope tracers: Enriching our perspectives and questions on sources, fates, rates, and pathways of major elements in aquatic systems. Limnol Oceanogr **64**: 950–981. doi:10.1002/LNO.11087

Glibert, P. M., F. P. Wilkerson, R. C. Dugdale, and others. 2016. Pluses and minuses of ammonium and nitrate uptake and assimilation by phytoplankton and implications for productivity and community composition, with emphasis on nitrogen-enriched conditions. Limnol Oceanogr **61**: 165–197. doi:10.1002/LNO.10203

Graf, D. R. H., C. M. Jones, and S. Hallin. 2014. Intergenomic Comparisons Highlight Modularity of the Denitrification Pathway and Underpin the Importance of Community Structure for N_2O Emissions V. De Crécy-Lagard [ed.]. PLoS One **9**: e114118. doi:10.1371/journal.pone.0114118

Graf, J. S., M. J. Mayr, H. K. Marchant, and others. 2018. Bloom of a denitrifying methanotroph, '*Candidatus* Methylomirabilis limnetica', in a deep stratified lake. Environ Microbiol **20**: 2598–2614. doi:10.1111/1462-2920.14285

Granger, J., M. G. Prokopenko, D. M. Sigman, C. W. Mordy, Z. M. Morse, L. V. Morales, R. N. Sambrotto, and B. Plessen. 2011. Coupled nitrification-denitrification in sediment of the eastern Bering Sea shelf leads to ^{15}N enrichment of fixed N in shelf waters. J Geophys Res Ocean **116**: C11006. doi:10.1029/2010JC006751

Granger, J., and D. M. Sigman. 2009. Removal of nitrite with sulfamic acid for nitrate N and O isotope analysis with the denitrifier method. Rapid Commun Mass Spectrom **23**: 3753–3762. doi:10.1002/rcm.4307

Granger, J., D. M. Sigman, M. F. Lehmann, and P. D. Tortell. 2008. Nitrogen and oxygen isotope fractionation during dissimilatory nitrate reduction by denitrifying bacteria. Limnol Oceanogr **53**: 2533–2545.

Granger, J., D. M. Sigman, J. A. Needoba, and P. J. Harrison. 2004. Coupled nitrogen and oxygen isotope fractionation of nitrate during assimilation by cultures of marine phytoplankton. Limnol Oceanogr **49**: 1763–1773. doi:10.4319/lo.2004.49.5.1763

Greenan, B. J. W., T. S. James, J. W. Loder, and others. 2019. Changes in Oceans Surrounding Canada, p. 343–423. *In* E. Bush and D. Lemmen [eds.], Canada's Changing Climate Report. Government of Canada.

Gregory, D. 1993. Oceanographic, geographic and hydrological parameters of Scotia-Fundy and southern Gulf of St. Lawrence inlets. Can Tech Rep Hydrogr Ocean Sci **143**: 1–248.

Griffin, B. M., J. Schott, and B. Schink. 2007. Nitrite, an Electron Donor for Anoxygenic Photosynthesis. Science **316**: 1870–1870. doi:10.1126/science.1139478

Groeneweg, J., B. Sellner, and W. Tappe. 1994. Ammonia Oxidation in Nitrosomonas at NH_3 Concentrations Near K_m: Effects of pH and Temperature. Water Res **28**: 2561–2566.

Großkopf, T., and J. LaRoche. 2012. Direct and indirect costs of dinitrogen fixation in *Crocosphaera watsonii* WH8501 and Possible Implications for the nitrogen cycle. Front Microbiol **3**: 236. doi:10.3389/fmicb.2012.00236

Gruber, N. 2008. The Marine Nitrogen Cycle: Overview and Challenges. Nitrogen Mar Environ **2**: 1–50. doi:10.1016/B978-0-12-372522-6.00001-3

Grundle, D. S., and S. K. Juniper. 2011. Nitrification from the lower euphotic zone to the sub-oxic waters of a highly productive British Columbia fjord. Mar Chem **126**: 173–181. doi:10.1016/j.marchem.2011.06.001

Grzymski, J. J., C. S. Riesenfeld, T. J. Williams, A. M. Dussaq, H. Ducklow, M. Erickson, R. Cavicchioli, and A. E. Murray. 2012. A metagenomic assessment of winter and summer bacterioplankton from Antarctica Peninsula coastal surface waters. ISME J **6**: 1901–1915. doi:10.1038/ismej.2012.31

Guildford, S. J., and R. E. Hecky. 2000. Total nitrogen, total phosphorus, and nutrient limitation in lakes and oceans: Is there a common relationship? Limnol Oceanogr **45**: 1213–1223. doi:10.4319/lo.2000.45.6.1213

Guillou, L., D. Bachar, S. Audic, and others. 2013. The Protist Ribosomal Reference database (PR2): a catalog of unicellular eukaryote Small Sub-Unit rRNA sequences with curated taxonomy. Nucleic Acids Res **41**: D597-604. doi:10.1093/nar/gks1160

Haas, S., D. de Beer, J. Klatt, and others. 2018. Low-light Anoxygenic Photosynthesis and Fe-S-Biogeochemistry in a Microbial Mat. Front Microbiol **9**: 858.

Haas, S., D. K. Desai, J. LaRoche, R. Pawlowicz, and D. W. R. Wallace. 2019. Geomicrobiology of the carbon, nitrogen and sulphur cycles in Powell Lake: a permanently stratified water column containing ancient seawater. Environ Microbiol **21**: 3927–3952. doi:10.1111/1462-2920.14743

Hallin, S., L. Philippot, F. E. Löffler, R. A. Sanford, and C. M. Jones. 2018. Genomics and Ecology of Novel N_2O-Reducing Microorganisms. Trends Microbiol **26**: 43–55. doi:10.1016/J.TIM.2017.07.003

Halm, H., N. Musat, P. Lam, and others. 2009. Co-occurrence of denitrification and nitrogen fixation in a meromictic lake, Lake Cadagno (Switzerland). Environ Microbiol **11**: 1945–1958. doi:10.1111/j.1462-2920.2009.01917.x

Hamilton, T. L., R. J. Bovee, S. R. Sattin, and others. 2016. Carbon and Sulfur Cycling below the Chemocline in a Meromictic Lake and the Identification of a Novel Taxonomic Lineage in the FCB Superphylum, Candidatus Aegiribacteria. Front Microbiol **7**: 598. doi:10.3389/fmicb.2016.00598

Hamilton, T. L., P. V. Welander, H. L. Albrecht, and others. 2017. Microbial communities and organic biomarkers in a Proterozoic-analog sinkhole. Geobiology **15**: 784–797. doi:10.1111/gbi.12252

Hansen, H. P., and F. Koroleff. 1999. Determination of nutrients, p. 159–228. *In* K. Grasshoff, K. Kremling, and M. Erhardt [eds.], Methods of Seawater Analysis. Wiley-VCH Verlag GmbH.

Happel, E., I. Bartl, M. Voss, and L. Riemann. 2018. Extensive nitrification and active ammonia oxidizers in two contrasting coastal systems of the Baltic Sea. Environ Microbiol **20**: 2913–2926. doi:10.1111/1462-2920.14293

Hardison, A. K., C. K. Algar, A. E. Giblin, and J. J. Rich. 2015. Influence of organic carbon and nitrate loading on partitioning between dissimilatory nitrate reduction to ammonium (DNRA) and N_2 production. Geochim Cosmochim Acta **164**: 146–160. doi:10.1016/j.gca.2015.04.049

Hargrave, B. T., and S. Taguchi. 1978. Origin of Deposited Material Sedimented in a Marine Bay. J Fish Res Board Canada **35**: 1604–1613. doi:10.1139/f78-250

Haroon, M. F., S. Hu, Y. Shi, M. Imelfort, J. Keller, P. Hugenholtz, Z. Yuan, and G. W. Tyson. 2013. Anaerobic oxidation of methane coupled to nitrate reduction in a novel archaeal lineage. Nature **500**: 567. doi:10.1038/nature12375

Harvey, H. W. 1953. Synthesis of Organic Nitrogen and Chlorophyll by *Nitzschia Closterium*. J Mar Biol Assoc United Kingdom **31**: 477–487. doi:10.1017/S0025315400011632

Hecky, R. E., P. Campbell, and L. L. Hendzel. 1993. The stoichiometry of carbon, nitrogen, and phosphorus in particulate matter of lakes and oceans. Limnol Oceanogr **38**: 709–724. doi:10.4319/lo.1993.38.4.0709

Heising, S., L. Richter, W. Ludwig, and B. Schink. 1999. *Chlorobium ferrooxidans* sp. nov., a phototrophic green sulfur bacterium that oxidizes ferrous iron in coculture with a "*Geospirillum*" sp. strain. Arch Microbiol **172**: 116–124. doi:10.1007/s002030050748

Heiss, E. M., and R. W. Fulweiler. 2016. Coastal water column ammonium and nitrite oxidation are decoupled in summer. Estuar Coast Shelf Sci **178**: 110–119. doi:10.1016/j.ecss.2016.06.002

Herfort, L., S. Schouten, B. Abbas, and others. 2007. Variations in spatial and temporal distribution of Archaea in the North Sea in relation to environmental variables. FEMS Microbiol Ecol **62**: 242–257. doi:10.1111/j.1574-6941.2007.00397.x

Hermes, J. D., P. M. Weiss, and W. W. Cleland. 1985. Use of nitrogen-15 and deuterium isotope effects to determine the chemical mechanism of phenylalanine ammonia-lyase. Biochemistry **24**: 2959–2967. doi:10.1021/bi00333a023

Hoch, M. P., M. L. Fogel, and D. L. Kirchman. 1992. Isotope fractionation associated with ammonium uptake by a marine bacterium. Limnol Oceanogr **37**: 1447–1459. doi:10.4319/lo.1992.37.7.1447

Hollibaugh, J. T., S. M. Gifford, M. A. Moran, M. J. Ross, S. Sharma, and B. B. Tolar. 2014. Seasonal variation in the metatranscriptomes of a Thaumarchaeota population from SE USA coastal waters. ISME J **8**: 685–698. doi:10.1038/ismej.2013.171

Horak, R. E. A., W. Qin, A. D. Bertagnolli, and others. 2018. Relative impacts of light, temperature, and reactive oxygen on thaumarchaeal ammonia oxidation in the North Pacific Ocean. Limnol Oceanogr **63**: 741–757. doi:10.1002/lno.10665

Horak, R. E. A., W. Qin, A. J. Schauer, E. V. Armbrust, A. E. Ingalls, J. W. Moffett, D. A. Stahl, and A. H. Devol. 2013. Ammonia oxidation kinetics and temperature sensitivity of a natural marine community dominated by Archaea. ISME J **7**: 2023–33. doi:10.1038/ismej.2013.75

Horrigan, S. G., J. P. Montoya, J. L. Nevins, and J. J. McCarthy. 1990a. Natural isotopic composition of dissolved inorganic nitrogen in the Chesapeake Bay. Estuar Coast Shelf Sci **30**: 393–410. doi:10.1016/0272-7714(90)90005-C

Horrigan, S. G., J. P. Montoya, J. L. Nevins, J. J. McCarthy, H. Ducklow, R. Goericke, and T. Malone. 1990b. Nitrogenous nutrient transformations in the spring and fall in the Chesapeake Bay. Estuar Coast Shelf Sci **30**: 369–391. doi:10.1016/0272-7714(90)90004-B

Horrigan, S. G., and A. L. Springer. 1990. Oceanic and estuarine ammonium oxidation: Effects of light. Limnol Oceanogr **35**: 479–482. doi:10.4319/lo.1990.35.2.0479

Howarth, R. W., and R. Marino. 2006. Nitrogen as the limiting nutrient for eutrophication in coastal marine ecosystems: Evolving views over three decades. *Limnology and Oceanography*. John Wiley & Sons, Ltd. 364–376.

Hsiao, S. S.-Y., T.-C. Hsu, J.-W. Liu, and others. 2014. Nitrification and its oxygen consumption along the turbid Chang Jiang River plume. Biogeosciences **11**: 2083–2098. doi:10.5194/bg-11-2083-2014

Hugerth, L. W., J. Larsson, J. Alneberg, M. V. Lindh, C. Legrand, J. Pinhassi, and A. F. Andersson. 2015. Metagenome-assembled genomes uncover a global brackish microbiome. Genome Biol **16**: 279. doi:10.1186/s13059-015-0834-7

Hugerth, L. W., H. A. Wefer, S. Lundin, H. E. Jakobsson, M. Lindberg, S. Rodin, L. Engstrand, and A. F. Andersson. 2014. DegePrime, a program for degenerate primer design for broad-taxonomic-range PCR in microbial ecology studies. Appl Environ Microbiol **80**: 5116–5123. doi:10.1128/AEM.01403-14

Hulth, S., R. C. Aller, and F. Gilbert. 1999. Coupled anoxic nitrification/ manganese reduction in marine sediments. Geochim Cosmochim Acta **63**: 49–66.

Huntsman, A. G. 1924. Circulation and Pollution of Water In and Near Halifax Harbour. Contrib to Can Biol Fish **2**: 71–81. doi:10.1139/f24-003

Hutchinson, G. 1957. A Treatise on Limnology, Geography, Physics and Chemistry, 1st ed. Wiley.

Hyatt, D., G.-L. Chen, P. F. LoCascio, M. L. Land, F. W. Larimer, and L. J. Hauser. 2010. Prodigal: prokaryotic gene recognition and translation initiation site identification. BMC Bioinformatics **11**: 119. doi:10.1186/1471-2105-11-119

Iino, T., K. Mori, Y. Uchino, T. Nakagawa, S. Harayama, and K.-I. Suzuki. 2010. Ignavibacterium album gen. nov., sp. nov., a moderately thermophilic anaerobic bacterium isolated from microbial mats at a terrestrial hot spring and proposal of Ignavibacteria classis nov., for a novel lineage at the periphery of green sulf. Int J Syst Evol Microbiol **60**: 1376–1382. doi:10.1099/ijs.0.012484-0

Inagaki, F., T. Nunoura, S. Nakagawa, and others. 2006. Biogeographical distribution and diversity of microbes in methane hydrate-bearing deep marine sediments on the Pacific Ocean Margin. Proc Natl Acad Sci USA **103**: 2815–2820. doi:10.1073/pnas.0511033103

İnceoğlu, Ö., M. Llirós, S. A. Crowe, and others. 2015a. Vertical Distribution of Functional Potential and Active Microbial Communities in Meromictic Lake Kivu. Microb Ecol **70**: 596–611. doi:10.1007/s00248-015-0612-9

İnceoğlu, Ö., M. Llirós, T. García-Armisen, S. A. Crowe, C. Michiels, F. Darchambeau, J. Descy, and P. Servais. 2015b. Distribution of Bacteria and Archaea in meromictic tropical Lake Kivu (Africa). Aquat Microb Ecol **74**: 215–233. doi:10.3354/ame01737

IOC, SCOR, and IAPSO. 2010. The international thermodynamic equation of seawater – 2010: Calculation and use of thermodynamic properties. Intergov Oceanogr Comm Manuals Guid No 56, UNESCO 196 pp.

Iversen, N., R. S. Oremland, and M. J. Klug. 1987. Big Soda Lake (Nevada). 3. Pelagic methanogenesis and anaerobic methane oxidation. Limnol Oceanogr **32**: 804–814. doi:10.4319/lo.1987.32.4.0804

Jensen, M. M., M. M. M. Kuypers, L. Gaute, and B. Thamdrup. 2008. Rates and regulation of anaerobic ammonium oxidation and denitrification in the Black Sea. Limnol Oceanogr **53**: 23–36. doi:10.4319/lo.2008.53.1.0023

Jensen, M. M., J. Petersen, T. Dalsgaard, and B. Thamdrup. 2009. Pathways, rates, and regulation of N_2 production in the chemocline of an anoxic basin, Mariager Fjord, Denmark. Mar Chem **113**: 102–113. doi:10.1016/j.marchem.2009.01.002

Jickells, T. D., E. Buitenhuis, K. Altieri, and others. 2017. A reevaluation of the magnitude and impacts of anthropogenic atmospheric nitrogen inputs on the ocean. Global Biogeochem Cycles **31**: 289–305. doi:10.1002/2016GB005586

Johnson, K. S., S. C. Riser, and D. M. Karl. 2010. Nitrate supply from deep to near-surface waters of the North Pacific subtropical gyre. Nature **465**: 1062–1065. doi:10.1038/nature09170

Jørgensen, B. B., and D. C. Nelson. 2004. Sulfide oxidation in marine sediments: Geochemistry meets microbiology. Geol Soc Am Spec Pap **379**: 63–81. doi:10.1130/0-8137-2379-5.63

Joye, S. B., T. L. Connell, L. G. Miller, R. S. Oremland, and R. S. Jellison. 1999. Oxidation of ammonia and methane in an alkaline, saline lake. Limnol Oceanogr **44**: 178–188. doi:10.4319/lo.1999.44.1.0178

Joye, S. B., and J. T. Hollibaugh. 1995. Influence of Sulfide Inhibition of Nitrification on Nitrogen Regeneration in Sediments. Science **270**: 623–625. doi:10.1126/science.270.5236.623

Kadnikov, V. V., A. V. Mardanov, A. V. Beletsky, O. V. Karnachuk, and N. V. Ravin. 2019. Genome of the candidate phylum *Aminicenantes* bacterium from a deep subsurface thermal aquifer revealed its fermentative saccharolytic lifestyle. Extremophiles **23**: 189–200. doi:10.1007/s00792-018-01073-5

Kalvelage, T., G. Lavik, P. Lam, and others. 2013. Nitrogen cycling driven by organic matter export in the South Pacific oxygen minimum zone. Nat Geosci **6**: 228–234. doi:10.1038/ngeo1739

Kalyuhznaya, M. G., W. Martens-Habbena, T. Wang, M. Hackett, S. M. Stolyar, D. A. Stahl, M. E. Lidstrom, and L. Chistoserdova. 2009. *Methylophilaceae* link methanol oxidation to denitrification in freshwater lake sediment as suggested by stable isotope probing and pure culture analysis. Environ Microbiol Rep **1**: 385–392. doi:10.1111/j.1758-2229.2009.00046.x

Kang, I., S. Kim, M. R. Islam, and J.-C. Cho. 2017. The first complete genome sequences of the acI lineage, the most abundant freshwater *Actinobacteria*, obtained by whole-genome-amplification of dilution-to-extinction cultures. Sci Rep **7**: 42252. doi:10.1038/srep42252

Katsev, S., and S. A. Crowe. 2015. Organic carbon burial efficiencies in sediments: The power law of mineralization revisited. Geology **43**: 607–610. doi:10.1130/G36626.1

Katsev, S., S. A. Crowe, A. Mucci, B. Sundby, S. Nomosatryo, G. Douglas Haffner, and D. A. Fowle. 2010. Mixing and its effects on biogeochemistry in the persistently stratified, deep, tropical Lake Matano, Indonesia. Limnol Oceanogr **55**: 763–776. doi:10.4319/lo.2010.55.2.0763

Kelley, D. E. 2018. The OCE Package, p. 91–101. *In* Oceanographic Analysis with R. Springer.

Kelly, S., E. Eyto, M. Dillane, R. Poole, and M. White. 2020. Characterizing ventilation events in an anoxic coastal basin: Observed dynamics and the role of climatic drivers. Limnol Oceanogr **9999**: 1–23. doi:10.1002/lno.11462

Kemeny, P. C., M. A. Weigand, R. Zhang, B. R. Carter, K. L. Karsh, S. E. Fawcett, and D. M. Sigman. 2016. Enzyme-level interconversion of nitrate and nitrite in the fall mixed layer of the Antarctic Ocean. Global Biogeochem Cycles **30**: 1069–1085. doi:10.1002/2015GB005350

Kérouel, R., and A. Aminot. 1997. Fluorometric determination of ammonia in sea and estuarine waters by direct segmented flow analysis. Mar Chem **57**: 265–275. doi:10.1016/S0304-4203(97)00040-6

Kerrigan, E. A., M. Kienast, H. Thomas, and D. W. R. Wallace. 2017. Using oxygen isotopes to establish freshwater sources in Bedford Basin, Nova Scotia, a Northwestern Atlantic fjord. Estuar Coast Shelf Sci **199**: 96–104. doi:10.1016/j.ecss.2017.09.003

van Kessel, M. A. H. J., D. R. Speth, M. Albertsen, P. H. Nielsen, H. J. M. Op den Camp, B. Kartal, M. S. M. Jetten, and S. Lücker. 2015. Complete nitrification by a single microorganism. Nature **528**: 555–559. doi:10.1038/nature16459

Khatiwala, S., F. Primeau, and M. Holzer. 2012. Ventilation of the deep ocean constrained with tracer observations and implications for radiocarbon estimates of ideal mean age. Earth Planet Sci Lett **325**–**326**: 116–125. doi:10.1016/J.EPSL.2012.01.038

Kim, D., L. Song, F. P. Breitwieser, and S. L. Salzberg. 2016. Centrifuge: rapid and sensitive classification of metagenomic sequences. Genome Res **26**: 1721–1729. doi:10.1101/gr.210641.116

Kim, T. W., K. Lee, R. G. Najjar, H. D. Jeong, and H. J. Jeong. 2011. Increasing N abundance in the northwestern pacific ocean due to atmospheric nitrogen deposition. Science **334**: 505–509. doi:10.1126/science.1206583

Kimura, M. 1980. A simple method for estimating evolutionary rates of base substitutions through comparative studies of nucleotide sequences. J Mol Evol **16**: 111–120. doi:10.1007/BF01731581

Kits, K. D., D. J. Campbell, A. R. Rosana, and L. Y. Stein. 2015a. Diverse electron sources support denitrification under hypoxia in the obligate methanotroph Methylomicrobium album strain BG8. Front Microbiol **6**: 1072. doi:10.3389/fmicb.2015.01072

Kits, K. D., M. G. Klotz, and L. Y. Stein. 2015b. Methane oxidation coupled to nitrate reduction under hypoxia by the Gammaproteobacterium Methylomonas denitrificans, sp. nov. type strain FJG1. Environ Microbiol **17**: 3219–3232. doi:10.1111/1462-2920.12772

Kitzinger, K., H. K. Marchant, L. A. Bristow, and others. 2020. Single cell analyses reveal contrasting life strategies of the two main nitrifiers in the ocean. Nat Commun **11**: 767. doi:10.1038/s41467-020-14542-3

Kitzinger, K., C. C. Padilla, H. K. Marchant, and others. 2019. Cyanate and urea are substrates for nitrification by *Thaumarchaeota* in the marine environment. Nat Microbiol **4**: 234–243. doi:10.1038/s41564-018-0316-2

Klepac-Ceraj, V., C. A. Hayes, W. P. Gilhooly, T. W. Lyons, R. Kolter, and A. Pearson. 2012. Microbial diversity under extreme euxinia: Mahoney Lake, Canada. Geobiology **10**: 223–235. doi:10.1111/j.1472-4669.2012.00317.x

Knapp, A. N. 2012. The sensitivity of marine N_2 fixation to dissolved inorganic nitrogen. Front Microbiol **3**: 374. doi:10.3389/fmicb.2012.00374

Kobayashi, M., Y. Matsuo, A. Takimoto, S. Suzuki, F. Maruo, and H. Shoun. 1996. Denitrification, a novel type of respiratory metabolism in fungal mitochondrion. J Biol Chem **271**: 16263–16267. doi:10.1074/jbc.271.27.16263

Koch, H., M. A. H. J. van Kessel, and S. Lücker. 2019. Complete nitrification: insights into the ecophysiology of comammox *Nitrospira*. Appl Microbiol Biotechnol **103**: 177–189. doi:10.1007/s00253-018-9486-3

Könneke, M., A. E. Bernhard, J. R. De La Torre, C. B. Walker, J. B. Waterbury, and D. A. Stahl. 2005. Isolation of an autotrophic ammonia-oxidizing marine archaeon. Nature **437**: 543–546. doi:10.1038/nature03911

Kopylova, E., L. Noé, and H. Touzet. 2012. SortMeRNA: fast and accurate filtering of ribosomal RNAs in metatranscriptomic data. Bioinformatics **28**: 3211–3217. doi:10.1093/bioinformatics/bts611

Kozlowski, J. A., M. Stieglmeier, C. Schleper, M. G. Klotz, and L. Y. Stein. 2016. Pathways and key intermediates required for obligate aerobic ammonia-dependent chemolithotrophy in bacteria and Thaumarchaeota. ISME J **10**: 1836–1845. doi:10.1038/ismej.2016.2

Kuever, J. 2014. The Family *Syntrophaceae*, p. 281–288. *In* E. Rosenberg, E.F. DeLong, S. Lory, E. Stackebrandt, and F. Thompson [eds.], The Prokaryotes. Springer Berlin Heidelberg.

Kumar, S., G. Stecher, and K. Tamura. 2016. MEGA7: Molecular Evolutionary Genetics Analysis Version 7.0 for Bigger Datasets. Mol Biol Evol **33**: 1870–1874. doi:10.1093/molbev/msw054

Kuypers, M. M. M., H. K. Marchant, and B. Kartal. 2018. The microbial nitrogen-cycling network. Nat Rev Microbiol. doi:10.1038/nrmicro.2018.9

Kuypers, M. M. M., A. O. Sliekers, G. Lavik, and others. 2003. Anaerobic ammonium oxidation by anammox bacteria in the Black Sea. Nature **422**: 608–11. doi:10.1038/nature01472

Laanbroek, H. J., P. L. E. Bodelier, and S. Gerards. 1994. Oxygen consumption kinetics of *Nitrosomonas europaea* and *Nitrobacter hamburgensis* grown in mixed continuous cultures at different oxygen concentrations. Arch Microbiol **161**: 156–162. doi:10.1007/BF00276477

Laanbroek, H. J., and S. Gerards. 1993. Competition for limiting amounts of oxygen between *Nitrosomonas europaea* and *Nitrobacter winogradskyi* grown in mixed continuous cultures. Arch Microbiol **159**: 453–459. doi:10.1007/BF00288593

Lam, P., M. M. Jensen, A. Kock, K. A. Lettmann, Y. Plancherel, G. Lavik, H. W. Bange, and M. M. M. Kuypers. 2011. Origin and fate of the secondary nitrite maximum in the Arabian Sea. Biogeosciences **8**: 1565–1577. doi:10.5194/bg-8-1565-2011

Lam, P., and M. M. M. Kuypers. 2011. Microbial Nitrogen Cycling Processes in Oxygen Minimum Zones. Ann Rev Mar Sci **3**: 317–345. doi:10.1146/annurev-marine-120709-142814

Landolfi, A., H. Dietze, W. Koeve, and A. Oschlies. 2013. Overlooked runaway feedback in the marine nitrogen cycle: the vicious cycle. Biogeosciences **10**: 1351–1363. doi:10.5194/bg-10-1351-2013

Langille. 2017. 16S Bacteria and Archaea Standard Operating Procedure · LangilleLab/microbiome_helper Wiki · GitHub.

Langmead, B., and S. L. Salzberg. 2012. Fast gapped-read alignment with Bowtie 2. Nat Methods **9**: 357–359. doi:10.1038/nmeth.1923

Laperriere, S. M., N. J. Nidzieko, R. J. Fox, A. W. Fisher, and A. E. Santoro. 2019. Observations of Variable Ammonia Oxidation and Nitrous Oxide Flux in a Eutrophic Estuary. Estuaries and Coasts **42**: 33–44. doi:10.1007/s12237-018-0441-4

LaRoche, J., R. Nuzzi, R. Waters, K. Wyman, P. Falkowski, and D. Wallace. 1997. Brown Tide blooms in Long Island's coastal waters linked to interannual variability in groundwater flow. Glob Chang Biol **3**: 397–410. doi:10.1046/j.1365-2486.1997.00117.x

Lau, E., M. C. Fisher, P. A. Steudler, and C. M. Cavanaugh. 2013. The methanol dehydrogenase gene, mxaF, as a functional and phylogenetic marker for proteobacterial methanotrophs in natural environments. PLoS One **8**: e56993. doi:10.1371/journal.pone.0056993

Lauro, F. M., M. Z. DeMaere, S. Yau, and others. 2011. An integrative study of a meromictic lake ecosystem in Antarctica. ISME J **5**: 879–895. doi:10.1038/ismej.2010.185

Lavik, G., T. Stührmann, V. Brüchert, and others. 2009. Detoxification of sulphidic African shelf waters by blooming chemolithotrophs. Nature **457**: 581–584. doi:10.1038/nature07588

Legrand, C., K. Rengefors, G. O. Fistarol, and E. Granéli. 2003. Allelopathy in phytoplankton - Biochemical, ecological and evolutionary aspects. Phycologia **42**: 406–419. doi:10.2216/i0031-8884-42-4-406.1

Lehours, A.-C., P. Evans, C. Bardot, K. Joblin, and F. Gérard. 2007. Phylogenetic Diversity of Archaea and Bacteria in the Anoxic Zone of a Meromictic Lake (Lake Pavin, France). Appl Environ Microbiol **73**: 2016–2019. doi:10.1128/AEM.01490-06

Lehtovirta-Morley, L. E., L. A. Sayavedra-Soto, N. Gallois, S. Schouten, L. Y. Stein, J. I. Prosser, and G. W. Nicol. 2016. Identifying Potential Mechanisms Enabling Acidophily in the Ammonia-Oxidizing Archaeon "*Candidatus*" Nitrosotalea devanaterra. Appl Environ Microbiol **82**: 2608–2619. doi:10.1128/AEM.04031-15

Letunic, I., and P. Bork. 2016. Interactive tree of life (iTOL) v3: an online tool for the display and annotation of phylogenetic and other trees. Nucleic Acids Res **44**: W242–W245. doi:10.1093/nar/gkw290

Li, D., C.-M. Liu, R. Luo, K. Sadakane, and T.-W. Lam. 2015a. MEGAHIT: an ultra-fast single-node solution for large and complex metagenomics assembly via succinct de Bruijn graph. Bioinformatics **31**: 1674–1676. doi:10.1093/bioinformatics/btv033

Li, J., D. B. Nedwell, J. Beddow, A. J. Dumbrell, B. A. McKew, E. L. Thorpe, and C. Whitby. 2015b. *amoA* gene abundances and nitrification potential rates suggest that benthic ammonia-oxidizing bacteria and not archaea dominate N cycling in the Colne estuary, United Kingdom. Appl Environ Microbiol **81**: 159–165. doi:10.1128/AEM.02654-14

Li, S.-J., Z.-S. Hua, L.-N. Huang, and others. 2015c. Microbial communities evolve faster in extreme environments. Sci Rep **4**: 6205. doi:10.1038/srep06205

Li, W. K. W. 2014. The state of phytoplankton and bacterioplankton at the Compass Buoy Station: Bedford Basin Monitoring Program 1992-2013. Can Tech Rep Hydrogr Ocean Sci **304**: 1–122.

Li, W. K. W., and P. M. Dickie. 2001. Monitoring phytoplankton, bacterioplankton, and virioplankton in a coastal inlet (Bedford Basin) by flow cytometry. Cytometry **44**: 236–246. doi:10.1002/1097-0320(20010701)44:3<236::AID-CYTO1116>3.0.CO;2-5

Li, W. K. W., and W. G. Harrison. 2008. Propagation of an atmospheric climate signal to phytoplankton in a small marine basin. Limnol Oceanogr **53**: 1734–1745. doi:10.4319/lo.2008.53.5.1734

Li, X., L. Hou, M. Liu, and others. 2015d. Evidence of Nitrogen Loss from Anaerobic Ammonium Oxidation Coupled with Ferric Iron Reduction in an Intertidal Wetland. Environ Sci Technol **49**: 11560–11568. doi:10.1021/acs.est.5b03419

Lin, H., and M. Taillefert. 2014. Key geochemical factors regulating Mn(IV)-catalyzed anaerobic nitrification in coastal marine sediments. Geochim Cosmochim Acta **133**: 17–33. doi:10.1016/j.gca.2014.01.025

Lindström, E. S., M. P. Kamst-Van Agterveld, and G. Zwart. 2005. Distribution of Typical Freshwater Bacterial groups is Associated with pH, Temperature, and Lake Water Retention Time. Appl Environ Microbiol **71**: 8201–8206. doi:10.1128/AEM.71.12.8201-8206.2005

Liu, S., F. Yang, Z. Gong, F. Meng, H. Chen, and Y. Xue. 2008. Application of anaerobic ammonium-oxidizing consortium to achieve completely autotrophic ammonium and sulfate removal. Bioresour Technol **99**: 6817–6825.

Liu, Z., N.-U. Frigaard, K. Vogl, T. Iino, M. Ohkuma, J. Overmann, and D. A. Bryant. 2012. Complete Genome of *Ignavibacterium album*, a Metabolically Versatile, Flagellated, Facultative Anaerobe from the Phylum *Chlorobi*. Front Microbiol **3**: 185. doi:10.3389/fmicb.2012.00185

Llorens-Marès, T., S. Yooseph, J. Goll, J. Hoffman, M. Vila-Costa, C. M. Borrego, C. L. Dupont, and E. O. Casamayor. 2015. Connecting biodiversity and potential functional role in modern euxinic environments by microbial metagenomics. ISME J **9**: 1648–1661. doi:10.1038/ismej.2014.254

Lomas, M. W., and F. Lipschultz. 2006. Forming the primary nitrite maximum: Nitrifiers or phytoplankton? Limnol Oceanogr **51**: 2453–2467. doi:10.4319/lo.2006.51.5.2453

Lorenzen, C. J. 1966. A method for the continuous measurement of *in vivo* chlorophyll concentration. Deep Sea Res Oceanogr Abstr **13**: 223–227. doi:10.1016/0011-7471(66)91102-8

Lourey, M. J., T. W. Trull, and D. M. Sigman. 2003. Sensitivity of $\delta^{15}N$ of nitrate, surface suspended and deep sinking particulate nitrogen to seasonal nitrate depletion in the Southern Ocean. Global Biogeochem Cycles **17**: 1081. doi:10.1029/2002gb001973

Ludwig, C. A. 1938. The Availability of Different forms of Nitrogen to a Green Alga. Am J Bot **25**: 448–458. doi:10.2307/2436419

Luther, G. W. 1991. Pyrite synthesis via polysulfide compounds. Geochim Cosmochim Acta **55**: 2839–2849. doi:10.1016/0016-7037(91)90449-F

Ma, X., S. T. Lennartz, and H. W. Bange. 2019. A multi-year observation of nitrous oxide at the Boknis Eck Time Series Station in the Eckernförde Bay (southwestern Baltic Sea). Biogeosciences **16**: 4097–4111. doi:10.5194/bg-16-4097-2019

Maalcke, W. J., J. Reimann, S. de Vries, and others. 2016. Characterization of Anammox Hydrazine Dehydrogenase, a Key N_2-producing Enzyme in the Global Nitrogen Cycle. J Biol Chem **291**: 17077–17092. doi:10.1074/jbc.M116.735530

MacGregor, B. J., D. P. Moser, B. J. Baker, E. W. Alm, M. Maurer, K. H. Nealson, and D. A. Stahl. 2001. Seasonal and spatial variability in Lake Michigan sediment small-subunit rRNA concentrations. Appl Environ Microbiol **67**: 3908–3922. doi:10.1128/AEM.67.9.3908-3922.2001

MacIsaac, J. J., R. C. Dugdale, R. T. Barber, D. Blasco, and T. T. Packard. 1985. Primary production cycle in an upwelling center. Deep Sea Res Part A, Oceanogr Res Pap **32**: 503–529. doi:10.1016/0198-0149(85)90042-1

Macko, S. A., M. Fogel, P. E. Hare, and T. C. Hoering. 1987. Isotopic fractionation of nitrogen and carbon in the synthesis of amino acids by microorganisms. Chem Geol Isot Geosci Sect **65**: 79–92. doi:10.1016/0168-9622(87)90064-9

Manske, A. K., J. Glaeser, M. M. M. Kuypers, and J. Overmann. 2005. Physiology and phylogeny of green sulfur bacteria forming a monospecific phototrophic assemblage at a depth of 100 meters in the Black Sea. Appl Environ Microbiol **71**: 8049–8060. doi:10.1128/AEM.71.12.8049-8060.2005

Mariotti, A., J. C. Germon, P. Hubert, P. Kaiser, R. Letolle, A. Tardieux, and P. Tardieux. 1981. Experimental Determination of Nitrogen Kinetic Isotope Fractionation: Some Principles; Illustration for the Denitrification and Nitrification Processes. Plant Soil **62**: 413–430.

Mariotti, A., C. Lancelot, and G. Billen. 1984. Natural isotopic composition of nitrogen as a tracer of origin for suspended organic matter in the Scheldt estuary. Geochim Cosmochim Acta **48**: 549–555. doi:10.1016/0016-7037(84)90283-7

Marschall, E., M. Jogler, U. Henßge, and J. Overmann. 2010. Large-scale distribution and activity patterns of an extremely low-light-adapted population of green sulfur bacteria in the Black Sea. Environ Microbiol **12**: 1348–1362. doi:10.1111/j.1462-2920.2010.02178.x

Martens-Habbena, W., P. M. Berube, H. Urakawa, J. R. de la Torre, and D. A. Stahl. 2009. Ammonia oxidation kinetics determine niche separation of nitrifying Archaea and Bacteria. Nature **461**: 976–979. doi:10.1038/nature08465

Martens-Habbena, W., W. Qin, R. E. A. Horak, and others. 2015. The production of nitric oxide by marine ammonia-oxidizing archaea and inhibition of archaeal ammonia oxidation by a nitric oxide scavenger. Environ Microbiol **17**: 2261–2274. doi:10.1111/1462-2920.12677

Martens-Habbena, W., and D. A. Stahl. 2011. Nitrogen metabolism and kinetics of ammonia-oxidizing archaea, p. 465–487. *In* M. Klotz and L. Stein [eds.], Methods in Enzymology: Research on Nitrification and Related Processes, Part B. Elsevier Academic Press Inc.

Massé, S., M. Botrel, D. A. Walsh, and R. Maranger. 2019. Annual nitrification dynamics in a seasonally ice-covered lake. PLoS One **14**: e0213748. doi:10.1371/journal.pone.0213748

Mathews, W. H. 1962. Bathymetry of Powell Lake, British Columbia. Ms. Rpt. No. 13, Institute of Oceanography, University of British Columbia.

McCarthy, J. J., W. Kaplan, and J. L. Nevins. 1984. Chesapeake Bay nutrient and plankton dynamics. 2. Sources and sinks of nitrite. Limnol Oceanogr **29**: 84–98. doi:10.4319/lo.1984.29.1.0084

McDougall, T. J., and O. A. Krzysik. 2015. Spiciness. J Mar Res **73**: 141–152. doi:10.1357/002224015816665589

McIlvin, M. R., and M. A. Altabet. 2005. Chemical conversion of nitrate and nitrite to nitrous oxide for nitrogen and oxygen isotopic analysis in freshwater and seawater. Anal Chem **77**: 5589–5595. doi:10.1021/ac050528s

Menten, L., and M. Michaelis. 1913. Die Kinetik der Invertinwirkung. Biochem Z **49**: 333–369.

Merbt, S. N., D. A. Stahl, E. O. Casamayor, E. Martí, G. W. Nicol, and J. I. Prosser. 2012. Differential photoinhibition of bacterial and archaeal ammonia oxidation. FEMS Microbiol Lett **327**: 41–46. doi:10.1111/j.1574-6968.2011.02457.x

Mercier, C., F. Boyer, A. Bonin, … E. C. A. of the S. 2013, and U. 2013. 2013. SUMATRA and SUMACLUST: fast and exact comparison and clustering of sequences. *Programs and Abstracts of the SeqBio 2013 workshop*. 27–29.

Michiels, C. C., F. Darchambeau, F. A. E. Roland, and others. 2017. Iron-dependent nitrogen cycling in a ferruginous lake and the nutrient status of Proterozoic oceans. Nat Geosci **18**: 1–19. doi:10.1038/ngeo2886

Middelburg, J. J. 1989. A simple rate model for organic matter decomposition in marine sediments. Geochim Cosmochim Acta **53**: 1577–1581. doi:10.1016/0016-7037(89)90239-1

Middelburg, J. J., and J. Nieuwenhuize. 2000. Uptake of dissolved inorganic nitrogen in turbid, tidal estuaries. Mar Ecol Prog Ser **192**: 79–88. doi:10.3354/meps192079

Middelburg, J. J., and J. Nieuwenhuize. 2001. Nitrogen isotope tracing of dissolved inorganic nitrogen behaviour in tidal estuaries. Estuar Coast Shelf Sci **53**: 385–391. doi:10.1006/ecss.2001.0805

Miloshevich, L. M., A. Paukkunen, H. Vömel, and S. J. Oltmans. 2004. Development and Validation of a Time-Lag Correction for Vaisala Radiosonde Humidity Measurements. J Atmos Ocean Technol **21**: 1305–1327. doi:10.1175/1520-0426(2004)021<1305:DAVOAT>2.0.CO;2

Mino, Y., C. Sukigara, M. C. Honda, and others. 2016. Seasonal variations in the nitrogen isotopic composition of settling particles at station K2 in the western subarctic North Pacific. J Oceanogr **72**: 819–836. doi:10.1007/s10872-016-0381-1

Minoche, A. E., J. C. Dohm, and H. Himmelbauer. 2011. Evaluation of genomic high-throughput sequencing data generated on Illumina HiSeq and Genome Analyzer systems. Genome Biol **12**: R112. doi:10.1186/gb-2011-12-11-r112

Mitchell, M., G. Harrison, K. Pauley, A. Gagné, G. Maillet, and P. Strain. 2002. Atlantic Zonal Monitoring Program Sampling Protocol. Can Tech Rep Hydrogr Ocean Sci **223**: 1–23.

Möbius, J. 2013. Isotope fractionation during nitrogen remineralization (ammonification): Implications for nitrogen isotope biogeochemistry. Geochim Cosmochim Acta **105**: 422–432. doi:10.1016/j.gca.2012.11.048

Morales, L. V., J. Granger, B. X. Chang, M. G. Prokopenko, B. Plessen, R. Gradinger, and D. M. Sigman. 2014. Elevated $^{15}N/^{14}N$ in particulate organic matter, zooplankton, and diatom frustule-bound nitrogen in the ice-covered water column of the Bering Sea eastern shelf. Deep Res Part II Top Stud Oceanogr **109**: 100–111. doi:10.1016/j.dsr2.2014.05.008

Mordy, C. W., L. B. Eisner, P. Proctor, P. Stabeno, A. H. Devol, D. H. Shull, J. M. Napp, and T. Whitledge. 2010. Temporary uncoupling of the marine nitrogen cycle: Accumulation of nitrite on the Bering Sea shelf. Mar Chem **121**: 157–166. doi:10.1016/j.marchem.2010.04.004

Morris, R. L., and T. M. Schmidt. 2013. Shallow breathing: bacterial life at low O_2. Nat Rev Microbiol **11**: 205–212. doi:10.1038/nrmicro2970

Mortimer, R. J. G., S. J. Harris, M. D. Krom, and others. 2004. Anoxic nitrification in marine sediments. Mar Ecol Prog Ser **276**: 37–51. doi:10.3354/meps276037

Murphy, A. E., A. N. Bulseco, R. Ackerman, J. H. Vineis, and J. L. Bowen. 2020. Sulphide addition favours respiratory ammonification (DNRA) over complete denitrification and alters the active microbial community in salt marsh sediments. Environ Microbiol **22**: 2124–2139. doi:10.1111/1462-2920.14969

Murphy, J., and J. P. Riley. 1962. A modified single solution method for the determination of phosphate in natural waters. Anal Chim Acta **27**: 31–36. doi:10.1016/S0003-2670(00)88444-5

Murray, A. E., C. M. Preston, R. Massana, L. T. Taylor, A. Blakis, K. Wu, and E. F. DeLong. 1998. Seasonal and Spatial Variability of Bacterial and Archaeal Assemblages in the Coastal Waters near Anvers Island, Antarctica. Appl Environ Microbiol **64**: 2585–2895.

Myers, C. R., and K. H. Nealson. 1988. Microbial reduction of manganese oxides: Interactions with iron and sulfur. Geochim Cosmochim Acta **52**: 2727–2732. doi:10.1016/0016-7037(88)90041-5

Naqvi, S. W. A., H. W. Bange, L. Farias, P. M. S. Monteiro, M. I. Scranton, and J. Zhang. 2010. Marine hypoxia/anoxia as a source of CH_4 and N_2O. Biogeosciences **7**: 2159–2190. doi:10.5194/bg-7-2159-2010

Nealson, K., and W. Berelson. 2003. Layered Microbial Communities and the Search for Life in the Universe. Geomicrobiol J **20**: 451–462. doi:10.1080/713851133

Nealson, K. H., C. R. Myers, and B. B. Wimpee. 1991. Isolation and identification of manganese-reducing bacteria and estimates of microbial Mn(IV)-reducing potential in the Black Sea. Deep Sea Res Part A Oceanogr Res Pap **38**: S907–S920. doi:10.1016/S0198-0149(10)80016-0

Neuenschwander, S. M., R. Ghai, J. Pernthaler, and M. M. Salcher. 2018. Microdiversification in genome-streamlined ubiquitous freshwater Actinobacteria. ISME J **12**: 185–198. doi:10.1038/ismej.2017.156

Newell, S. E., S. E. Fawcett, and B. B. Ward. 2013. Depth distribution of ammonia oxidation rates and ammonia-oxidizer community composition in the Sargasso Sea. Limnol Oceanogr **58**: 1491–1500. doi:10.4319/lo.2013.58.4.1491

Newton, R. J., S. E. Jones, M. R. Helmus, and K. D. McMahon. 2007. Phylogenetic Ecology of the Freshwater *Actinobacteria* acI Lineage. Appl Environ Microbiol **73**: 7169–7176. doi:10.1128/AEM.00794-07

Nishizawa, M., K. Koba, A. Makabe, and others. 2013. Nitrification-driven forms of nitrogen metabolism in microbial mat communities thriving along an ammonium-enriched subsurface geothermal stream. Geochim Cosmochim Acta **113**: 152–173. doi:10.1016/j.gca.2013.03.027

Nishizawa, M., S. Sakai, U. Konno, and others. 2016. Nitrogen and oxygen isotope effects of ammonia oxidation by thermophilic *Thaumarchaeota* from a geothermal water stream. Appl Environ Microbiol **82**: 4492–4504. doi:10.1128/AEM.00250-16

Northcote, T. G., and K. J. Hall. 1983. Limnological contrasts and anomalies in two adjacent saline lakes. Hydrobiologia **105**: 179–194. doi:10.1007/BF00025187

Nowka, B., H. Daims, and E. Spieck. 2015. Comparison of oxidation kinetics of nitrite-oxidizing bacteria: Nitrite availability as a key factor in niche differentiation. Appl Environ Microbiol **81**: 745–753. doi:10.1128/AEM.02734-14

Ohkouchi, N., Y. Nakajima, and H. Okada. 2005. Biogeochemical processes in the saline meromictic Lake Kaiike, Japan: implications from molecular isotopic evidences of photosynthetic pigments. Environ Microbiol **7**: 1009–1016.

Olson, R. 1981. Differential photoinhibition of marine nitrifying bacteria: a possible mechanism for the formation of the primary nitrite maximum. J Mar Res **39**: 227–238.

Oren, A., E. Padan, and M. Avron. 1977. Quantum yields for oxygenic and anoxygenic photosynthesis in the cyanobacterium *Oscillatoria limnetica*. Proc Natl Acad Sci USA **74**: 2152–2156. doi:10.1073/PNAS.74.5.2152

Ostrom, N. E., A. Piit, R. Sutka, P. H. Ostrom, A. S. Grandy, K. M. Huizinga, and G. P. Robertson. 2007. Isotopologue effects during N_2O reduction in soils and in pure cultures of denitrifiers. J Geophys Res Biogeosciences **112**. doi:10.1029/2006JG000287

Oswald, K., J. S. Graf, S. Littmann, and others. 2017. *Crenothrix* are major methane consumers in stratified lakes. ISME J **11**: 2124–2140. doi:10.1038/ismej.2017.77

Oswald, K., J. Milucka, A. Brand, P. Hach, S. Littmann, B. Wehrli, M. M. M. Kuypers, and C. J. Schubert. 2016. Aerobic gammaproteobacterial methanotrophs mitigate methane emissions from oxic and anoxic lake waters. Limnol Oceanogr **61**: S101–S118. doi:10.1002/lno.10312

Overbeek, R., R. Olson, G. D. Pusch, and others. 2014. The SEED and the Rapid Annotation of microbial genomes using Subsystems Technology (RAST). Nucleic Acids Res **42**: D206–D214. doi:10.1093/nar/gkt1226

Overmann, J., H. Cypionka, and N. Pfennig. 1992. An extremely low-light adapted phototrophic sulfur bacterium from the Black Sea. Limnol Oceanogr **37**: 150–155. doi:10.4319/lo.1992.37.1.0150

Overmann, J., and M. M. Tilzer. 1989. Control of primary productivity and the significance of photosynthetic bacteria in a meromictic kettle lake. Mittlerer Buchensee, West-Germany. Aquat Sci **51**: 261–278. doi:10.1007/BF00877171

Pachiadaki, M. G., M. M. Yakimov, V. LaCono, E. Leadbetter, and V. Edgcomb. 2014. Unveiling microbial activities along the halocline of Thetis, a deep-sea hypersaline anoxic basin. ISME J **8**: 2478–2489. doi:10.1038/ismej.2014.100

Padilla, C. C., A. D. Bertagnolli, L. A. Bristow, N. Sarode, J. B. Glass, B. Thamdrup, and F. J. Stewart. 2017. Metagenomic Binning Recovers a Transcriptionally Active Gammaproteobacterium Linking Methanotrophy to Partial Denitrification in an Anoxic Oxygen Minimum Zone. Front Mar Sci **4**: 23. doi:10.3389/fmars.2017.00023

Parada, A. E., D. M. Needham, and J. A. Fuhrman. 2016. Every base matters: assessing small subunit rRNA primers for marine microbiomes with mock communities, time series and global field samples. Environ Microbiol **18**: 1403–1414. doi:10.1111/1462-2920.13023

Parks, D. H., M. Imelfort, C. T. Skennerton, P. Hugenholtz, and G. W. Tyson. 2015. CheckM: assessing the quality of microbial genomes recovered from isolates, single cells, and metagenomes. Genome Res **25**: 1043–1055. doi:10.1101/gr.186072.114

Peña, M. A., K. L. Denman, S. E. Calvert, R. E. Thomson, and J. R. Forbes. 1999. The seasonal cycle in sinking particle fluxes off Vancouver Island, British Columbia. Deep Res Part II Top Stud Oceanogr **46**: 2969–2992. doi:10.1016/S0967-0645(99)00090-9

Peng, X., C. A. Fuchsman, A. Jayakumar, M. J. Warner, A. H. Devol, and B. B. Ward. 2016. Revisiting nitrification in the Eastern Tropical South Pacific : A focus on controls. J Geophys Res Ocean **121**: 1667–1684. doi:10.1002/2015JC011455.Received

Peñuelas, J., B. Poulter, J. Sardans, and others. 2013. Human-induced nitrogen-phosphorus imbalances alter natural and managed ecosystems across the globe. Nat Commun **4**: 2934. doi:10.1038/ncomms3934

Peñuelas, J., J. Sardans, A. Rivas-ubach, and I. A. Janssens. 2012. The human-induced imbalance between C, N and P in Earth's life system. Glob Chang Biol **18**: 3–6. doi:10.1111/j.1365-2486.2011.02568.x

Perry, K. A. 1990. The Chemical Limnology of Two Meromictic Lakes with Emphasis on Pyrite Formation. University of British Columbia.

Perry, K. A., and T. F. Pedersen. 1993. Sulphur speciation and pyrite formation in meromictic ex-fjords. Geochim Cosmochim Acta **57**: 4405–4418. doi:10.1016/0016-7037(93)90491-E

Petrie, B., and P. Yeats. 1990. Simple models of the circulation, dissolved metals, suspended solids and nutrients in Halifax Harbour. Water Qual Res J Canada **25**: 325–349.

Philippot, L. 2002. Denitrifying genes in bacterial and Archaeal genomes. Biochim Biophys Acta - Gene Struct Expr **1577**: 355–376. doi:10.1016/S0167-4781(02)00420-7

Philips, S., H. Laanbroek, and W. Verstraete. 2002. Origin, causes and effects of increased nitrite concentrations in aquatic environments. Rev Environ **1**: 115–141.

Pianka, E. R. 1970. On r- and K-Selection. Am Nat **104**: 592–597. doi:10.1086/282697

Pimenov, N. V., and L. N. Neretin. 2006. Composition and activities of microbial communities involved in carbon, sulfur, nitrogen and manganese cycling in oxic/anoxic interface of the Black Sea, p. 501–521. *In* L.N. Neretin [ed.], Past and Present Water Column Anoxia. Nato Science Series: IV: Earth and Environmental Sciences. Springer.

Pitcher, A., C. Wuchter, K. Siedenberg, S. Schouten, and J. S. Sinninghe Damsté. 2011. Crenarchaeol tracks winter blooms of ammonia-oxidizing Thaumarchaeota in the coastal North Sea. Limnol Oceanogr **56**: 2308–2318. doi:10.4319/lo.2011.56.6.2308

Pjevac, P., C. Schauberger, L. Poghosyan, and others. 2017. *AmoA*-Targeted Polymerase Chain Reaction Primers for the Specific Detection and Quantification of Comammox *Nitrospira* in the Environment. Front Microbiol **8**: 1508. doi:10.3389/fmicb.2017.01508

Platt, T., A. Prakash, and B. Irwin. 1972. Phytoplankton nutrients and flushing of inlets on the coast of Nova Scotia. Le Nat Can **99**: 253–261.

Podosokorskaya, O. A., V. V. Kadnikov, S. N. Gavrilov, and others. 2013. Characterization of *Melioribacter roseus* gen. nov., sp. nov., a novel facultatively anaerobic thermophilic cellulolytic bacterium from the class *Ignavibacteria*, and a proposal of a novel bacterial phylum *Ignavibacteriae*. Environ Microbiol **15**: 1759–1771. doi:10.1111/1462-2920.12067

Pouliot, J., P. E. Galand, C. Lovejoy, and W. F. Vincent. 2009. Vertical structure of archaeal communities and the distribution of ammonia monooxygenase A gene variants in two meromictic High Arctic lakes. Environ Microbiol **11**: 687–699. doi:10.1111/j.1462-2920.2008.01846.x

Priscu, J. C. 1997. The biogeochemistry of nitrous oxide in permanently ice-covered lakes of the McMurdo Dry Valleys, Antarctica. Glob Chang Biol **3**: 301–315. doi:10.1046/j.1365-2486.1997.00147.x

Pruesse, E., J. Peplies, and F. O. Glöckner. 2012. SINA: Accurate high-throughput multiple sequence alignment of ribosomal RNA genes. Bioinformatics **28**: 1823–1829. doi:10.1093/bioinformatics/bts252

Pruitt, K. D., T. Tatusova, and D. R. Maglott. 2007. NCBI reference sequences (RefSeq): a curated non-redundant sequence database of genomes, transcripts and proteins. Nucleic Acids Res **35**: D61–D65. doi:10.1093/nar/gkl842

Punshon, S., and R. M. Moore. 2004. Nitrous oxide production and consumption in a eutrophic coastal embayment. Mar Chem **91**: 37–51. doi:10.1016/j.marchem.2004.04.003

Qin, W., S. A. Amin, W. Martens-Habbena, and others. 2014. Marine ammonia-oxidizing archaeal isolates display obligate mixotrophy and wide ecotypic variation. Proc Natl Acad Sci USA **111**: 12504–12509. doi:10.1073/pnas.1324115111

Qin, W., K. A. Meinhardt, J. W. Moffett, A. H. Devol, E. Virginia Armbrust, A. E. Ingalls, and D. A. Stahl. 2017. Influence of oxygen availability on the activities of ammonia-oxidizing archaea. Environ Microbiol Rep **9**: 250–256. doi:10.1111/1758-2229.12525

Reed, D. C., C. K. Algar, J. A. Huber, and G. J. Dick. 2014. Gene-centric approach to integrating environmental genomics and biogeochemical models. Proc Natl Acad Sci USA **111**: 1879–1884. doi:10.1073/pnas.1313713111

Revsbech, N. P., B. Thamdrup, T. Dalsgaard, and D. E. Canfield. 2011. Construction of STOX oxygen sensors and their application for determination of O_2 concentrations in oxygen minimum zones, p. 325–341. *In* Methods in Enzymology. Academic Press Inc.

Rikmann, E., I. Zekker, M. Tomingas, T. Tenno, A. Menert, L. Loorits, and T. Tenno. 2012. Sulfate-reducing anaerobic ammonium oxidation as a potential treatment method for high nitrogen-content wastewater. Biodegradation **23**: 509–524. doi:10.1007/s10532-011-9529-2

Rios-Del Toro, E. E., E. I. Valenzuela, N. E. López-Lozano, M. G. Cortés-Martínez, M. A. Sánchez-Rodríguez, O. Calvario-Martínez, S. Sánchez-Carrillo, and F. J. Cervantes. 2018. Anaerobic ammonium oxidation linked to sulfate and ferric iron reduction fuels nitrogen loss in marine sediments. Biodegradation **29**: 429–442. doi:10.1007/s10532-018-9839-8

Robidart, J. C., C. M. Preston, R. W. Paerl, K. A. Turk, A. C. Mosier, C. A. Francis, C. A. Scholin, and J. P. Zehr. 2012. Seasonal *Synechococcus* and *Thaumarchaeal* population dynamics examined with high resolution with remote *in situ* instrumentation. ISME J **6**: 513–523. doi:10.1038/ismej.2011.127

Robinson, R. S., M. Kienast, A. Luiza Albuquerque, and others. 2012. A review of nitrogen isotopic alteration in marine sediments. Paleoceanography **27**: PA4203. doi:10.1029/2012PA002321

Rodriguez-R, L. M., and K. T. Konstantinidis. 2014. Nonpareil: a redundancy-based approach to assess the level of coverage in metagenomic datasets. Bioinformatics **30**: 629–635. doi:10.1093/bioinformatics/btt584

Rognes, T., T. Flouri, B. Nichols, C. Quince, and F. Mahé. 2016. VSEARCH: a versatile open source tool for metagenomics. PeerJ **4**: e2584. doi:10.7717/peerj.2584

Ruijter, J. M., C. Ramakers, W. M. H. Hoogaars, Y. Karlen, O. Bakker, M. J. B. van den Hoff, and A. F. M. Moorman. 2009. Amplification efficiency: linking baseline and bias in the analysis of quantitative PCR data. Nucleic Acids Res **37**: e45. doi:10.1093/nar/gkp045

Ryabenko, E., M. A. Altabet, and D. W. R. Wallace. 2009. Effect of chloride on the chemical conversion of nitrate to nitrous oxide for $\delta^{15}N$ analysis. Limnol Oceanogr Methods **7**: 545–552. doi:10.4319/lom.2009.7.545

Saccà, A., L. Guglielmo, and V. Bruni. 2008. Vertical and temporal microbial community patterns in a meromictic coastal lake influenced by the Straits of Messina upwelling system. Hydrobiologia **600**: 89–104. doi:10.1007/s10750-007-9179-x

Sakamoto, C. M., K. S. Johnson, and L. J. Coletti. 2009. Improved algorithm for the computation of nitrate concentrations in seawater using an in situ ultraviolet spectrophotometer. Limnol Oceanogr Methods **7**: 132–143. doi:10.4319/lom.2009.7.132

Salmaso, N. 2005. Effects of climatic fluctuations and vertical mixing on the interannual trophic variability of Lake Garda, Italy. Limnol Oceanogr **50**: 553–565. doi:10.4319/lo.2005.50.2.0553

Sanderson, B., K. Perry, and T. Pedersen. 1986. Vertical Diffusion in Meromictic Powell Lake, British Columbia. J Geophys Res **91**: 7647–7655.

Santoro, A. E., C. Buchwald, M. R. McIlvin, and K. L. Casciotti. 2011. Isotopic signature of N_2O produced by marine ammonia-oxidizing archaea. Science **332**: 1282–1285. doi:10.1016/0024-4937(90)90045-3

Santoro, A. E., and K. L. Casciotti. 2011. Enrichment and characterization of ammonia-oxidizing archaea from the open ocean: phylogeny, physiology and stable isotope fractionation. ISME J **5**: 1796–1808. doi:10.1038/ismej.2011.58

Santoro, A. E., R. A. Richter, and C. L. Dupont. 2019. Planktonic Marine Archaea. Ann Rev Mar Sci **11**: 131–158. doi:10.1146/annurev-marine-121916-063141

Santoro, A. E., M. A. Saito, T. J. Goepfert, C. H. Lamborg, C. L. Dupont, and G. R. DiTullio. 2017. Thaumarchaeal ecotype distributions across the equatorial Pacific Ocean and their potential roles in nitrification and sinking flux attenuation. Limnol Oceanogr **62**: 1984–2003. doi:10.1002/lno.10547

Santoro, A. E., C. M. Sakamoto, J. M. Smith, and others. 2013. Measurements of nitrite production in and around the primary nitrite maximum in the central California Current. Biogeosciences **10**: 7395–7410. doi:10.5194/bg-10-7395-2013

Sass, H., and H. Cypionka. 2004. Isolation of Sulfate-Reducing Bacteria from the Terrestrial Deep Subsurface and Description of *Desulfovibrio cavernae* sp. nov. Syst Appl Microbiol **27**: 541–548. doi:10.1078/0723202041748181

Schaefer, S. C., and J. T. Hollibaugh. 2017. Temperature Decouples Ammonium and Nitrite Oxidation in Coastal Waters. Environ Sci Technol **51**: 3157–3164. doi:10.1021/acs.est.6b03483

Scheifele, B., R. Pawlowicz, T. Sommer, and A. Wüest. 2014. Double Diffusion in Saline Powell Lake, British Columbia. J Phys Oceanogr **44**: 2893–2908. doi:10.1175/JPO-D-14-0070.1

Schramm, A., D. De Beer, J. C. Van Den Heuvel, S. Ottengraf, and R. Amann. 1999. Microscale distribution of populations and activities of *Nitrosospira* and *Nitrospira* spp. along a macroscale gradient in a nitrifying bioreactor: Quantification by in situ hybridization and the use of microsensors. Appl Environ Microbiol **65**: 3690–3696.

Schubert, C. J., E. Durisch-Kaiser, L. Klauser, and others. 2006. Recent studies on sources and sinks of methane in the Black Sea, p. 419–441. *In* L.N. Neretin [ed.], Past and Present Water Column Anoxia. Nato Science Series: IV: Earth and Environmental Sciences. Springer.

Schultze, M., B. Boehrer, K. Wendt-Potthoff, S. Katsev, and E. T. Brown. 2017. Chemical Setting and Biogeochemical Reactions in Meromictic Lakes, p. 35–59. *In* R.D. Gulatei, E.S. Zadereev, and A.G. Degermendzhi [eds.], Ecology of Meromictic Lakes. Ecological Studies (Analysis and Synthesis). Springer.

Schweiger, B., H. P. Hansen, and H. W. Bange. 2007. A time series of hydroxylamine (NH2OH) in the southwestern Baltic Sea. Geophys Res Lett **34**: L24608. doi:10.1029/2007GL031086

Sebilo, M., G. Billen, B. Mayer, D. Billiou, M. Grably, J. Garnier, and A. Mariotti. 2006. Assessing Nitrification and Denitrification in the Seine River and Estuary Using Chemical and Isotopic Techniques. Ecosystems **9**: 564–577. doi:10.1007/s10021-006-0151-9

Shan, S., J. Sheng, K. R. Thompson, and D. A. Greenberg. 2011. Simulating the three-dimensional circulation and hydrography of Halifax Harbour using a multi-nested coastal ocean circulation model. Ocean Dyn **61**: 951–976. doi:10.1007/s10236-011-0398-3

Sharples, J., J. J. Middelburg, K. Fennel, and T. D. Jickells. 2017. What proportion of riverine nutrients reaches the open ocean? Global Biogeochem Cycles **31**: 39–58. doi:10.1002/2016GB005483

Shi, Q., and D. Wallace. 2018. A 3-year time series of volatile organic iodocarbons in Bedford Basin, Nova Scotia: a northwestern Atlantic fjord. Ocean Sci **14**: 1385–1403. doi:10.5194/os-14-1385-2018

Sigman, D., K. Karsh, and K. L. Casciotti. 2009. Ocean Process Tracers: Nitrogen Isotopes in the Ocean, p. 4138–4153. *In* J. Steele, S. Thorpe, and K. Turekian [eds.], Encyclopedia of Ocean Sciences. Academic Press.

Sintes, E., D. De Corte, E. Haberleitner, and G. J. Herndl. 2016. Geographic Distribution of Archaeal Ammonia Oxidizing Ecotypes in the Atlantic Ocean. Front Microbiol **7**: 77. doi:10.3389/fmicb.2016.00077

Smart, S. M., S. E. Fawcett, S. J. Thomalla, M. A. Weigand, C. J. C. Reason, and D. M. Sigman. 2015. Isotopic evidence for nitrification in the Antarctic winter mixed layer. Global Biogeochem Cycles **29**: 427–445. doi:10.1002/2014GB005013

Soetaert, K., J. J. Middelburg, C. Heip, P. Meire, S. Van Damme, and T. Maris. 2006. Long-term change in dissolved inorganic nutrients in the heterotrophic Scheldt estuary (Belgium, The Netherlands). Limnol Oceanogr **51**: 409–423. doi:10.4319/lo.2006.51.1_part_2.0409

Soetaert, K., and T. Petzoldt. 2010. Inverse modelling, sensitivity and monte carlo analysis in R using package FME. J Stat Softw **33**: 1–28. doi:10.18637/jss.v033.i03

Soetaert, K., T. Petzoldt, and R. W. Setzer. 2010. Solving differential equations in R: Package deSolve. J Stat Softw **33**: 1–25. doi:10.18637/jss.v033.i09

Soulet, G., L. Giosan, C. Flaux, and V. Galy. 2019. Using stable carbon isotopes to quantify radiocarbon reservoir age offsets in the coastal black sea. Radiocarbon **61**: 309–318. doi:10.1017/RDC.2018.61

Southwell, M. W., B. N. Popp, and C. S. Martens. 2008. Nitrification controls on fluxes and isotopic composition of nitrate from Florida Keys sponges. Mar Chem **108**: 96–108. doi:10.1016/J.MARCHEM.2007.10.005

Spieck, E., and E. Bock. 2005. The Lithoautotrophic Nitrite-Oxidizing Bacteria, p. 149–153. *In* D. Brenner, N. Krieg, J. Staley, and G. Garrity [eds.], Bergey's Manual® of Systematic Bacteriology. Springer.

Stamatakis, A. 2014. RAxML version 8: a tool for phylogenetic analysis and post-analysis of large phylogenies. Bioinformatics **30**: 1312–1313. doi:10.1093/bioinformatics/btu033

Statham, P. J. 2012. Nutrients in estuaries - An overview and the potential impacts of climate change. Sci Total Environ **434**: 213–227. doi:10.1016/j.scitotenv.2011.09.088

Stein, L. Y. 2019. Insights into the physiology of ammonia-oxidizing microorganisms. Curr Opin Chem Biol **49**: 9–15. doi:10.1016/j.cbpa.2018.09.003

Stephens, B. M., S. D. Wankel, J. M. Beman, A. J. Rabines, A. E. Allen, and L. I. Aluwihare. 2019. Euphotic zone nitrification in the California Current Ecosystem. Limnol Oceanogr **9999**: 1–17. doi:10.1002/lno.11348

Stramma, L., S. Schmidtko, L. A. Levin, and G. C. Johnson. 2010. Ocean oxygen minima expansions and their biological impacts. Deep Res Part I Oceanogr Res Pap **57**: 587–595. doi:10.1016/j.dsr.2010.01.005

Straub, K. L., M. Benz, B. Schink, and F. Widdel. 1996. Anaerobic, nitrate-dependent microbial oxidation of ferrous iron. Appl Environ Microbiol **62**: 1458–1460.

Strous, M., J. A. Fuerst, E. H. M. Kramer, and others. 1999. Missing Lithotroph Identified as New Planctomycete. Nature **400**: 446.

Strous, M., E. Van Gerven, P. Zheng, J. G. Kuenen, and M. S. M. Jetten. 1997. Ammonium removal from concentrated waste streams with the anaerobic ammonium oxidation (anammox) process in different reactor configurations. Water Res **31**: 1955–1962. doi:10.1016/S0043-1354(97)00055-9

Strous, M., E. Pelletier, S. Mangenot, and others. 2006. Deciphering the evolution and metabolism of an anammox bacterium from a community genome. Nature **440**: 790–794. doi:10.1038/nature04647

Sugimoto, R., A. Kasai, T. Miyajima, and K. Fujita. 2008. Nitrogen isotopic discrimination by water column nitrification in a shallow coastal environment. J Oceanogr **64**: 39–48. doi:10.1007/s10872-008-0003-7

Sugimoto, R., A. Kasai, T. Miyajima, and K. Fujita. 2009. Controlling factors of seasonal variation in the nitrogen isotope ratio of nitrate in a eutrophic coastal environment. Estuar Coast Shelf Sci **85**: 231–240. doi:10.1016/J.ECSS.2009.08.006

Sun, X., Q. Ji, A. Jayakumar, and B. B. Ward. 2017. Dependence of nitrite oxidation on nitrite and oxygen in low-oxygen seawater. Geophys Res Lett **44**: 7883–7891. doi:10.1002/2017GL074355

Sun, X., L. F. M. Kop, M. C. Y. Lau, J. Frank, A. Jayakumar, S. Lücker, and B. B. Ward. 2019. Uncultured *Nitrospina*-like species are major nitrite oxidizing bacteria in oxygen minimum zones. ISME J **13**: 2391–2402. doi:10.1038/s41396-019-0443-7

Suzuki, I., U. Dular, and S. C. Kwok. 1974. Ammonia or ammonium ion as substrate for oxidation by *Nitrosomonas europaea* cells and extracts. J Bacteriol **120**: 556–558.

Suzuki, M. T., and S. J. Giovannoni. 1996. Bias caused by template annealing in the amplification of mixtures of 16S rRNA genes by PCR. Appl Environ Microbiol **62**: 625–630.

Sverdrup, H. 1953. On Conditions for the Vernal Blooming of Phytoplankton. ICES J Mar Sci **18**: 287–295.

Taguchi, S., and T. Platt. 1977. Assimilation of $^{14}CO_2$ in the dark compared to phytoplankton production in a small coastal inlet. Estuar Coast Mar Sci **5**: 679–684. doi:10.1016/0302-3524(77)90092-5

Tezuka, Y. 1985. C:N:P ratios of seston in Lake Biwa as indicators of nutrient deficiency in phytoplankton and decomposition process of hypolimnetic particulate matter. Japanese J Limnol (Rikusuigaku Zasshi) **46**: 239–246. doi:10.3739/rikusui.46.239

Thamdrup, B., and T. Dalsgaard. 2002. Production of N_2 through anaerobic ammonium oxidation coupled to nitrate reduction in marine sediments. Appl Environ Microbiol **68**: 1312–1318. doi:10.1128/AEM.68.3.1312-1318.2002

Thomazo, C., and D. Papineau. 2013. Biogeochemical Cycling of Nitrogen on the Early Earth. Elements **9**: 345–351.

Tiodjio, R. E., A. Sakatoku, A. Nakamura, and others. 2015. Bacterial and archaeal communities in Lake Nyos (Cameroon, Central Africa). Sci Rep **4**: srep6151. doi:10.1038/srep06151

Tolar, B. B., G. M. King, and J. T. Hollibaugh. 2013. An Analysis of Thaumarchaeota Populations from the Northern Gulf of Mexico. Front Microbiol **4**: 72. doi:10.3389/fmicb.2013.00072

Torgersen, T., D. E. Hammond, W. B. Clarke, and T.-H. Peng. 1981. Fayetteville, Green Lake, New York: ^{3}He-^{3}He water mass ages and secondary chemical structure. Limnol Oceanogr **26**: 110–122. doi:10.4319/lo.1981.26.1.0110

Tremblay, J., K. Simpson, J. Martin, L. Miller, Y. Gratton, D. Barber, and N. M. Price. 2008. Vertical stability and the annual dynamics of nutrients and chlorophyll fluorescence in the coastal, southeast Beaufort Sea. J Geophys Res Ocean **113**. doi:10.1029/2007JC004547

Tsementzi, D., J. Wu, S. Deutsch, and others. 2016. SAR11 bacteria linked to ocean anoxia and nitrogen loss. Nature **536**: 179–183. doi:10.1038/nature19068

Tyrrell, T. 1999. The relative influences of nitrogen and phosphorus on oceanic primary production. Nature **400**: 525–531. doi:10.1038/22941

Ushiki, N., M. Jinno, H. Fujitani, T. Suenaga, A. Terada, and S. Tsuneda. 2017. Nitrite oxidation kinetics of two *Nitrospira* strains: The quest for competition and ecological niche differentiation. J Biosci Bioeng **123**: 581–589. doi:10.1016/j.jbiosc.2016.12.016

Vaccaro, R. F., and J. H. Ryther. 1960. Marine Phytoplankton and the Distribution of Nitrite in the Sea. ICES J Mar Sci **25**: 260–271.

Vajrala, N., W. Martens-Habbena, L. A. Sayavedra-Soto, A. Schauer, P. J. Bottomley, D. A. Stahl, and D. J. Arp. 2013. Hydroxylamine as an intermediate in ammonia oxidation by globally abundant marine archaea. Proc Natl Acad Sci USA **110**: 1006–1011. doi:10.1073/pnas.1214272110

Vallino, J. J. 2011. Differences and implications in biogeochemistry from maximizing entropy production locally versus globally. Earth Syst Dyn **2**: 69–85. doi:10.5194/esd-2-69-2011

Verhagen, F. J., and H. J. Laanbroek. 1992. Effects of Grazing by Flagellates on Competition for Ammonium between Nitrifying and Heterotrophic Bacteria in Chemostats. Appl Environ Microbiol **58**: 1962–1969.

Veuger, B., J. J. Middelburg, H. T. S. Boschker, J. Nieuwenhuize, P. Van Rijswijk, E. J. Rochelle-Newall, and N. Navarro. 2004. Microbial uptake of dissolved organic and inorganic nitrogen in Randers Fjord. Estuar Coast Shelf Sci **61**: 507–515. doi:10.1016/j.ecss.2004.06.014

Voss, M., M. A. Altabet, and B. V. Bodungen. 1996. $\delta^{15}N$ in sedimenting particles as indicator of euphotic-zone processes. Deep Res Part I Oceanogr Res Pap **43**: 33–47. doi:10.1016/0967-0637(95)00099-2

Voss, M., H. W. Bange, J. W. Dippner, J. J. Middelburg, J. P. Montoya, and B. Ward. 2013. The marine nitrogen cycle: Recent discoveries, uncertaintiesand the potential relevance of climate change. Philos Trans R Soc B Biol Sci **368**: 20130121. doi:10.1098/rstb.2013.0121

Walker, C. B., J. R. de la Torre, M. G. Klotz, and others. 2010. *Nitrosopumilus maritimus* genome reveals unique mechanisms for nitrification and autotrophy in globally distributed marine crenarchaea. Proc Natl Acad Sci USA **107**: 8818–8823. doi:10.1073/pnas.0913533107

Walsh, D. A., E. Zaikova, C. G. Howes, Y. C. Song, J. J. Wright, S. G. Tringe, P. D. Tortell, and S. J. Hallam. 2009. Metagenome of a Versatile Chemolithoautotroph from Expanding Oceanic Dead Zones. Science **326**: 578–582.

Walsh, E. A., J. B. Kirkpatrick, S. D. Rutherford, D. C. Smith, M. Sogin, and S. D'Hondt. 2016. Bacterial diversity and community composition from seasurface to subseafloor. ISME J **10**: 979–989. doi:10.1038/ismej.2015.175

Walters, W., E. R. Hyde, D. Berg-Lyons, and others. 2016. Improved Bacterial 16S rRNA Gene (V4 and V4-5) and Fungal Internal Transcribed Spacer Marker Gene Primers for Microbial Community Surveys. mSystems **1**: e00009-15. doi:10.1128/mSystems.00009-15

Wankel, S., C. Kendall, J. Pennington, F. Chavez, and A. Paytan. 2007. Nitrification in the euphotic zone as evidenced by nitrate dual isotopic composition: Observations from Monterey Bay, California. Global Biogeochem Cycles **21**: 1–13.

Ward, B. B. 1987. Kinetic studies on ammonia and methane oxidation by *Nitrosococcus oceanus*. Arch Microbiol **147**: 126–133. doi:10.1007/BF00415273

Ward, B. B. 1990. Kinetics of ammonia oxidation by a marine nitrifying bacterium: Methane as a substrate analogue. Microb Ecol **19**: 211–225. doi:10.1007/BF02017166

Waser, N. A. D., P. J. Harrison, B. Nielsen, S. E. Calvert, and D. H. Turpin. 1998a. Nitrogen isotope fractionation during the uptake and assimilation of nitrate, nitrite, ammonium, and urea by a marine diatom. Limnol Oceanogr **43**: 215–224. doi:10.4319/lo.1998.43.2.0215

Waser, N., K. Yin, Z. Yu, K. Tada, P. Harrison, D. Turpin, and S. Calvert. 1998b. Nitrogen isotope fractionation during nitrate, ammonium and urea uptake by marine diatoms and coccolithophores under various conditions of N availability. Mar Ecol Prog Ser **169**: 29–41. doi:10.3354/meps169029

Wenk, C. B., J. Blees, J. Zopfi, M. Veronesi, A. Bourbonnais, C. J. Schubert, H. Niemann, and M. F. Lehmann. 2013. Anaerobic ammonium oxidation (anammox) bacteria and sulfide-dependent denitrifiers coexist in the water column of a meromictic south-alpine lake. Limnol Oceanogr **58**: 1–12. doi:10.4319/lo.2013.58.1.0001

Wenk, C. B., C. H. Frame, K. Koba, and others. 2016. Differential N_2O dynamics in two oxygen-deficient lake basins revealed by stable isotope and isotopomer distributions. Limnol Oceanogr **61**: 1735–1749. doi:10.1002/lno.10329

Westley, M. B., H. Yamagishi, B. N. Popp, and N. Yoshida. 2006. Nitrous oxide cycling in the Black Sea inferred from stable isotope and isotopomer distributions. Deep Res Part II Top Stud Oceanogr **53**: 1802–1816. doi:10.1016/j.dsr2.2006.03.012

Williams, P. M., W. H. Mathews, and G. L. Pickard. 1961. A Lake in British Columbia containing Old Sea-Water. Nature **191**: 830–832. doi:10.1038/191830b0

Willis, C., D. Desai, and J. LaRoche. 2019. Influence of 16S rRNA variable region on perceived diversity of marine microbial communities of the Northern North Atlantic. FEMS Microbiol Lett **366**: fnz152. doi:10.1093/femsle/fnz152

Wollast, R. 1978. Modelling of biological and chemical processes in the Scheldt Estuary. Elsevier Oceanogr Ser **23**: 63–77.

Wright, J. J., K. M. Konwar, and S. J. Hallam. 2012. Microbial ecology of expanding oxygen minimum zones. Nat Rev Microbiol **10**: 381–394. doi:10.1038/nrmicro2778

Wu, J., S. E. Calvert, C. S. Wong, and F. A. Whitney. 1999. Carbon and nitrogen isotopic composition of sedimenting particulate material at Station Papa in the subarctic northeast Pacific. Deep Res Part II Top Stud Oceanogr **46**: 2793–2832. doi:10.1016/S0967-0645(99)00084-3

Wu, Q. L., G. Zwart, M. Schauer, M. P. Kamst-van Agterveld, and M. W. Hahn. 2006. Bacterioplankton community composition along a salinity gradient of sixteen high-mountain lakes located on the Tibetan Plateau, China. Appl Environ Microbiol **72**: 5478–5485. doi:10.1128/AEM.00767-06

Wuchter, C., B. Abbas, M. J. L. Coolen, and others. 2006. Archaeal nitrification in the ocean. Proc Natl Acad Sci USA **103**: 12317–12322. doi:10.1073/pnas.0600756103

Xia, F., J. G. Wang, T. Zhu, B. Zou, S. K. Rhee, and Z. X. Quan. 2018. Ubiquity and Diversity of Complete Ammonia Oxidizers (Comammox). Appl Environ Microbiol **84**: e01390-18. doi:10.1128/AEM.01390-18

Xiong, Y., R. Guilbaud, C. L. Peacock, R. P. Cox, D. E. Canfield, M. D. Krom, and S. W. Poulton. 2019. Phosphorus cycling in Lake Cadagno, Switzerland: A low sulfate euxinic ocean analogue. Geochim Cosmochim Acta **251**: 116–135. doi:10.1016/J.GCA.2019.02.011

Xu, H., H. W. Paerl, B. Qin, G. Zhu, and G. Gao. 2010. Nitrogen and phosphorus inputs control phytoplankton growth in eutrophic Lake Taihu, China. Limnol Oceanogr **55**: 420–432. doi:10.4319/lo.2010.55.1.0420

Yan, X., X. S. Wan, L. Liu, and others. 2019. Biogeochemical Dynamics in a Eutrophic Tidal Estuary Revealed by Isotopic Compositions of Multiple Nitrogen Species. J Geophys Res Biogeosciences **124**: 2018JG004959. doi:10.1029/2018JG004959

Yang, W. H., K. A. Weber, and W. L. Silver. 2012. Nitrogen loss from soil through anaerobic ammonium oxidation coupled to iron reduction. Nat Geosci **5**: 538–541. doi:10.1038/ngeo1530

Yanko-Hombach, V., P. J. Mudie, S. Kadurin, and E. Larchenkov. 2014. Holocene marine transgression in the Black Sea: New evidence from the northwestern Black Sea shelf. Quat Int **345**: 100–118. doi:10.1016/J.QUAINT.2013.07.027

Yilmaz, P., L. W. Parfrey, P. Yarza, and others. 2014. The SILVA and "All-species Living Tree Project (LTP)" taxonomic frameworks. Nucleic Acids Res **42**: D643–D648. doi:10.1093/nar/gkt1209

Yool, A., A. P. Martin, C. Fernández, and D. R. Clark. 2007. The significance of nitrification for oceanic new production. Nature **447**: 999–1002. doi:10.1038/nature05885

Yoon, S., S. Nissen, D. Park, R. A. Sanford, and F. E. Löffler. 2016. Nitrous Oxide Reduction Kinetics Distinguish Bacteria Harboring Clade I NosZ from Those Harboring Clade II NosZ. Appl Environ Microbiol **82**: 3793–800. doi:10.1128/AEM.00409-16

Yoshida, N. 1988. ^{15}N-depleted N_2O as a product of nitrification. Nature **335**: 528–529. doi:10.1038/335528a0

Yoshikawa, C., Y. Yamanaka, and T. Nakatsuka. 2005. An ecosystem model including nitrogen isotopes: Perspectives on a study of the marine nitrogen cycle. J Oceanogr **61**: 921–942. doi:10.1007/s10872-006-0010-5

Yoshiyama, K., and J. H. Sharp. 2006. Phytoplankton response to nutrient enrichment in an urbanized estuary: Apparent inhibition of primary production by overeutrophication. Limnol Oceanogr **51**: 424–434. doi:10.4319/lo.2006.51.1_part_2.0424

Yu, C., L. Hou, Y. Zheng, and others. 2018. Evidence for complete nitrification in enrichment culture of tidal sediments and diversity analysis of clade a comammox *Nitrospira* in natural environments. Appl Microbiol Biotechnol **102**: 9363–9377. doi:10.1007/s00253-018-9274-0

Yurkov, V. V, and J. T. Beatty. 1998. Aerobic anoxygenic phototrophic bacteria. Microbiol Mol Biol Rev **62**: 695–724.

Zadereev, E. S., R. D. Gulati, and A. Camacho. 2017. Biological and Ecological Features, Trophic Structure and Energy Flow in Meromictic Lakes, p. 61–86. *In* R.D. Gulatei, E.S. Zadereev, and A.G. Degermendzhi [eds.], Ecology of Meromictic Lakes. Ecological Studies (Analysis and Synthesis). Springer, Cham.

Zakem, E. J., A. Al-Haj, M. J. Church, and others. 2018. Ecological control of nitrite in the upper ocean. Nat Commun **9**: 1206. doi:10.1038/s41467-018-03553-w

Zhang, J., K. Kobert, T. Flouri, and A. Stamatakis. 2014a. PEAR: a fast and accurate Illumina Paired-End reAd mergeR. Bioinformatics **30**: 614–620. doi:10.1093/bioinformatics/btt593

Zhang, L., M. A. Altabet, T. Wu, and O. Hadas. 2007. Sensitive Measurement of NH_4^+ $^{15}N/^{14}N$ ($\delta^{15}NH_4^+$) at Natural Abundance Levels in Fresh and Saltwaters. Anal Chem **79**: 5589–5595. doi:10.1021/ac070106d

Zhang, X., G. Flato, M. Kirchmeier-Young, and others. 2019. Changes in Temperature and Precipitation Across Canada, p. 112–193. *In* E. Bush and D. Lemmen [eds.], Canada's Changing Climate Report. Government of Canada.

Zhang, X., D. M. Sigman, F. M. M. Morel, and A. M. L. Kraepiel. 2014b. Nitrogen isotope fractionation by alternative nitrogenases and past ocean anoxia. Proc Natl Acad Sci USA **111**: 4782–4787. doi:10.1073/pnas.1402976111

Zorz, J., C. Willis, A. M. Comeau, M. G. I. Langille, C. L. Johnson, W. K. W. Li, and J. LaRoche. 2019. Drivers of Regional Bacterial Community Structure and Diversity in the Northwest Atlantic Ocean. Front Microbiol **10**: 281. doi:10.3389/fmicb.2019.00281

Zwart, G., E. J. van Hannen, M. P. Kamst-van Agterveld, and others. 2003. Rapid screening for freshwater bacterial groups by using reverse line blot hybridization. Appl Environ Microbiol **69**: 5875–5883. doi:10.1128/AEM.69.10.5875-5883.2003

APPENDIX A: SUPPORTING INFORMATION TO CHAPTER 2

THREE PARALLEL APPROACHES TO THE CHARACTERIZATION OF THE GEOMICROBIOLOGY OF POWELL LAKE USING NEXT GENERATION SEQUENCING OF DNA

Three types of analyses were carried out to characterize the microbial community along the vertical geochemical gradient of Powell Lake, each with their associated benefits and limitation. First, the high throughput Illumina sequencing of small subunit (ssu) rRNA (16S and 18S) amplicons was used primarily to assess the variation in overall microbial community structure associated with each geochemical zone along the stratified water column. Primer bias associated with ssu rRNA amplicons sequencing is a known limitation of this type of analysis (Suzuki and Giovannoni 1996; Hugerth et al. 2014; Walters et al. 2016). However, it is considered a useful approach for comparing the overall taxonomic composition of communities along chemical or environmental gradients (Crowe et al. 2011; Hollibaugh et al. 2014; Gies et al. 2014; Bristow et al. 2015; Andrei et al. 2015; Baatar et al. 2016), while restricted in providing information on the metabolic potential of these communities. Second, to address the latter, we carried out metagenomic sequencing of the microbial community at selected depths exhibiting specific chemical properties. Unlike ssu amplicon sequencing, metagenomic reads are not subject to primer bias but reflect the relative abundance of microorganisms in the community more accurately, with most of the reads belonging to the abundant microorganisms. Annotation of the metagenomic reads (bulk metagenome) allows the assignment of functions, however, the taxonomic affiliation of functional genes is not as well curated as that of ssu rRNA amplicons, for which large databases are available (DeSantis et al. 2006; Yilmaz et al. 2014). Third, we used metagenomic bins to link taxonomy and function. However, the assembly of genomes from metagenomes is restricted to the microorganisms with high relative abundance within the microbial community, again reducing the taxonomic coverage to the 72 (= number of metagenomic bins identified) most abundant microorganisms. Each type of analysis yields slightly different information about the microbial diversity at the taxonomic and functional levels.

We examined the congruence between the ssu rRNA and the metagenomic approaches by comparing the taxonomic diversity based on 16S rRNA amplicon sequencing to that based on metagenome generated bins (Figure A2). As indicated by the slope of the linear fit, several phyla were over- (*Thaumarchaeota*, *Chloroflexi*, *Actinobacteria*) or underestimated (*Chlorobi*/*Ignaviabacteria*, *Planctomycetes*) by metagenomic binning as compared to the 16S rRNA amplicon approach (Figure A2B). This is to be expected given differential biases mentioned above and reflects under- or overestimation of the relative abundance. Importantly, however, for most phyla, high positive correlations (high R^2) were shown between the relative abundance based on 16S rRNA amplicons as compared to relative abundance based on the metagenomic bins (Figure A2B). The only exception (negative correlation) was the phylum *Spirochaetes* for which only a single bin was available, and which was quantitatively insignificant based on both approaches (Figure 2.3B, Figures S2A). The high correlation for most phyla indicates that the changes in relative abundance of a given phylum across the vertical profile were reflected similarly by both methods.

ALPHA-DIVERSITY INDICES AS FUNCTIONS OF DEPTH IN THE POWELL LAKE WATER COLUMN

Alpha-diversity based on rarefied 16S rRNA gene sequence data showed a distinct minimum at the chemocline (130 m; Figure A1A). Similar observations have been made for more shallow chemoclines and explained by the dominance of anoxygenic phototrophs. In the deep chemocline of Powell Lake such microorganisms were absent, and the diversity minimum was probably due to the predominance of the actinobacterial lineage acI (34.8%). Below the chemocline minimum, a notable increase was observed to the zone of highest diversity that roughly overlapped with the ferruginous zone. Diversity was highest at the surface and at 200-230 m, coinciding with the dissolved iron and manganese peaks. Alpha-diversity decreased again in the deep water below 230 m. Overall, diversity in Powell Lake's water column was extremely high compared to other meromictic lakes (Lehours et al. 2007; Dimitriu et al. 2008; Casamayor et al. 2013; Tiodjio et al. 2015; Andrei et al. 2015; Baatar et al. 2016). Moreover, observations in other meromictic lakes have frequently shown consistently elevated diversity in the monimolimnion compared to the

oxic and hypoxic parts of the water column (Lauro et al. 2011; Klepac-Ceraj et al. 2012; Gies et al. 2014; Andrei et al. 2015; Baatar et al. 2016). In this study, only results based on the Shannon-Weaver index were consistent with this report pattern. Evenness and Simpson index showed lower values below 230 m compared to parts of the oxic zone. Interestingly, the previous observations were on lakes much shallower than Powell Lake. Here we observed declining diversity in the deeper half of the monimolimnion with lower Simpson diversity and Evenness than in parts of the oxycline zone (Figure A1A,B). This pattern is similar to marine sediments, where the upper meters harbor much higher microbial diversity than deep sediments (> 10 m below surface; Walsh et al., 2016). It may thus be speculated whether the geochemical zones that promote low diversity in deeper marine subsurface sediments and Powell Lake's deep monimolimnion are located within the sediments of shallower lakes. Observations of high diversity in shallow monimolimnia are most convincingly explained by a need for a more diverse community to degrade increasingly refractory organic carbon at depth (Lauro et al. 2011; Baatar et al. 2016). DOC accumulation increased with depth in Powell Lake (Figure 2.2D), which is analogous to marine sediments where organic matter becomes increasingly refractory with age (Middelburg 1989; Katsev and Crowe 2015). Thus, the observed increase in the ferruginous zone, but not the observed decrease in microbial diversity in parts of the deep monimolimnion was consistent with the explanation stated above. In Powell Lake's deep monimolimnion, this principle may be offset by reduced diversity commonly associated with extreme environments (Frontier 1985; Li et al. 2015c). Thus, the observed variations in diversity in the monimolimnion may reflect a balance between the increasingly extreme conditions (e.g. high H_2S) driving reduced microbial diversity and the parallel increase in the relative complexity of the available organic matter, warranting increased diversity.

METAL CYCLING BETWEEN THE FERRUGINOUS AND EUXINIC ZONES

Microbial groups that are potentially involved in metal oxidation were identified by correlation analysis to identify correlation of microbial groups (based on 16S rRNA amplicon sequencing) with dissolved iron (Fe) and manganese (Mn) accumulation. For this, a simple correlation function implemented in MATLAB (MathWorks, USA) was used to determine correlation of microbial groups on the phylum and genus levels with dissolved

Fe and Mn concentrations (Table A8, Table A9).Given the unusually broad manganous zone with the dissolved manganese maximum at the top of the euxinic zone, this aids in the identification of microbial groups potentially associated with manganese reduction, which may be found in the manganous, ferruginous or euxinic zone.

The phyla OD1 and *Chlorobi* showed the strongest positive correlation with dissolved manganese (Table A8). Among the *Chlorobi*, *Ignavibacteriales* showed the strongest correlation (Table A9). Additionally, several OTUs affiliated with the *Deltaproteobacteria* showed maxima coinciding with the dissolved Mn peak (Table A9). This included *Desulfobacca*, affiliated with the most abundant OTU (NCBI: AB426203.1) at the depth of the dissolved Mn peak (3.7%) as well as *Desulfovibrio* (max. 1.0%), a genus previously linked to Mn reduction (Sass and Cypionka, 2004). Of the taxonomic groups affiliated with other indicator OTUs from the ferruginous and euxinic zones (Table 2.1), C20 (*Chlorobi*) showed relatively strong correlation with dissolved manganese concentration, while SB-45 (*Atribacteria*) and SHA-114 (AC1) showed weak or no correlation, suggesting that the latter were not involved in manganese reduction outside of the manganous zone.

Aminacenantes, NC10 and *Chlorobi* were among the phyla that were both abundant and whose distribution correlated with dissolved Fe concentration (Figure 2.3B, Table A8). Among the *Chlorobi*, *Ignavibacteriales* and the lineage BSV26/C20 correlated well with dissolved Fe (Table A9). 16S rRNA gene sequences affiliated with BSV26/C20 best matched with *Ignavibacterium album* strain JCM 16511 (86% ID; blastN against NCBI 16S ribosomal RNA gene sequences database; Liu et al., 2012) and were affiliated with the most abundant OTU (NCBI: HM243831.1) at the depth of the dissolved Fe peak, indicating possible involvement of *Ignavibacteria* in Fe reduction. Ferric iron reduction capability has been found among the *Ignavibacteria*, a heterotrophic, non-phototrophic class in the phylum *Chlorobi* (Iino et al. 2010; Podosokorskaya et al. 2013).

INDICATIONS FOR SYNTROPHIC INTERACTIONS BASED ON CORRELATIONS BETWEEN FORMER CANDIDATE PHYLA AND METHANOGENS AND DISTINCT SYNTROPHIC COMMUNITIES IN THE TWO DEEPEST ZONES

A simple correlation function implemented in MATLAB (MathWorks, USA) was used to determine correlation between microbial groups (based on 16S rRNA amplicon sequencing) on the phylum and genus levels (Table A8, Table A9).

Results from a study at Sakinaw Lake, a meromictic lake geographically close to Powell Lake with a similar geological history (Perry 1990; Perry and Pedersen 1993), suggested syntrophic interactions between certain candidate phyla and archaeal methanogens in the deep water (Gies et al. 2014). Co-occurrence of *Methanomicrobiales* with *Atribacteria* and *Aminacenantes*, respectively, was interpreted by Gies et al. as acetate-oxidizing *Aminacenantes* and *Atribacteria* supplying H_2 to hydrogenotrophic *Methanomicrobiales*. Consistent with that, we observed correlations on the genus level between *Methanomicrobiales* and each of these two groups, respectively (Table A9). Meanwhile, maxima of *Aminacenantes* and *Atribacteria* were separated by depth (Figure 2.3B, Table A8, Table A9), which supports previously suggested niche partitioning based on competition for acetate by these groups (Gies et al. 2014). However, despite putative competition for acetate with these groups (Gies *et al.*, 2014), *Methanosaeta* (*Methanosarcinales*) did correlate with lineages of the *Aminacenantes* and *Atribacteria* on the genus level (Table A8), suggesting independence of acetate utilization by at least one of these groups. Weak correlation was found between *Cloacimonetes* and subgroups of *Aminacenantes* and *Methanosarcinales*, respectively, not clearly supporting previously suggested syntrophy through acetate provision by *Cloacimonetes* to these groups (Table A9; Gies *et al.*, 2014).

Significant difference in the community structure between the euxinic and ancient seawater zones of Powell Lake suggested that the syntrophic partners and interactions within each zone are distinct (Figure 2.3A; Table A1). The syntrophic interactions of the euxinic zone might be centered around *Syntrophaceae*, while members of the Miscellaneous Crenarchaeota Group, *Omnitrophica* and *Cloacimonetes* may play the dominant roles in the syntrophic community of the ASW zone (Table 2.1, Table A3). A

simple, bottom-up explanation for this distinction may be the different quantity of reduced compounds (DOC, ammonium, sulfide and presumably methane) between the two zones (Figure 2). Other factors like the differences in salinity and the composition of organic matter may also play a role. While the genetic potential for methanogenesis is similar in these zones (Figure 2.4A), it is also possible that active methanogenesis occurs in only one of the two zones, which may greatly affect the microbial community composition.

ABSENCE OF CLEAR EVIDENCE FOR ANAMMOX POTENTIAL

Only tentative evidence for anammox potential was found in Powell Lake. Despite high relative abundance of 16S rRNA gene sequences affiliated with *Planctomycetes* (Figure 2.3B), no *Planctomycetes* OTUs of abundance > 0.7% in any sample clustered with known anammox strains (Figure A7). The marker gene *hao* was at low relative abundance in the metagenomes from the nitrogenous and manganous zones, where the occurrence of anammox would be most plausible (Thamdrup and Dalsgaard 2002; Kuypers et al. 2003; Jensen et al. 2008; Algar and Vallino 2014). Furthermore, *hao* may also be affiliated with *Nitrosomonadales*-AOBs, which were more abundant than *Planctomycetes* at these depths (Figure 2.3B, Figure A3A; Kozlowski *et al.*, 2016; Maalcke *et al.*, 2016). Blast searches of functional gene sequences from known anammox bacteria (*hdh*, *hzs*) against the two *Planctomycetes*-affiliated bins (Bin55, MAG15) yielded no significant matches.

Lifestyles as heterotrophic degraders in the *Planctomycetes* of Powell Lake would be consistent with the distribution of the abundant *Planctomycetes*-affiliated 16S rRNA gene sequences. They were of highest relative abundance in the lower oxycline and in the ancient seawater (Figure 2.3B), i.e. zones of organic matter degradation. The largest relative abundance of *hao* was found in the metagenome from 310 m, where the absence of oxygen, nitrite and the presence of high concentrations of sulfide provide hostile environments for both AOBs and anammox bacteria. This may be explained by the high relative abundance of 16S rRNA gene sequences affiliated with the *Planctomycetes* lineage MSBL-9 at 310 m (11.8% of 16S rRNA gene sequences; data not shown). Members of the lineage may contain *hao* as an evolutionary relict or for different metabolic purposes. MSBL-9 was first found in a deep-sea hypersaline lake where no sign of anammox was found (Pachiadaki et al. 2014).

Hao was found in two metagenomic bins, one unrelated to *Planctomycetes* (MAG11), another (MAG13) not confidently assigned beyond kingdom level (Table A5), leaving open the possibility that the latter is in fact affiliated with *Planctomycetes*. PSI-blast suggested that the *hao* from MAG11 was unrelated to anammox genes, but that both *hao* genes contained in MAG13 were closely related to hydroxylamine oxidoreductase from *Cd.* Brocadia sp. (NCBI: RIK00143), a known anammox lineage. However, other genes typical for anammox bacteria, including *nirK*, *hzs* or genes for the acetyl-CoA carbon fixation pathway (Strous et al. 2006; Berg et al. 2010; Kuypers et al. 2018), were not found in MAG13. Metagenomic reads mapping to MAG13 were almost exclusively from the ferruginous zone with a maximum in the metagenome from 200 m (Table A5), where anammox would be expected to be unfavorable due to high amounts of organic carbon and sulfide (Jensen et al. 2008; Algar and Vallino 2014). While potential for anammox may occur in Powell Lake, this dataset does not provide clear evidence for it.

VERTICAL PROFILES OF N_2O IN POWELL LAKE AND THE DETECTION OF *nosZ* CLADE II IN METAGENOMIC BINS WITH ANAEROBIC METABOLISM

Duplicate or triplicate nitrous oxide samples were collected along a vertical profile in Powell Lake's Southern Basin, without headspace, in 20 ml Wheaton borosilicate glass vials using tubing that inserts the sample to the bottom of the vial. Each sample was allowed to overflow gently several times to avoid any influence from bubbles inserting atmospheric gasses. Subsequently, any biological activity within the samples was stopped by the addition of 0.1 mL concentrated $HgCl_2$ and vials were then capped with PTFE-lined flat butyl septa and aluminum crimped seals (Wheaton cat #: seals: 20-0000as, vials: 20-2300, septa: 22-4168). In the laboratory, 10 ml of water sample was displaced by 10 ml ultra-pure helium to create the headspace. The vials were then shaken for gas equilibration and subsequently analyzed on a gas chromatograph coupled to a headspace sampler (GCHS; Agilent 789B GC and 7697A Headspace Sampler).

The vertical profile of N_2O in the Southern Basin of Powell Lake created from these measurements showed a distinct maximum of 20.3 nM around 120 m depth (Figure A8). Similar maxima have been frequently found in meromictic water columns and are often associated with N_2O production associated with nitrification (Cohen 1978; Westley et al.

2006; Wenk et al. 2016). Similarly, the depth of the N_2O maximum in Powell Lake, suggested an association with nitrification, given that it coincided with the depth of the nitrate maximum and at which oxygen was available at concentrations of ~80 µM precluding a significant role for N_2O production by incomplete denitrification.

At 135 m and below, concentrations were consistently below 4 nM and the strong decrease between 120 and 135 m indicated N_2O consumption around the depth of the oxic-suboxic interface, probably by biological N_2O reduction. This is consistent with the maximum genetic potential for denitrification (including *nosZ*) in the 130 m metagenome (Figure 2.4). Such a decrease at the base of the oxycline has also been documented in other meromictic water columns (Cohen 1978; Westley et al. 2006).

The *nosZ* subunit of the gene coding for the nitrous oxide reductase is commonly used to detect the genetic potential for N_2O reduction, the final step of the denitrification process (Lauro et al. 2011; Llorens-Marès et al. 2015; Hallin et al. 2018). Interestingly, it was the sole dissimilatory N reduction marker gene in several metagenomic bins isolated from Powell Lake. These bins were affiliated with *Sphingobacteriales* (*Bacteroidetes*; Bin53, Bin64), *Ignavibacteria* (MAG6), *Planctomycetaceae* (MAG15), *Actinobacteria* (MAG30) and unspecified Bacteria (MAG38). Among these groups, the *nosZ* gene has not previously been observed in *Actinobacteria* and *Planctomycetes* (Graf et al. 2014; Hallin et al. 2018) and both MAG15 and MAG30 also contain *nos* maturation protein genes (*nosF*, *nosY* plus *nosL* in MAG15 and *nosD* in MAG30). They both have the genetic makeup of heterotrophic degraders (central carbohydrate metabolism, fermentation) and contain cytochrome *c* oxidases I, II and III, indicating a potential for aerobic respiration despite their exclusive occurrence in the deeper half of the water column (Table 2.2, Table A3). Based on a PSI-Blast against the NCBI nucleotide database, the best matching sequences were affiliated with cytochrome *c* and *nosZ* genes from *Chloroflexi*, respectively, which contain *nosZ* clade II (Hallin et al. 2018). Similarly, the *nosZ* of bins 53 and 64 as well as MAG6 matched best with *nosZ* from clade II taxa *Bacteroidetes* and *Ignavibacteria*, respectively. A lower half-saturation constant for clade II NosZ has been suggested to functionally distinguish it from conventional NosZ (Yoon et al. 2016), which is consistent with the occurrence of these five bins in the low-N_2O (≤4 nM) water below the chemocline

of Powell Lake (Figure A8; Table A3). Further research is recommended to inquire whether N_2O might be used as an electron donor by some of the microbial groups represented by these bins.

VERTICAL PROFILES OF CH_4 IN POWELL LAKE INDICATED THAT THE "ASW" IS A METHANOGENIC ZONE

Samples for methane (CH_4) concentration measurements were taken in June 2018 from the center of South Basin of Powell Lake, approximately at the same site at which samples were taken in 2016 (Chapter 2). Samples were taken in the same way as described for N_2O concentration samples and analyzed on the same gas chromatograph.

Methane concentrations were lowest in the oxic water column (<0.50 μM, 80–131 m) and started to increase below 131 m to maxima of 2340–4680 μM in the ancient seawater (ASW) zone (Figure A8). The variations in measured methane concentrations in samples from within the ASW zone may be due to problems with outgassing from these samples following sampling. However, the sharp increase of methane below the halocline along with the peak in genetic potential for methanogenesis (Figure 2.4A) suggest that the ASW zone may be a zone of active methanogenesis (Figure A8). Within the framework of Canfield and Thamdrup (2009), this indicates that the ASW zone of Powell Lake represents a methanogenic zone.

Table A1. Comparison (ANOSIM) of the microbial community composition between groups of samples predicted by geochemical zonation. The significance level quantifies the probability of the null hypothesis that no differences between groups exist.

Zones predicted by geochemistry	R statistic	Significance level [%]	Possible permutations	Actual permutations
surface, oxycline	1.0	6.7	15	15
surface, nitrogenous	1.0	33.3	3	3
surface, manganous	1.0	6.7	15	15
surface, ferruginous	1.0	10.0	10	10
surface, euxinic	1.0	10.0	10	10
surface, ancient seawater	1.0	6.7	15	15
oxycline, nitrogenous	1.0	20.0	5	5
oxycline, manganous	1.0	2.9	35	35
oxycline, ferruginous	1.0	2.9	35	35
oxycline, euxinic	1.0	2.9	35	35
oxycline, ancient seawater	1.0	2.9	35	35
nitrogenous, manganous	1.0	20.0	5	5
nitrogenous, ferruginous	1.0	25.0	4	4
nitrogenous, euxinic	1.0	25.0	4	4
nitrogenous, ancient seawater	1.0	20.0	5	5
manganous, ferruginous	0.8	2.9	35	35
manganous, euxinic	1.0	2.9	35	35
manganous, ancient seawater	1.0	2.9	35	35
ferruginous, euxinic	0.9	10.0	10	10
ferruginous, ancient seawater	1.0	2.9	35	35
euxinic, ancient seawater	1.0	2.9	35	35

Table A2. Metagenome summary statistics

	Metagenomes (from depth [m])									
	120 m	**130 m**	**150 m**	**160 m**	**180 m**	**200 m**	**280 m**	**310 m**	**330 m**	**350 m**
Sequencing type	NextSeq	MiSeq	NextSeq	MiSeq	NextSeq	NextSeq	NextSeq	NextSeq	NextSeq	MiSeq
Reads (initial)	4.22E+06	5.56E+06	4.77E+06	6.23E+06	8.00E+06	4.58E+06	1.54E+06	3.18E+05	4.50E+06	5.44E+06
Reads passed trimming and filtering	3.75E+06	5.53E+06	4.17E+06	6.19E+06	7.00E+06	3.97E+06	1.29E+06	2.62E+05	3.83E+06	5.41E+06
Passed reads [%]	88.79	99.37	87.39	99.39	87.45	86.68	84.02	82.27	85.02	99.41
Sequencing depth [Gb]	0.58	1.78	0.63	1.93	1.06	0.59	0.18	0.04	0.54	1.68
Reads mapped to KEGG pathway [%]	26.45	53.33	23.88	43.59	22.41	21.38	19.21	18.04	17.56	35.68
Reads mapped to Metagenomic bins [%]	41.97	68.91	41.60	25.34	29.57	26.62	5.06	11.71	20.02	14.79

Table A3. Indicator OTUs distinguishing the microbial communities between geomicrobiological zones (Figure 2.3A), where high percentage of contribution to between-zone dissimilarities (SIMPER) indicates OTUs that are highly distinct between zones. For each combination of geomicrobiological zones outlined in Table 2.1, the three OTUs with the largest contributions are shown. They are rank-ordered (highlighted by heat-color-coding) and are specified by their taxonomic affiliation and NCBI accession numbers if existent. The zone projected on the x-axis of the matrix is the zone in which a given OTU was abundant compared to the corresponding zone on the y-axis, where it was rare.

	Surface	Oxycline	Nitrogenous Zone	Manganous Zone	Ferruginous Zone	Euxinic Zone	Ancient Seawater Zone
Surface		acI, Actinobacteria (FN668226.2)	acI, Actinobacteria (FN668226.2)	Sterolibacterium (NR_025450.1)	Desulfobacca (AB426203.1)	SB-45, Atribacteria (JQ087016.1)	Omnitrophica (New.ReferenceOTU12)
		Nitrospiraceae (AM167945.1)	Crenothrix (FJ502272.1)	acI, Actinobacteria (FN668226.2)	Syntrophaceae (HQ003553.1)	SHA-114, AC1 (AB186797.1)	SB-45, Atribacteria (JQ087016.1)
		Rhodospirillaceae (GQ396920.1)	Sterolibacterium (NR_025450.1)	Bacteroidales (AM162484.1)	C20, Chlorobi (HM243831.1)	Syntrophaceae (HQ003553.1)	B10, Crenarchaeota (FN428815.1)
Oxycline	Chitinophagaceae (HM129183.1)		Crenothrix (FJ502272.1)	Sterolibacterium (NR_025450.1)	Desulfobacca (AB426203.1)	SB-45, Atribacteria (JQ087016.1)	Omnitrophica (New.ReferenceOTU12)
	Synechococcus (FJ382618.1)		Comamonadaceae (GU208444.1)	Bacteroidales (AM162484.1)	Syntrophaceae (HQ003553.1)	SHA-114, AC1 (AB186797.1)	SB-45, Atribacteria (JQ087016.1)
	Roseococcus (New.ReferenceOTU8)		Sterolibacterium (NR_025450.1)	Desulfobacca (AB426203.1)	C20, Chlorobi (HM243831.1)	Syntrophaceae (HQ003553.1)	B10, Crenarchaeota (FN428815.1)
Nitrogenous Zone	Chitinophagaceae (HM129183.1)	Nitrospiraceae (AM167945.1)		Bacteroidales (AM162484.1)	Desulfobacca (AB426203.1)	SB-45 (JQ087016.1)	Omnitrophica (New.ReferenceOTU12)
	Synechococcus (FJ382618.1)	Rhodospirillaceae (GQ396920.1)		Desulfobacca (AB426203.1)	Syntrophaceae (HQ003553.1)	SHA-114, AC1 (AB186797.1)	SB-45 (JQ087016.1)
	Roseococcus (New.ReferenceOTU8)	Phycisphaerales (AF316766.1)		SJA-28 (Chlorobi)	C20, Chlorobi (HM243831.1)	C20, Chlorobi (EU644261.1)	B10, Crenarchaeota (FN428815.1)
Manganous Zone	Chitinophagaceae (HM129183.1)	acI, Actinobacteria (FN668226.2)	Crenothrix (FJ502272.1)		Pirellulaceae (New.ReferenceOTU11)	SB-45, Atribacteria (JQ087016.1)	Omnitrophica (New.ReferenceOTU12)
	Synechococcus (FJ382618.1)	Nitrospiraceae (AM167945.1)	acI, Actinobacteria (FN668226.2)		Bacteroidales (AM162484.1)	C20, Chlorobi (EU644261.1)	SB-45, Atribacteria (JQ087016.1)
	Roseococcus (New.ReferenceOTU8)	Rhodospirillaceae (GQ396920.1)	Sediminibacterium (JN656812.1)		C20, Chlorobi (HM243831.1)	SHA-114, AC1 (AB186797.1)	B10, Crenarchaeota (FN428815.1)
Ferruginous Zone	Chitinophagaceae (HM129183.1)	acI, Actinobacteria (FN668226.2)	acI, Actinobacteria (FN668226.2)	acI, Actinobacteria (FN668226.2)		SB-45, Atribacteria (JQ087016.1)	Omnitrophica (New.ReferenceOTU12)
	Synechococcus (FJ382618.1)	Nitrospiraceae (AM167945.1)	Crenothrix (FJ502272.1)	Sterolibacterium (NR_025450.1)		C20, Chlorobi (EU644261.1)	B10, Crenarchaeota (FN428815.1)
	Roseococcus (New.ReferenceOTU8)	acI, Actinobacteria (FN668218.2)	Comamonadaceae (GU208444.1)	Betaproteobacteria (FR667762.1)		Pirellulaceae (New.ReferenceOTU31)	SB-45, Atribacteria (JQ087016.1)
Euxinic Zone	Chitinophagaceae (HM129183.1)	acI, Actinobacteria (FN668226.2)	acI, Actinobacteria (FN668226.2)	acI, Actinobacteria (FN668226.2)	Sterolibacterium (NR_025450.1)		B10, Crenarchaeota (FN428815.1)
	Haliscomenobacter (EF520596.1)	Nitrospiraceae (AM167945.1)	Crenothrix (FJ502272.1)	Sterolibacterium (NR_025450.1)	Bacteroidales (AM162484.1)		Omnitrophica (New.ReferenceOTU12)
	Roseococcus (New.ReferenceOTU8)	acI, Actinobacteria (FN668218.2)	Comamonadaceae (GU208444.1)	Betaproteobacteria (FR667762.1)	GIF10, Omnitrophica (New.RefeOTU1)		MSBL2, Cloacimonetes (HQ691904.1)
Ancient Seawater	Chitinophagaceae (HM129183.1)	acI, Actinobacteria (FN668226.2)	acI, Actinobacteria (FN668226.2)	acI, Actinobacteria (FN668226.2)	Desulfobacca (AB426203.1)	Syntrophaceae (HQ003553.1)	
	Roseococcus (New.ReferenceOTU8)	Nitrospiraceae (AM167945.1)	Crenothrix (FJ502272.1)	Sterolibacterium (NR_025450.1)	Syntrophaceae (HQ003553.1)	Syntrophaceae (AB630476.1)	
	Haliscomenobacter (EF520596.1)	acI, Actinobacteria (FN668218.2)	Comamonadaceae (GU208444.1)	Bacteroidales (AM162484.1)	C20, Chlorobi (HM243831.1)	Desulfobacca (AB426203.1)	

Contribution to dissimilarity [%]
2.6
0.42

Table A4. Distribution of marker genes for anoxygenic photosynthesis (derived from HUMAnN) as well as additional functional marker genes for other processes derived from Hidden Markov Models over the metagenomes from different water column depths. Gene numbers are normalized to total gene numbers per metagenome and color-coded to highlight gene distributions.

	Metagenome depth [m]	120 m	130 m	150 m	160 m	180 m	200 m	280 m	310 m	330 m	350 m
Methane oxidation	Soluble methane monooxygenase (*mmoX*)	1.1E-06	9.3E-06	2.6E-07	7.6E-07	1.5E-07	5.4E-07	0.0E+00	0.0E+00	0.0E+00	1.0E-06
	Particulate methane monooxygenase (*pmoA*)	1.2E-05	3.5E-05	5.4E-06	5.5E-06	1.8E-06	2.4E-06	8.3E-07	0.0E+00	8.5E-07	2.3E-06
Methanol oxidation	Methanol Dehydrogenase (*xoxF*)	3.9E-04	2.8E-04	1.1E-04	2.4E-04	7.4E-05	6.7E-05	6.4E-05	6.2E-05	6.2E-05	2.2E-04
Denitrification	Nitrite reductase (*nirS*)	1.7E-05	9.7E-05	5.2E-05	6.4E-05	1.2E-05	9.7E-06	2.5E-06	4.1E-06	5.6E-07	2.1E-06
Sulfur mineralization	Cystathionine gamma-lyase (*mccB*)	8.1E-04	1.7E-03	6.2E-04	1.1E-03	5.4E-04	5.4E-04	4.0E-04	3.6E-04	2.8E-04	7.0E-04
Sulfur reduction/ -oxidation	Sulfide-quinone reductase (*sqr*)	6.5E-04	1.8E-03	5.1E-04	9.9E-04	4.2E-04	3.7E-04	3.6E-04	2.9E-04	3.3E-04	7.9E-04

	Metagenome depth [m]	120 m	130 m	150 m	160 m	180 m	200 m	280 m	310 m	330 m	350 m
Anoxygenic Photosynthesis	K11336: 2-vinyl bacteriochlorophyllide hydratase (*bchF*)	1.8E-06	4.5E-06	1.8E-06	7.1E-07	0.0E+00	2.3E-06	0.0E+00	3.4E-05	0.0E+00	0.0E+00
	K11337: 3-hydroxyethyl bacteriochlorophyllide *a* dehydrogenase (*bchC*)	2.1E-06	5.6E-06	1.7E-06	3.9E-06	7.3E-07	0.0E+00	3.9E-06	0.0E+00	4.3E-06	2.9E-06
	K08944: bacteriochlorophyll *a* protein (*fmoA*)	0.0E+00	0.0E+00	0.0E+00	0.0E+00	0.0E+00	0.0E+00	0.0E+00	0.0E+00	0.0E+00	0.0E+00
	K09879: isorenieratene synthase	7.8E-06	5.2E-06	3.5E-06	8.9E-06	3.5E-06	5.0E-06	6.9E-06	4.8E-07	1.5E-06	4.2E-06
	K08940: photosystem P840 reaction center large subunit (*pscA*)	0.0E+00	0.0E+00	0.0E+00	0.0E+00	0.0E+00	0.0E+00	0.0E+00	0.0E+00	0.0E+00	0.0E+00
	K08941: photosystem P840 reaction center iron-sulfur protein (*pscB*)	0.0E+00	0.0E+00	0.0E+00	0.0E+00	0.0E+00	0.0E+00	0.0E+00	0.0E+00	0.0E+00	0.0E+00
	K08942: photosystem P840 reaction center cytochrome c551 (*pscC*)	9.9E-07	3.5E-06	0.0E+00	1.0E-06	9.3E-07	0.0E+00	0.0E+00	0.0E+00	0.0E+00	0.0E+00
	K08943: photosystem P840 reaction center protein (*pscD*)	0.0E+00	0.0E+00	0.0E+00	0.0E+00	0.0E+00	0.0E+00	0.0E+00	0.0E+00	0.0E+00	0.0E+00
	K08928: photosynthetic reaction center L subunit (*pufL*)	3.5E-06	1.6E-06	3.4E-06	6.6E-07	7.7E-07	3.0E-06	4.2E-06	2.2E-05	3.3E-06	1.3E-06
	K08929: photosynthetic reaction center M subunit (*pufM*)	1.1E-05	4.2E-06	4.0E-06	5.6E-07	6.0E-07	9.0E-07	3.9E-06	0.0E+00	1.4E-06	1.9E-08

Table A5. Taxonomic classification and vertical distribution of metagenomic bins including metagenome-annotated genomes (MAGs) over the ten metagenomes from different depths. Taxonomy and nearest neighbor are based on CheckM and SEED, respectively. Vertical distribution of each bin is represented by percentage of reads recruited from a given metagenome that map to the contigs of a given bin and visualized by gray background if percentage >0.5%. For each bin, completion and redundancy based on number of unique and redundant marker genes are also provided. *(Electronic Supplement)*

Table A6. OTUs forming isolated clades in the phylogenetic tree of 16S rRNA sequences from then ancient seawater zone (Figure A5). Occurrence in a given zone is indicated if the OTU is >0.5% in at least one sample from this zone.

Local OTU ID	OTU ID (Greengenes)	OTU ID (NCBI)	Occurrence	Taxonomic affiliation (phylum)
-	4297148	JQ087016	Euxinic, ASW	*Atribacteria*
-	4410644	JQ816281	ASW	*Atribacteria*
New.ReferenceOTU15	-	-	Euxinic, ASW	Unaffiliated
New.ReferenceOTU50	-	-	ASW	Unaffiliated
-	581539	GQ259268	ASW	*Bacteroidetes*
-	548731	EU592421	ASW	*Deltaproteobacteria*
-	3003711	HQ395178	ASW	*Deltaproteobacteria*
New.ReferenceOTU6	-	-	ASW	*Planctomycetes* (*Phycisphaerae*)
New.ReferenceOTU25	-	-	Euxinic, ASW	*Planctomycetes* (*Phycisphaerae*)
New.ReferenceOTU37	-	-	Ferruginous, Euxinic ASW	*Planctomycetes* (*Phycisphaerae*)

Table A7. Marker genes used to quantify genetic potential for processes in the carbon, nitrogen and sulfur cycles.

Carbon cycle

Process	KEGG orthology	Gene name	Marker gene
Aerobic respiration ((K02256+K02262)/2)+((K02274+K02276)/2)	K02256	coxI	cytochrome c oxidase subunit I (coxI)
	K02262	coxIII	cytochrome c oxidase subunit III (coxIII)
	K02274	coxA	cytochrome c oxidase subunit I (coxA)
	K02276	coxC	cytochrome c oxidase subunit III (coxC)
High-O2 affinity respiration	K00404	ccoN, fixN	cb-type cytochrome c oxidase subunit I
	K00425	cydA	cytochrome bd-I oxidase subunit I
Calvin cycle (K00855+K01602)/2	K00855	PRK, prkB	phosphoribulokinase
	K01602	rbcS	ribulose bisphosphate carboxylase small chain
Aerobic methane oxidation	K08684		methane monooxygenase
Aerobic methanol oxidation	K14028	mxaF	methanol dehydrogenase (cytochrome c) subunit 1
CO oxidation (K03518+K03519+K03520)/3	K03518	coxS	aerobic carbon-monoxide dehydrogenase small subunit
	K03519	coxM	aerobic carbon-monoxide dehydrogenase medium subunit
	K03520	coxL	aerobic carbon-monoxide dehydrogenase large subunit
Anaerobic C fixation Reductive Tricarboxylic Acid Cycle: (K00174+K00175+K00244+K01648)/4; Reductive Acetyl-CoA: (K00194+K00197)/2	K00174	korA, oorA	2-oxoglutarate:ferredoxin oxidoreductase subunit alpha
	K00175	korB, oorB	2-oxoglutarate:ferredoxin oxidoreductase subunit beta
	K00244	frdA	fumarate reductase flavoprotein subunit
	K01648	aclY	adenosinetriphosphate (ATP) citrate lyase
	K00194	cdhD, acsD	CO dehydrogenase subunit delta
	K00197	cdhE, acsC	CO dehydrogenase subunit gamma
Fermentation	K00016	LDH, ldh	L-lactate dehydrogenase
Methanogenesis (K00400+K00401)/2	K00400	mcrA	methyl coenzyme M reductase system, component A2
	K00401	mcrB	methyl-coenzyme M reductase beta subunit

Nitrogen cycle

Process	KEGG orthology	Gene name	Marker gene
N assimilation (K00360+K00367+K01915+K00265+K00284)/3	K00360	nasB	assimilatory nitrate reductase
	K00367	narB	ferredoxin-nitrate reductase (assimilatory)
	K01915	glnA	glutamine synthetase
	K00265	gltB	glutamate synthase (NADPH/NADH) large chain
	K00284	gltS	glutamate synthase (ferredoxin-dependent)
Ammonification (Remineralization) (K00260+K00261+K00262+K01428)/2	K00260	gudB, rocG	glutamate dehydrogenase
	K00261	gdhA, glud1	glutamate dehydrogenase
	K00262	gdhA	glutamate dehydrogenase
	K01428	ureC	urease alpha subunit
N fixation (K00531+K02586+K02588+K02591)/3	K00531	anfG	nitrogenase delta subunit
	K02586	nifD	nitrogenase molybdenum-iron protein alpha chain
	K02588	nifH	nitrogenase iron protein NifH
	K02591	nifK	nitrogenase molybdenum-iron protein beta chain
Ammonium oxidation (K10944+K10945+K10946)/3	K10944	amoA	ammonia monooxygenase subunit A
	K10945	amoB	ammonia monooxygenase subunit B
	K10946	amoC	ammonia monooxygenase subunit C
Nitrite reduction (to NO)	K00368	nirK	nitrite reductase (NO-forming)
Nitrate reduction / nitrite oxidation (K00370+K00371)/2	K00370	narG, nxrA	nitrate reductase / nitrite oxidoreductase, alpha subunit
	K00371	narH, nxrB	nitrate reductase / nitrite oxidoreductase, beta subunit
Nitrate reduction (K02567+K02568)/2	K02567	napA	periplasmic nitrate reductase NapA
	K02568	napB	cytochrome c-type protein NapB

Nitrogen cycle (continued)

Process	KEGG orthology	Gene name	Marker gene
Denitrification (K02305+K04561+K00376)/3	K02305	norC	nitric-oxide reductase, cytochrome c-containing subunit II
	K04561	norB	nitric-oxide reductase, cytochrome b-containing subunit I
	K00376	nosZ	nitrous-oxide reductase
Anammox/ bacterial ammonium oxidation	K10535	HAO, hdh	hydroxylamine oxidoreductase / hydrazine dehydrogenase
DNRA (K03385+K05904)	K03385	nrfA	formate-dependent nitrite reductase, periplasmic cytochrome c552
	K05904	nrfA	cytochrome c nitrite reductase

Sulfur cycle

Process	KEGG orthology	Gene name	Marker gene
Assimilatory sulfate reduction (K00860+K00956+K00957)/3	K00860	cysC	adenylylsulfate kinase
	K00956	cysN	sulfate adenylyltransferase subunit 1
	K00957	cysD	sulfate adenylyltransferase subunit 2
S mineralization (K00456+K01011)	K00456	CDO1	cysteine dioxygenase CDO1
	K01011	sseA	thiosulfate/ 3-mercaptopyruvate sulfurtransferase
Dissimilatory sulfate reduction/ sulfide oxidation (K00394+K00395+K11180)/3	K00394	aprA	adenylylsulfate reductase, subunit A
	K00395	aprB	adenylylsulfate reductase, subunit B
	K11180	dsrA	sulfite reductase, dissimilatory-type alpha subunit
Thiosulfate/ Polysulfide reduction	K08352	phsA	thiosulfate reductase / polysulfide reductase chain A

Table A8. Correlations among different phylum-level taxonomic groups based on 16S rRNA gene sequences and between taxonomic groups and geochemical parameters in different samples over the vertical range of the water column. The table shows correlation coefficients with negative correlations color-coded in blue. *(Electronic Supplement)*

Table A9. Correlations among different genus-level taxonomic groups based on 16S rRNA gene sequences and between taxonomic groups and geochemical parameters in different samples over the vertical range of the water column. The table shows correlation coefficients with negative correlations color-coded in blue. *(Electronic Supplement)*

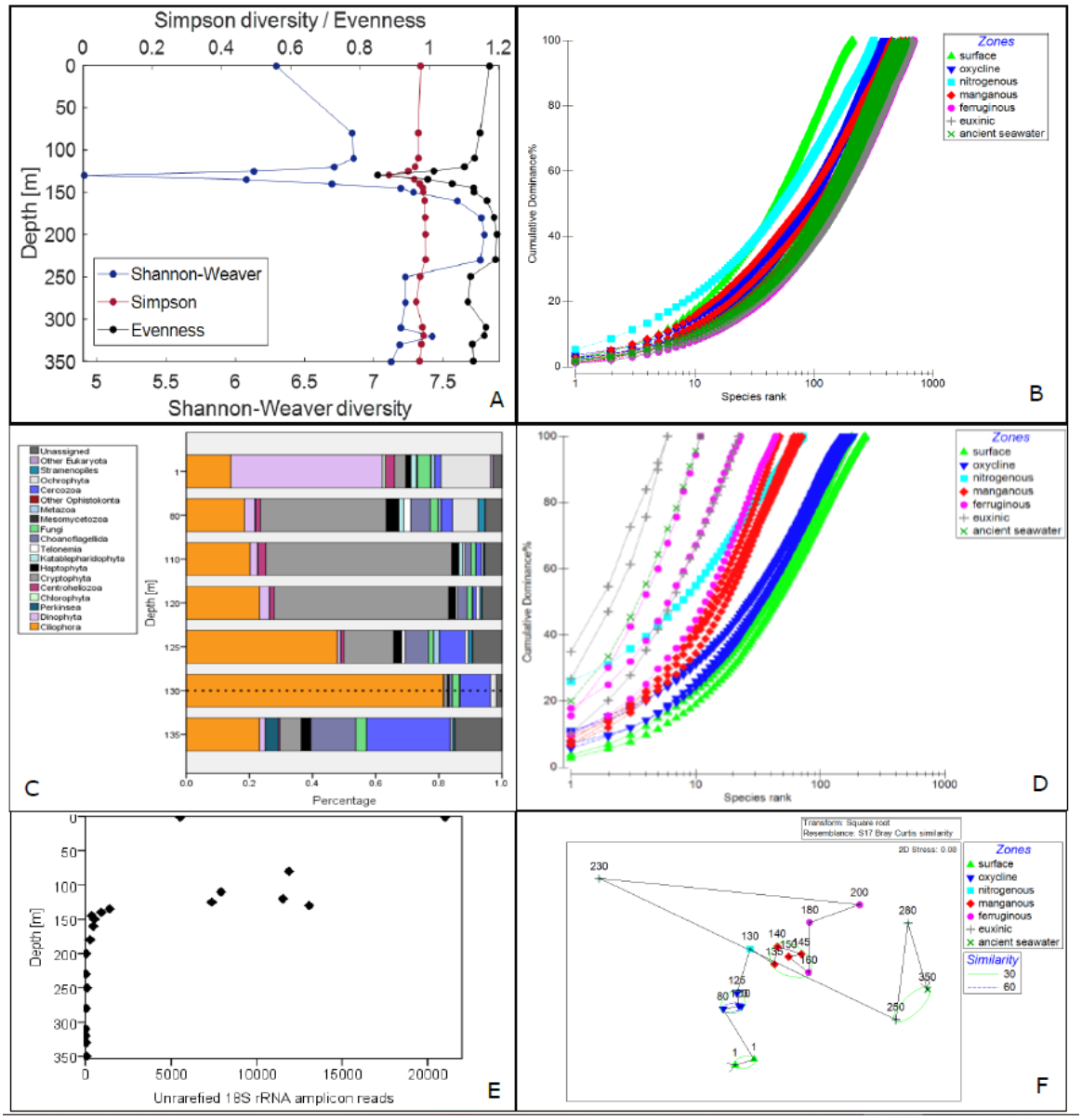

Figure A1. Prokaryotic and eukaryotic diversity based on small subunit rRNA gene sequencing. (A) Vertical profile of Evenness, Shannon-Weaver and Simpson diversity indices based on 16S rRNA gene sequencing. (B) Rank-dominance plot of 16S rRNA gene sequencing based OTUs in samples from different geomicrobiological zones. (C) Vertical profile of relative abundance of eukaryotic phyla based on 18S rRNA gene sequences. The 1-meter bar represents the average of a duplicate sample. The oxic-suboxic interface is indicated by a dotted line. Note that samples below 135 m fell below the rarefication threshold. (D) Rank-dominance plot of 18S rRNA gene sequencing based OTUs in samples from different geomicrobiological zones. (E) Unrarefied 18S rRNA amplicon reads as a function of depth. (F) Non-parametric multidimensional scaling (NMDS) plot of eukaryotic community composition based on Bray-Curtis similarity, showing the clustering of microbial communities from different depths referenced to predicted

geomicrobiological zones (Table 2.1). Geomicrobiological zones are indicated by different symbols and colors. Numbers in the plot indicate sample depths [m] and samples from neighboring depths are connected by a line. The 60%-threshold of between-sample similarity is indicated.

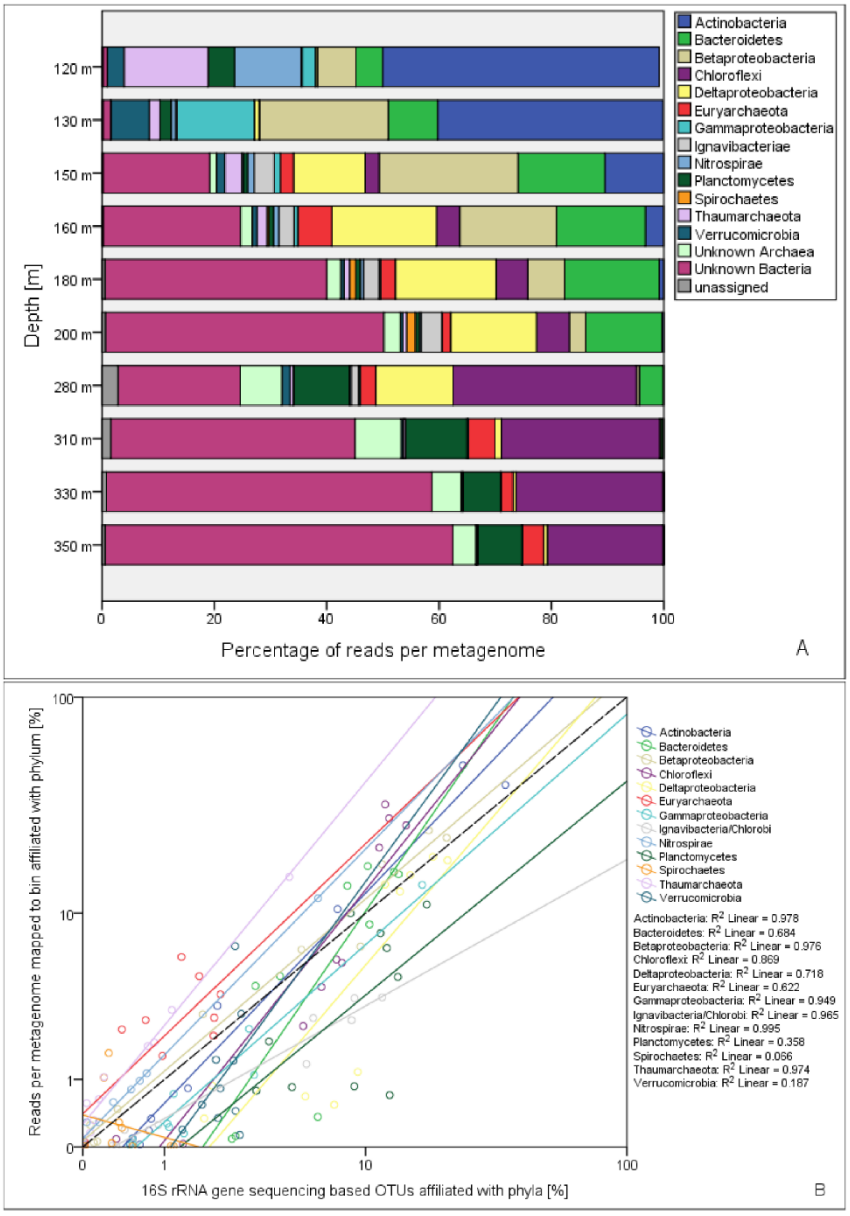

Figure A2: Vertical distribution of the relative abundance of microbial phyla based on affiliation with metagenomic bins and their correlation with phyla distribution based on 16S rRNA gene sequencing. (A) Percentage of metagenomic reads mapping to metagenomic bins with identical taxonomic affiliation at the phylum level (CheckM; Table A5) were summed up to construct the phylum-level depth profile. (B) For each phylum, the relative abundances were correlated with relative abundances based on 16S rRNA gene sequencing (Figure 2.3B) and the R^2 of the linear regression was provided. The dashed black line indicates a slope of 1. Logarithmic scales were used for better readability.

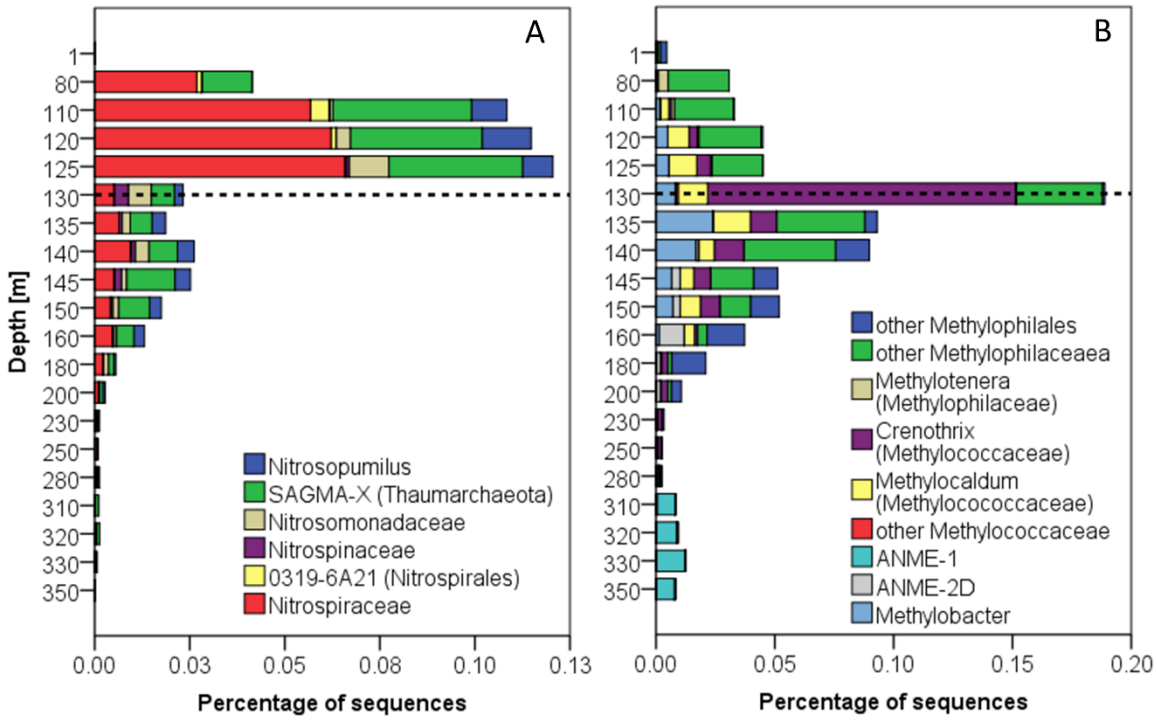

Figure A3. Relative abundance of 16S rRNA gene sequences affiliated with (A) potential nitrifiers and (B) potential methylotrophs and methanotrophs by depth. The oxic-suboxic interface is indicated by dashed lines.

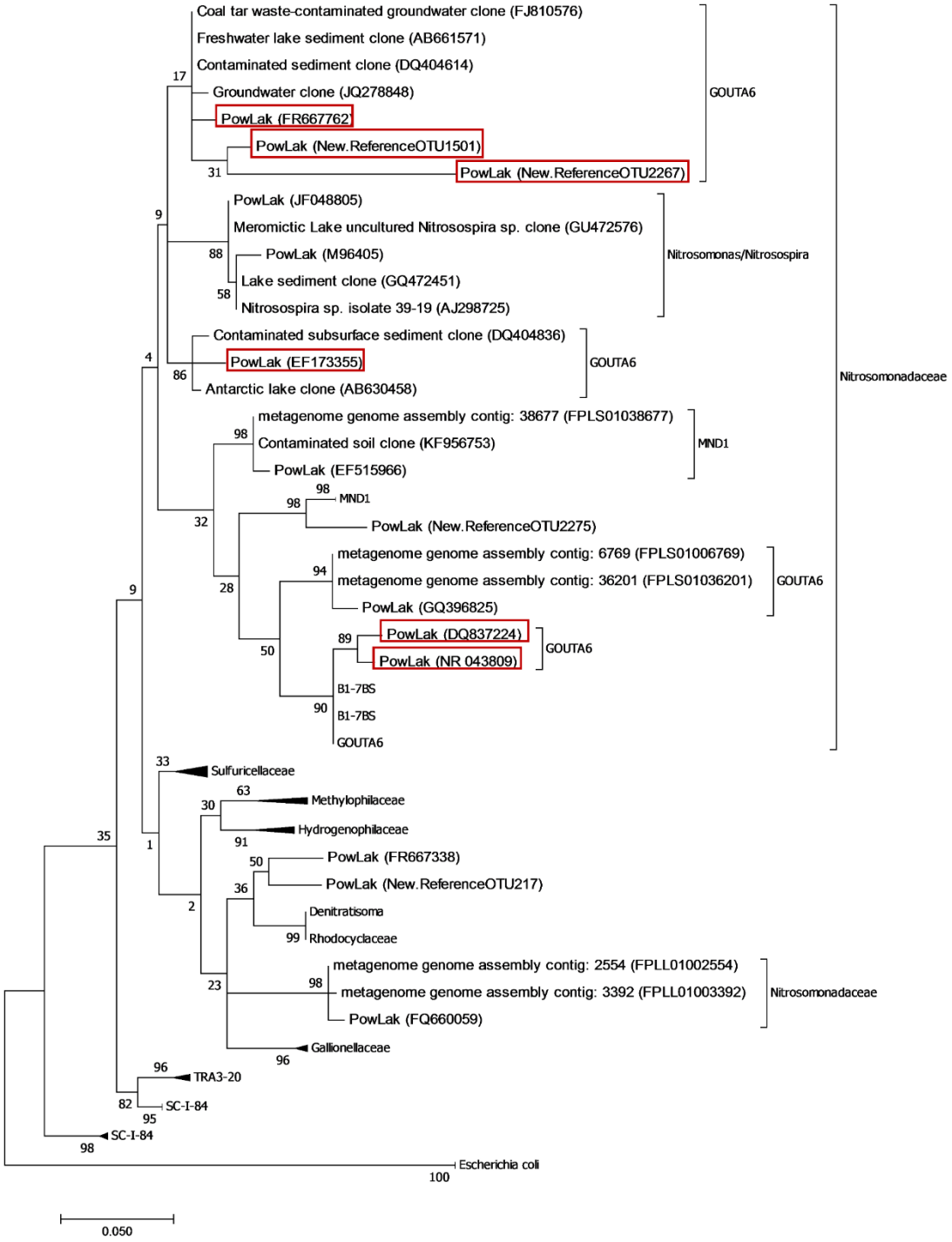

Figure A4. Phylogenetic tree (Kimura two-parameter model) of 16S rRNA gene sequences affiliated (based on Greengenes) with *Nitrosomonadaceae* and unclassified *Betaproteobacteria* that had a quantitatively significant presence (≥0.2%) in the oxycline, nitrogenous and manganous zones as well as their closest neighbors (>80% similarity) from the SILVA database. Powell Lake OTUs with highest shares in the manganous zone are

highlighted. The numbers at the branching nodes represent bootstrap support based on maximum likelihood (1000 replications). NCBI accession numbers are given in brackets behind ‘PowLak’ (indicating sequences from this study) or the NCBI descriptor (reference sequences). Sequences that could not be assigned to an existing sequence at the 97% similarity level are labeled ‘New.ReferenceOTU’. The branch identifiers are based on SILVA annotation.

Figure A5. Phylogenetic tree of the 16S rRNA gene sequences representing the top indicator OTUs for the Ancient Seawater Zone. The top 30 indicator OTUs (based on 16S rRNA gene sequencing) for the ancient seawater zone were chosen based on SIMPER analysis. SINA was used to identify and align the ten closest neighbors (>80% identity) for each OTU from the SILVA database. A maximum likelihood tree (100 bootstraps) was then constructed in RAxML, visualized and annotated in iTOL. Bootstrap support (0-100%) is indicated by numbers at the branch nodes. Powell Lake OTUs are highlighted and represented by the Greengenes accession number of their closest relative or labeled ‘New.ReferenceOTU' for OTUs that could not be assigned to an existing sequence at the 97% similarity level. Reference sequences are identified by their NCBI accession number and their SILVA-based taxonomic affiliation (left-hand color spectrum) and isolation source (right-hand color spectrum) are indicated. *(Electronic Supplement)*

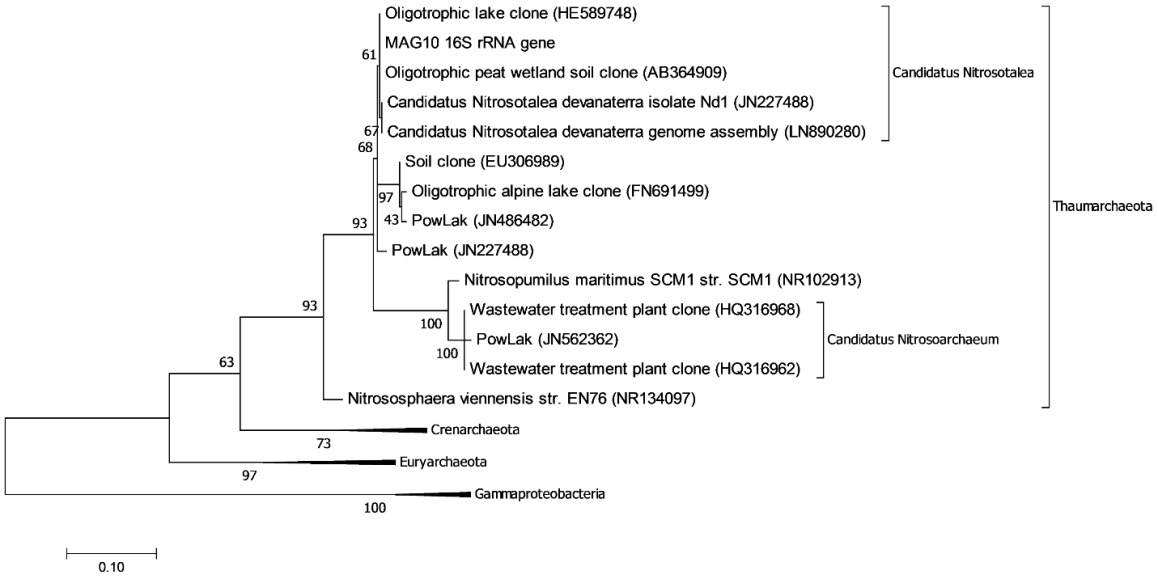

Figure A6. Phylogenetic tree (Kimura two-parameter model) of 16S rRNA gene sequences affiliated with *Thaumarchaeota,* their closest neighbors (>90% similarity) from the SILVA database as well as handpicked reference sequences from the NCBI RefSeq database. The numbers at the branching nodes represent bootstrap support based on maximum likelihood (1000 replications). NCBI accession numbers are given in brackets behind 'PowLak' (indicating sequences from this study) or the NCBI descriptor (reference sequences). The branch identifiers are based on SILVA annotation.

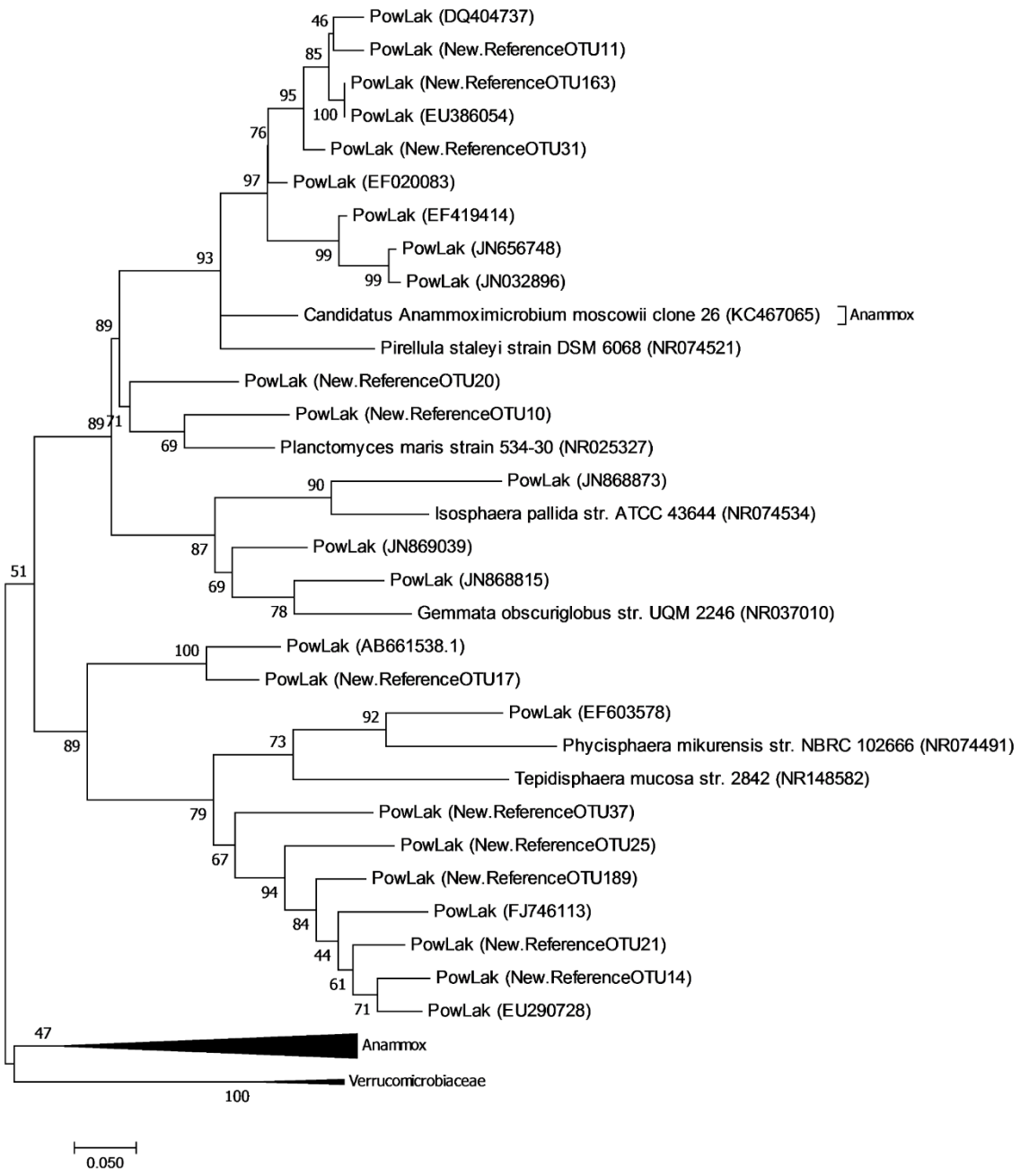

Figure A7. Phylogenetic tree (Kimura two-parameter model) of abundant (≥0.7% in any sample) OTUs affiliated with *Planctomycetes* from 16S rRNA gene sequencing. Representatives of *Planctomycetes* subgroups were handpicked from NCBI RefSeq database as references. The numbers at the branching nodes represent bootstrap support based on maximum likelihood (1000 replications). NCBI accession numbers are given in brackets behind 'PowLak' (indicating sequences from this study) or the NCBI descriptor (reference sequences). Sequences that could not be assigned to an existing sequence at the 97% similarity level are labeled 'New.ReferenceOTU'.

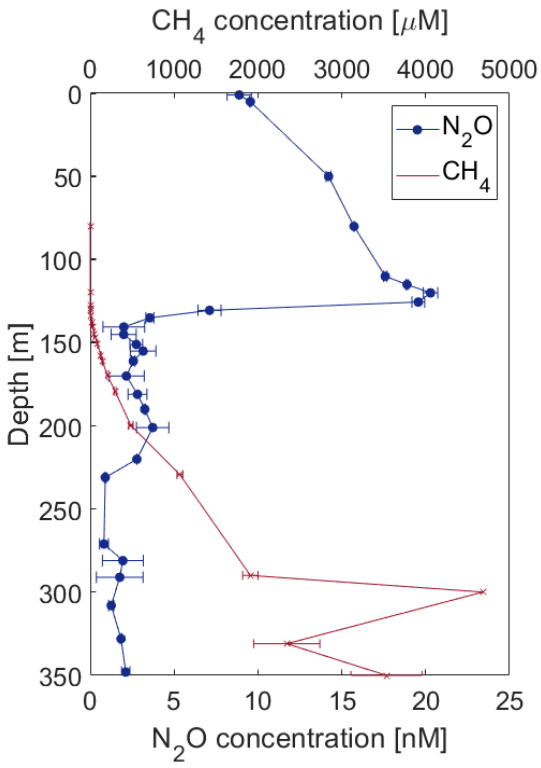

Figure A8. N_2O and CH_4 concentrations along the vertical profile measured in Powell Lake.

APPENDIX B: SUPPORTING INFORMATION TO CHAPTER 3

BEDFORD BASIN: STUDY SITE

The BB is a fjord-like embayment within the Halifax Regional Municipality (Nova Scotia), the largest urban center in Atlantic Canada. The 17 km^2 basin is connected to the Halifax Harbour and ultimately the Scotian Shelf (North Atlantic) via a narrow channel, forming a ~20 m deep sill. The main freshwater inflow is from the Sackville River, which is small in volume (5.3 $m^3 s^{-1}$) compared to the mean tidal volume entering the basin (2.5×10^7 m^3) and the total basin volume of 5.1×10^8 m^3 (Petrie and Yeats 1990; Gregory 1993). BB has a 2-layer estuarine type circulation, with relatively fresh water leaving the basin toward the harbor near-surface and relatively saline water entering the basin in the deeper layer (Huntsman 1924; Petrie and Yeats 1990; Fader and Miller 2008; Shan et al. 2011). The basin and adjacent harbor are subject to intense anthropogenic use, most importantly a municipal wastewater treatment plant drains into the BB and four additional ones can be found in the extended harbor area (Kerrigan et al. 2017).

SENSOR MEASUREMENTS, WATER SAMPLING AND ATMOSPHERIC DATA

Sampling for this study was conducted within the framework of the BB Monitoring Program led by the Bedford Institute of Oceanography (BIO), which has conducted a weekly oceanographic monitoring (1992 to present) at the Compass Buoy Station, (44°41'37"N, 63°38'25"W), situated at the central deep point of the basin (~70 m; Li 2014). From this time series, data from weekly CTD measurements with a Seabird SBE-25 CTD (including SBE-43 O_2 sensor) as well as particulate organic carbon (POC), particulate organic nitrogen (PON), chlorophyll *a* and nutrient data from four discrete depths (5 m, 60 m) were used in the present study. As of March 2015, the O_2 sensor data were cross-calibrated against discrete water samples analyzed by Winkler titration. Starting in 2014, the BIO monitoring has been augmented with additional measurements used in this study. Nitrate sensor (SUNA, Seabird Scientific; accuracy range: 2 μmol L^{-1}, manufacturer information) water column profiles were taken almost weekly, corrected for

salinity and dissolved organic matter as previously described (Sakamoto et al. 2009), and calibrated against nitrate concentrations analyzed in discrete water samples (see below).

Beginning in January 2014, weekly water samples for molecular analyses were transported to the laboratory in cooled, dark bottles. Samples for DNA extraction were pre-filtered through 160 µm nylon mesh and concentrated on polycarbonate filters (0.2 µm, 47 mm; Isopore, Millipore) by a peristaltic pump. Filters were flash-frozen in liquid N_2 and stored at -80°C until DNA extraction. Samples for cell counts were analyzed on the same day or fixed in 1% paraformaldehyde for 10 minutes, flash-frozen in liquid N_2 and stored at -80°C for later analysis. Atmospheric data (temperature and wind speed) were retrieved from the Environment and Climate Change Canada database (https://climate.weather.gc.ca/historical_data/search_historic_data_e.html, Bedford Basin station, 44°42'36"N, 63°37'48"W).

ANALYSIS OF BULK NUTRIENT, PARTICULATE AND CHLOROPHYLL A CONCENTRATIONS

DIN concentrations were analyzed using standard analytical methods for total ammonium (NH_3+NH_4^+; Kérouel and Aminot, 1997), nitrite (NO_2^-) and nitrate (NO_3^-; Hansen and Koroleff, 1999) with a precision (determined as the average standard deviation of all duplicate sample measurements) of 0.11 µmol kg_{sw}^{-1} (ammonium), 0.13 µmol kg_{sw}^{-1} (nitrate) and 0.01 µmol kg_{sw}^{-1} (nitrite). For the years 2016–2017, DIN concentrations were analyzed in the Canada Excellence Research Chair for Ocean Science and Technology (CERC.OCEAN) laboratory at Dalhousie University on a continuous flow auto-analyzer (San++, Skalar). For the years 2014–2015, mostly publicly available data from BIO were used, which were produced on similar instruments (Technicon II, Alpkem RFA300 or Seal Analytical AA3). Additional data from produced by BIO according to standard methods (phosphate and silicate (Murphy and Riley 1962; Hansen and Koroleff 1999; Mitchell et al. 2002), chlorophyll *a* (Lorenzen 1966; Li and Dickie 2001), POC and PON (Perkin Elmer Series II CHNS/O Analyzer 2400; Li and Harrison, 2008; Li 2014) were used for statistical evaluation of the long-term dataset.

STATISTICAL ANALYSES

Annual mean values as well as weekly standard anomalies, the weekly anomaly of a given parameter compared to the inter-annual weekly average of this parameter, standardized by the week-appropriate standard deviation (Li and Harrison 2008), were calculated for various parameters from the BB time series, 1994 to 2018 (Li 2014). Years for which a parameter was incompletely monitored (i.e. several consecutive weeks without measurements) were excluded from annual averaging but not from the standard anomalies. As a mixing proxy, the water spiciness was calculated from salinity, temperature and pressure, using the command 'swSPICE' from the R package OCE (Kelley 2018). The minimum spiciness during the winter mixing period (January–April) for each year was then used as a proxy for winter mixing intensity. Since winter mixing decreases temperature and salinity in BB bottom water (Figure 3.1A; Shan et al. 2011; Li 2014), spiciness represents a more relevant proxy than density. Sackville River water discharge data (at Bedford station: 44°43'53"N, 63°39'37"W) were retrieved from the Environment and Climate Change Canada website (https://wateroffice.ec.gc.ca/mainmenu/historical_data_index_e.html). Statistical tests were implemented in R software, using the command 'shapiro.test' for the Shapiro-Wilk normality test, 'corr.test' from the 'psych' package for Pearson, Spearman's rho and Kendall's tau correlation tests, and the command 'lm' for multiple regressions.

MICROBIAL CELL COUNTS

For cell counting, water was filtered through a 35 μm mesh and stained with 1× SYBR™ Green I (Invitrogen) for 10 min in the dark at room temperature. Cells were enumerated on an Accuri C6 (BD) flow cytometer with excitation at 488nm and detection using FL1 (533/30) and FL3 (670LP).

ANALYSIS OF 16S rRNA AMPLICON SEQUENCES

16S rRNA amplicon sequences were processed using a QIIME-2 based workflow (Bolyen et al. 2019). Paired-end sequences were joined using VSEARCH (Rognes et al. 2016) and low-quality reads were filtered out using the Demux command and its default parameters.

Deblur (Amir et al. 2017) was applied, with a trim-length of 354 bp, to correct reads and assign amplicon sequence variants (ASVs). Taxonomy was assigned to ASVs using a Naive-Bayes approach implemented in the *scikit learn* Python library and the SILVA database (Yilmaz et al. 2014) using a QIIME 2 associated full-length 16S rRNA gene classifier (available online: https://docs.qiime2.org/2019.7/data-resources/#taxonomy-classifiers-for-use-with-q2-feature-classifier). The dataset was refined by removal of rare (<0.1% of mean sample depth; likely due to MiSeq (Illumina) between-run bleed-through) and mitochondrial ASVs, as well as those unclassified at the phylum level. Samples were rarefied to a sequencing depth of 2995 reads, a value which allowed to retain all samples from 60 meters. For further analysis, the ASVs assigned by SILVA to taxonomic groups of known nitrifiers (*Thaumarchaeota*, *Nitrosomonadaceae*, *Nitrosococcaceae*, *Nitrospinaceae* and *Nitrospirae*) were subset and their share in total 16S rRNA amplicon sequences scaled to total cell counts.

Representative sequences closely related to the nitrifier ASVs were collected from the NCBI 'Nucleotide' and 'RefSeq Representative Genomes' databases through comparison via BLAST (Pruitt et al. 2007) for the phylogenetic tree depicted in Figure B2. The accession codes for all previously published reference sequences used in the phylogenies are provided in a version of the bacterial tree without any collapsed nodes (Figure B12). For Figure B9 and Figure B10, sequences of operational taxonomic units affiliated with *Thaumarchaeota* and *Nitrospina*, respectively, identified by Kitzinger et al. from samples taken in the Gulf of Mexico were added (Kitzinger et al. 2019, 2020). For each tree, these sequences along with the ASVs from BB were aligned using MUSCLE (Edgar 2004) and maximum-likelihood phylogenies were constructed in MEGA7 (Kumar et al. 2016). Trees were then visualized in iTOL (Letunic and Bork 2016).

QUANTITATIVE PCRs

Quantitative PCR (qPCR) was used to measure the abundance of the ammonia monooxygenase subunit A gene (*amoA*). Using Primer Express 3.0.1 software (Applied Biosystems), *de novo* assays were developed to target representative sequences for each of the six oceanic phylotypes of archaeal *amoA* defined in reference 26. Table B7 lists for each assay: designed primers, the accession code corresponding to the relevant phylotype

representative, and the nucleotide sequence of the dsDNA (gBlock; Integrated DNA Technologies). qPCR reactions were carried out on a ViiA 7 real time PCR system with QuantStudio software (Applied Biosystems); cycling conditions were: an initiation/hold step of 50°C for 2 min then 95°C for 10 min, followed by 45 qPCR cycles of 95°C for 15 sec and 60°C for 1 min. Additionally, a melt curve for temperatures between 60°C and 95°C was run to determine any non-specific amplification. The 16-µL reactions included: 8 µL 1× Power SYBR Green PCR Master Mix (Applied Biosystems), 200 nM of each primer (IDT), 6.4 µg BSA (NEB), and 5µL of template (either time-series DNA or standard DNA). Ultrapure DNase/RNase-free water (Invitrogen) was used for no-template controls. A standard curve of 10^1–10^7 gene copies per reaction was used to determine gene copy numbers; dsDNA stocks were freshly quantified on a Qubit 4 Fluorometer using the 1× dsDNA HS Assay Kit (both from Invitrogen). The range of average qPCR efficiencies for the six assays as calculated from standards was 86–91%, as determined using LinRegPCR software (Ruijter et al. 2009). We also confirmed the specificity of each qPCR *amoA* assay to its intended *amoA* phylotype target by testing all combinations of primer sets and standards (Table B8). Due to limited DNA volume and since *amoA* phylotypes amoA-A3 to A6 were consistently much rarer than phylotypes amoA-A1 and amoA-A2 (based on DNA from the years 2015–2017), we did not run qPCR assays for these much rarer types in 2014.

SUPPLEMENTARY DISCUSSION B1: THE TEMPORAL DISTRIBUTION OF THE ARCHAEAL *amoA* PHYLOTYPES QUANTIFIED BY qPCR

Six phylotypes of archaeal *amoA* were quantified by qPCR in 60-meter BB samples. AmoA-A3, amoA-A4, amoA-A5 and amoA-A6 were measured in 2015, 2016 and 2017. Gene copies of amoA-A1 and amoA-A2 were measured additionally in 2014. The different phylotypes displayed very different quantitative and qualitative temporal distributions (Figure B3). AmoA-A1, the most abundant phylotype (up to 4.4×10^5 copies g_{sw}^{-1}; Figure B3A), decreased in copy numbers during major mixing events (winter mixing, intrusions), while it increased in number during each stratified period with maxima coinciding with periods of maximum nitrate increase, suggesting that it represented the overall dominant ammonia oxidizer as discussed in the main text. Its abundance was well described as a

function of temperature (positive), dissolved oxygen and POC concentrations (negative; Table B1), reflecting the conditions at the end of stratified periods when nitrification tended to be strongest and amoA-A1 tended to be most abundant (Figure B3).

AmoA-A2 was the second most abundant phylotype (up to 1.1×10^4 copies g_{sw}^{-1}). Like amoA-A1, it has previously been associated with the surface ocean, whereas the remaining four phylotypes examined here have been associated with the deep ocean (Sintes et al. 2016). Interestingly, amoA-A2 displayed a distribution very similar to amoA-A6 and amoA-A3, which are associated with the deep oceanic realm (Sintes et al. 2016). With the exception of the year 2014, when only low amoA-A2 copy numbers were present exclusively during the stratified period, each of these phylotypes tended to appear at their highest numbers during the winter mixing period of each year (Figure B3B, E, F). This is reflected by the statistically significant and positive association of each of these phylotypes with dissolved oxygen concentration (Table B1). The sharp increases in copy numbers of *amoA* phylotypes A2, A3 and A6 coinciding with sharp salinity increases (shelf water intrusion events) in November 2016, March 2017 and December 2017 indicate that they may be brought to the BB bottom water from the Scotian Shelf by physical transport and mixing. Additionally, the growth of AOAs that are represented by these phylotypes may be favored by the conditions prevailing during the winter mixing period and they may represent ammonia oxidizers that are active in BB bottom waters during those times, but further research is necessary to establish this. The covariation of the surface-ocean associated amoA-A2 with the deep-ocean associated amoA-A6 and amoA-A3, respectively, is intriguing and further research may reveal why their appearance in BB bottom water is linked with the same mixing events.

AmoA-A4 displayed exceedingly low copy numbers (<2 copies g_{sw}^{-1}) and no clear temporal pattern (Figure B3D). AmoA-A5 was among the more abundant phylotypes (0–6.5×10^3 copies $g_{sw}^{-1)}$ but had no clear temporal distribution pattern (Figure B3E; Table B1).

SUPPLEMENTARY DISCUSSION B2: THE RATE INCREASING EFFECT OF WARMER WATER FROM INTRUSION EVENTS

Based on our observations, the intrusion events during the time period 2014–2017 decreased nutrient concentrations and amoA-A1 copy number, but in no case did they

deplete ammonium and/or the AOO community enough to significantly delay nitrification in their aftermath (Figure 3.2). This suggests that the mixing induced by intrusion events affected nitrification less than strong winter mixing. Following intrusion events, the associated temperature and oxygen increase may partly compensate for the small observed nitrifier biomass dilution by allowing for increased AO, NO and N remineralization rates. Both marine AOA and AOB have AO rate maxima at much higher temperatures (20–35°C; Groeneweg et al. 1994; Ruijter et al. 2009; Qin et al. 2014) than occur in BB bottom water (0.6–5.9°C). The temperature range in BB bottom water is small during stratified periods (~1–4°C) with the largest increases associated with the intrusion events (0.5–2.3°C; Figure B3). A very high Q_{10} value (Table B4) provided the best fit for the model, accounting for a strong nitrification rate increase after the intrusion events. The applied Q_{10} value is much higher than found in other AOA dominated, oligotrophic systems (Horak et al. 2013, 2018; Baer et al. 2014), but is similar to Q_{10} values observed in nutrient-rich parts of marine Narragansett Bay (Berounsky and Nixon 1990). This may suggest that high ammonium availability can lead to higher temperature-dependence of AO rates in AOA than has been observed in oligotrophic AOA (Horak et al. 2013, 2018; Qin et al. 2014; Baer et al. 2014).

SUPPLEMENTARY DISCUSSION B3: STATISTICAL VALIDATION OF CONCLUSIONS USING LONG-THERM BB TIME SERIES DATA

The findings for the years 2014–2017 were further constrained in the context of the long-term BB time series, for which weekly measurements started in 1994 (temperature, salinity, nitrate, phosphate, silicate, chlorophyll *a*), 1999 (dissolved oxygen) or 2002 (ammonium, nitrite, POC, PON). Statistical tests (*SI Materials and Methods*) suggested an important role for mixing intensity on nitrification indicators in BB bottom water. The annual average nitrate:ammonium ratio correlated negatively with the annual averages (all at 60 m) of POC and dissolved oxygen concentrations, and positively with high silicate concentrations (Table B5). Rather than reflecting a direct connection of these parameters with nitrification, these factors may both co-vary with winter mixing intensity, reflecting the delaying effect of intense winter mixing on nitrification as demonstrated by the empirical results and model observations in the years 2014–17 (Figure 3.2C,D,E). Indeed, each of these factors was also correlated with minimum spiciness, which was used as a proxy for winter mixing

intensity (Table B5). Quantification of mixing intensity is not straightforward, especially since winter mixing brings colder and fresher water to BB bottom water (Figure 3.1; Figure B1), therefore working approximately orthogonal to density. This is captured by spiciness, a parameter that is directly proportional to both temperature and salinity (Flament 2002; McDougall and Krzysik 2015). Annual spiciness minima appeared in the late phases of the winter mixing periods in each year 2014–17 due to mixing of low-temperature-low-salinity surface water into the bottom water (Figure 3.1A). Therefore, we used the minimum spiciness observed during annual winter mixing of each recorded year as a proxy for annual winter mixing intensity. Low intensity of winter mixing (indicated by less negative minimum spiciness) correlated significantly with low annual average O_2, POC and PON concentrations at 60 m, as well as high annual average nitrate:ammonium ratio, salinity, nitrate, and silicate concentrations (Table B5). The correlations of minimum spiciness with high nitrate concentrations and nitrate:ammonium ratios are consistent with a controlling influence of winter mixing on nitrification, with more intense mixing causing weaker nitrification.

Since the annual averages of POC and dissolved O_2 correlated positively, variations in annual O_2 are likely driven primarily by variations in mixing-induced reoxygenation and only secondarily by variations in remineralization. Winter mixing may also cause higher POC concentrations in the BB bottom water, explaining the correlation of POC with minimum spiciness. Measurements by Hargrave and Taguchi (Hargrave and Taguchi 1978) suggested that winter destratification favored sedimentation to 60 m relative to shallower depths in BB. The same authors report a chlorophyll *a* maximum within sedimented material in January. While it is not clear that stronger winter mixing increases the positive effect of destratification on POC deposition at 60 m observed by Hargrave and Taguchi (Hargrave and Taguchi 1978), this may provide an explanation for the correlation of intense winter mixing (low minimum spiciness) with increased POC concentrations observed here.

A multiple regression of weekly standard anomalies throughout the long-term time series suggested positive effects of temperature and negative effects of POC and oxygen concentrations on the nitrate:ammonium ratio (Table B6). The positive effect of temperature may reflect nitrification rate increase due to warmer temperatures (Appendix

B). As discussed above, low salinity and high dissolved oxygen and POC are probably caused primarily by high intensity winter mixing (Table B5). Hence, this test also suggests a role for the winter mixing intensity as a negative control on nitrification in BB (Table B6).

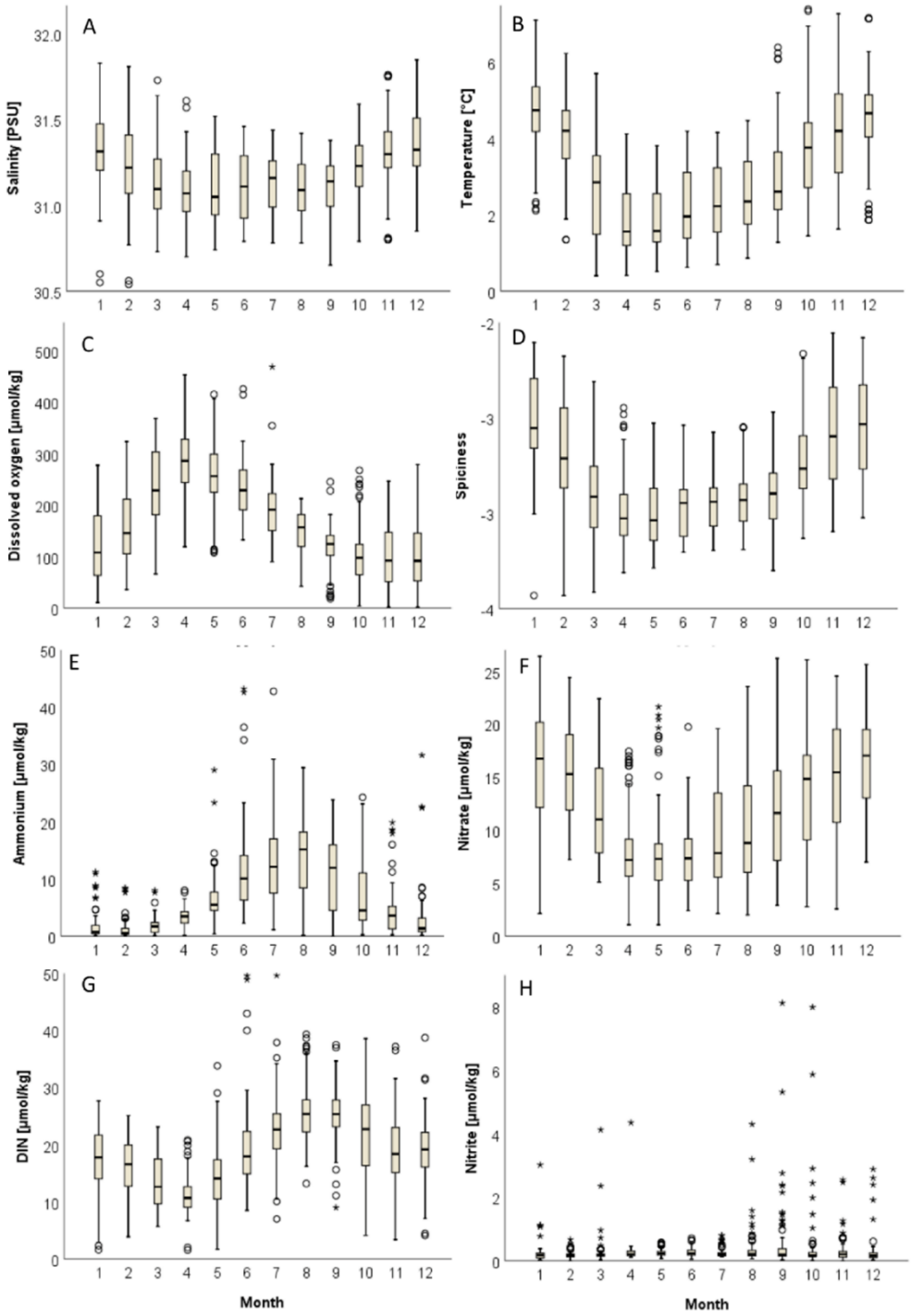

Figure B1. Monthly averages using weekly long-term time series data until 2018, starting in 1994 (temperature, salinity, spiciness, nitrate), 1999 (dissolved oxygen) or 2002 (ammonium, nitrite, DIN).

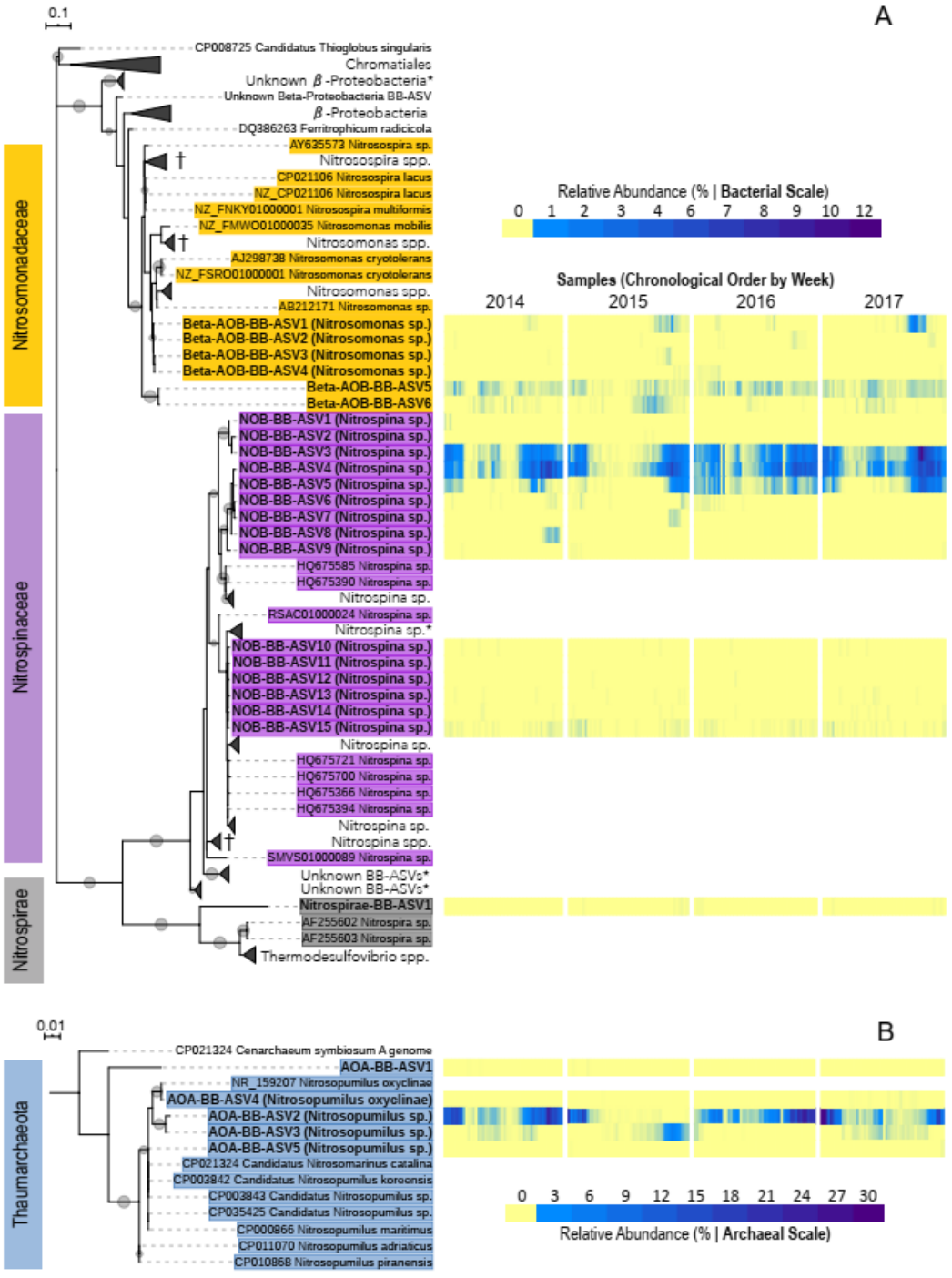

Figure B2. Phylogenetic maximum likelihood trees (1000 bootstraps) of A) bacterial and B) archaeal ASVs from 16S rRNA amplicon sequencing of the Bedford Basin bottom water community (bold) affiliated by SILVA with known nitrifier taxa, and their abundances in total 16S rRNA genes shown as heatmaps. Bedford Basin ASVs within collapsed branches (marked by *) were all quantitatively insignificant (≤0.2% in each sample) or, in the case of *Gammaproteobacteria*, blasting did not support their functional classification as

nitrifiers. Gray nodes indicate >80% bootstrap support. Collapsed nodes containing type species of a relevant AOB or NOB genus are marked with † and the full bacterial tree (A) can be seen in Figure B12. Relative ASV abundances are shown in chronological order and the weekly time steps are interrupted only at the end of each year and in March 2016 due to missing samples.

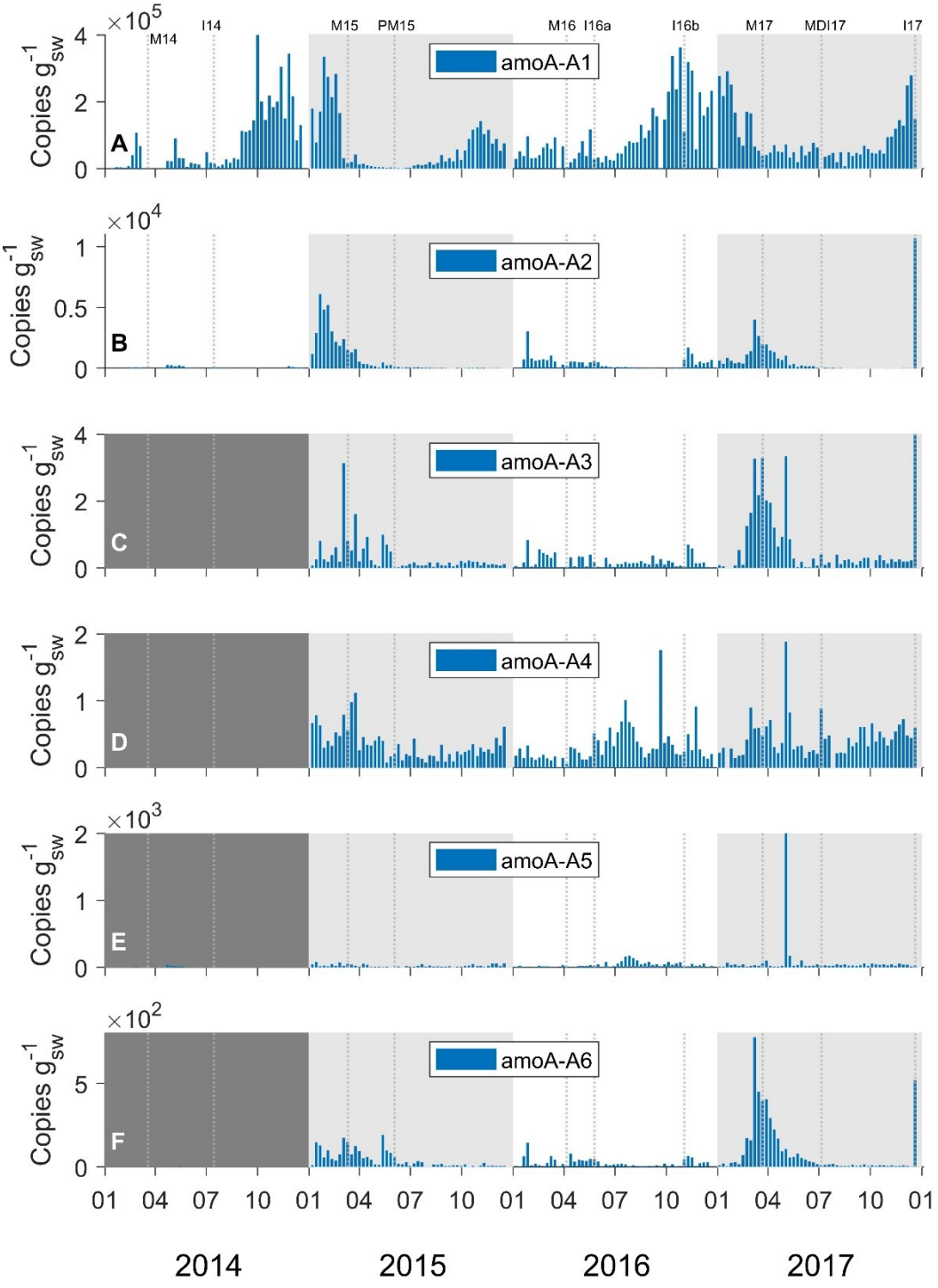

Figure B3. Temporal distribution of the phylotypes of archaeal *amoA*, A1 – A6, quantified by qPCR as well as salinity at 60 m in Bedford Basin, 2014–2017. Dotted lines indicate shelf water intrusion events.

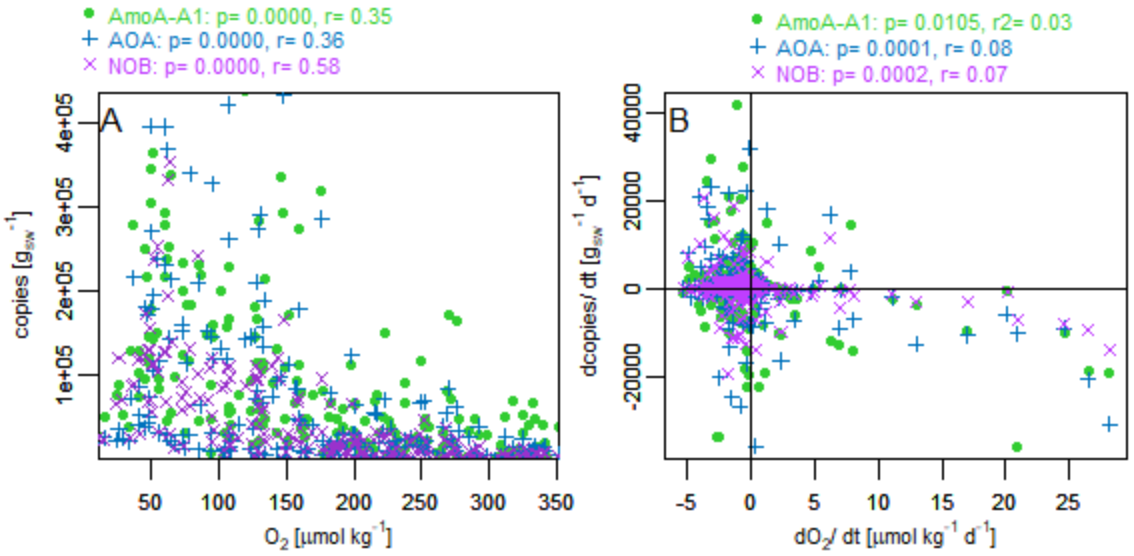

Figure B4. Concentrations (A) and time derivatives (B) of oxygen plotted against nitrifier abundances. Results from a Spearman's Rho correlation test (Table 3.1) are shown in the panel legends.

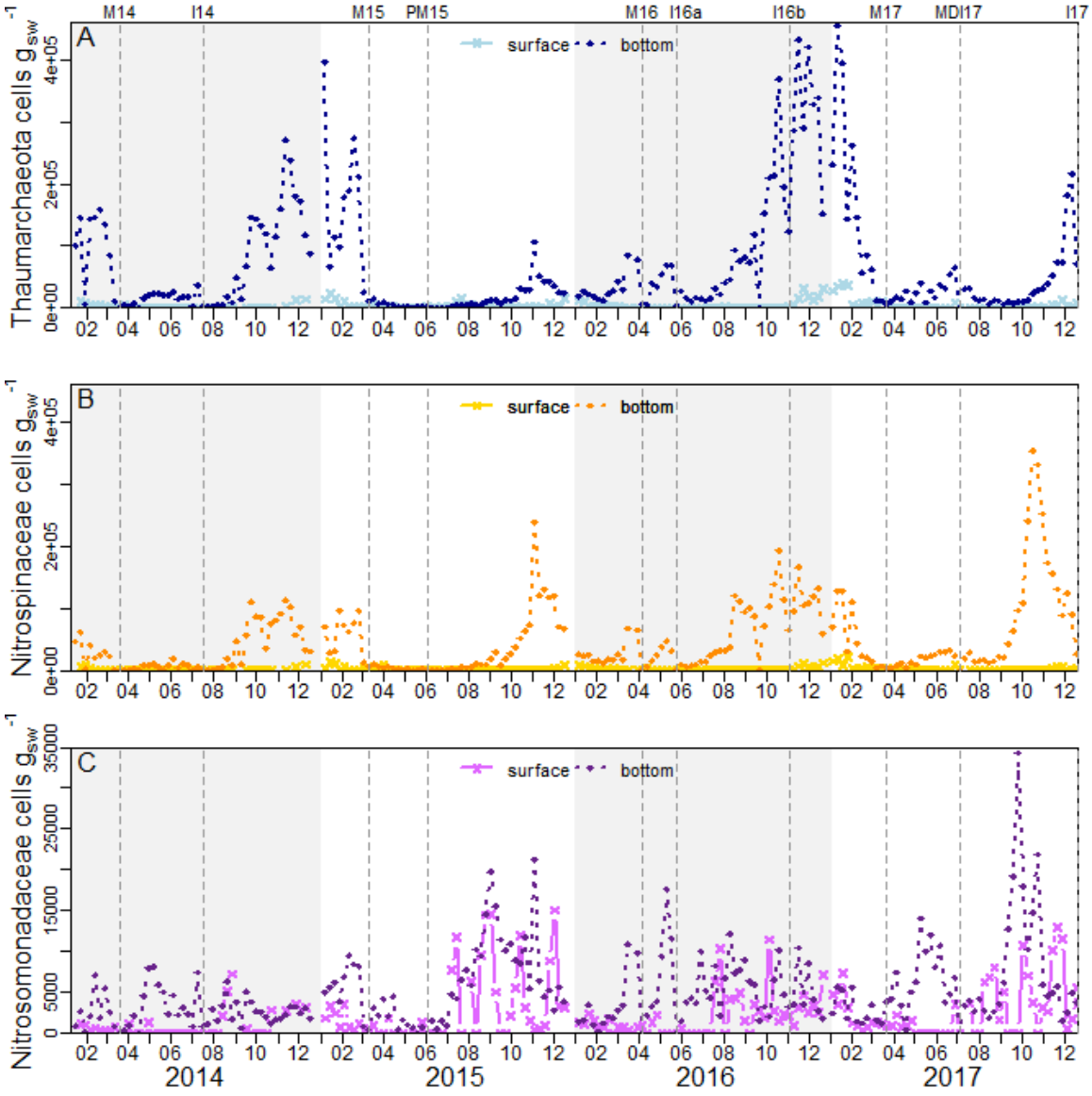

Figure B5. Time series of nitrifier abundance at the surface (5 m) and in the bottom water (60 m) of Bedford Basin: A) *Thaumarchaeota* (AOA), B) *Nitrospinaceae* (NOB), C) *Nitrosomonadaceae* (AOB). Note the different scale for *Nitrosomonadaceae*.

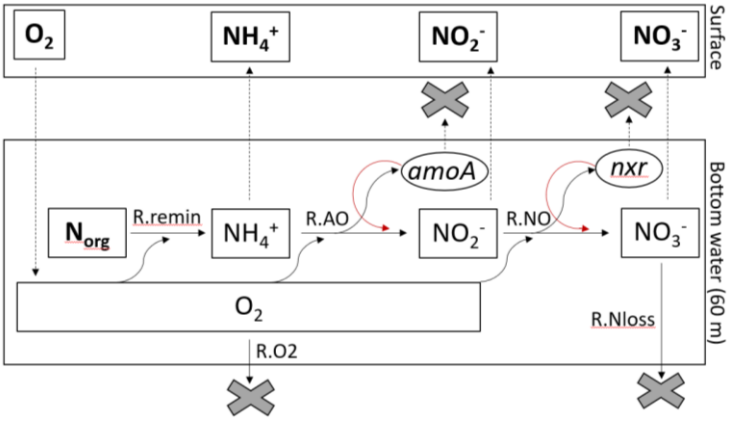

Figure B6. Network of biogeochemical reactions (solid arrows) and transport in and out of the 60-meter box of the model by physical mixing (dashed arrows). Direction of dashed arrows indicates the typical net flow of a given substance caused by mixing, which could be reversed in cases where the concentration gradient is reversed. As indicated by the red arrows, *amoA* and *nxr* increase reinforces the reactions catalyzed by them, AO and NO, respectively. Arrows toward 'X' indicate losses from the model. N_{org} (organic nitrogen) as well as all concentrations in the surface box are based on observations at 5 m depth (bold), the remaining variables in the 60-meter box are modeled. R.remin = remineralization rate; R.AO = ammonia oxidation rate; R.NO = nitrite oxidation rate; R.Nloss = N loss rate (= denitrification + assimilation + loss to sediment); R.O2 = respiration rate + loss to sediment.

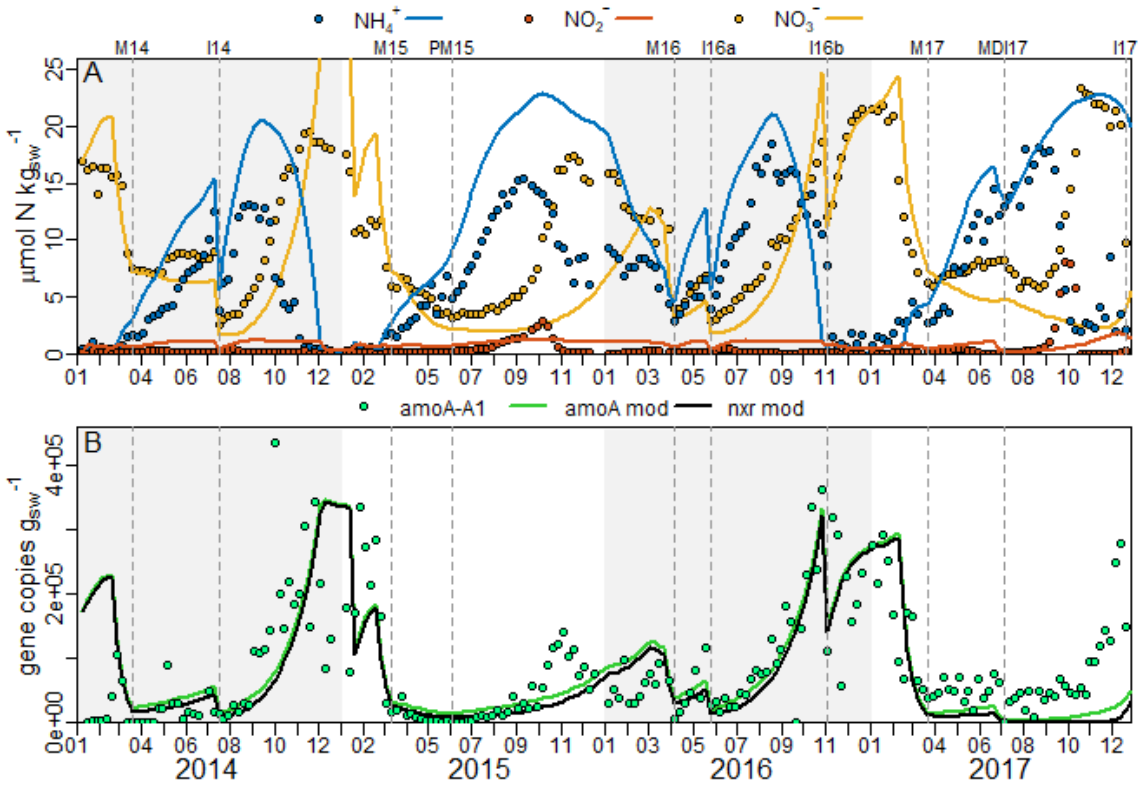

Figure B7. Time series of observed (scatter or bar) and modeled (lines: "mod") biogeochemical parameters at 60 m in Bedford Basin, 2014–2017, with modeled AO rate parameters adjusted to fit the observations in the year 2016 but otherwise identical to the model shown in Figure 3.3. A) Observed and modeled ammonium, nitrite and nitrate concentrations. B) AmoA-A1 (modeled and observed) and *nxr* (modeled) gene abundance.

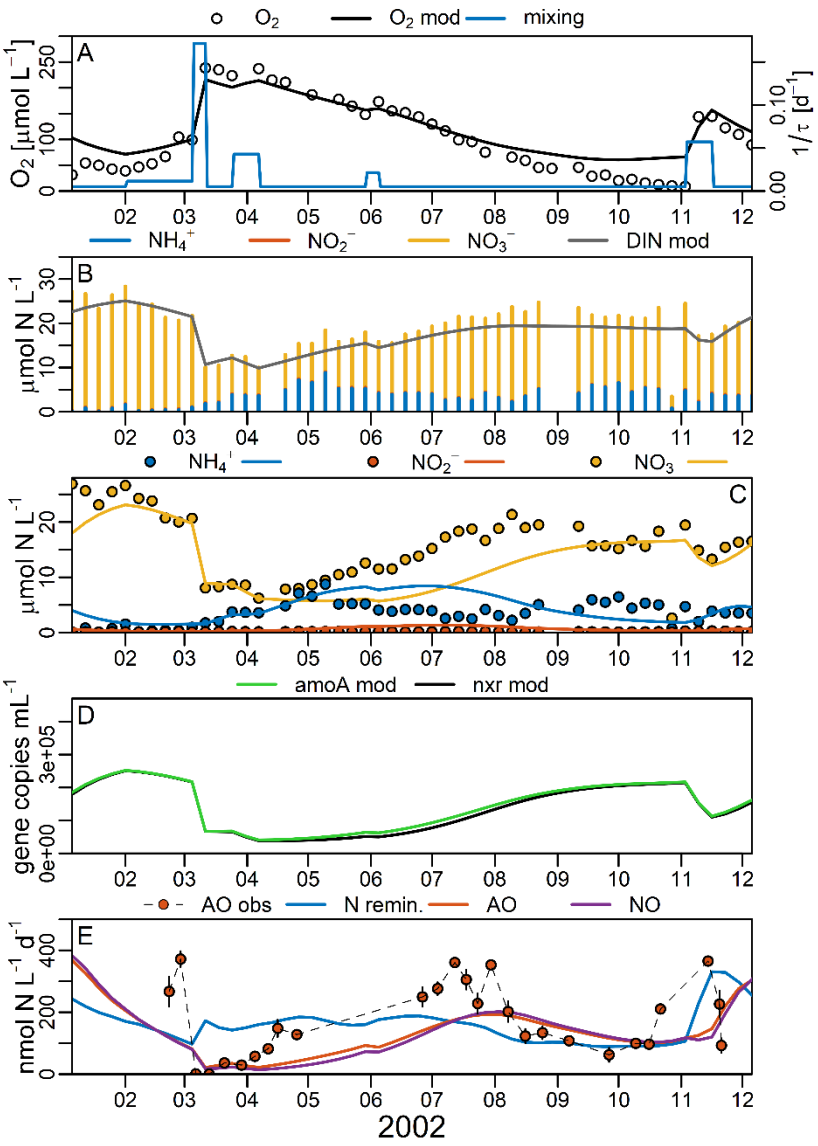

Figure B8**.** Model output for the year 2002 compared to empirical ammonia oxidation rates ("AO obs") from Punshon and Moore (Punshon and Moore 2004). Scatter plots represent data, line plots represent model output. To ensure accurate comparability with rates from Punshon and Moore (Punshon and Moore 2004), volumetric units were used for concentrations and rates in this model. Since POC data for 2002 were only available as of October 2002 this model is forced by a the weekly POC average 2014–2017 prior to October 2002. Note that two positive outliers (April 2nd, May 1st) were omitted from the oxygen data plotted in panel A, after we verified based on the full water column profiles that they most likely stemmed from methodological error.

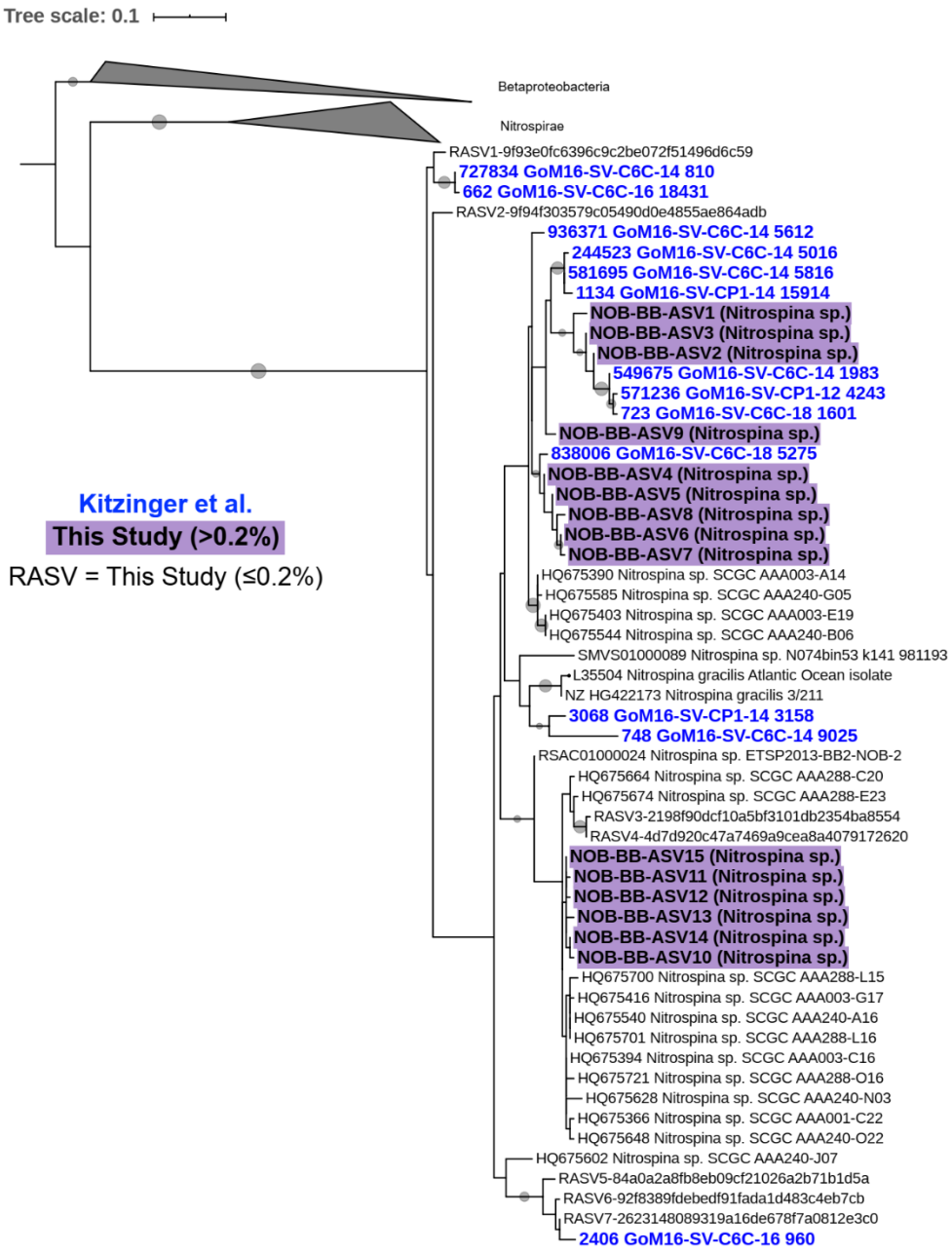

Figure B9. Phylogenetic Maximum Likelihood tree (1000 bootstraps) of *Nitrospina*-affiliated ASVs from this study, the reference sequences from Figure B2 and additional *Nitrospina*-affiliated reference sequences from the Gulf of Mexico, identified by Kitzinger et al. (Kitzinger et al. 2019, 2020) and shown in Table B9. Gray nodes indicate >50% bootstrap support.

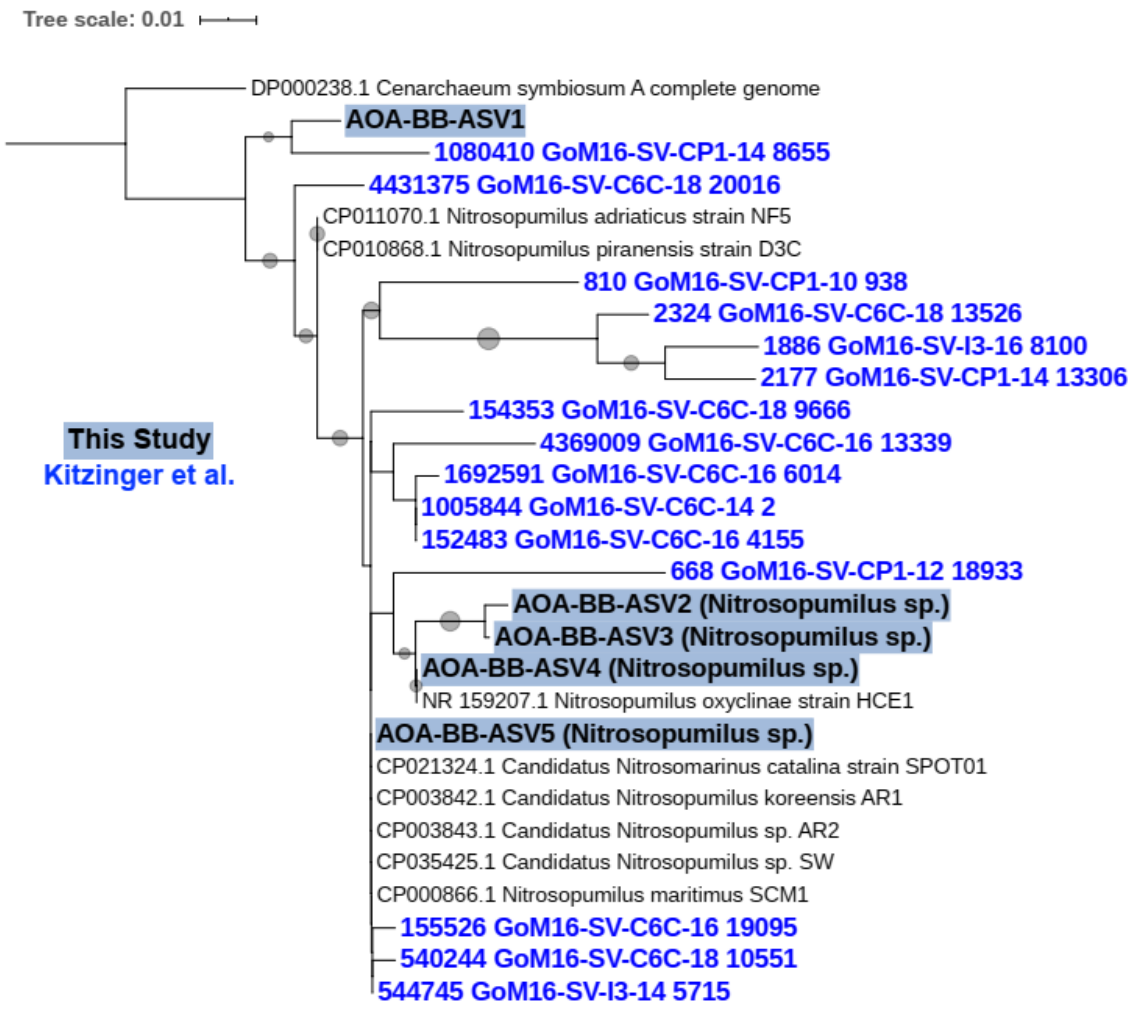

Figure B10. Phylogenetic Maximum Likelihood tree (1000 bootstraps) of *Thaumarchaeota*-affiliated ASVs from this study, the reference sequences from Figure B2 and additional *Thaumarchaeota*-affiliated reference sequences from the Gulf of Mexico, identified by Kitzinger et al. (Kitzinger et al. 2019, 2020) and shown in Table B9. Gray nodes indicate >50% bootstrap support.

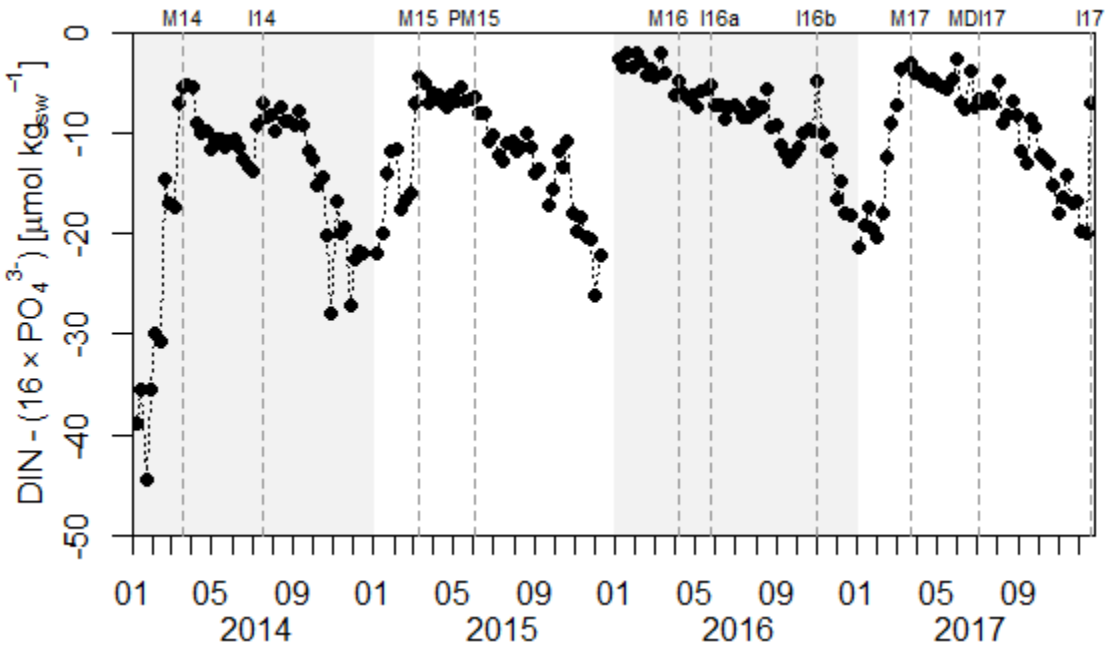

Figure B11. Observed Difference between DIN and phosphate concentrations corrected for the Redfield Ratio (factor 16) in the BB bottom water (60 m).

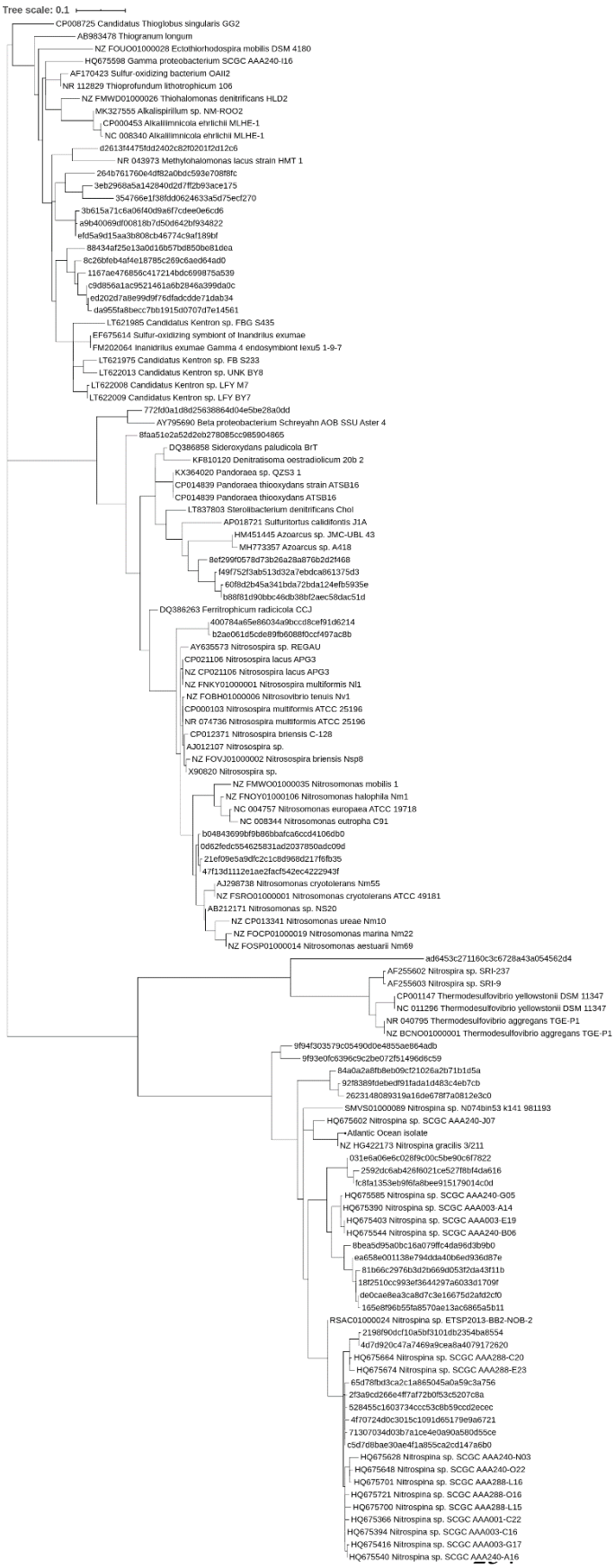
Tree scale: 0.1
CP008725 Candidatus Thioglobus singularis GG2
AB983478 Thiogranum longum
NZ FOUO01000028 Ectothiorhodospira mobilis DSM 4180
HQ675598 Gamma proteobacterium SCGC AAA240-I16
AF170423 Sulfur-oxidizing bacterium OAII2
NR 112829 Thioprofundum lithotrophicum 106
NZ FMWD01000026 Thiohalomonas denitrificans HLD2
MK327555 Alkalispirillum sp. NM-ROO2
CP000453 Alkalilimnicola ehrlichii MLHE-1
NC 008340 Alkalilimnicola ehrlichii MLHE-1
d2613f44751dd2402c82f02012d12c6
NR 043973 Methylohalomonas lacus strain HMT 1
264b761760e4df82a0bdc593e708f8fc
3eb2968a5a142840d2d7ff2b93ace175
354786e1f38fdfd062f4633a5d75ecf270
3b615a71c6a06f40d8a8f7cdee0e6cd6
a9b40069df008818b7d50d642bf934822
efd5a9d15aa3b808cb46774c9af189bf
88434af25e13a0d16b57bd850be81dea
8c26bfeb4af4e18785c269c6ad64ad0
1167ae476856c417214bdc699875a539
c9d856a1ac9521461a6b2846a399da0c
ed202d7a8e99d9f76dfadcdde71dab34
da955fa8becc7bb1915d0707d7e14561
LT621985 Candidatus Kentron sp. FBG S435
EF675614 Sulfur-oxidizing symbiont of Inandrilus exumae
FM202064 Inanidrilus exumae Gamma 4 endosymbiont lexu5 1-9-7
LT621975 Candidatus Kentron sp. FB S233
LT622013 Candidatus Kentron sp. UNK BY8
LT622008 Candidatus Kentron sp. LFY M7
LT622009 Candidatus Kentron sp. LFY BY7
772fd0a1d8d25638864d04e5be28a0dd
AY795690 Beta proteobacterium Schreyahn AOB SSU Aster 4
8faa51o2a52d2eb278085cc985904865
DQ386858 Sideroxydans paludicola BrT
KF810120 Denitratisoma oestradiolicum 20b 2
KX364020 Pandoraea sp. QZS3 1
CP014839 Pandoraea thiooxydans strain ATSB16
CP014839 Pandoraea thiooxydans ATSB16
LT837803 Sterolibacterium denitrificans Chol
AP018721 Sulfuritortus calidifontis J1A
HM451445 Azoarcus sp. JMC-UBL 43
MH773357 Azoarcus sp. A418
8ef299f0578d73b26a28a876b2d2f468
f49f752f3ab513d32a7ebdca861375d3
60f8d2b45a341bda72bda124efb5935e
b88f81d90bbc46db38bf2aec58dac51d
DQ386263 Ferritrophicum radicicola CCJ
400784a65e86034a9bccd8cef91d6214
b2ae061d5cde89fb6088f0ccf497ac8b
AY635573 Nitrosospira sp. REGAU
CP021106 Nitrosospira lacus APG3
NZ CP021106 Nitrosospira lacus APG3
NZ FNKY01000001 Nitrosospira multiformis Nl1
NZ FOBH01000006 Nitrosovibrio tenuis Nv1
CP000103 Nitrosospira multiformis ATCC 25196
NR 074736 Nitrosospira multiformis ATCC 25196
CP012371 Nitrosospira briensis C-128
AJ012107 Nitrosospira sp.
NZ FOVJ01000002 Nitrosospira briensis Nsp8
X90820 Nitrosospira sp.
NZ FMWO01000035 Nitrosomonas mobilis 1
NZ FNOY01000106 Nitrosomonas halophila Nm1
NC 004757 Nitrosomonas europaea ATCC 19718
NC 008344 Nitrosomonas eutropha C91
b04843699bf9b86bbafca6ccd4106db0
0d62fedc554625831ad2037850adc09d
21ef09e5a9dfc2c1c8d968d217f6fb35
47f13d1112e1ae2facf542ec4222943f
AJ298738 Nitrosomonas cryotolerans Nm55
NZ FSRO01000001 Nitrosomonas cryotolerans ATCC 49181
AB212171 Nitrosomonas sp. NS20
NZ CP013341 Nitrosomonas ureae Nm10
NZ FOCP01000019 Nitrosomonas marina Nm22
NZ FOSP01000014 Nitrosomonas aestuarii Nm69
ad6453c271160c3c6728a43a054562d4
AF255602 Nitrospira sp. SRI-237
AF255603 Nitrospira sp. SRI-9
CP001147 Thermodesulfovibrio yellowstonii DSM 11347
NC 011296 Thermodesulfovibrio yellowstonii DSM 11347
NR 040795 Thermodesulfovibrio aggregans TGE-P1
NZ BCNO01000001 Thermodesulfovibrio aggregans TGE-P1
9f94f303579c05490d0e4855ae864adb
9f93e0fc6396c9c2be072f51496d6c59
84a0a2a8fb8eb09cf21026a2b71b1d5a
92f8389fdebedf91fada1d483c4eb7cb
2623148089319a16de678f7a0812e3c0
SMVS01000089 Nitrospina sp. N074bin53 k141 981193
HQ675602 Nitrospina sp. SCGC AAA240-J07
Atlantic Ocean isolate
NZ HG422173 Nitrospina gracilis 3/211
031e6a06e6c028f9c00c5be90c6f7822
2592dc6ab426f6021ce527f8bf4da616
fc8fa1353eb9f6fa8bee915179014c0d
HQ675585 Nitrospina sp. SCGC AAA240-G05
HQ675390 Nitrospina sp. SCGC AAA003-A14
HQ675403 Nitrospina sp. SCGC AAA003-E19
HQ675544 Nitrospina sp. SCGC AAA240-B06
8bea5d95a0bc16a079ffc4da96d3b9b0
ea658e001138e794dda40b6ed936d87e
81b66c2976b3d2b669d053f2da43f11b
18f2510cc993ef3644297a6033d1709f
de0cae8ea3ca8d7c3e16675d2afd2cf0
165e8f96b55fa8570ae13ac6865a5b11
RSAC01000024 Nitrospina sp. ETSP2013-BB2-NOB-2
2198f90dcf10a5bf3101db2354ba8554
4d7d920c47a7469a9cea8a407917262O
HQ675664 Nitrospina sp. SCGC AAA288-C20
HQ675674 Nitrospina sp. SCGC AAA288-E23
65d78fbf3ca2c1a865045a0a59c3a756
2f3a9cd266e4ff7af72b0f53c5207c8a
528455c1603734ccc53c8b59cd2ecec
4f7072440c3015c1091d65179e9a6721
71307034d03b7a1ce4e0a90a580d55ce
c5d7d8bae30ae4f1a855ca2cd147a6b0
HQ675628 Nitrospina sp. SCGC AAA240-N03
HQ675648 Nitrospina sp. SCGC AAA240-O22
HQ675701 Nitrospina sp. SCGC AAA288-L16
HQ675721 Nitrospina sp. SCGC AAA288-O16
HQ675700 Nitrospina sp. SCGC AAA288-L15
HQ675366 Nitrospina sp. SCGC AAA001-C22
HQ675394 Nitrospina sp. SCGC AAA003-C16
HQ675416 Nitrospina sp. SCGC AAA003-G17
HQ675540 Nitrospina sp. SCGC AAA240-A16

Figure B12. Phylogenetic maximum likelihood trees (1000 bootstraps) of bacterial and archaeal ASVs from 16S rRNA amplicon sequencing of the Bedford Basin bottom water community (bold) affiliated by SILVA with known nitrifier taxa. Same as bacterial tree in Figure B2A without any collapsed clades to show the names of all used sequences from Bedford Basin and reference database.

Table B1. Multiple regression analyses with each amoA phylotype quantified by qPCR tested as a dependent variable against independent variables that may predict their presence in Bedford Basin bottom water. Significant parameters ($p<0.01$) are highlighted in bold font.

Dependent:	amoA-A1		amoA-A2		amoA-A3		amoA-A4		amoA-A5		amoA-A6	
	t value	Sign.	t value	Sign.	t value	Sign.	t value	Sign.	t value	Sign.	t value	Sign.
(Intercept)	-0.74	0.46	**-2.66**	**0.01**	**-3.49**	**6E-04**	-0.03	0.97	-0.27	0.79	-2.02	0.04
Temperature [°C]	**4.74**	**4E-06**	2.50	0.01	-1.60	0.11	0.72	0.47	-0.60	0.55	-0.69	0.49
Dissolved O_2 [µmol kg_{sw}^{-1}]	**-3.99**	**1E-04**	**4.31**	**3E-05**	**3.62**	**4E-04**	1.50	0.14	0.45	0.65	**4.91**	**2E-06**
NH_4^+ concentration [µmol kg_{sw}^{-1}]	-1.30	0.19	-1.89	0.06	-2.06	0.04	-0.19	0.85	-0.08	0.94	-2.05	0.04
POC concentration [µmol kg_{sw}^{-1}]	**-3.08**	**2E-03**	**-2.96**	**3E-03**	-1.57	0.12	-0.53	0.60	0.63	0.53	-2.18	0.03
Salinity [PSU]	0.81	0.42	**2.63**	**0.01**	**3.51**	**6E-04**	0.07	0.95	0.27	0.79	2.02	0.04
Multiple R^2	0.48		0.26		0.26		0.03		0.01		0.24	

Table B2. Model equations.

$\frac{dO2}{dt} = -R.remin - 1.5 \times R.AO - 0.5 \times R.ON - R.O2 + \frac{1}{\tau} \times (O2.sw - O2)$
$\frac{dNH4}{dt} = rNC \times R.remin - R.AO + \frac{1}{\tau} \times (NH4.sw - NH4)$
$\frac{dNO2}{dt} = R.AO - R.NO + \frac{1}{\tau} \times (NO2.sw - NO2)$
$\frac{dNO3}{dt} = R.NO - R.Nloss + \frac{1}{\tau} \times (NO3.sw - NO3)$
$\frac{dAmoA}{dt} = R.AO + \frac{1}{\tau} \times (0 - AmoA)$
$\frac{dNxr}{dt} = R.NO + \frac{1}{\tau} \times (0 - Nxr)$

Table B3. Reaction terms used in the numerical box model. Modeled state variables are shown in bold.

$R.remin = k.remin \times (\exp(T) \times \ln(Q10_{remin})/10) \times POC \times \boldsymbol{O2}$
$R.AO = k.AO \times (\exp(T) \times \ln(Q10_{nitr})/10) \times \boldsymbol{AmoA} \times \boldsymbol{NH4} \times \frac{\boldsymbol{O2}}{K_s.O2.AO + \boldsymbol{O2}}$
$R.NO = k.NO \times (\exp(T) \times \ln(Q10_{nitr})/10) \times \boldsymbol{Nxr} \times \boldsymbol{NO2} \times \frac{\boldsymbol{O2}}{K_s.O2.NO + \boldsymbol{O2}}$
$R.Nloss = k.Nloss \times \boldsymbol{NO3}$
$R.O2 = k.sedi.o2 \times \boldsymbol{O2}$

Table B4. Kinetic parameter values used in the numerical box model.

Parameter	Description	Value	Unit	Reference
k.remin	rate constant for N remineralization	0.0002	kg μmol^{-1} d^{-1}	-
k.AO	rate constant for ammonia oxidation	0.0011	kg (gene copies)$^{-1}$ d^{-1}	-
k.NO	rate constant for nitrite oxidation	0.0091	kg (gene copies)$^{-1}$ d^{-1}	-
ks.O2.AO	Half-saturation constant for O_2 in AO	3	$\mu mol\ kg_{SW}^{-1}$	a, b
ks.O2.NO	Half-saturation constant for O_2 in NO	22	$\mu mol\ kg_{SW}^{-1}$	a
k.Nloss	rate constant for N loss (denitrification, assimilation)	0.0014	d^{-1}	-
k.sedi.O2	rate constant for O_2 uptake by sediment/higher organisms	0.0014	d^{-1}	-
rNC	Redfield ratio for nitrogen/carbon	0.15	-	-
$Q10_{remin}$	Q_{10}-type temperature dependence affecting N remineralization	20	-	-
$Q10_{nitr}$	Q_{10}-type temperature dependence affecting ammonia and nitrite oxidation	20	-	-
τ	Residence time	194 (lowered by mixing)	d	c

References: [a]Laanbroek and Gerards (1993); [b]Martens-Habbena et al. (2009); [c]Burt et al. (2013).

Table B5. Results from Spearman's Rho and Kendall's Tau and Pearson's, tests, testing the correlation between oceanographic parameters from the long-term Bedford Basin time series with i) the annual NO_3^-/NH_4^+, and ii) winter mixing proxied by the minimum spiciness during each annual winter mixing period. With the exception of the minimum spiciness during winter mixing, all parameters represent annual means from n tested years between 1994 and 2018. Results from the parametric Pearson's test are given if both tested parameters are normally distributed (Shapiro-Wilk test p>0.05). Bold numbers highlight significance below the 5% level.

	annual (NO_3^-/NH_4^+) ratio (60 m)							Minimum spiciness during winter (60m)						
		Spearman		Kendall		Pearson			Spearman		Kendall		Pearson	
	n	r	p	r	p	r	p	n	r	p	r	p	r	p
Minimum spiciness during winter (60m)	15	**0.53**	**0.041**	0.37	0.173									
Stratification [kg m^{-4}]	17	0.32	0.213	0.22	0.395			17	-0.04	0.874	-0.03	0.911	0.08	0.756
Dissolved O_2 (60 m) [µmol kg_{sw}^{-1}]	17	**-0.59**	**0.012**	-0.41	0.101			17	**-0.52**	**0.034**	-0.37	0.147	**-0.53**	**0.029**
Nitrate (60 m) [µmol kg_{sw}^{-1}]	17	**0.91**	**0.000**	**0.74**	**0.001**			18	**0.57**	**0.014**	0.40	0.101	**0.65**	**0.00**
Phosphate (60 m) [µmol kg_{sw}^{-1}]	17	0.48	0.051	0.34	0.184			18	0.44	0.070	0.32	0.195	SW p<0.05	
Salinity (60 m) [PSU]	17	0.30	0.244	0.18	0.498			19	**0.80**	**0.000**	**0.60**	**0.006**	**0.81**	**0.000**
Silicate (60 m) [µmol kg_{sw}^{-1}]	17	**0.72**	**0.001**	**0.49**	**0.048**			18	**0.49**	**0.038**	0.35	0.159	**0.55**	**0.018**
Temperature (60 m) [°C]	17	0.41	0.103	0.31	0.228			19	0.12	0.637	0.06	0.794	0.17	0.474
Ammonium (60 m) [µmol kg_{sw}^{-1}]	17	**-0.93**	**0.000**	**-0.81**	**0.000**	SW p<0.05		15	-0.44	0.098	-0.30	0.285	**-0.58**	**0.024**
Nitrite (60 m) [µmol kg_{sw}^{-1}]	17	-0.33	0.191	-0.24	0.363			16	-0.47	0.068	-0.35	0.184	SW p<0.05	
DIN (60 m) [µmol kg_{sw}^{-1}]	17	0.05	0.837	0.01	0.955			15	0.24	0.398	0.12	0.660	0.23	0.41
POC (60 m) [µmol kg_{sw}^{-1}]	15	**-0.61**	**0.016**	-0.45	0.094			14	**-0.57**	**0.034**	-0.41	0.149	**-0.63**	**0.015**
PON (60 m) [µmol kg_{sw}^{-1}]	15	-0.21	0.451	-0.14	0.612			14	**-0.53**	**0.049**	-0.41	0.149	**-0.53**	**0.050**
POC (5 m) [µmol kg_{sw}^{-1}]	15	-0.32	0.243	-0.26	0.355			14	-0.11	0.714	-0.08	0.794	-0.21	0.465
PON (5 m) [µmol kg_{sw}^{-1}]	15	-0.29	0.289	-0.24	0.393			14	-0.09	0.771	-0.03	0.911	-0.05	0.875
Chlorophyll *a* (5 m) [µg kg_{sw}^{-1}]	17	-0.27	0.286	-0.21	0.428			18	-0.24	0.341	-0.18	0.484	-0.18	0.484
Sackville River discharge [m^3 s^{-1}]	16	0.24	0.368	0.15	0.579			17	-0.36	0.154	-0.26	0.317	-0.33	0.191

Table B6. Results from a multiple linear regression using weekly standard anomalies for each variable. The multiple R^2 of the regression was 0.25. Significant parameters ($p<0.01$) are highlighted in bold font.

Dependent	Independent	Estimate	Std error	t value	Significance
$NO_3^-/[NO_3^- + NH_4^+]$	(Intercept)	0.04	0.03	1.31	0.191
	dissolved O_2 [µmol kg_{SW}^{-1}]	**-0.33**	**0.03**	**-10.62**	**2.00E-16**
	Temperature [°C]	**0.22**	**0.03**	**7.62**	**7.76E-14**
	POC [µmol kg_{SW}^{-1}]	-0.08	0.03	-2.46	0.014
	Salinity [PSU]	**0.14**	**0.03**	**4.47**	**9.04E-06**

Table B7. Primer sets and dsDNA standards used to quantify archaeal *amoA* phylotypes. Primers and standards are written 5' to 3'. GenBank accession codes for larger reference sequences used to design primers and their standards are provided in parentheses.

Assay	**Forward Primer** **Name**: sequence	**Reverse Primer** **Name**: sequence	**dsDNA Standard** **Name** (reference sequence): nucleotides
amoA-A1	**amoA-A1-F:** GGCGGCGTACTGGTAGGA	**amoA-A1-R:** TGGGTCTGCTACTGTTATCAGGTTTA	**amoA-A1-STD (KJ807556):** TTCGTACACGGTATTTTCAGTATCGCAAACGTTGATGCTAATTGTAGGTGCATGTTATTACTTGACATTTACAGGCGTTCCAGGCACAGCGACGTACTACGCTCTAATTATGACAGTATACACATGGGTAGCAAAAGCCGCATGGTTTTCGCTAGGATATCCATATGACTTCATTGTAACTCCAGTTTGGCTTCCATCAGCAATGCTGTTGGACTTGGTCTACTGGGCGACAAAGAAGAACAAGCACTCCTTGATACTGTTTGGCGGCGTACTGGTAGGAATGTCTTTACCATTATTCAACATGGTAAACCTGATAACAGTAGCAGACCCACTAGAAACGGCATTCAAATA
amoA-A2	**amoA-A2-F:** GCGGAGTCTTAGTTGGAATGTCA	**amoA-A2-R:** GGGTCAGCCACTGTGATCAA	**amoA-A2-STD (KF727168):** ATCGTTTGTAGTATTCTCAATATCTCAAACACTTATGCTCACTGTAGGTGCGTGTTACTATCTCACCTTCACTGGAGTTCCAGGAACCGCAACGTATTATGCACTTATCATGACAGTCTACACTTGGATTGCAAAAGGTGCATGGTTCGCATTAGGTTACCCATATGACTTCATCGTTACACCAGTTTGGCTACCATCAGCAATGCTGTTGGATTTGGCGTACTGGGCAACAAAGAAGAATAAGCACTCTCTGATACTGTTCGGCGGAGTCTTAGTTGGAATGTCATTACCACTATTCAACATGGTCAATTTGATCACAGTGGCTGACCCACTAGAGACTGCATTCAAGTA
amoA-A3	**amoA-A3-F:** TGATGACGGTAGTCGGAGCTG	**amoA-A3-R:** AATACGCGCCTGTACCAGGAA	**amoA-A3-STD (KF727043.1):** ATCATTCGTAGTTTTCTCTATCGCCAACACTTTGATGACGGTAGTCGGAGCTGTGTATTACATTACATTTACGGGTGTTCCTGGTACAGGCGCGTATTACGGCTTAATAATGCAGGTCTATACATGGGTCGCTAAAGTTGCATGGTTTGCACTTGGTTATCCGGTGGATTTCATTGTTCATCCAATGTGGATTCCATCATGCATGTTGTTGGATTTGGCATATTGGGCTACGAAGAAGAATAAGCACTCGCTGATATTCTTTGGAGGAGTTTTGGTCGGTATGTCAATGCCGCTGTTCAATATGGTACAGCTGATGCTGATCGCCGATCCGCTAGAAACTGCATTCAAATA

Assay	Forward Primer **Name**: sequence	Reverse Primer **Name**: sequence	dsDNA Standard **Name** (reference sequence): nucleotides
amoA-A4	**amoA-A4-F:** CCTTGATGACAGTG GTAGGTGCT	**amoA-A4-R:** GCCATAATATGCG CCTGTGC	**amoA-A4-STD (KF727066.1):** ATCATTTGTAGTATTTTCCATAGCTAATACCTTG ATGACAGTGGTAGGTGCTGTTTACTATATCACG TTTACAGGTGTTCCTGGCACAGGCGCATATTAT GGCCTAATTATGCAAGTCTATACTTGGGTTGCT AAAGTTGCATGGTTTGCACTTGGCTATCCTGTG GATTTCATTGTTCATCCAATGTGGATTCCATCTT GTATGCTATTGGACTTGGCGTATTGGGCTACAA AGAAGAATAAGCACTCGCTGATATTCTTTGGTG GAGTTTTGGTTGGTATGTCAATGCCGCTGTTCA ATATGGTACAGTTGATGTTGATCGCCGATCCG CTAGAAACTGCATTCAAGTA
amoA-A5	**amoA-A5-F:** TGACAGTCGTCGGA GCAGTC	**amoA-A5-R:** TTGGCGACCCAAG TATACACC	**amoA-A5-STD (KF727042):** TTCCTTTGTAGTTTTCTCCATTGCCAACACTCTC ATGACAGTCGTCGGAGCAGTCTATTATATCACA TTTACAGGCGTGCCTGGAACAGGCGCATATTA TGGTTTAATTATGCAGGTGTATACTTGGGTCGC CAAAGTGGCATGGTTTGCACTTGGCTATCCTG CAGATTTCATCGTTCATCCAATGTGGATTCCAT CATGCATGTTGTTGGATTTGGCATATTGGGCTA CGAAGAAGAATAAGCACTCGCTGATATTCTTTG GTGGGGTTTTAGTTGGAATGTCAATGCCACTGT TCAATATGGTACAGTTGATGTTGATAGCAGATC CACTAGAAACTGCATTCAAGTA
amoA-A6	**amoA-A6-F:** TTGATGACTATTGTT GGTGCTGTG	**amoA-A6-R:** TCAGACCATAGTA CGTTGCAGTACC	**amoA-A6-STD (KF727089):** ATCATTTGTCGTATTCTCAATTGCCAATACTTTG ATGACTATTGTTGGTGCTGTGTATTATCTTACAT TTACGGGCGTACCTGGTACTGCAACGTACTAT GGTCTGATTATGCAAGTCTATACTTGGGTTGCA AAAGTTGCATGGTTTGCACTTGGCTATCCAGTA GATTTCATCGTTCATCCGATGTGGATTCCATCT TGTATGTTATTGGACTTGGCGTATTGGGCTACG AAGAAGAATAAGCACTCGCTGATATTCTTTGGA GGAGTTTTGGTCGGTATGTCAATGCCGCTGTT CAATATGGTACAGTTGATGTTGATCGCCGATCC GCTAGAAACTGCATTCAAGTA

Table B8. Target specificity of qPCR assays analyzed by cross-reaction test. F/R = Primers, STD = double stranded DNA standard, green = positive amplification. 10^7 copies of each standard were added to each reaction. With the ViiA7 and SYBR chemistry, 10^7 copies of amoA were typically detected after 14 cycles of DNA amplification. Detection at ≥31 cycles would equate to approximately ≤0.01% copies as false positives.

		Approximate Number of Cycles to Detection					
		dsDNA Standard Template					
		A1 STD	A2 STD	A3 STD	A4 STD	A5 STD	A6 STD
Assay / Primer Set	A1 F/R	14	–	–	–	–	–
	A2 F/R	32	14	–	–	–	–
	A3 F/R	–	–	14	36	–	–
	A4 F/R	–	–	35	14	–	–
	A5 F/R	–	–	–	–	16	–
	A6 F/R	34	34	34	36	36	14

Table B9. 16S rRNA gene sequences of OTUs affiliated with *Thaumarchaeota* and *Nitrospina* found in the Gulf of Mexico (Kitzinger et al. 2019, 2020). These sequences are used in Figure B9 and Figure B10, respectively. Raw sequences these OTUs were picked from were deposited by the authors of the original publication at NCBI under Bioproject PRJNA397176 and BioSample numbers SAMN07461114–SAMN07461122.

Thaumarchaeota
>1005844 GoM16-SV-C6C-14_2
AACCAGCACCTCAAGTGGTCAGGATGATTATTGGGCCTAAAGCATCCGTAGCCG GCTCTGTAAGTTTTCGGTTAAATCTGTACGCTCAACGTACAGGCTGCCGGGAATA CTGCAAAGCTAGGGAGTGGGAGAGGTAGACGGTACTCGGTAGGAAGGGGTAAA ATCCTTTGATCTATTGATGACCACCTGTGGCGAAGGCGGTCTACCAGAACACGTC CGACGGTGAGGGATGAAAGCTGGGGGAGCAAACCGG
>1080410 GoM16-SV-CP1-14_8655
AACCAGCACCTCAAGTGGTCAGGAGGATTATTGGGCCTAAAGCATCCGTAGCCG GCTCTGTAAGTTTTCGGTTAAATCTATGCGCTCAACGTATGGGCTGCCGAAAATA CTGTAGAGATAGGGAGTGGGAGAGGTAGACGGTACTCGGTAGGAAGGGGTAAA ATCCTTTGATCTATCGATGACCACCTGTGGCGAAGGCGGTCTACCAGAACACGTT CGACGGTGAGGGATGAAAGCTGGGGGAGCAAACCGG
>152483 GoM16-SV-C6C-16_4155
AACCAGCACCTCAAGTGGTCAGGATGATTATTGGGCCTAAAGCATCCGTAGCCG GCTCTGTAAGTTTTCGGTTAAATCTGTACGCTCAACGTACAGGCTGCCGGGAATA CTGCAAAGCTAGGGAGTGGGAGAGGTAGACGGTACTCGGTAGGAAGGGGTAAA ATCCTTTGATCTATTGATGACCACCTGTGGCGAAGGCGGTCTACCAGAACACGTC CGACGGTGAGGGATGAAAGCTGGGGGAGCAAACCGG
>154353 GoM16-SV-C6C-18_9666
AACCAGCACCTCAAGTGGTCAGGATGATTATTGGGCCTAAAGCATCCGTAGCCG GCGCTATAAGTTTTCGGTTAAATCTGTACGCTCAACGTACAGGCTGCCGGGAATA CTGTAGCGCTAGGGAGTGGGAGAGGTAGACGGTACTCGGTAGGAAGGGGTAAA ATCCTTTGATCTATTGATGACCACCTGTGGCGAAGGCGGTCTACCAGAACACGTC CGACGGTGAGGGATGAAAGCTGGGGGAGCAAACCGG
>155526 GoM16-SV-C6C-16_19095
AACCAGCACCTCAAGTGGTCAGGATGATTATTGGGCCTAAAGCATCCGTAGCCG GCTCTGTAAGTTTTCGGTTAAATCTGTACGCTCAACGTACAGGCTGCCGGGAATA CTGCAGAGCTAGGGAGTGGGAGAGGTAGACGGTACTTGGTAGGAAGGGGTAAA ATCCTTTGATCTATTGATGACCACCTGTGGCGAAGGCGGTCTACCAGAACACGTC CGACGGTGAGGGATGAAAGCTGGGGGAGCAAACCGG
>1692591 GoM16-SV-C6C-16_6014
AACCAACACCTCAAGTGGTCAGGATGATTATTGGGCCTAAAGCATCCGTAGCCG GCTCTGTAAGTTTTCGGTTAAATCTGTACGCTCAACGTACAGGCTGCCGGGAATA CTGCAAAGCTAGGGAGTGGGAGAGGTAGACGGTACTCGGTAGGAAGGGGTAAA ATCCTTTGATCTATTGATGACCACCTGTGGCGAAGGCGGTCTACCAGAACACGTC CGACGGTGAGGGATGAAAGCTGGGGGAGCAAACCGG

Thaumarchaeota
>4369009 GoM16-SV-C6C-16_13339
AACCTGCACCTCAAGTGGTCAGGATGTTTATTGGGCCTAAAGCATCCGTAGCCG GCGCTGTAAGTTTTCGGTTAAATCTGTACGCTCAACGTACAGGCTGCCGGGAATA CTGCAAAGCTAGGGAGTGGGAGAGGTAGACGGTACTCGGTAGGAAGGGGTAAA ATCCTTTGATCTATTGAGGACCACCTGTGGCGAAGGCGGTCTACCAGACCACGT CCGACGGTGAGGGATGAAAGCTGGGGGAGCAAACAGG
>4431375 GoM16-SV-C6C-18_20016
AACCAGCACCTCAAGTGGTCAGGATGATTATTGGGCCTAAAGCATCCGTAGCCT GCTTTGTAAGTTTTCGGTTAAATCTATACGCTCAACGTATGGGCTGCCGGGAATA CTGCAAAGCTAGGGAGTGGGAGAGGTAGACGGTACTCGGTAGGAAGGGGTAAA ATCCTTTGATCTATTGATGACCACCTGTGGCGAAGGCGGTCTACCAGAACACGTC CGACGGTGAGGGATGAAAGCTGGGGGAGCAAACCGG
>540244 GoM16-SV-C6C-18_10551
AACCAGCACCTCAAGTGGTCAGGATGATTATTGGGCCTAAAGCATCCGTAGCCG GCTCTGTAAGTTTTCGGTTAAATCTGTACGCTCAACGTACAGGCTGCTGGGAATA CTGCAGAGCTAGGGAGTGGGAGAGGTAGACGGTACTCGGTAGGAAGGGGTAAA ATCCTTTGATCTATTGATGACCACCTGTGCGAAGGCGGTCTACCAGAACACGTCC GACGGTGAGGGATGAAAGCTGGGGGAGCAAACCGG
>544745 GoM16-SV-I3-14_5715
AACCAGCACCTCAAGTGGTCAGGATGATTATTGGGCCTAAAGCATCCGTAGCCG GCTCTGTAAGTTTTCGGTTAAATCTGTACGCTCAACGTACAGGCTGCCGGGAATA CTGCAGAGCTAGGAGTGGGAGAGGTAGACGGTACTCGGTAGGAAGGGGTAAAA TCCTTTGATCTATTGATGACCACCTGTGGCGAAGGCGGTCTACCAGAACACGTC CGACGGTGAGGGATGAAAGCTGGGGGAGCAAACCGG
>New.CleanUp.ReferenceOTU1886 GoM16-SV-I3-16_8100
AACCAGCACCTCACTTGGTCAGGATGATTATTGGGCCTAAAGCATCCGTCGCCG GCTCTGTAAGTTTTCGGTTAAATCTGTACGCTCAACGTACAGGCTGCCGGGCCTC CGGCAGAGCTAGGGAGTGGGAGAGTTCTACGGTCCTCGGTAGGAAGGGGTAAA ATCCTTTGATCTATTGATGACCACCTGTGGCGAAGGCGGTCTACCAGAACACGTC CGACGGTGAGGGAGGAAAGCTGGGGGAGCCCCCCGG
>New.CleanUp.ReferenceOTU2177 GoM16-SV-CP1-14_13306
AACCAGCACCTCCCGTGGTCAGGATGATTATTGGGCCTAAAGCATCCGTCGCCG GCTCTGTAAGTTTTCGGTTAAATCTGTACGCTCAACGTACAGGCTGCCGGGCATC CGGCAAAGCTAGGGAGTGGGAGAGGTCTCCGGTACTCGGTAGGAAGGGGTAAA ATCCTTTGCTCTATTGATGACCACCTGTGGCGAAGGCGGTCTACCAGAACACGT CCGACGGTGAGGGAGGAAAGCTGGGGGAGCCCCCCGG

Thaumarchaeota
>New.CleanUp.ReferenceOTU2324 GoM16-SV-C6C-18_13526
AACCAGCACCTCAATTGGTCAGGATGATTATTGGGCCTAAAGCATCCGTCGCCG GCTCTGTAAGTTTTCGGTTAAATCTGTACGCTCAACGTACAGGATGCCGGGCATC CGGCAGAGCTAGGGAGTGGGAGAGGTATCCGGTACTCGGTAGGAAGGGGTAAA ATCCTTTGATCTATTGATGACCACCTGTGGCGAAGGCGGTCTACCAGAACACGTC CGACGGTGAGGGAGGAAAGCTGGGGGAGCCACCCTG
>New.CleanUp.ReferenceOTU668 GoM16-SV-CP1-12_18933
AACCAGCACCTCAAGTGGTCAGGATGATTATTGGGCCTAAAGCATCCGTAGCCG GCTCTGTAAGGGGAAGGGAAAATCAGTACGCTCAACGTACAGGCTGCCGGGAAT ACTGCAGAGCCAGGGAGAGGGAGAGGTAGACGGTACTCGGTAGGAAGGGGTAA AATCCTTTGATCTATTGATGACAACCTGTGGCGAAGGCGGTCTACCAGAACACGT CCGACGGTGAGGGATGAAAGCTGGGGGAGCAAACCGG
>New.CleanUp.ReferenceOTU810 GoM16-SV-CP1-10_938
AACCAGCACCTCAAGTGGTCAGGATGATTATTGGGCCTAAAGCATCCGTAGCCG GCTCTGTAAGTTTTCGGTTAAATCTGTACGCTCAACGTACAGGCTGCCGGGAATA CTGCAGAGCTAGGGAGTGGGAGAGGTCGCCGGTGCTCGGTAGCCCCCGGTAAA ATCCTTTGATCTATTGATGACCACCTGTGGCGAAGGCGGTCTACCAGAACACGTC CGACGGTGAGGGATGAAAGCTGGGGGAGCAAACCCG
>244523 GoM16-SV-C6C-14_5016
TACGGAGGGGGCAAGCGTTGTTCGGAATCATTGGGCGTAAAGAGTATGTAGGCG GCTGAATAAGTCAGACGTGTAAGCCCACGGCTCAACCGTGGAATTGCGTTTGAA ACTGTTTAGCTTGAGTGCAGAAGAGGAAAGCGGAATTCCCAGTGTAGCGGTGAA ATGCATTGATATTGGGAAGAACACCGGTGGCGAAGGCGGCTTTCTGGTCTGCTA CTGACGCTGAGATACGAAAGCCAGGGGAGCAAAGGGG
>549675 GoM16-SV-C6C-14_1983
TACGGAGGGGGCAAGCGTTGTTCGGAATCATTGGGCGTAAAGAGTATGTAGGCG GCTATTTAAGTCAGACGTGTAAGCCCACGGCTCAACCGTGGAATTGCGTTTGAAA CTATTTAGCTTGAGTTCGGGAGAGGAAAGCGGAATTCCCAGTGTAGCGGTGAAA TGCATTGATATTGGGAAGAACACCGGTGGCGAAGGCGGCTTTCTGGTCCGATAC TGACGCTGAGATACGAAAGCCAGGGGAGCGAACGGG
Nitrospina
>571236 GoM16-SV-CP1-12_4243
TACGGAGGGGGCAGGCGTTGTTCGGAATCATTGGGCGTAAAGAGTATGTAGGC GGCTATTTAAGTCAGACGTGTAAGCCCACGGCTCAACCGTGGAATTGCGTTTGA AACTATTTAGCTTGAGTTCGGGAGAGGAAAGCGGAATTCCCAGTGTAGCGGTGA AATGCATTGATATTGGGAAGAACACCAGTGGCGAAGGCGGCTTTCTGGTCCGAT ACTGACGCTGAGATACGAAAGCCAGGGGAGCGAACGGG

Nitrospina
>581695 GoM16-SV-C6C-14_5816
TACGGAGGGGGCAAGCGTTGTTCGGAATCATTGGGCGTAAAGAGTATGTAGGCG GCTGGATAAGTCAGACGTGTAAGCCCACGGCTCAACCGTGGAATTGCGTTTGAA ACTGTTTAGCTTGAGTGCAGAAGAGGAAAGCGGAATTCCCAGTGTAGCGGTGAA ATGCATTGATATTGGGAAGAACACCGGTGGCGAAGGCGGCTTTCTGGTCTGCTA CTGACGCTGAGATACGAAAGCCAGGGGAGCAAAGGGG
>727834 GoM16-SV-C6C-14_810
TACGGAGGGGGCAAGCGTTGTTCGGAATTATTGGGCGTAAAGAGTATGTAGGCG GTTAGGTAAGTCAGGCGTGTAAGCCCTCGGCTCAACCGAGGAATTGCGTTTGAA ACTACCTAACTTGAGTACGAAAGAGGAAAGCGGAATTCCCAGTGTAGCGGTGAA ATGCATTGATATTGGGAAGAACATCGGTGGCGAAGGCGGCTTTCTGGTTCGATA CTGACGCTGAGATACGAAAGCCAGGGGAGCAAACGGG
>838006 GoM16-SV-C6C-18_5275
TACGGAGGGGGCAAGCGTTGTTCGGAATTATTGGGCGTAAAGAGTATGTAGGCG GCTGGATAAGTCAGACGTGTAAGCCCACGGCTCAACCGTGGAATTGCGTTTGAA ACTATTCAGCTTGAGTGCAGGAGAGGAAGGCGGAATTCCCAGTGTAGCGGTGAA ATGCATTGATATTGGGAAGAACACCGGTGGCGAAGGCGGCCTTCTGGTCTGTTA CTGACGCTGAGATACGAAAGCCAGGGGAGCAAAGGGG
>936371 GoM16-SV-C6C-14_5612
TACGGAGGGGGCAAGCGTTGTTCGGAATTATTGGGCGTAAAGAGTATGTAGGCG GCTGGATAAGTCAGGTGTGTAAGCCCACGGCTCAACCGTGGAATTGCACTTGAA ACTATTCAGCTTGAGTACAGGAGAGGAAAGCGGAATTCCCAGTGTAGCGGTGAA ATGCATTGATATTGGGAAGAACACCGGTGGCGAAGGCGGCTTTCTGGTCTGTTA CTGACGCTGAGATACGAAAGCCAGGGGAGCAAAGGGG
>New.CleanUp.ReferenceOTU1134 GoM16-SV-CP1-14_15914
TACGGAGGGGGCAAGCGTTGTTCGGAATCATTGGGCGTAAAGAGTATGTAGGCG GCTGGATAAGTCAGACGTGTAAGCCCACGGCTCAACCGTGGAATTGCGTTTGGA ACTGTTTAGCTTGAGTGCAGAAGAGGAAAGCGGAATTCCCAGTGTAGCGGTGAA ATGCATTGATATTGGGAAGAACACCGGTGGCGAAGGCGGCTTTCTGGTCTGCTA CTGACGCTGAGATACGAAAGCCAGGGGAGCAAAGGGC
>New.CleanUp.ReferenceOTU2406 GoM16-SV-C6C-16_960
TACGGAGGGGGCAAGCGTTGTTCGGAATCATTGGGCGTAAAGAGTATGTAGGCG GTTAGATAAGTCAGGTGTGTAAGCCCAGGGCTCAACCTTGGAATTGCACTTGAAA CTGTTTAACTTGAGTTCAGGAGAGGAAAGCGGAATTCCCAGTGTAGCGGTGAAA TGCATTGATATTGGGAAGAACATCGGTGGCGAAGGCGGCTTTCTGGTCTGATAC TGACGCTGAGATACGAAAGCCAGGGGAGCGAACGGG

Nitrospina
>New.CleanUp.ReferenceOTU3068 GoM16-SV-CP1-14_3158
TACGAAGGGGGCAAGCGTTGTTCGGAATCATTGGGCGTAAAGCGTATGTAGGCG GCCGAATAAGTCGGGCGTGCAAGCCCATGGCTCAACCATGGAATTGCGTTTGAA ACTGTTCGGCTTGAGTGCAGGAGAGGAAGGCGGAATTCCCAGTGTAGCGGTGA AATGCGTTGATATTGGGAAGAACACCGGTGGCGAAGGCGGCCTTCTGGCCTGCT ACTGACGCTGAGATACGAAAGCCAGGGGAGCGAACGGG
>New.CleanUp.ReferenceOTU662 GoM16-SV-C6C-16_18431
TACGGAGGGGGCAAGCGTTGTTCGGAATTATTGGGCGTAAAGAGTATGTAGGCG GTTAGGTAAGTCAGGCGTGTAAGCCCTCGGCTCAACCGAGGAATTGCGTTTGAA ACTACCTACCTTGAGTACGAAAGAGGAAAGCGGAATTCCCAGTGTAGCGGTGAA ATGCATTGATATTGGGAAGAACATCGGTGGCGAAGGCGGCTTTCTGGTTCGATA CTGACGCTGAGATACGAAAGCCAGGGGAGCAAACGGG
>New.CleanUp.ReferenceOTU723 GoM16-SV-C6C-18_1601
TACGGAGGGGGCAAGCGTTGTTCGGAATCATTGGGCGTAAAGAGTATGTAGGCG GCTATTTAAGTCAGACGTGTAAGCCCACGGCTCAACCGTGGAATTGCGTTTGAAA CTATTTAGCTTGAGTTCGGGAGAGGAAAGCGGAATTCCCAGTGTAGCGGTGAAA TGCATTGATATTGGGAAGAACACCAGTGGCGAAGGCGGCTTTCTGGTCCGATAC TGACGCTGAGATACGAAAGCCAGGGTAGCGAACGGG
>New.CleanUp.ReferenceOTU748 GoM16-SV-C6C-14_9025
TACGAAGGGGGCAAGCGTTGTTCGGAATCATTGGGCGTAAAGCGTATGTAGGCG GCTAGATAAGTCGGGCGTGCAAGCCCGCGGCTCAACCGCGGAATTGCGCTCGA AACTGTCTGGCTTGAGTGCAAGAGAGGGAAGCGGAATTCCCAGTGTAGCGGTGA AATGCGTTGATATTGGGAAGAACACCAGTGGCGAAGGCGGCTTTCTGGCTTGCA ACTGACGCTGAGATACGAAAGCCAGGGGAGCGAACGGG

APPENDIX C: SUPPORTING INFORMATION TO CHAPTER 4

POST-ANALYSIS CORRECTIONS AND ADJUSTMENT OF THE ERROR MARGIN AROUND $\delta^{15}N_{NO3}$ VALUES

A decrease in accuracy of $\delta^{15}N_{NO3}$ with decreasing nitrate concentrations was observed for *in-house* standards (Figure C1). We corrected for this by increasing the error margin around each $\delta^{15}N_{NO3}$ datapoint based on the nitrate concentration of a given sample. For this, we first quantified the relationship between initial nitrate concentration of a given sample and the deviation from the accurate $\delta^{15}N$ value based on *in-house* data obtained over many different batches of analysis (Figure C1). The average value (-5.04‰) of $\delta^{15}N_{NO3}$ *in-house* standards, which was determined over many mass-spectrometer runs with standards run at 20 µM, was taken as the accurate $\delta^{15}N_{NO3}$ value. Available *in-house* standard $\delta^{15}N_{NO3}$ values measured at initial concentrations from 1 to 20 µM (Figure C1) were binned on the basis of their initial nitrate concentrations into 10 bins between 1 and 20 µM. Next, a Wilcoxon Signed Ranks test was used to identify bins significantly different from the 20-µM bin. Most bins <5 µM, but no bin >5uM fell below the 10% significance level suggestive of a significant difference to the 20-µM bin. We therefore applied an adjustment of the error margin around $\delta^{15}N$ values only for samples with nitrate concentrations ≤ 5 µM.

The adjustment of the error margin was based on the regression line fitted through available $\delta^{15}N$ values of *in-house* standards with different nitrate concentrations (Figure C1). If a sample had a nitrate concentration ≤5 µM, the $\delta^{15}N$ offset between the sample's nitrate concentration and the $\delta^{15}N$ at 20 µM nitrate was calculated using the equation of the regression line. This offset was then added to the error margin. In all cases, the other error margin component was the precision of analysis, instantiated as the standard deviation between duplicates of a given sample.

OVERVIEW OF IMPROVEMENTS MADE TO STABLE ISOTOPE METHODS THROUGHOUT THE BEDFORD BASIN TIME SERIES 2014–2017

Throughout the duration of the time series (2014–2017), improvements and additions were made to the previously published methodology for chemical conversion of nitrate and nitrite (McIlvin and Altabet 2005; Ryabenko et al. 2009) to N_2O for stable isotope analysis. These methodological adjustments are summarized below for each compound.

For nitrate, there were variations in the approach with which nitrate concentrations of samples were adjusted to those of standards prior to the cadmium reduction step. Samples were either i) adjusted to the concentration of calibration standards, or ii) run with standards at 20 μM despite a nitrate concentration of <20 μM in the standards. Samples run with approach i) warranted no further corrections (Figure C3), while for samples run with approach ii), we increased the margin of error around samples with low nitrate concentrations as described above. For future analyses, we recommend the adjustment of nitrate concentrations in calibration standards and samples (approach i) for optimal, concentration-independent accuracy (Figure C3).

Additionally, we determined that using 1M NaCl solution instead of deionized water for sample dilution before the azide reduction step resulted in an improved calibration slope (closer to 1.0) for $\delta^{18}O$, while not affecting $\delta^{15}N$ values (Figure C2). This approach was suggested by Dr. Mark A. Altabet (personal communication). It was implemented for BB time series samples from August 10th, 2016, and after.

For nitrite, a methodological change was instantiated as of August 2016, which allowed to preserve (Casciotti et al. 2007) and measure the $\delta^{18}O$ signature in nitrite. For this purpose, samples were alkalinized to pH13 using 6 M NaOH after sampling and prior to frozen storage. Additionally, sample dilution to achieve uniform nitrite concentration was performed with 1 M NaCl solution instead of deionized water, as discussed for nitrate above. To properly adjust the pH during the azide reaction, the recipe for the azide-acetic acid mixture was modified to allow for a higher concentration of acetic acid in the reagent (following suggestions by M. Altabet; personal communication). For calibration, three new nitrite isotope standards were created from commercial $NaNO_2$ salts as well as from a pre-existing calibration standard (MAA1; Bourbonnais *et al.*, 2017). The $\delta^{15}N$ and $\delta^{18}O$ of these

salts was altered by adding commercially available ^{15}N-enriched $NaNO_2$ salts and ^{18}O-enriched H_2O (10% $H_2{}^{18}O$), respectively. The newly created nitrite isotope standards were calibrated against the standards WILIS10, WILIS11, WILIS20 (Buchwald et al. 2016) and the determined isotope values are summarized in Table C1.

DOCUMENTING THE LINEARITY OF THE DIN STABLE ISOTOPE METHODS

Linearity corrections for isotope methods for the determination of the $\delta^{15}N$ and $\delta^{18}O$ in nitrate, nitrite and ammonium were usually made using the linearity of the N_2O reference gas on the mass spectrometer. For this, the N_2O reference gas linearity was determined prior to each mass spectrometer run, by taking a $\delta^{15}N$ and $\delta^{18}O$ sample at different reference gas pressures over a range corresponding to the expected peak heights of the standards and samples about to be measured. Using linear or polynomial regressions in the N_2O reference gas linearity, the $\delta^{15}N$ and $\delta^{18}O$ of each sample deviating from the average peak height of the corresponding standards could then be corrected according to the degree of its deviation.

For samples for which no reference gas linearity test was available (samples from the year 2014 as well as January-May 2015), any linearity effects either remained uncorrected for (ammonium until April 29th, 2015; nitrate until May 20th, 2015), or were corrected (nitrite until April 1st, 2015) via *in-house* standards of varying nitrite concentrations run in parallel. To ensure data quality for samples that could not be linearity-corrected in any way, samples <75% of standard size in the resulting N_2O amplitude were not reported (ammonium, nitrate).

Long-term linearity effects Linearity effects were small in the isotope methods for nitrite and ammonium after instrument linearity corrections. This was shown by a compilation of $\delta^{15}N$ values of *in-house* standards at different initial ammonium and nitrite concentrations, respectively, measured with standards at 20 µM, which showed no significant slope in the linear regression, respectively (Figure C4, Figure C5). For nitrate, however, it proved crucial that sample concentration be adjusted to standard concentration prior to the cadmium reduction step (Figure C3). If this was not done, linearity effects that could not

be corrected for by instrument linearity (Figure C1) and necessitated an increased margin of error as described above.

AMMONIUM ASSIMILATION CORRECTION

The steady increase of $\delta^{15}N_{PON}$ observed in fall 2014, which we have attributed to assimilation of the increasingly ^{15}N-enriched ammonium (see 4.5.1), was associated with only a minor increase (<1 μmol kg^{-1}) in PON (Figure 4.4C). This PON increase was an order of magnitude smaller than the simultaneous increase of nitrate due to nitrification (13.9 μmol kg^{-1} overall, 7.5 μmol kg^{-1} during the "Rayleigh closed-system period").

Despite this indication that the effect of ammonium assimilation was likely to be small, we corrected for its influence on the isotopic enrichment factor for AO ($^{15}\varepsilon_{AO}$). In a first step, the estimated amount of PON that was added by ammonium assimilation at each weekly time point *t* was subtracted from the ammonium pool:

$$NH_4^+{}_{AO}(t) = NH4(t) + (PON(t) - PON(t\text{-}1)) \qquad \text{C.1}$$

with PON(t-1) representing the PON concentration in the previous week. However, this correction was only applied for weeks at which PON(t) > PON(t-1); otherwise: NH_4^+-AO(t) = NH_4^+(t). We also estimated a $\delta^{15}N_{NH4}AO$ for each weekly time point during this period, which equaled $\delta^{15}N_{NH4}$ if $\delta^{15}N_{PON}(t) \leq \delta^{15}N_{PON}(t\text{-}1)$, but was calculated as follows for time points at which $\delta^{15}N_{PON}(t) > \delta^{15}N_{PON}(t\text{-}1)$:

$$\delta^{15}N_{ammonium}AO(t) = \left(\left(\frac{\left({}^{15}NH_4^+(t) - (PO^{15}N(t) - PO^{15}N(t-1)) \right)}{{}^{14}NH_4^+(t) - (PO^{14}N(t) - PO^{14}N(t-1))} \right) - 1 \right) \times 1000 \qquad \text{C.2}$$

with 0.0036765 representing the atom percentage of ^{15}N in air-N_2, and with $^{15}NH_4^+$, $^{14}NH_4^+$, $PO^{15}N$ and $PO^{14}N$ representing concentrations [μmol kg^{-1}] of the light and heavy stable isotope in ammonium and PON, respectively, which were derived from each compound's $\delta^{15}N$ and concentration values at a given time point *t*. Assuming that all of the increase in PON during that period is due to ammonium assimilation, any effect of ammonium

assimilation on the ammonium pool and on $\delta^{15}N_{NH4}$ is thus removed in the inferred parameters $NH_4^+{}_{AO}$ and $\delta^{15}N_{NH4}AO$, respectively, so that changes in these parameters should solely reflect AO. If $\delta^{15}N_{NH4}AO$ is substituted for $\delta^{15}N_{NH4}$ in the Rayleigh model and $NH_4^+{}_{AO}$ is used to calculate $f(NH_4^+)$, the slope of the ammonium curve becomes 21.8 ±2.2‰ (Figure 4.6B; Table 4.1). This represents a corrected, accurate $^{15}\varepsilon_{AO}$ which is statistically indistinguishable from $^{15}\varepsilon_{AU}$ which reflects the combined effects of AO and ammonium assimilation (Figure 4.6A; Table 4.1). In the absence of $\delta^{15}N_{PON}$ data for 2017, this negligible difference observed for the 2014 data was assumed to hold similarly during the Rayleigh closed-system period of 2017 so that we assume that the $^{15}\varepsilon_{AU}$ determined for that year (24.1 ±1.1‰; Figure 4.6C) is similarly close to the $^{15}\varepsilon_{AO}$.

NEGLIGIBLE OR SMALL INFLUENCE OF N_2O PRODUCTION AND THE NH_4^+/NH_3 EQILIBRIUM ISOTOPE EFFECT ON $^{15}\varepsilon_{AO}$

The equilibrium isotope effect ($\varepsilon_{eq\text{-}amm}$ = -21‰) between NH_4^+ and NH_3 is another potential source of inaccuracy in estimating $^{15}\varepsilon_{AO}$ (Bigeleisen 1965; Hermes et al. 1985; Casciotti et al. 2003). However, as in laboratory-based studies (Casciotti et al. 2010a), this effect is subsumed under the reported $^{15}\varepsilon_{AO}$, because $\delta^{15}N$ of total ammonium (NH_3+NH_4^+) is measured by standard methods, including the method employed here (high pH during bromate oxidation turns all ammonium into NH_3; Zhang *et al.*, 2007).

Finally, N_2O production during nitrification (Santoro et al. 2011; Wenk et al. 2016) might impact the Rayleigh fits. N_2O concentrations in BB bottom water increased steadily as nitrification proceeded, however, peak concentrations did not exceed 26 nmol kg^{-1} (unpublished data for 2014 and 2017; see also Punshon and Moore, 2004), which is negligible compared to the ~1000× higher ammonium and nitrate concentrations. We conclude that the influence of N_2O production and the NH_4^+/NH_3 equilibrium isotope effect on the $^{15}\varepsilon_{AO}$ determined during the "Rayleigh closed-system periods" was likely negligible.

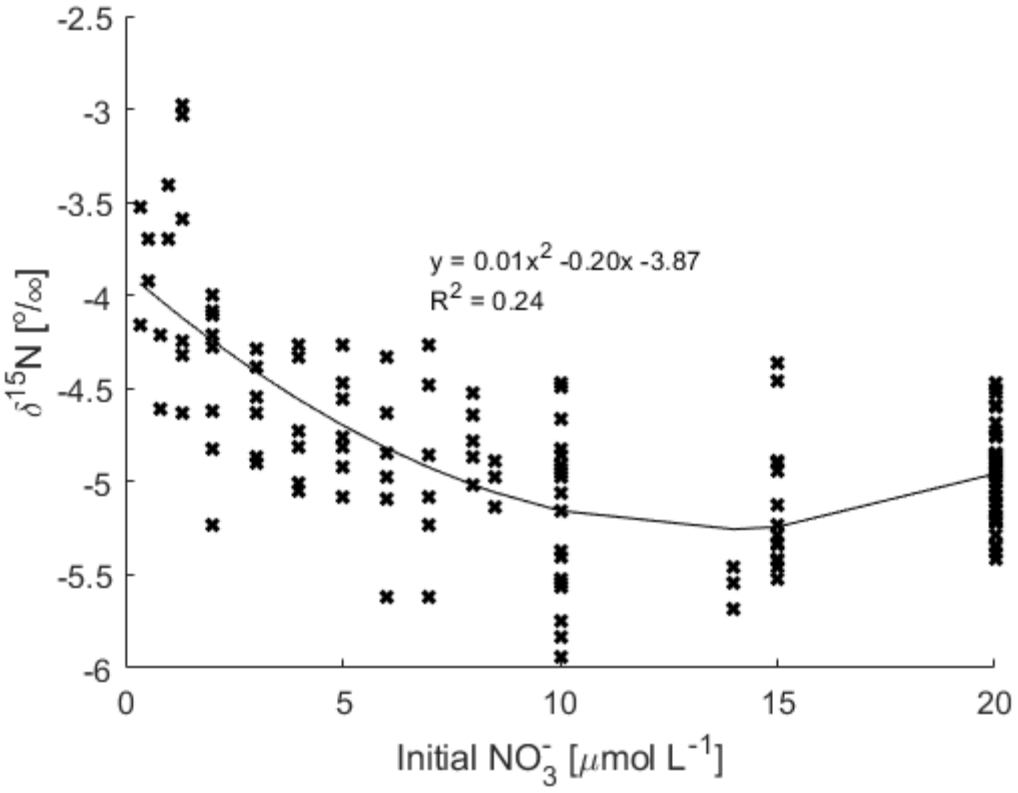

Figure C1. The $\delta^{15}N_{NO3}$ of *in-house* standards as a function of initial nitrate concentration before cadmium and azide reduction when measured with standards of 20 µM initial nitrate concentration.

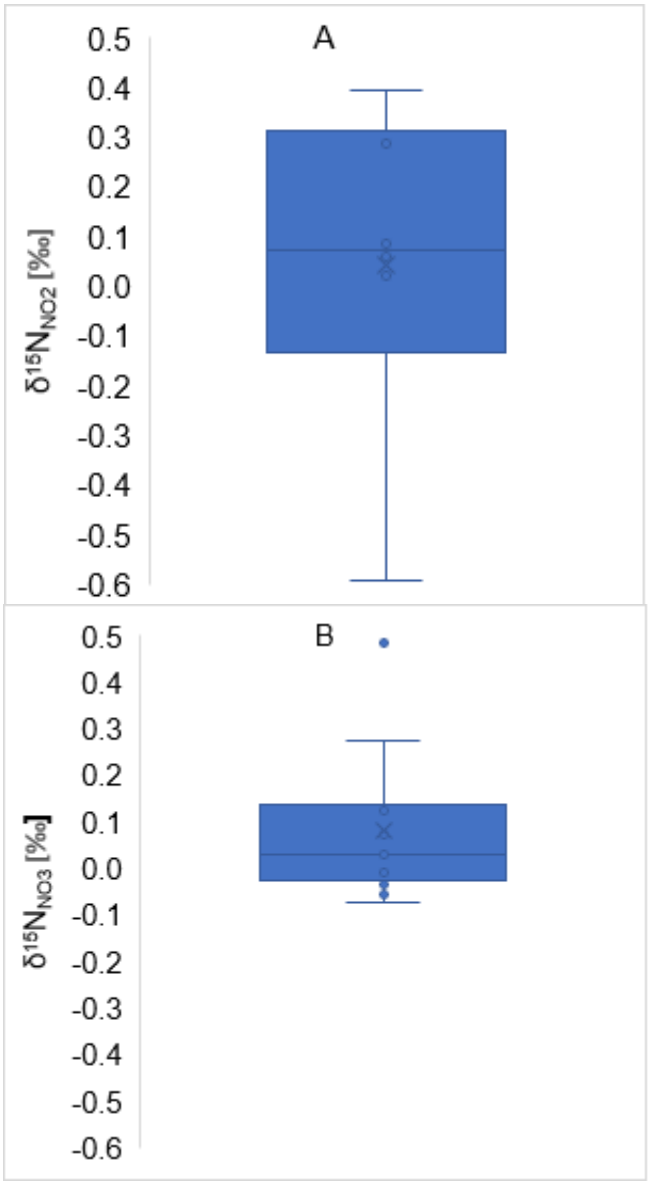

Figure C2. Range of differences in $\delta^{15}N$ measured if samples were diluted with deionized water compared to dilution with 1 M NaCl solution prior to azide reduction, for A) $\delta^{15}N_{NO2}$ (n = 6), and B) $\delta^{15}N_{NO3}$ (n = 12).

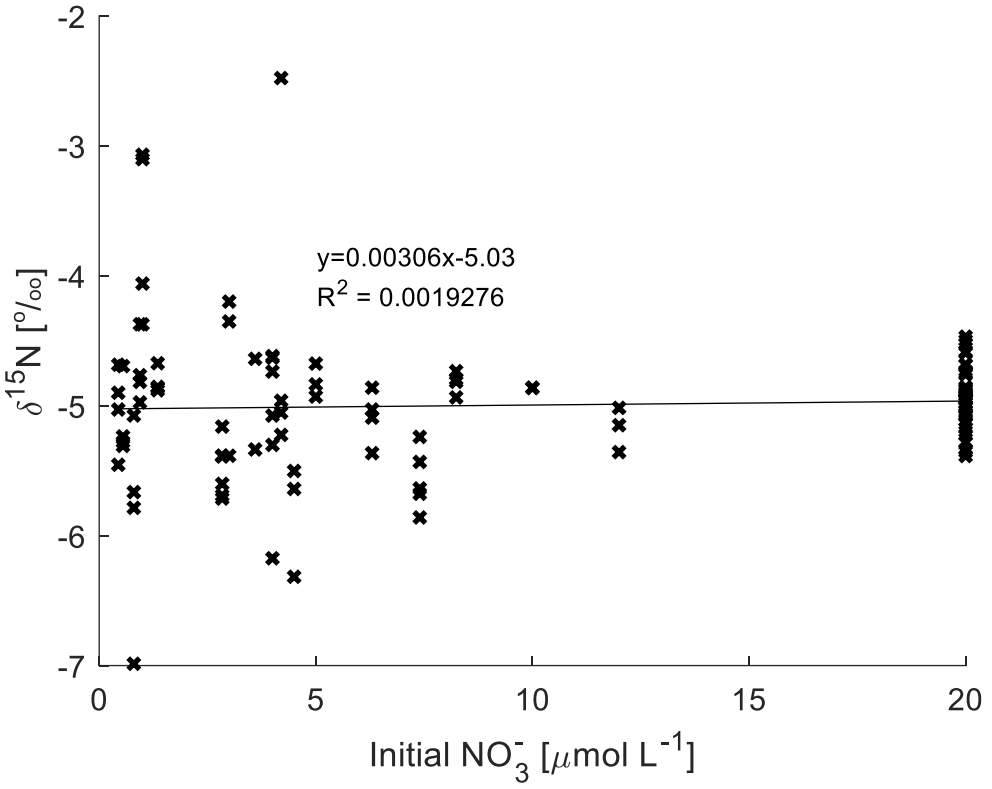

Figure C3. The concentration-dependence $\delta^{15}N_{NO3}$ in our *in-house* standard as a function of initial nitrate concentration before cadmium and azide reduction if measured with calibration standards adjusted to nitrate concentration of the *in-house* standard.

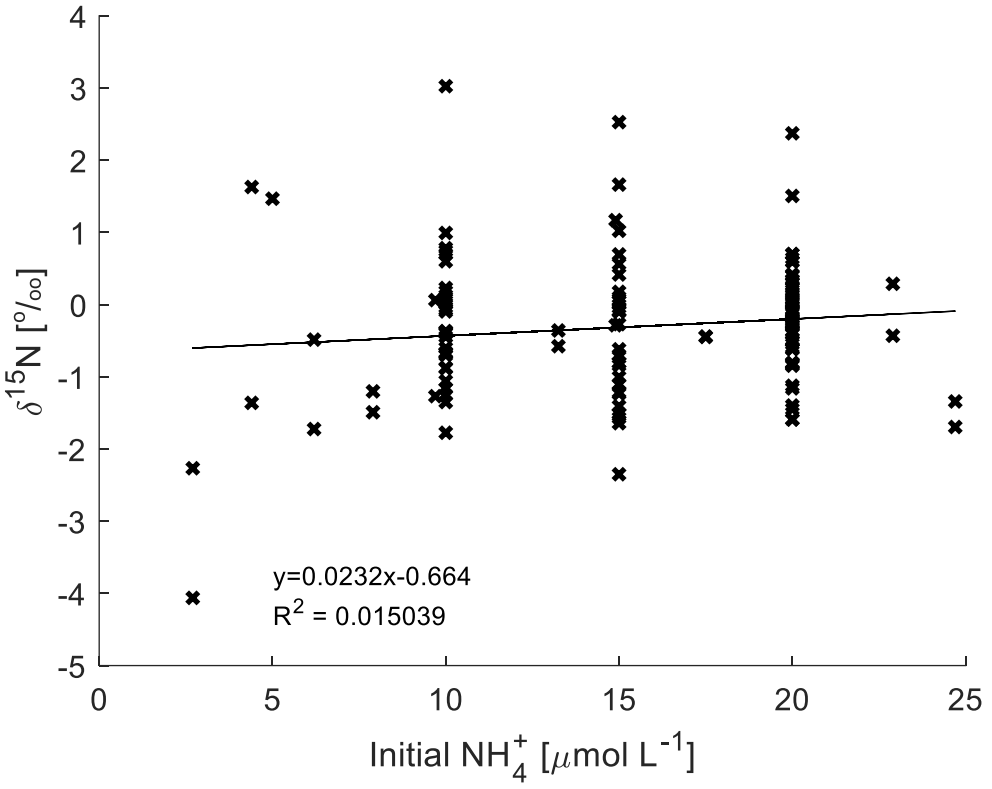

Figure C4. The $\delta^{15}N_{NH4}$ of *in-house* standards analyzed with calibration standards at 20 µM as a function of initial ammonium concentration in the *in-house* standards.

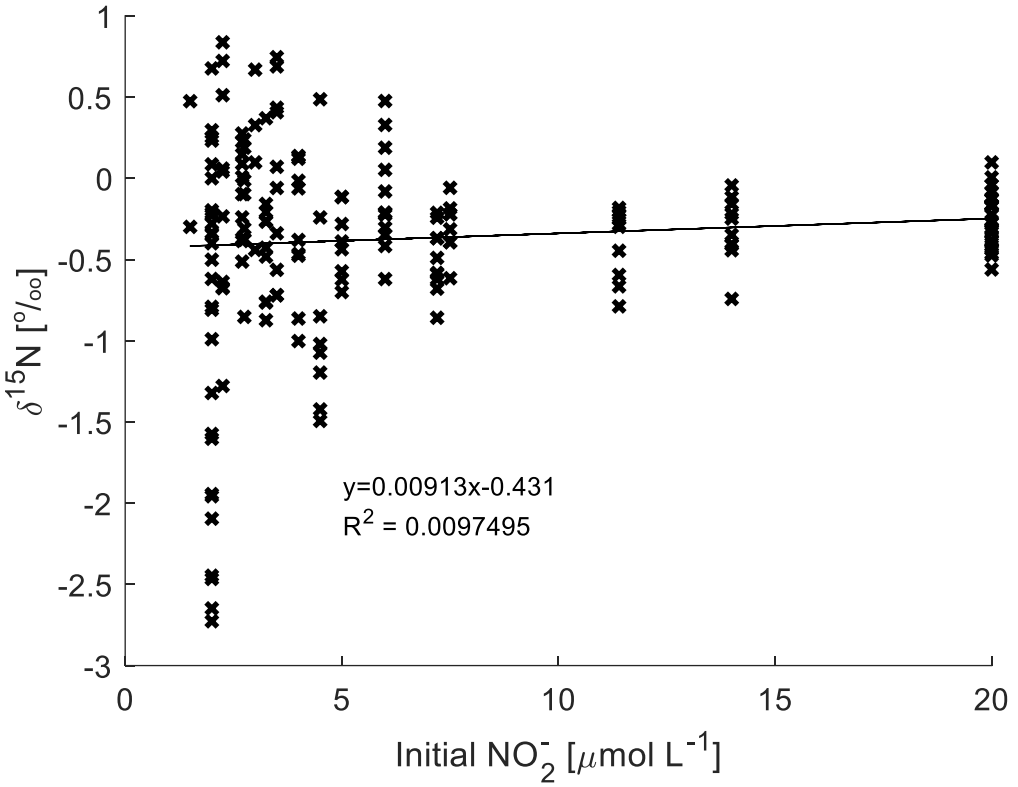

Figure C5. The $\delta^{15}N_{NO2}$ of *in-house* standards analyzed with calibration standards at 20 µM as a function of initial nitrite concentration in the *in-house* standards.

Table C1. Isotopic composition ($\delta^{15}N$, $\delta^{18}O$) of $NaNO_2$ salts calibrated for isotope standardization, including standard deviation (SD).

	$\delta^{15}N$	SD($\delta^{15}N$)	$\delta^{18}O$	SD($\delta^{18}O$)
SHA1	17.51	0.21	35.90	0.08
SHA2	118.88	0.07	46.14	0.10
MAA1_NEW	-59.18	0.32	19.72	0.09

Table C2. Model equations. Sw = surface water.

$\frac{dNH4}{dt} = rNC \times R.remin - R.AO + k.mix(t) \times (NH4.sw - NH4)$
$\frac{dN15H4}{dt} = rNC \times R.remin \times a.PON.d15N.60m - R.AO + k.mix(t) \times (N15H4.sw - N15H4)$
$\frac{dNO2}{dt} = R.AO - R.NO + k.mix(t) \times (NO2.sw - NO2)$
$\frac{dN15O2}{dt} = R.AO.15 - R.NO.15 + k.mix(t) \times (N15O2.sw - N15O2)$
$\frac{dNO3}{dt} = R.NO - R.Nloss + k.mix(t) \times (NO3.sw - NO3)$
$\frac{dN15O3}{dt} = R.NO.15 - R.Nloss.15 + k.mix(t) \times (N15O3.sw - N15O3)$
$\frac{dAmoA}{dt} = (R.AO + R.AO.15) + k.mix(t) \times (0 - amoA)$
$\frac{dNxr}{dt} = (R.NO + R.NO.15) + k.mix(t) \times (0 - Nxr)$

Table C3. Model reactions. Modelled state variables shown in bold.

$R.remin = k.remin \times (\exp(T) \times \ln(Q10_{remin})/10) \times POC \times O2$
$R.AO = k.AO \times (\exp(T) \times \ln(Q10_{nitr})/10) \times \boldsymbol{AmoA} \times \boldsymbol{NH4} \times \frac{O2}{K_s.O2.AO + O2}$
$R.AO.15 = \frac{k.AO}{\alpha.AO} \times (\exp(T) \times \ln(Q10_{nitr})/10) \times \boldsymbol{AmoA} \times \boldsymbol{N15H4} \times \frac{O2}{K_s.O2.AO + O2}$
$R.NO = k.NO \times (\exp(T) \times \ln(Q10_{nitr})/10) \times \boldsymbol{Nxr} \times \frac{\boldsymbol{NO2}}{K_s.NO + \boldsymbol{NO2}} \times \frac{O2}{K_s.O2.NO + O2}$
$R.NO.15 = \frac{k.NO}{\alpha.NO} \times \left(\exp(T) \times \frac{\ln(Q10_{nitr})}{10}\right) \times \boldsymbol{Nxr} \times \frac{15NO2}{NO2} \times \frac{\boldsymbol{NO2}}{K_s.NO + \boldsymbol{NO2}} \times \frac{O2}{K_s.O2.NO + O2}$
$R.Nloss = k.Nloss \times \boldsymbol{NO3}$
$R.Nloss.15 = \frac{k.Nloss}{\alpha.Nloss} \times \boldsymbol{N15O3}$

Table C4. Model parameters

Parameter	Description	2014	2017	Unit	Ref.
τ	Residence time	193.9 (lowered by mixing)	193.9 (lowered by mixing)	Days	a
k.remin	rate constant for remineralization	0.00014	0.00016	kg_{sw} μmol^{-1} day^{-1}	
k.AO	rate constant for ammonia oxidation (AO)	0.00143	0.00114	kg_{sw} (gene copies)$^{-1}$ day^{-1}	
k.NO	rate constant for nitrite oxidation (NO)	0.03857	0.03857	kg_{sw} (gene copies)$^{-1}$ day^{-1}	
ks.NO	Half saturation constant for NO	0.8	0.8	$\mu mol\ kg_{sw}^{-1}$	
ε.AO	Enrichment factor for ammonia oxidation	21.4	26.0	‰	
ε.NO	Enrichment factor for nitrite oxidation	-0.4	-4.6, -11.1	‰	
ε.Nloss	Enrich. fac. for denitrification (not considered)	0	0	‰	
k.Nloss	rate constant for N loss (denitrification, assimilation)	0.0014	0.0014	day^{-1}	
a.PON.d15N	Abundance of ^{15}N in PON calculated from $\delta^{15}N_{PON}$	Empirical (dynamic)	Empirical (dynamic)	μmol^{-1} kg^{-1}	
ks.O2.AO	Half-saturation constant for O_2 in AO	3	3		b,c, d
ks.O2.NO	Half-saturation constant for O_2 in NO	22	22	$\mu mol\ kg_{sw}^{-1}$	b
rNC	Redfield ratio for nitrogen/carbon	0.15	0.15	-	
$Q10_{remin}$	Q_{10}-type temperature dependence affecting remineralization	20	20	-	
$Q10_{nitr}$	Q_{10}-type temperature dependence affecting AO and NO.	20	20	-	

References: [a]Burt et al. (2013); [b]Laanbroek and Gerards (1993); [c]Martens-Habbena et al. (2009); [d]Qin et al. (2017).

APPENDIX D: DATA DEPOSITION

All data produced in the context of my doctoral research, including data not presented in this thesis, has been deposited on the Scholars Portal Dataverse platform and can be accessed under the following DOI: https://doi.org/10.5683/SP2/0QQOX9. It contains a description of the deposited data (file: Appendix_D_data_deposition_description.docx) as well as files containing data and protocols.

APPENDIX E: COPYRIGHT AGREEMENTS

JOHN WILEY AND SONS LICENSE
TERMS AND CONDITIONS

Aug 14, 2020

This Agreement between Dalhousie University -- Sebastian Haas ("You") and John Wiley and Sons ("John Wiley and Sons") consists of your license details and the terms and conditions provided by John Wiley and Sons and Copyright Clearance Center.

License Number	4887820040801
License date	Aug 14, 2020
Licensed Content Publisher	John Wiley and Sons
Licensed Content Publication	Environmental Microbiology
Licensed Content Title	Geomicrobiology of the carbon, nitrogen and sulphur cycles in Powell Lake: a permanently stratified water column containing ancient seawater
Licensed Content Author	Sebastian Haas, Dhwani K. Desai, Julie LaRoche, et al
Licensed Content Date	Aug 5, 2019
Licensed Content Volume	21
Licensed Content Issue	10

Licensed Content Pages	26
Type of use	Dissertation/Thesis
Requestor type	Author of this Wiley article
Format	Electronic
Portion	Full article
Will you be translating?	No
Title	BIOGEOCHEMICAL NITROGEN TRANSFORMATIONS UNDER CONTRASTING MIXING REGIMES IN TWO COASTAL WATER COLUMNS
Institution name	Dalhousie University
Expected presentation date	Oct 2020
Order reference number	1112
Requestor Location	Dalhousie University 1355 Oxford Street, PO BOX 15000 Halifax, NS B3H 4R2 Canada Attn: Dalhousie University
Publisher Tax ID	EU826007151
Total	0.00 CAD

TERMS AND CONDITIONS

- The Wiley Materials and all of the intellectual property rights therein shall at all times remain the exclusive property of John Wiley & Sons Inc, the Wiley Companies, or their respective licensors, and your interest therein is only that of having possession of and the right to reproduce the Wiley Materials pursuant to Section 2 herein during the continuance of this Agreement. You agree that you own no right, title or interest in or to the Wiley Materials or any of the intellectual property rights therein. You shall have no rights hereunder other than the license as provided for above in Section 2. No right, license or interest to any trademark, trade name, service mark or other branding ("Marks") of WILEY or its licensors is granted hereunder, and you agree that you shall not assert any such right, license or interest with respect thereto

- NEITHER WILEY NOR ITS LICENSORS MAKES ANY WARRANTY OR REPRESENTATION OF ANY KIND TO YOU OR ANY THIRD PARTY, EXPRESS, IMPLIED OR STATUTORY, WITH RESPECT TO THE MATERIALS OR THE ACCURACY OF ANY INFORMATION CONTAINED IN THE MATERIALS, INCLUDING, WITHOUT LIMITATION, ANY IMPLIED WARRANTY OF MERCHANTABILITY, ACCURACY, SATISFACTORY QUALITY, FITNESS FOR A PARTICULAR PURPOSE, USABILITY, INTEGRATION OR NON-INFRINGEMENT AND ALL SUCH WARRANTIES ARE HEREBY EXCLUDED BY WILEY AND ITS LICENSORS AND WAIVED BY YOU.

- WILEY shall have the right to terminate this Agreement immediately upon breach of this Agreement by you.

- You shall indemnify, defend and hold harmless WILEY, its Licensors and their respective directors, officers, agents and employees, from and against any actual or threatened claims, demands, causes of action or proceedings arising from any breach of this Agreement by you.

- IN NO EVENT SHALL WILEY OR ITS LICENSORS BE LIABLE TO YOU OR ANY OTHER PARTY OR ANY OTHER PERSON OR ENTITY FOR ANY SPECIAL, CONSEQUENTIAL, INCIDENTAL, INDIRECT, EXEMPLARY OR PUNITIVE DAMAGES, HOWEVER CAUSED, ARISING OUT OF OR IN CONNECTION WITH THE DOWNLOADING, PROVISIONING, VIEWING OR USE OF THE MATERIALS REGARDLESS OF THE FORM OF ACTION, WHETHER FOR BREACH OF CONTRACT, BREACH OF WARRANTY, TORT, NEGLIGENCE, INFRINGEMENT OR OTHERWISE (INCLUDING, WITHOUT LIMITATION, DAMAGES BASED ON LOSS OF PROFITS, DATA, FILES, USE, BUSINESS OPPORTUNITY OR CLAIMS OF THIRD PARTIES), AND WHETHER OR NOT THE PARTY HAS BEEN ADVISED OF THE POSSIBILITY OF SUCH DAMAGES. THIS LIMITATION SHALL APPLY NOTWITHSTANDING ANY FAILURE OF ESSENTIAL PURPOSE OF ANY LIMITED REMEDY PROVIDED HEREIN.

- Should any provision of this Agreement be held by a court of competent jurisdiction to be illegal, invalid, or unenforceable, that provision shall be deemed amended to achieve as nearly as possible the same economic effect as the original provision, and the legality, validity and enforceability of the remaining provisions of this Agreement shall not be affected or impaired thereby.

Screenshot from https://www.pnas.org/page/authors/licenses , taken on 12/08/2020:

Default License for PNAS Articles

Except, as noted above, for open access articles submitted beginning September 2017, authors retain copyright, but grant to PNAS an exclusive License to Publish. Authors and their employing institution or company retain extensive rights for use of their materials after publication in PNAS and for intellectual property. These rights are retained without requiring explicit permission from PNAS, provided the full journal reference is cited and, for articles published in 90–105 (1993–2008), "Copyright (copyright year) National Academy of Sciences." Users may view, reproduce, or store journal content, provided that the information is only for their personal, noncommercial use.

Anyone may, without requesting permission, use original figures or tables published in PNAS for noncommercial and educational use (i.e., in a review article, in a book that is not for sale), provided that the full journal reference is cited and, for articles published in volumes 90–105 (1993–2008), "Copyright (copyright year) National Academy of Sciences." Commercial reuse of figures and tables (i.e., in promotional materials, in a textbook for sale) requires permission from PNAS.

Authors retain the following rights under the PNAS default license:

- The right to post the manuscript on preprint servers such as arXiv or bioRxiv, as long as authors retain distribution rights to the work, that PNAS-formatted files (HTML and PDF) are not used, and that a link to the article in PNAS is included.
- The right to archive a postprint (accepted manuscript) on personal web pages.
- The right to archive a postprint (accepted manuscript) in their funding body's archive or designated noncommercial institutional repository upon publication in PNAS, provided that a link to the article in PNAS is included, and the right to request public access 6 months after publication (unless the PNAS open access option was chosen).
- The right to post the PNAS-formatted PDF of their article on their personal website 6 months after publication, or immediately on publication if the PNAS open access option was chosen. A link to the article in PNAS must be included.
- The right to make electronic or hard copies of articles for their personal use, including classroom use, or for the personal use of colleagues, provided those copies are not for sale and are not distributed in a systematic way outside of their employing institution.
- Authors must retain copyright of the work. The PNAS News Office asks that authors refrain from posting accepted manuscripts on publicly accessible preprint servers until after the media embargo has expired.
- The right to use all or part of their article in a compilation of their own works, such as collected writings or lecture notes.
- If the article is a "work for hire" made within the scope of the author's employment, the employer may use all or part of the information in the article for intracompany use.
- The right to include the article in the author's thesis or dissertation.
- The right to publish a new or extended version of the article provided that it is sufficiently different to be considered a new work.
- The right to expand the article into book-length form for publication.
- The right to permit others to use the original figures or tables published in PNAS for noncommercial and educational use (i.e., in a review article, in a book that is not for sale), provided that the full journal reference is cited and, for articles published in volumes 90–105 (1993–2008), "Copyright (copyright year) National Academy of Sciences."
- The right to reuse the original figures and tables in future works.
- Patent and trademark rights or rights to any process or procedure described in the article.
- The right to present all or part of the paper at a meeting or conference, including ones that are webcast, and to give copies of the paper to meeting attendees before or after publication in PNAS. For interactions with the media prior to publication, see the PNAS Embargo Policy.

For other uses by authors, please contact PNASpermissions@nas.edu.

License to publish:

PNAS License to Publish

1. In consideration of publication of the WORK (including but not limited to figures, tables, artwork, abstracts, cover images, or summaries submitted with the WORK) in the *Proceedings of the National Academy of Sciences* USA (PNAS), the author(s) hereby grants to the National Academy of Sciences (NAS) for the full term of copyright and any extensions thereto the sole and exclusive, irrevocable license to publish, reproduce, distribute, transmit, display, store, translate, create derivative works from and otherwise use the WORK in any language or in any form, manner, format, or medium now known or hereafter developed without limitation throughout the world, and to license others to do any or all of the above. In the event that PNAS decides not to publish the WORK, this license shall be terminated.
2. In consideration of publication of the WORK in PNAS, the author(s) also grants to the NAS for the full term of copyright and any extensions thereto all of the same rights provided for in clause 1 above, for the supporting information as defined in the PNAS Information for Authors, but on a nonexclusive basis.
3. Ownership of copyright in the WORK remains with the author(s). Provided that the author(s) credits first publication of the WORK in PNAS when reproducing the WORK or extracts from it, the author(s) retains the following nonexclusive rights:
    a. The author(s) reserves the right after publication of the WORK by PNAS, to use all or part of the WORK in compilations or other publications of the author's own works, to use figures and tables created by them and contained in the WORK, and to make copies of all or part of the WORK for the author's use for lectures, classroom instruction, or similar uses.
    b. The author(s) reserves the right, after publication in PNAS, to post the WORK (including the PNAS-formatted PDF) on the author's personal web page provided that a link to the article in PNAS is included.
    c. The author(s) reserves the right to post the WORK on preprint servers such as arXiv provided that the author retains distribution rights to the WORK, that PNAS-formatted files (HTML and PDF) are not used, and that a link to the WORK in PNAS is included.
    d. The author(s) reserves the right on acceptance for publication of the WORK in PNAS to deposit his or her accepted manuscript in the author(s)'s funding body's archive or designated noncommercial institutional repository, provided that a link to the WORK in PNAS is included; and the right to request public access 6 months after publication, or immediately on publication if the author(s) has chosen either the PNAS Open Access CC BY-NC-ND or the Open Access CC BY option, depending on which CC license option was chosen for deposition in the repository. (NOTE: PNAS automatically deposits the PNAS-formatted version of all papers in PubMed Central.)
4. After publication of the WORK by PNAS, third parties are automatically granted permission to use figures and tables created by the author(s) and contained in the WORK for noncommercial use (e.g., not for sale or for commercial advantage).
5. The author(s) warrants that the WORK is original research by the authors, that all the facts it contains are true and accurate, that it does not infringe upon any copyright, proprietary, or personal right of any third party, and that permissions have been obtained and are attached for any portions of the WORK owned or controlled by a third party. The corresponding author of the WORK must sign this form. The signing author(s) represents and warrants that he or she signs this license as authorized agent(s) for and on behalf of all the authors and that this license is made on behalf of all the authors. The author(s) shall indemnify the NAS and/or its successors and assigns for any and all claims, costs, and expenses, including attorney's fees, arising out of any breach of this warranty or other representations contained herein.
6. The author(s) authorizes NAS to take such steps as it considers necessary at its own

expense in the author(s)'s name and on their behalf if it believes that a third party is infringing or is likely to infringe the copyright in the WORK.

7. If the WORK has been prepared by an employee within the scope of his or her employment, the license recognizes the employer's reserved right to make copies of the WORK for its own internal use.

Documentation Report:

If any of the following items are pertinent to your paper, we must receive the appropriate documentation or statements before we can publish your paper.

Please check the appropriate boxes below:

☐ **None of the three items below applies to this paper.**

☐ **Structural Coordinate Deposition and Release.** Authors of papers reporting new or revised structures must deposit their coordinates in the Protein Data Bank or an equivalent public archive, and the accession numbers must be supplied for publication. You agree, by signing below, that the coordinates will be released when the article is published. A footnote reporting the accession numbers will be added to your paper. You must provide the accession numbers on the page proof.

☑ **Sequence Database Deposition.** Authors of papers reporting new sequences must submit these data to an appropriate database, and the accession numbers must be supplied for publication. A footnote reporting the accession numbers will be added to your paper. You must provide the accession numbers on the page proof.

☐ **Permission to Print Previously Published Material.** If your paper includes material (e.g., figures or tables) that were published previously or modified from a previous publication, whether or not you are an author of the earlier publication, you must provide the previous publisher's permission to republish this material in print and online. We acknowledge that copyright is held by the original publisher. Please state which items were published previously and where:

Please select one:

◉ If **any authors** are not U.S. government employees: I warrant that I am an authorized agent for and on behalf of all authors. I have read the PNAS License to Publish and agree to the terms and conditions therein. PNAS and all authors agree that this agreement will be executed electronically.

○ If **all authors** are U.S. government employees: I certify that the WORK was written as part of the official duties of the authors as employees of the U.S. Government. On behalf of all authors, I authorize publication of the WORK in PNAS under terms equivalent to those provided for in the license and agree to all of the warranties specified in the license.

○ If WORK is a Work Made for Hire and the employer of the author(s) owns the copyright.

Please visit the PNAS FAQ for more information. You will need to complete a hardcopy version of this form. Please click here.

local_p_id: 1348358
time: 1584379732
ip address: 168.149.237.22